

**Department of Mechanical Engineering**

**Flexural Behaviour of Hybrid Fibre-Reinforced Polymer (FRP)  
Matrix Composites**

**Sударisman**

**This thesis is presented for the Degree of  
Doctor of Philosophy  
of  
Curtin University of Technology**

**December 2009**

## **DECLARATION**

To the best of my knowledge and belief this thesis contains no materials previously published by any other person except where due acknowledgement has been made.

This thesis contains no material which has been accepted for the award of any other degree or diploma in any university.

Signature: .....

Date: .....

## PUBLICATIONS

Some of the work presented in this thesis has been published in the following:

### *Journals:*

1. Sudarisman and I. J. Davies, "The effect of processing parameters on the flexural properties of unidirectional carbon fibre-reinforced polymer (CFRP) composites," *Materials Science and Engineering: A*, vol. 498, pp. 65-68, 2008.
2. Sudarisman and I. J. Davies, "Influence of compressive pressure, vacuum pressure, and holding temperature applied during autoclave curing on the microstructure of unidirectional CFRP composites," *Advanced Materials Research*, vol. 41-42, pp. 323-328, 2008.
3. Sudarisman and I. J. Davies, "Flexural failure of unidirectional hybrid fibre-reinforced polymer FRP) composites containing different grades of glass fibre," *Advanced Materials Research*, vol. 41-42, pp. 357-362, 2008.

### *Conference Proceedings:*

1. Sudarisman, B. de San Miguel, and I. J. Davies, "Failure mechanism of unidirectional hybrid FRP composites containing carbon and E-glass fibres subjected to three-point bend loading," in *Proceedings of the International Conference on Materials and Metallurgical Engineering 2009 (ICOMMET 2009)*, 24-25 June, Surabaya, Indonesia, 2009, pp. FA 6-9.
2. Sudarisman, B. de San Miguel, and I. J. Davies, "The Effect of Partial Substitution of E-glass Fibre for Carbon Fibre on the Mechanical Properties of CFRP Composites," in *Proceedings of the International Conference on Materials and Metallurgical Engineering 2009 (ICOMMET 2009)*, 24-25 June, Surabaya, Indonesia, 2009, pp. MI 126-129.

## ACKNOWLEDGEMENT

I would like express my gratitude and sincere thanks to many individuals who have contributed to the writing and completion of this PhD thesis.

Firstly, the individual to whom I most owe thanks is Dr. Ian J. Davies, who has been my principal supervisor, as well as a source of support throughout my postgraduate study in this university. His endless patience and encouragement to develop my understanding and comprehension of the research topic is highly appreciated. Secondly, I would also like to thank my other committee members - Dr. Garry Leadbeater (Co-supervisor), Associate Professor Jim Low of the Department of Applied Physics (Associate supervisor), Associate Professor Tilak T. Chandratilleke (Chairperson and currently Head of the Department) and also to Associate Professor Ian Howard - for the improvements of the experimental procedures together with the help and support in accessing the laboratory facilities in the Department of Mechanical Engineering. Another person whom I have to thank is my former Academic Supervisor, Professor Dahsin Liu of the Composite Vehicle Research Center (CVRC), Michigan State University, USA who, almost seventeen years ago, introduced me to composite materials and eventually I found it to be a very interesting and challenging subject in my career.

The financial support provided by the Technological and Professional Skill Development Project (TPSDP) Universitas Muhammadiyah Yogyakarta, from the Directorate of Manpower, the Directorate General of Higher Education, the Department of National Education of the Republic of Indonesia, and from Universitas Muhammadiyah Yogyakarta covering the major period of my postgraduate study is greatly appreciated.

My sincere thanks also go to David Collier, Philips Cesoria, and Graeme Watson for manufacturing the apparatus required for producing composite plates and for material testing. I am also grateful for the help given by Karen Haynes in providing and handling chemicals used in this project. I would also like to thank Jeff N. Pickle and John R. Murray for their discussion on strain gauges, to Peter G. Bruce, Michael J. Ellis, Derek Oxley and Robert Cutter for their assistance in



performing mechanical testing using the INSTRON machine. Thanks also go to Amanda and Elaine of the Centre for Microscope for their assistance in taking the micrographs.

Thanks to my colleagues, Lorenzo Mascaro, Bradley de San Miguel and Michael Andrew Klita, for their help in composite plate fabrication process. Special thank goes to Bradley for preparing the spreadsheet template for flexural property calculations. Thanks also to all my colleagues in postgraduate study in the Department of Mechanical Engineering for the support and sincere friendship. To all my colleagues in the Department of Mechanical Engineering, Universitas Muhammadiyah Yogyakarta, Indonesia, I would also like to thank for their support and trust during this study and through the years.

Support from my parents and my mother-in-law is also greatly appreciated. Last but not least, I would like to sincerely thank my wife, Rustiawati, my sons Wahid and Aziz, and my daughter, Rahmah, for their everlasting support, understanding, sacrifices and love during my study and throughout the years.

## ABSTRACT

The flexural behaviour of three different hybrid fibre-reinforced polymer (FRP) matrix composites, *i.e.* S2-glass/E-glass/epoxy, TR50S carbon/IM7 carbon/epoxy, and E-glass/TR50S carbon/epoxy hybrid FRP composites, has been investigated. The main objectives of this study were to: (i) improve the flexural properties of the parent composite materials, *i.e.* E-glass/epoxy and TR50S carbon fibre/epoxy composites, through substitution of stronger fibres, *i.e.* S2-glass and IM7 carbon fibres, for the fibres of the parent composite materials, and (ii) determine the optimum stacking configurations that produced the maximum increase in flexural properties of the resulting hybrid composites. In addition to these, two secondary objectives related to the preliminary investigation of determining the optimum stacking configurations have also been established. The two secondary objectives were to: (i) determine the optimum values of the processing parameters of the composites under investigation, and (ii) determine the compressive strength and compressive modulus of the parent materials.

The investigation was carried out experimentally, thus data presented and analysed were obtained from laboratory work. Optimum values of five processing parameters, *i.e.* (i) the concentration of matrix precursor within the solvent solution utilised to wet the fibres, (ii) the compressive pressure applied during hot-press curing, (iii) the vacuum pressure of the atmosphere inside the curing chamber, (iv) the dwell time during hot-press curing, and (v) the holding temperature during hot-press curing, have been established. The criteria for determining the optimum values of these parameters were optimum fibre content, minimum void content, and optimum flexural properties. Compressive strength and compressive modulus of the parent composite materials have also been determined.

Specimens were cut from flat composite plates using a diamond-tipped circular blade saw. The longitudinal edges of the specimens were carefully polished to remove any possible edge damage due to cutting. The composite plates were produced from preforms comprised of a number of glass fibre/epoxy preregs, carbon fibre/epoxy preregs or a combination of these. All the

fabrication procedures were carried out using manual techniques. Whilst the compressive tests were conducted in accordance with the ASTM D3410-03 standard, flexural tests were carried out according to Procedure A of the ASTM D790-07 standard. Span-to depth ratios,  $S/d$ , of 16, 32, and 64 were selected for flexural testing in order to determine the minimum value of  $S/d$  required to ensure flexural failure rather than shear failure. Fibre and void contents were evaluated from optical micrograph images of the slices perpendicular to the fibre direction of the samples.

It was concluded that the optimum values of the five processing parameters under investigations were: (i) epoxy concentration,  $C_e \sim 50$  wt%, (ii) compressive pressure,  $p_c \sim 1.00$  MPa, (iii) vacuum pressure,  $p_v \sim 0.035$  MPa, (iv) dwell time,  $t \sim 30$  minutes, and (v) holding temperature,  $T \sim 120$  °C. Compressive tests revealed that the order of compressive strength for the parent composite materials were arranged as follows: S2-glass fibre/epoxy (476 MPa), E-glass fibre/epoxy (430 MPa), IM7 carbon fibre/epoxy (426 MPa), and TR50S carbon fibre/epoxy (384 MPa). The compressive modulus of these parent composite materials were found to be ordered as follows: IM7 carbon fibre/epoxy (67.9 GPa), TR50S carbon fibre/epoxy (61.8 GPa), S2-glass fibre/epoxy (45.1 GPa), and E-glass fibre/epoxy (32.9 GPa). After considering these compressive properties, three different hybrid combinations, as mentioned earlier, were manufactured and evaluated with the prepreg layers of the fibre composites possessing higher compressive strength being placed at the compressively loaded side of the flexural specimens.

Shorter beam specimens ( $S/d = 16$ ) of the three hybrid systems exhibited increased flexural strength as the amount of stronger fibre content was increased, but no hybrid effect was noted. The increase appeared to follow the rule of mixtures and this was attributed to their failure mode being shear failure. For beams tested at  $S/d = 32$  and  $S/d = 64$ , the three hybrid systems demonstrated three different trends. The S2-glass fibre/E-glass fibre/epoxy hybrid system, where the S2-glass fibre (substituted at the compressive loading face) was slightly stronger and stiffer compared to the E-glass fibre at the tensile side, demonstrated increases in flexural strength together with the presence of a hybrid effect following partial substitution of the S2-glass fibre for E-glass fibres at the

compressive side. The IM7 carbon fibre/TR50S carbon fibre/epoxy hybrid system, where the IM7 carbon fibre (substituted at the compressive side) was slightly stronger but significantly stiffer in compression compared to the TR50S fibre at the tensile side, exhibited a slight increase in flexural strength that appeared to obey the rule of mixtures. This result was attributed to the strength increase in the compressive side introduced by the substituted fibres not being sufficient to suppress the increase of internal compressive stress due to the increase in compressive modulus of the substituted fibres. The E-glass fibre/TR50S carbon fibre/epoxy hybrid system, where the E-glass fibre (substituted at the compressive side) was found to be slightly stronger but significantly less stiff in compression compared to the TR50S fibre at the tensile side, demonstrated a significant increase in flexural modulus and also exhibited a significant hybrid effect. The decrease in internal compressive stresses generated at the compressive side due to the decreased compressive modulus of the substituted fibre, when combined with the increase in compressive strength of the substituted fibre, was thought to lead to the significant increase of flexural strength for this hybrid system.

General trends observed in flexural modulus for the three hybrid systems were reasonably similar with any change in flexural modulus appearing to obey the rule of mixtures. Whilst an increase in flexural modulus was noted for higher contents of stronger fibre in the case of the S2-glass fibre/E-glass fibre/epoxy hybrid system and IM7 carbon fibre/TR50S carbon fibre/epoxy hybrid system, a decrease in flexural modulus with increased quantities of stronger fibre was exhibited by the E-glass fibre/TR50S carbon fibre/epoxy hybrid system. The increase or decrease in flexural modulus was attributed to the relative stiffness in compression of the substituted fibre when compared to that of the respective parent composite materials.

Unlike the S2-glass fibre/E-glass fibre/epoxy hybrid system and IM7 carbon fibre/TR50S carbon fibre/epoxy hybrid system that did not exhibit any significant trend with regards the effect of the substitution of stronger fibre at the compressive side, the E-glass fibre/TR50S carbon fibre hybrid system demonstrated a significant increase in the energy stored to maximum stress with increasing content of the stronger fibre. This increase was mainly attributed to the

increased strain-to-maximum stress of the hybrid system with respect to that of the parent composite material.

In addition, for the three hybrid systems under investigation, the most significant change in flexural properties was noticed following substitution of the first layer at the compressive face. The relative position with respect to the neutral plane of the substituted layer was thought to be the reason for this phenomenon. It was also noted that flexural properties increased with the increase in  $S/d$ . A change in failure morphology was noted with the change of  $S/d$  from 16 to 32. It was thus determined that a  $S/d$  ratio of at least 32 was required in order to promote flexural failure (as opposed to shear failure). For the S2-glass fibre/E-glass fibre/epoxy hybrid system, this change appeared more obvious in comparison with that the other two hybrid systems with this change being accompanied by a significant increase in flexural strength.

The main general conclusions that could be drawn from this investigation were that, although the flexural modulus appeared to obey the rule of mixture, an increase in flexural strength together with the presence of a hybrid effect, would most probably be observed when the fibre substituted at the compressive side possessed a significantly lower modulus combined with significantly higher compressive strength as demonstrated by the hybrid TR50S carbon - E-glass FRP composites. The most significant change in properties was exhibited by the first layer substitution whilst increasing the value of  $S/d$  resulted in an increase of flexural strength, with  $S/d = 32$  being determined to be sufficient in order to promote flexural failure as opposed to shear failure.

## LIST OF CONTENTS

Chapters	Page
<b>TITLE PAGE</b> .....	i
<b>DECLARATION</b> .....	ii
<b>PUBLICATIONS</b> .....	iii
<b>ACKNOWLEDEMENT</b> .....	iv
<b>ABSTRACT</b> .....	vi
<b>LIST OF CONTENTS</b> .....	x
<b>LIST OF FIGURES</b> .....	xvi
<b>LIST OF TABLES</b> .....	xxiii
 <b>CHAPTER 1</b> <b>INTRODUCTION</b>	
1.1. GENERAL INTRODUCTION .....	1
1.2. RESEARCH BACKGROUND .....	1
1.3. RESEARCH POBLEMS .....	5
1.4. RESEARCH OBJECTIVES .....	5
1.5. RESEARCHSIGNIFICANCE .....	6
1.6. STRUCTURE OF THE THESIS .....	6
REFERENCES .....	8
 <b>CHAPTER 2</b> <b>LITERATURE REVIEW AND THEORETICAL BACKGROUND</b>	
2.1. INTRODUCTION .....	13
2.1.1. Definition .....	19
2.1.2. Classification of Composite Materials .....	24
2.1.2.1. Relative Dimensions of Reinforcements .....	24
2.1.2.2. Geometry of Reinforcement .....	25
2.1.2.3. Fibre Architecture .....	28
2.1.2.4. Matrix Types .....	29
2.2. CONSTITUENT MATERIALS .....	31
2.2.1. Fibres .....	31

2.2.1.1. Glass Fibres .....	33
2.2.1.2. Carbon Fibres and Graphite Fibres .....	37
2.2.2. Epoxy Matrix .....	41
2.3. FIBRE-MATRIX INTERFACE .....	45
2.4. FABRICATION TECHNIQUES OF FIBRE-REINFORCED (FRP) COMPOSITES .....	46
2.4.1. Hand Lay-up .....	47
2.4.1. Wet Lay-up .....	48
2.4.2. Dry Lay-up or Prepreg Lay-up .....	49
2.4.2. Other Fabrication Techniques .....	53
2.5. FIBRE-REINFORCED POLYMER (FRP) COMPOSITES .....	56
2.5.1. Glass Fibre-Reinforced Polymer (GFRP) Composites .....	56
2.5.1.1. Tensile properties .....	57
2.5.1.2. Compressive properties .....	60
2.5.1.3. Flexural properties .....	63
2.5.1.4. GFRP summary .....	65
2.5.2. Carbon Fibre-Reinforced Polymer (CFRP) Composites .....	66
2.5.2.1. Tensile properties .....	66
2.5.2.2. Compressive properties .....	70
2.5.2.3. Flexural properties .....	74
2.5.2.4. CFRP summary .....	92
2.5.3 Hybrid Fibre-Reinforced Polymer (HFRP) Composites .....	93
2.5.3.1. Hybrid effect .....	94
2.5.3.2. Tensile properties .....	95
2.5.3.3. Compressive properties .....	98
2.5.3.4. Flexural properties .....	100
2.5.3.5. Hybrid FRP summary .....	108
REFERENCES .....	109

### **CHAPTER 3**

### **MECHANICS OF COMPOSITE MATERIALS**

3.1. CLASSICAL BEAM THEORY .....	127
3.1.1. Normal Stress and Normal Strain Distribution .....	127

3.1.2. Shear Stress Distribution .....	130
3.1.3. 'Composite' Cross Section of Beams .....	131
3.1.4. Beam Deflection .....	134
3.2. THE RULE OF MIXTURES .....	138
3.2.1. Volume Fraction and Composite Density .....	138
3.2.2. Longitudinal Strengths .....	139
3.2.3. Modulus of Elasticity .....	140
3.3. LAMINATED BEAM THEORY .....	141
3.4. THE WORK OF FRACTURE .....	146
3.4. FAILURE THEORIES .....	146
REFERENCES .....	148

## **CHAPTER 4**

### **EXPERIMENTAL PROCEDURE**

4.1. EQUIPMENT DESIGN AND MANUFACTURING .....	149
4.1.1. Composite Plate Fabrication Equipment .....	149
4.1.1.1. Rectangular stainless steel frames .....	149
4.1.1.2. Frame holder .....	150
4.1.1.3. Oven .....	150
4.1.1.4. Hot-press .....	152
4.1.2. Mechanical Test Equipment .....	152
4.1.2.1. Tabbing press .....	152
4.1.2.2. Alignment jig .....	153
4.1.2.3. Compression test fixture .....	154
4.1.2.4. Flexural test fixture and loading nose .....	154
4.2. COMPOSITE PLATE FABRICATION .....	155
4.2.1. Materials .....	155
4.2.1.1. Fibres .....	155
4.2.1.2. Matrix .....	157
4.2.2. Stacking Configuration .....	157
4.2.3. Plate Fabrication Development .....	158
4.2.3.1. Fabrication parameters .....	158
4.2.3.2. Fabrication parameter optimisation .....	159



4.2.3.3. Composite plate fabrication procedure .....	160
4.3. FIBRE VOLUME FRACTION AND VOID CONTENT DETERMINATION .....	162
4.4. MECHANICAL TESTING .....	164
4.4.1. Compressive Test .....	164
4.4.1.1. Specimen preparation .....	164
4.4.1.2. Testing .....	166
4.4.2. Flexural Test .....	166
4.4.2.1. Specimen preparation .....	166
4.4.2.2. Testing .....	167
4.5. OPTICAL MICROGRAPHY .....	169
4.5.1. Specimen Preparation .....	169
4.5.2. Image Capturing .....	169
4.5.3. Image Analysis .....	169
REFERENCES .....	171

## **CHAPTER 5**

### **FABRICATION PARAMETER OPTIMISATION**

5.1. FABRICATION PARAMETERS .....	175
5.2. EXPERIMENTAL PROCEDURE .....	178
5.2.1. Materials .....	178
5.2.2. Optimisation Procedure .....	178
5.2.3. Testing and Evaluation .....	179
5.3. RESULT AND DISCUSSION .....	180
5.3.1. Epoxy Concentration Determination .....	181
5.3.2. Hot-press Curing Compressive Pressure .....	183
5.3.3. Hot-press Curing Holding Time .....	187
5.3.4. Hot-press Curing Vacuum Pressure .....	189
5.3.5. Hot-press Curing Holding Temperature .....	191
5.4. CONCLUSIONS .....	193
REFERENCES .....	194

## CHAPTER 6

### RESULTS AND DISCUSSION

6.1. PRELIMINARY TEST: COMPRESSIVE TEST .....	199
6.1.1. Specimens .....	199
6.1.2. Stress-Strain Relation .....	200
6.1.3. Compressive Properties .....	202
6.2. HYBRID FRP COMPOSITES CONTAINING DIFFERENT TYPES OF GLASS FIBRE .....	204
6.2.1. Physical properties .....	205
6.2.1.1. Stacking configurations .....	205
6.2.1.2. Density, fibre content and void content .....	206
6.2.2. Mechanical Properties .....	208
6.2.2.1. Stress-strain response .....	208
6.2.2.2. Failure mechanism .....	215
6.2.2.3. Flexural strength .....	217
6.2.2.4. Flexural modulus .....	220
6.2.2.5. Energy storage capacity to maximum stress, $\gamma_{\max}$ .....	222
6.2.3. Summary .....	225
6.3. HYBRID FRP COMPOSITES CONTAINING DIFFERENT GRADES OF CARBON FIBRE .....	226
6.3.1. Physical properties .....	227
6.3.1.1. Stacking configurations .....	227
6.3.1.2. Density, fibre content and void content .....	228
6.3.2. Mechanical Properties .....	230
6.3.2.1. Stress-strain response .....	230
6.3.2.2. Failure mechanism .....	237
6.3.2.3. Flexural strength .....	239
6.3.2.4. Flexural modulus .....	242
6.3.2.5. Energy storage capacity to maximum stress, $\gamma_{\max}$ .....	243
6.3.3. Summary .....	245
6.4. HYBRID FRP COMPOSITES CONTAINING MIXED GLASS AND MEDIUM STRENGTH CARBON FIBRES .....	246
6.4.1. Physical properties .....	247
6.4.1.1. Stacking configurations .....	247

6.4.1.2. Density and fibre content .....	248
6.4.2. Mechanical Properties .....	249
6.4.2.1. Stress-strain response .....	249
6.4.2.2. Failure mechanism .....	256
6.4.2.3. Flexural strength .....	260
6.4.2.4. Flexural modulus .....	263
6.4.2.5. Energy storage capacity to maximum stress, $\gamma_{\max}$ .....	264
6.4.3. Summary .....	265
REFERENCES .....	266

## **CHAPTER 7**

### **CONCLUSSIONS AND RECOMMENDATIONS**

7.1. CONCLUSIONS .....	272
7.1.1. Fabrication Parameters Optimisation .....	272
7.1.2. Compressive Properties of Parent Composite Materials .....	273
7.1.3. Hybrid FRP Composites Containing Different Types of Glass Fibre .....	273
7.1.4. Hybrid FRP Composites Containing Different Grades of Carbon Fibre .....	274
7.1.5. Hybrid FRP Composites Containing Glass and Carbon Fibres ....	275
7.2. RECOMMENDATIONS FOR FUTURE WORK .....	276
REFERENCES .....	277

<b>APPENDICES</b> .....	279
-------------------------	-----

## LIST OF FIGURES

FIGURES	Page
2.1. Classification of materials for engineering structures (Summarised from a number references) .....	14
2.2. Strengths and moduli of typical structural materials showing that, in general, those of the metallic materials are superior. (a) Yield strength, (b) Young's modulus .....	15
2.3. Specific strength and specific modulus of typical structural materials showing that, in terms of specific strength and specific modulus, a typical carbon fibre-reinforced epoxy (CFRP) composite (appears close to top-right corner) is the optimum material. Alumina ( $\text{Al}_2\text{O}_3$ , appears close to top-left corner) ceramic, whilst it possesses high specific modulus, has a very low specific strength, whilst materials that appear close to the bottom-left corner (phenolic, polypropylene, epoxy, and nylon), which are, except for magnesia, all polymers, possess both low specific strength and modulus .....	16
2.4. The utilisation of composite materials in aircraft structures from the 1930s – current. (a) Weight proportion of materials used in aircraft manufactured from 1930 – 1980, (b) Proportion of materials in modern aircraft, the Boeing 787 – Dreamliner .....	17
2.5. Engineering material evolution through the ages showing, in the second layer from the bottom of the figure, the relative importance of composite materials .....	18
2.6. Carbon fibre-reinforced epoxy composite showing distinct phases between fibres (bright region) and matrix (dark region). (a) Transverse to fibre direction, (b) Parallel with fibre direction .....	20
2.7. Impact properties of various engineering materials. Unidirectional fibre-reinforced polymer composite materials with approximately 60% fibre volume fraction .....	20
2.8. Specific strengths and specific moduli of typical structural materials showing that, in general, those of composite materials are superior in comparison with those of conventional metals .....	23
2.9. Three main types of composite system based on the reinforcing material geometry: (a) SEM micrographs of a typical nickel-based particle-reinforced lead-based matrix particulate composite with 0.3 mol fraction of $\text{Ni}_{0.93}\text{Co}_{0.02}\text{Mn}_{0.5}\text{Fe}_{1.95}\text{O}_{4-\delta}$ and 0.7 mol fraction of $\text{PbZr}_{0.52}\text{Ti}_{0.48}\text{O}_3$ , (b) Mica flake-reinforced poly-dimethylsiloxane, and (c) Unidirectional continuous carbon-silicon carbide fibres hybrid-reinforced polymer matrix composite containing four layers of carbon fibre prepreg in the lower part and four layers of silicon carbide fibres in the upper part illustrating shear failure along its neutral plane after being loaded in bending .....	26

2.10. Spool of E-glass fibre E2350-11 supplied by Owens Corning Asia-Pacific. Net weight of the spool is 17 kgs .....	34
2.11. Direct-melt glass fibre manufacturing process .....	36
2.12. A roll of S2-glass fibre mat Unitex UT-S500 supplied by SP System, Newport, Isle of Wight, UK .....	37
2.13. Two rolls of 12k tow size PAN-based carbon fibre from two different manufacturers .....	40
2.14. Illustration of amine curing reaction of epoxide and amine hardener showing that each of hydrogen atom of the amine curing agent reacts with each of the epoxide groups to form a strong covalent bond .....	43
2.15. Classification of polymer matrix composite fabrication techniques ..	47
2.16. Schematic illustration of simple wet lay-up moulding .....	49
2.17. A small-sized autoclave showing its important elements. Thermostat that is installed to control its temperature is not shown. Element geometry is shown in the inset. (Basic design by Nick Jensen, improvement and instrumentation by Sudarisman) .....	51
2.18. Compressive strength comparison between E-glass fibre/vinylester and IM7-12k carbon fibre/vinylester composites showing, within the range of given fibre volume fraction, that of the GFRP composite is higher than that of the CFRP composites .....	81
3.1. A beam subjected to a three-point bending: (a) A simply supported beam of span $S$ deformed with curvature radius of $r$ due to a shear force $F$ acting in the mid-span, (b) Magnification of an arbitrary segment of the beam showing the deformation of a layer located at a distance of $y$ from the neutral axis, (c) Arbitrary cross section of the beam showing an elementary cross section $dA$ experiencing a normal stress of magnitude $\sigma_x$ , (d) Schematic representation of normal stress distribution along the $y$ axis .....	130
3.2. Enlarged view of beam segments as seen in Figure 3.1(a): (a) Normal and shear stresses generated over the segment due to lateral force $F$ , (b) Shear stress distribution over the depth of the beam .....	132
3.3. A typical composite cross section comprising of two different materials of rectangular shapes. (a) Cross section, (b) Normal strain distribution along the $y$ -axis, (c) Normal stress distribution along the $y$ -axis showing discontinuity at the interface of the two materials ...	134
3.4. Deflection of a beam: (a) A simply supported beam subjected to a lateral force $F$ acting at the mid-span of the beam, (b) Magnified view of segment DE of the beam showing the slope and deflection $y$ and $\theta$ , respectively, at D, and $\theta + d\theta$ and $y + dy$ , respectively at E ...	137

3.5. Deflection of a simply supported beam after the origin has been moved to point A .....	139
3.6. A representative sectional view a three-layer laminated composite beam showing the layer numbers ( <i>i.e.</i> $k = 1, k = 2$ , and $k = 3$ ), the number of layer ( <i>i.e.</i> $n = 3$ ), and for $k = 1$ : $h_k = h_1$ and $h_{k-1} = h_0$ , for $k = 2$ : $h_k = h_2$ and $h_{k-1} = h_1$ , and for $k = 3$ : $h_k = h_3$ and $h_{k-1} = h_2$ . .....	143
4.1. Rectangular stainless steel frames. (a) Top view, (b) Photograph ...	152
4.2. Frame holder. (a) Front view of the holder, (b) Photograph showing: 1. Glass fibre roll, 2. Stainless steel frame, and 3. Holder .....	153
4.3. Oven for producing fibre/epoxy prepregs. (a) Shop drawing showing its details and dimensions, (b) Photograph showing: 1. Digital thermometer and timer, 2. Rotating handle, and 3. Door ....	154
4.4. Tabbing press. (a) Front view showing: 1. Bottom plate, 2. Top plate, 3. Hooks, 4. Guiding Pins, 5. Bolt, and 6. Arm, (b) Photograph .....	155
4.5. Alignment jig. (a) Top view showing: 1. Holding plates, 2. Parallel holders, 3. Bases, (b) Front view showing: 4. Gauge length spacers, and (c) Photograph showing fixture grips separated 2.54 mm apart ..	156
4.6. Compressive test fixture. (a) Front view showing: 1. Clamping screws, 2 and 3. Grips, 4. Load pins, and (b) Photograph .....	157
4.7. Flexural test fixture. (a) Front view, and (b) Photograph showing the support along with the three-point bend loading nose .....	157
4.8. Schematic illustration of the composite plate manufacturing procedure .....	164
4.9. Schematic illustration of hybrid FRP composites containing two types of fibres in a common matrix .....	166
4.10. Compressive test specimen showing nominal dimensions. (a) Top view, (b) Front view, note that $t$ is specimen thickness which depends on the thickness of the composite plate panel .....	169
5.1. Photo micrograph of the calibration bar captured under $5\times$ optical magnification showing two scale bars of the same length, one in micron and the other in pixels (px) .....	183
5.2. Optical micrographs of two specimens manufactured from different epoxy resin contents: (a) 45 wt% of epoxy content showing less matrix-rich areas as narrower dark bands (white arrows), and (b) 65 wt% of epoxy concentration showing matrix-rich areas as wider diagonal dark bands (dark arrows) and voids (white arrows) between layers .....	185

5.3. Influence of epoxy resin content (within an acetone solution) on flexural properties and estimated fibre volume and void volume contents .....	186
5.4. Optical micrographs of composite specimens: (a) manufactured at 0.25 MPa compressive pressure illustrating matrix-rich regions and voids (dark spots in matrix area), and (b) manufactured at 1.00 MPa compressive pressure indicating the presence of denser fibre packing and less voids .....	187
5.5. The effect of hot-press compressive pressure on fibre alignment showing negligible difference in the degree of fibre misalignment: (a) $p_c = 0.25$ MPa, and (b) $p_c = 1.25$ MPa .....	188
5.6. Influence of compressive pressure during the vacuum hot-press curing procedure on flexural properties and estimated fibre volume fraction .....	189
5.7. Optical micrographs illustrating: (a) imperfect fibre wetting (dark arrows) and the presence of voids (white arrows) between individual prepreg layers for a 20 minute holding time specimen, and (b) fibre misalignment within a 40 minute holding time specimen (dark arrows) .....	190
5.8. Influence of holding time during the vacuum hot-press curing procedure on flexural properties and estimated fibre volume fraction .....	191
5.9. Samples of in-plane micrographs: (a) at $p_v = 0.085$ MPa showing $\sim 1.5\%$ up to $5^\circ$ fibre misalignment, (b) at $p_v = 0.035$ MPa showing the lack of fibre misalignment .....	192
5.10. The influence of vacuum pressure on flexural strength, flexural modulus, and predicted fibre volume fraction at $p_c = 1.00$ MPa, $T = 120^\circ\text{C}$ , and $t = 30$ minutes .....	193
5.11. The influence of holding temperature on flexural strength, flexural modulus, and predicted fibre volume and void volume content at $p_c = 1.00$ MPa, $T = 120^\circ\text{C}$ , $t = 30$ minutes and $p_v = 0.035$ MPa .....	195
6.1. Representative stress-strain relationship curves of compressive FRP composite specimens showing a considerably linear stress-stress relation up to close to failure .....	201
6.2. Compressive properties of single fibre-type composite specimens under investigation .....	203
6.3. Visual illustration of the stacking configurations of the hybrid composites under investigation .....	206
6.4. Optical micrograph of hybrid GFRP composites containing one layer of E-glass epoxy prepreg and four layers of S2-glass/epoxy prepreps showing unevenly distributed fibres, matrix rich areas and voids .....	207

6.5. Representative load-displacement and stress-stress relationships for $S_3E_2$ samples tested at $S/d = 16$ . (a) Load-displacement relationship before toe correction, (b) After toe correction, (c) Stress-strain relationship .....	211
6.6. The effect of hybrid ratio on stress-strain relationship for each of the hybrid GFRP composite plates: (a) $S/d = 16$ , (b) $S/d = 32$ , (c) $S/d = 64$ .....	212
6.7. The effect of span-to-depth ratio on stress-strain relationship for representative composite plates: (a) $S_0E_5$ (E-glass/epoxy) composite plate, (b) $S_3E_2$ (hybrid S2-E-glass/epoxy) composite plate, (c) $S_5E_0$ (S2-glass/epoxy) composite plate .....	214
6.8. A typical compressive side fracture region for specimens tested at $S/d = 16$ showing splitting (dark arrows) and fibre buckling .....	215
6.9. A typical fracture region for specimens tested at $S/d = 32$ illustrating fibre buckling (top) and less splitting .....	216
6.10. A typical fracture surface for specimens tested at $S/d = 64$ showing fibre buckling and kinking domination (top) and less splitting (white arrows) .....	217
6.11. The influence of hybrid ratio (S2-glass fibre volume/total fibre volume) on the flexural strength of hybrid GFRP composites showing an increase of flexural strength with the increase in S2-glass fibre volume .....	218
6.12. The influence of hybrid ratio (S2-glass fibre volume/total fibre volume) on the flexural modulus of hybrid GFRP composites showing an increase of flexural strength with the increase in S2-glass fibre volume .....	221
6.13. The influence of hybrid ratio on the energy absorption capacity to maximum stress, $\gamma_{\max}$ , of hybrid GFRP composites .....	222
6.14. Visual illustration of the stacking configurations of the hybrid CFRP composites under investigation .....	228
6.15. Optical micrograph of hybrid CFRP composites containing TR50S and IM7 carbon fibres showing unevenly distributed fibres, matrix rich areas and voids. (a) Matrix rich area present at the interface of TR50S/epoxy-IM7/epoxy prepreg layers, (b) Uneven fibre distribution, with smaller variation was also observed within a IM7/epoxy prepreg layer .....	230
6.16. Shift of loading point after first failure for specimens tested at $S/d = 16$ resulting in the length of the moment arm being reduced or the load recorded by the load cell to produce the same magnitude of moment force being increased .....	232
6.17. Representative load-displacement and stress-stress relationships for $IM_1TR_5$ samples tested at $S/d = 16$ . (a) Load-displacement	



relationship before toe correction, (b) After toe correction, (c) Stress-strain relationship .....	234
6.18. The effect of hybrid ratio on stress-strain relationships for each of the hybrid CFRP composite plates: (a) $S/d = 16$ , (b) $S/d = 32$ , (c) $S/d = 64$ .....	235
6.19. The effect of hybrid ratio on stress-strain relationships for each of the hybrid CFRP composite plates: (a) $TR_6$ samples, (b) $IM_1TR_5$ samples, (c) $IM_6$ samples .....	236
6.20. A typical shear failure region for hybrid CFRP specimens tested at $S/d = 16$ . (a) Low magnification image showing interlaminar delamination (white arrows), and (b) Larger magnification image showing interlaminar delamination and fibre buckling and kinking at the top side .....	237
6.21. A typical fracture region for hybrid CFRP specimens tested at $S/d = 32$ showing fibre buckling and kinking .....	238
6.22. A typical fracture region for hybrid CFRP specimens tested at $S/d = 64$ showing out-of-plane fibre buckling and kinking domination at the compressive side .....	239
6.23. The influence of hybrid ratio ( $IM_7$ carbon fibre volume/total fibre volume) on flexural strength for hybrid CFRP composites illustrating an insignificant increase in flexural strength with the increase in $IM_7$ carbon fibre volume .....	239
6.24. The influence of hybrid ratio on flexural modulus for hybrid CFRP composites showing an increase in flexural modulus with the increase in $IM_7$ carbon fibre volume content .....	242
6.25. The influence of hybrid ratio on the energy absorption capacity to maximum stress, $\gamma_{max}$ , of hybrid CFRP composites .....	243
6.26. Schematic illustration of the stacking configurations of the hybrid CFRP composites under investigation .....	247
6.27. Representative load-displacement and stress-strain relationships for hybrid composite samples ( $C_1G_3$ ). (a) Before toe correction, (b) After toe correction, and (c) Stress-strain relationship .....	251
6.28. Representative illustration of the effect of hybrid ratio on stress-strain relationships. (a) $S/d = 16$ , (b) $S/d = 32$ , (c) $S/d = 64$ .....	254
6.29. Representative illustration of the effect of $S/d$ on stress-strain relationships. (a) $C_0G_5$ samples, (b) $C_3G_2$ samples, (c) $C_6G_0$ samples .....	255
6.30. Fracture region of a $C_2G_2$ specimen tested at $S/d = 16$ showing: (a) fibre kinking, (b) fibre breakage, (c) delamination in a matrix rich ..	257
6.31. Fracture region of a $C_2G_2$ specimen with $S/d = 32$ . (a) Compressive face showing out-of-plane buckling and kinking (white arrow) and splitting (dark arrow), and (b) tensile surface showing fibre breakage (dark arrow) and delamination (white arrow) .....	258

6.32. Compressive side of the fracture region for a C <sub>2</sub> G <sub>2</sub> specimen with $S/d = 64$ : (a) splitting, (b) in-plane buckling producing kink band, (c) out-of-plane buckling at the carbon fibre side, (d) matrix-rich areas between two prepreg layers .....	259
6.33. The effect of hybrid ratio on flexural strength showing an increase of flexural strength with the increase of hybrid ratio .....	260
6.34. The effect of hybrid ratio on flexural modulus illustrating a decrease in flexural strength with the increase of hybrid ratio .....	263
6.35. The effect of hybrid ratio on specific energy storage capacity-to-maximum stress showing an increase of $\gamma_{\max}$ as the hybrid ratio increased .....	264

## LIST OF TABLES

Tables	Page
2.1. Properties of typical structural materials.....	22
2.2. Global market for advanced composite fibres in 2006 .....	32
2.3. Cost and properties of E-glass and standard modulus carbon fibre ...	33
2.4. Typical chemical composition of E- and S-glass fibres (wt%) .....	35
2.5. Typical properties of E- and S-glass fibres .....	37
2.6. Typical properties of carbon fibres from different precursors .....	41
2.7. Typical properties of cured epoxy resin .....	45
2.8. Average compressive mechanical properties of E-glass/polyester C-channel composites at elevated temperatures .....	62
2.9. Compressive strength calculation for Khalid <i>et al.</i> , 2005 .....	63
2.10. Flexural strength calculation from Khalid <i>et al.</i> , 2005 .....	68
2.11. Typical properties of GFRP composites .....	70
2.12. Typical properties of CFRP composites .....	88
2.13. Typical properties of hybrid FRP composites .....	103
4.1. Properties of the constituent materials .....	160
4.2. Stacking configurations .....	161
5.1. Selected values of the processing parameters .....	181
5.2. Optimum values of the processing parameters .....	193
6.1. Predicted fibre volume and void content of single fibre-type composite plates .....	200
6.2. Predicted tensile properties of FRP composites under investigation according to the rule of mixtures .....	203
6.3. Calculated density, predicted fibre volume content and void volume content of the hybrid GFRP composites .....	206
6.4. Strain at maximum stress for hybrid GFRP specimens .....	220
6.5. Calculated density, predicted fibre volume content and void volume content for the hybrid CFRP composites .....	228
6.6. Strain at maximum stress for the hybrid GFRP specimens (%) .....	241
6.7. Physical characteristics of the hybrid composite plates .....	248

6.8. Strain at maximum stress (%) for the hybrid carbon-glass FRP composites under investigation .....	262
--	-----

## **CHAPTER 1**

# **INTRODUCTION**

### **1.1. GENERAL INTRODUCTION**

The flexural behaviour of hybrid fibre-reinforced polymer (FRP) matrix composites has been investigated experimentally. Thus, all the data presented and analysed were obtained from laboratory work. The current research can be divided into three parts. The first part deals with the parameter optimisation of composite plate fabrication that will be presented in Chapter 5. The second part, referred to as “preliminary work”, consists of compressive testing of the parent composite materials that were later used to manufacture the hybrid composite system – this part will be presented in section 6.1. The final part contends with hybrid composite materials containing three different hybrid systems where each hybrid system contains two different reinforcing fibres embedded within a common matrix – these hybrid composite systems will be presented in sections 6.2 to 6.4.

### **1.2. RESEARCH BACKGROUND**

The specific mechanical properties, *i.e.*, mechanical properties-to-density ratio, of composite materials being generally higher than those of conventional materials [1](pp. 3-4) is one amongst many reasons behind the wide acceptance of composite materials ranging from household appliances, sporting [2] and leisure goods, civil and construction structures [3, 4], transportation [5-7], and aerospace [8] and high performance structures. The fact that their properties can be engineered and tailored [1](pp. 6-9) according to their required applications, *e.g.*, through: (i) selecting the type of matrix and reinforcing materials, (ii) controlling

the proportions of matrix and reinforcement, or else for the case of fibre-reinforced composites, through (iii) controlling their fibre architecture, is a major advantage of these materials.

The utilisation of different types of reinforcing material within a common matrix to produce hybrid composites has been the subject of research in materials science since the 1970s [9-12]. For example, combinations of reinforcement being studied have included: glass fibre and carbon fibre [10, 13-15], glass fibre and graphite fibre [16, 17], glass fibre and aramid fibre [18], glass fibre and steel fibre [19], glass fibre and bamboo fibre [20, 21], aramid fibre and carbon fibre [22], aramid fibre and glass fibre [22], carbon fibre and silicon carbide fibre [23, 24], as well as ultra high modulus polyethylene fibre and carbon fibre [25].

Different properties of various hybrid FRP systems have also been reported. For example, investigations have previously focussed on: (i) tensile properties (*e.g.*, short glass and short carbon fibres in polypropylene [26], jute and chopped strand glass fibre mat in polyethylene [27]), (ii) compressive properties (*e.g.*, sisal fibre and chopped strand glass fibre mat in polyethylene [28], ultra high modulus polyethylene and carbon fibres in epoxy [25], aramid and glass fibres in polyethylene [29]), (iii) compression after impact properties (*e.g.*, Kevlar and carbon fibres in epoxy [30]), (iv) impact properties (*e.g.*, Kevlar and carbon fibres in epoxy [30], sisal fibre and chopped strand glass fibre mat in polyethylene [28], jute fibre and chopped strand glass fibre mat in polyethylene [27]), (v) ductility (*e.g.*, ultra high modulus polyethylene fibres in epoxy [25]), (vi) flexural properties (*e.g.*, sisal fibre and chopped strand glass fibre mat in polyethylene [31], graphite and E-glass fibres in polypropylene chloride [16], ultra high modulus polyethylene fibres in epoxy [25], jute and chopped strand glass fibre mat in polyethylene [27]), and (vii) flexural fatigue properties (*e.g.*, shaft of aluminium core reinforced with GFRP composite jacket [32], glass and carbon fibres in epoxy [13, 14]). However, there has been very limited information published concerning the improvement of flexural properties for low cost unidirectional E-glass/epoxy composites through the partial substitution of superior mechanical property S2-glass fibre, as well as improving the flexural properties of unidirectional standard quality carbon fibre/epoxy composites by

introducing high strength carbon fibres in order to produce hybrid fibre-reinforced polymer (FRP) composites.

The existence of a hybrid effect, *i.e.*, any deviation of hybrid composite properties from those predicted by the rule of mixtures [33], may still be debatable; some researchers have reported the existence of a positive hybrid effect, some have reported an increase in properties but did not observe a hybrid effect (*i.e.*, only obeying the rule of mixtures), whilst others have reported a negative hybrid effect.

Positive hybrid effects have been reported by You *et al.* [34] who studied the tensile properties of cylindrical carbon-glass fibre hybrid FRP composite rods. Li *et al.* [25] reported that the substitution of carbon fibre for ultra high modulus polyethylene (UHMPE) fibre at moderate amounts, up to ~46%, showed a positive hybrid effect with regards the compressive strain at ultimate strength. A significant positive hybrid effect for fracture toughness (approximately 100% increase with 15 vol.% substitution of S-glass fibre for carbon fibre), flexural strength and flexural modulus was observed by Chaudhuri and Garala [35]. Meanwhile, Davies and colleagues [23, 36] reported that the substitution of 12.5% silicon carbide (SiC) fibre into the parent CFRP composite material produced a significant increase in flexural strength and exhibited a positive hybrid effect.

An improvement in the retention of tensile strength and modulus with regards to environmental aging has been reported by Thwe and Liao [21] for their chopped strand glass fibre – bamboo fibre-reinforced polypropylene composites, but they did not report whether or not they observed a hybrid effect. Poor wetting leading to weak fibre-matrix interfacial bonding resulted in an increase of tensile properties but absence of a hybrid effect for flax FRP composites through substitution of glass fibre has been reported [37]. Although Dickson *et al.* [38] reported an increase in strain-to-failure of CFRP layers due to partial incorporation of E-glass fibre, a hybrid effect was not observed. Furthermore, a significant increase in compressive strain-to-failure has been observed, although a hybrid effect was not noticed, with regards to compressive strength due to the compressive strength of the incorporated UHMPE fibre being noticeably lower

than that of the original carbon fibre [49]. Meanwhile, compressive strength and modulus were observed to increase with an increase of S-glass fibre content in CFRP composite samples although a positive hybrid effect was not observed [35]. Substitution of higher compressive strength SiC fibre for carbon fibre within CFRP parent composite materials did not exhibit any significant increase in compressive strength, compressive modulus, or work of fracture for the hybrid SiC and carbon fibre-reinforced epoxy composites [24]. Wang *et al.* reported that their boron-carbon and silicon carbide-carbon hybrid FRP composites demonstrated a remarkable increase in flexural strength [39], but this may be attributed to the fibre content in their hybrid systems (~75%) being significantly higher than that of the parent CFRP composite material (53.1%). Arbelaiz *et al.* [37] reported that poor fibre wetting, noticed in their SEM micrographs, resulted in weak fibre-matrix interfacial bonding of their flax-glass fibre hybrid FRP composites that limit an increase in flexural strength and flexural modulus, resulting in a restricted improvement in flexural properties together with the absence of a hybrid effect.

In contrast to these examples, a negative hybrid effect for the case of tensile properties has been reported by Hariharan and Khalil [40]. This result was attributed to the coefficient of thermal expansion for the two fibre types utilised in their research, *i.e.*, oil palm fibre and chopped strand E-glass fibre mat, being significantly different leading to the presence of high residual thermal stresses upon cooling down following curing. Similarly, a small negative hybrid effect in tensile strength for mixed continuous and spun fabric carbon fibre-reinforced phenolic due to weak fibre-matrix interfacial bonding was observed by Kang *et al.* [41]. Finally, although a positive hybrid effect for flexural strength was noticed, the flexural modulus exhibited a slight negative hybrid effect from the substitution of ~12.5% silicon carbide fibre into the parent CFRP composite [23, 36] that may be attributed to the elastic modulus of the SiC fibre being slightly lower than that of the carbon fibre.

Most of the previous research discussed above observed an increase in mechanical properties through hybridisation. Three different categories of this hybridisation effect have been reported in a number of previously published



papers, namely: (i) remarkable increase in mechanical properties in conjunction with a positive hybrid effect, (ii) reasonable increase in properties without a noticeable hybrid effect, and (iii) decrease in properties with a negative hybrid effect.

### **1.3. RESEARCH PROBLEMS**

The overall research problem analysed within the present work can be stated as: “To investigate how to improve the flexural properties of parent fibre-reinforced polymer composite materials through the production of hybrid composite materials”.

As the manufacture of composite plates has also been investigated by the present author, a research question relating to this aspect of work may also be included. In addition, considering that the failure of composite beams mostly initiates at their compressively loaded side [36, 42-48], the compressive properties of parent composite materials have also been investigated and, thus, another research question regarding this work may also be included. Two additional research questions may therefore be derived from the research problem stated above. Thus, the following four main research questions or themes may be proposed.

1. What are the optimum values of processing parameters required in order to produce the most favourable flexural properties for the composites under investigation?
2. How do the compressive strength and compressive modulus of the parent composite materials differ from one another, so that an optimum stacking sequence and/or stacking configuration can be determined?
3. Can the flexural strength, flexural modulus and energy storage capacity-to-maximum stress of fibre-reinforced polymer matrix composites be improved through hybridisation?

4. How does the stacking configuration influence the hybrid effect with regards to flexural strength, flexural modulus and energy storage capacity-to-maximum stress?

#### **1.4. RESEARCH OBJECTIVES**

The following suppositions were defined to be the main themes of the current research.

1. The optimum values of the processing parameters of the composites under investigation can be determined.
2. The compressive strength and compressive modulus of the parent composite materials can be determined.
3. The flexural properties of the parent composite materials can be improved through hybridisation.
4. The optimum stacking hybrid configuration in terms of producing relative optimum increase can be identified.

#### **1.5. RESEARCH SIGNIFICANCE**

Through achieving the research objectives mentioned above, the following positive multiplier effects may further be obtained.

1. Material saving. Improving the flexural properties of the parent composites through hybridisation means an improvement in harnessing the property potential of the materials and thus reducing the demand for materials of the products.
2. Weight saving and/or increase of load carrying capacity. Improving the performance of materials leads to a reduction in the structure dimensions to

support the same magnitude of load, or *vice versa*, increase the load carrying capacity of a structure of the same dimensions.

3. If the materials are utilised in mobile structures, such as transportation vehicles, weight saving results in a reduction in the amount of energy required to move it and thus produces savings in fuel consumption.
4. Fuel consumption savings further reduce the amount of pollutants emitted from fuel combustion to the atmosphere.

## 1.6. STRUCTURE OF THE THESIS

The body of this thesis comprises of seven chapters, after which specific data and calculations have been included within an appendix. The seven chapters of the thesis, together with their brief description, are presented below.

Chapter 1. **Introduction** presents a brief description of the whole thesis, *i.e.*, general introduction, research background, research problems, research objectives, research significance, and the structure of the thesis.

Chapter 2. **Literature Review and Theoretical Background** reviews previous research related to the subject of the current investigations in more detail. This chapter is divided into five sections with each section being divided into sub-sections. The subjects discussed within this chapter include: general description of composite materials, constituent materials of FRP composites, fibre-matrix interface characteristics, general description of available fabrication techniques, and discussion of mechanical behaviour of FRP composites.

Chapter 3. **Mechanics of Materials** contains a discussion on the loading-response relationships of the materials and includes classical beam theory, the rule of mixtures, laminated beam theory, and failure theories.

Chapter 4. **Experimental Procedure** describes the method adopted in order to solve the problems stated and presented in Chapter 1. This includes equipment design and manufacture, composite plate fabrication

procedures, fibre volume content and void content determination methods, mechanical testing procedures adopted, and optical micrography analysis for the investigation of fracture regions.

Chapter 5. **Fabrication Parameters Optimisation** was divided into four sections, namely, determination of fabrication parameters, experimental procedure, results and discussion, and conclusions.

Chapter 6. **Results and Discussion** presents the description, analyses and discussion of the data obtained from the experimental work. It contains four sections, namely, preliminary test (compressive test) of the parent composite materials, hybrid FRP composites containing two different types of glass fibres, hybrid FRP composites containing two different grades of carbon fibres, and hybrid FRP composites containing combination of glass and carbon fibres.

Chapter 7. **Conclusion and Recommendations for Future Work** summarises the outcomes of the investigation and presents recommendations that may be carried out in order to enhance the current findings.

## REFERENCES

- [1] S. K. Mazumdar, *Composites Manufacturing: Materials, Product, and Process Engineering*. Boca Raton: CRC Press, 2002.
- [2] B. E. Spencer, "69. Composites in the sporting goods industry," in *Handbook of Composites*, Second ed, S. T. Peters, Ed. London: Chapman and Hall, 1998, pp. 1044-1052.
- [3] E. J. Barbero, "46. Construction," in *Handbook of Composites*, Second ed, S. T. Peters, Ed. London: Chapman and Hall, 1998, pp. 982-1003.
- [4] S. N. Loud, "63. Commercial and industrial application of composites," in *Handbook of Composites*, Second ed, S. T. Peters, Ed. London: Chapman and Hall, 1998, pp. 931-956.
- [5] D. L. Denton, "61. Land transportation application," in *Handbook of Composites*, Second ed, S. T. Peters, Ed. London: Chapman and Hall, 1998, pp. 905-915.

- [6] R. N. Hadcock, "Aircraft applications," in *Handbook of Composites*, Second ed, S. T. Peters, Ed. London: Chapman and Hall, 1998, pp. 1044-1052.
- [7] W. C. Tucker and T. Juska, "62. Marine application," in *Handbook of Composites*, Second ed, S. T. Peters, Ed. London: Chapman and Hall, 1998, pp. 916-930.
- [8] G. C. Krumweide and E. A. derby, "67. Aerospace equipment and instrument structure," in *Handbook of Composites*, Second ed, S. T. Peters, Ed. London: Chapman and Hall, 1998, pp. 1004-1043.
- [9] C. Zweben, "Tensile strength of hybrid composites," *Journal of Materials Science (Historical Archive)*, vol. 12, pp. 1325-1337, 1977.
- [10] A. R. Bunsell and B. Harris, "Hybrid carbon and glass fibre composites," *Composites*, vol. 5, pp. 157-164, 1974.
- [11] B. Harris and A. R. Bunsell, "Impact properties of glass fibre/carbon fibre hybrid composites," *Composites*, vol. 6, pp. 197-201, 1975.
- [12] J. L. Perry and D. F. Adams, "Charpy impact experiments on graphite/epoxy hybrid composites," *Composites*, vol. 6, pp. 166-172, 1975.
- [13] G. Belingardi and M. P. Cavatorta, "Bending fatigue stiffness and strength degradation in carbon-glass/epoxy hybrid laminates: Cross-ply vs. angle-ply specimens," *International Journal of Fatigue*, vol. 28, pp. 815-825, 2006.
- [14] G. Belingardi, M. P. Cavatorta, and C. Frasca, "Bending fatigue behavior of glass-carbon/epoxy hybrid composites," *Composites Science and Technology, Experimental Techniques and Design in Composite Materials*, vol. 66, pp. 222-232, 2006.
- [15] S.-Y. Fu, Y.-W. Mai, B. Lauke, and C.-Y. Yue, "Synergistic effect on the fracture toughness of hybrid short glass fibre and short carbon fibre reinforced polypropylene composites," *Materials Science and Engineering: A*, vol. 323, pp. 326-335, 2002.
- [16] S. C. Khatri and M. J. Koczak, "Thick-section AS4-graphite/E-glass/PPS hybrid composites: Part II. Flexural response," *Composites Science and Technology*, vol. 56, pp. 473-482, 1996.
- [17] S. C. Khatri and M. J. Koczak, "Thick-section AS4-graphite/E-glass/PPS hybrid composites: Part I. Tensile behavior," *Composites Science and Technology*, vol. 56, pp. 181-192, 1996.
- [18] R. Park and J. Jang, "Impact behavior of aramid fiber/glass fiber hybrid composite: Evaluation of four-layer hybrid composites," *Journal of Materials Science*, vol. 36, pp. 2359-2367, 2001.
- [19] I. R. McColl and J. G. Morley, "Crack growth in hybrid fibrous composites," *Journal of Materials Science*, vol. 12, pp. 1165-1175, 1977.
- [20] M. M. Thwe and K. Liao, "Effects of environmental aging on the mechanical properties of bamboo-glass fiber reinforced polymer matrix

- hybrid composites," *Composites Part A: Applied Science and Manufacturing*, vol. 33, pp. 43-52, 2002.
- [21] M. M. Thwe and K. Liao, "Durability of bamboo-glass fiber reinforced polymer matrix hybrid composites," *Composites Science and Technology*, vol. 63, pp. 375-387, 2003.
  - [22] S. Fischer and G. Marom, "The flexural behaviour of aramid fibre hybrid composite materials," *Composites Science and Technology*, vol. 28, pp. 291-314, 1987.
  - [23] I. J. Davies and H. Hamada, "Flexural properties of a hybrid composite containing carbon and silicon carbide fibres," *Advanced Composite Materials*, vol. 10, pp. 77-96, 2001.
  - [24] Sudarisman, I. J. Davies, and H. Hamada, "Compressive failure of unidirectional hybrid fibre-reinforced epoxy composites containing carbon and silicon carbide fibres," *Composites Part A: Applied Science and Manufacturing*, vol. 38, pp. 1070-1074, 2007.
  - [25] Y. Li, X. J. Xian, C. L. Choy, M. Guo, and Z. Zhang, "Compressive and flexural behavior of ultra-high-modulus polyethylene fiber and carbon fiber hybrid composites," *Composites Science and Technology*, vol. 59, pp. 13-18, 1999.
  - [26] S.-Y. Fu, B. Lauke, E. Mäder, C.-Y. Yue, X. Hu, and Y.-W. Mai, "Hybrid effects on tensile properties of hybrid short-glass-fiber-and short-carbon-fiber-reinforced polypropylene composites," *Journal of Materials Science*, vol. 36, pp. 1243-1251, 2001.
  - [27] A. a. Kafi, M. Z. Abedin, M. D. H. Beg, K. L. Pickering, and M. A. Khan, "Study on the mechanical properties of jute/glass fiber-reinforced unsaturated polyester hybrid composites: effect of surface modification by ultraviolet radiation," *Journal of Reinforced Plastics and Composites*, vol. 25, pp. 575-588, 2006.
  - [28] K. John and S. V. Naidu, "Sisal fiber/glass fiber hybrid composites: The impact and compressive properties," *Journal of Reinforced Plastics and Composites*, vol. 23, pp. 1253-1258, 2004.
  - [29] R. Park and J. Jang, "Effect of stacking sequence on the compressive performance of impacted aramid fiber/glass fiber hybrid composite," *Polymer Composites*, vol. 21, pp. 231-237, 2000.
  - [30] J. Gustin, A. Joneson, M. Mahinfalah, and J. Stone, "Low velocity impact of combination Kevlar/carbon fiber sandwich composites," *Composite Structures*, vol. 69, pp. 396-406, 2005.
  - [31] K. John and S. V. Naidu, "Effect of Fiber Content and Fiber Treatment on Flexural Properties of Sisal Fiber/Glass Fiber Hybrid Composites," *Journal of Reinforced Plastics and Composites*, vol. 23, pp. 1601-1605, 2004.

- [32] Y. A. Khalid, S. A. Mutasher, B. B. Sahari, and A. M. S. Hamouda, "Bending fatigue behavior of hybrid aluminum/composite drive shafts," *Materials & Design*, vol. 28, pp. 329-334, 2007.
- [33] T. Hayashi, "On the improvement of mechanical properties of composites by hybrid composition," in *Proceedings of the 8th International Reinforced Plastics Conference, Paper No. 22*, Brighton, U.K., 10-12 October 1972, pp. 149-152.
- [34] Y. J. You, Y. H. Park, H. Y. Kim, and J. S. Park, "Hybrid effect in tensile properties rods with various material compositions," *Composite Structures*, vol. 80, pp. 117-122, 2007.
- [35] R. A. Chaudhuri and H. J. Garala, "Analytical/experimental evaluation of hybrid commingled carbon/glass/epoxy thick-section composites under compression," *Journal of Composite Materials*, vol. 29, pp. 1695-1718, 1995.
- [36] I. J. Davies, H. Hamada, and M. Shibuya, "Compressive and flexural strength of polymer composites containing a mixture of carbon and silicon carbide fibres: Part 1 - Flexural properties," in *T. Tanimoto and T. Morii (editors): Proceedings of the 6th Japan International SAMPE Symposium*, Tokyo, Japan, October 26-29, 1999, pp. 571-574, Japan Chapter of SAMPE, Tokyo, Japan.
- [37] A. Arbelaiz, B. Fernandez, G. Cantero, R. Llano-Ponte, A. Valea, and I. Mondragon, "Mechanical properties of flax fibre/polypropylene composites. Influence of fibre/matrix modification and glass fibre hybridization," *Composites Part A: Applied Science and Manufacturing*, vol. 36(12), pp. 1637-1644, 2005.
- [38] R. F. Dickson, G. Fernando, T. Adam, H. Reiter, and B. Harris, "Fatigue behaviour of hybrid composites," *Journal of Materials Science (Historical Archive)*, vol. 24, pp. 227-233, 1989.
- [39] M. Wang, Z. Zhang, and Z. Sun, "The Hybrid Model and Mechanical Properties of Hybrid Composites Reinforced with Different Diameter Fibers," *Journal of Reinforced Plastics and Composites*, vol. 28, pp. 257-264, 2009.
- [40] A. B. A. Hariharan and H. P. S. A. Khalil, "Lignocellulose-based hybrid bilayer laminate composite: Part I - Studies on tensile and impact behavior of oil palm fiber-reinforced epoxy resin," *Journal of Composite Materials*, vol. 39, pp. 663-684, 2005.
- [41] T. J. Kang, S. J. Shin, K. Jung, and J. K. Park, "Mechanical, thermal and ablative properties of interply continuous/spun hybrid carbon composites," *Carbon*, vol. 44, pp. 833-839, 2006.
- [42] P.-O. Hagstrand, F. Bonjour, and J.-A. E. Manson, "The influence of void content on the structural flexural performance of unidirectional glass fibre reinforced polypropylene composites," *Composites Part A: Applied Science and Manufacturing*, vol. 36, pp. 705-714, 2005.

- [43] D. Liu and Sudarisman, "Photoelastic study of fully-stressed composite beams," in *Proceedings of the 1995 Spring Conference, Society for Experimental Mechanics*, Grand Rapids, MI, U.S.A., June 12-14, 1995, pp. 861-866.
- [44] M. Ramulu, P. B. Stickler, N. S. McDevitt, I. P. Datar, D. Kim, and M. G. Jenkins, "Influence of processing methods on the tensile and flexure properties of high temperature composites," *Composites Science and Technology*, vol. 64, pp. 1763-1772, 2004.
- [45] Sudarisman and I. J. Davies, "Flexural failure of unidirectional hybrid fibre-reinforced polymer FRP) composites containing different grades of glass fibre," *Advanced Materials Research*, vol. 41-42, pp. 357-362, 2008.
- [46] Sudarisman, B. de San Miguel, and I. J. Davies, "Failure mechanism of unidirectional hybrid FRP composites containing carbon and E-glass fibres subjected to three-point bend loading," in *Proceedings of the International Conference on Materials and Metallurgical Engineering 2009*, 24-25 June, Surabaya, Indonesia, 2009, pp. FA 5-8.
- [47] Z. Zheng and J. J. Engblom, "Computational and experimental characterization of continuously fiber reinforced plastic extrusions: Part I - Short-term flexural loading," *Journal of Reinforced Plastics and Composites*, vol. 23, pp. 777-793, 2004.
- [48] Z. Zheng and J. J. Engblom, "Computational and experimental characterization of continuously fiber reinforced plastic extrusions: Part II - Long-term flexural loading," *Journal of Reinforced Plastics and Composites*, vol. 23, pp. 799-810, 2004.
- [49] Y. Li, X. J. Xian, C. L. Choy, M. Guo, and Z. Zhang, "Compressive and flexural behavior of ultra-high-modulus polyethylene fiber and carbon fiber hybrid composites," *Composites Science and Technology*, vol. 59, pp. 13-18, 1999.

Every reasonable effort has been made to acknowledge the owners of copyright materials. I would be pleased to hear from any copyright owner who has been omitted or incorrectly acknowledged.



## **CHAPTER 2**

# **LITERATURE REVIEW AND THEORETICAL BACKGROUND**

### **2.1. INTRODUCTION**

In the broadest point of view, there exists a vast diversity of engineering materials which can be in solid, liquid or gaseous states, but structural materials are almost entirely found in the solid state. Based on their similarities in processing conditions, microstructures, properties, and applications, structural materials can be classified into four main groups, *i.e.*, metals and their alloys, ceramics and glasses, polymers and elastomers, and composites, with details of this classification being presented in Figure 2.1.

The history of human progress shows that the development of civilisation has been closely related to the advancement of materials being used in a particular era, with the development of materials mainly being triggered by the need for superior quality materials for weapons [1] (p. 3). The development of structural materials through human history can be traced back from pre-history and is summarised from a number of references ([1] (pp. 3-6), [2, 3]) below. During the Stone Age, prior to 10000 B.C., most structures were made from stone which is a ceramic. Following this, during the Bronze Age, 4000 B.C. – 1000 B.C., copper and bronze were discovered with the rapid expansion of weapons and tools from these metals. Pins, daggers, blades, fragments, and ornaments made from copper (Cu) containing 0.5% – 3.0% of tin (Sn) and up to 1.5% of arsenic (As), dated to 1800 B.C. – 3900 B.C., have been found in Egypt, India, Iran, Iraq, and Turkey [3]. In addition, some ornaments, swords, daggers, spear-heads, and battle-axes

dating to ~1300 B.C. have been found in Egypt with the main manufacturing method being determined to be forging except for sphere-heads that were fabricated by metal casting [2]. The next era was the Iron Age (1000 B.C. – A.D. 1620) in which the previous generation of materials used to produce tools and weapons were replaced by iron. The manufacture of weapons and tools from iron by the Anatolians and Iranians manufacturing has been traced back to 1500 B.C. – 1000 B.C. It is believed that iron reached Asia, North Africa and Europe in 500 B.C. – 1000 B.C., Greece in ~900 B.C., and Sudan in ~200 B.C. [3]. Following the invention of metal production technologies, such as iron casting in 1620, and the manufacture of different grades of steel which began in 1850, together with light weight alloys during the 1940s, metals have played a primary role as the main structural material and also the main engineering material in the broader sense.

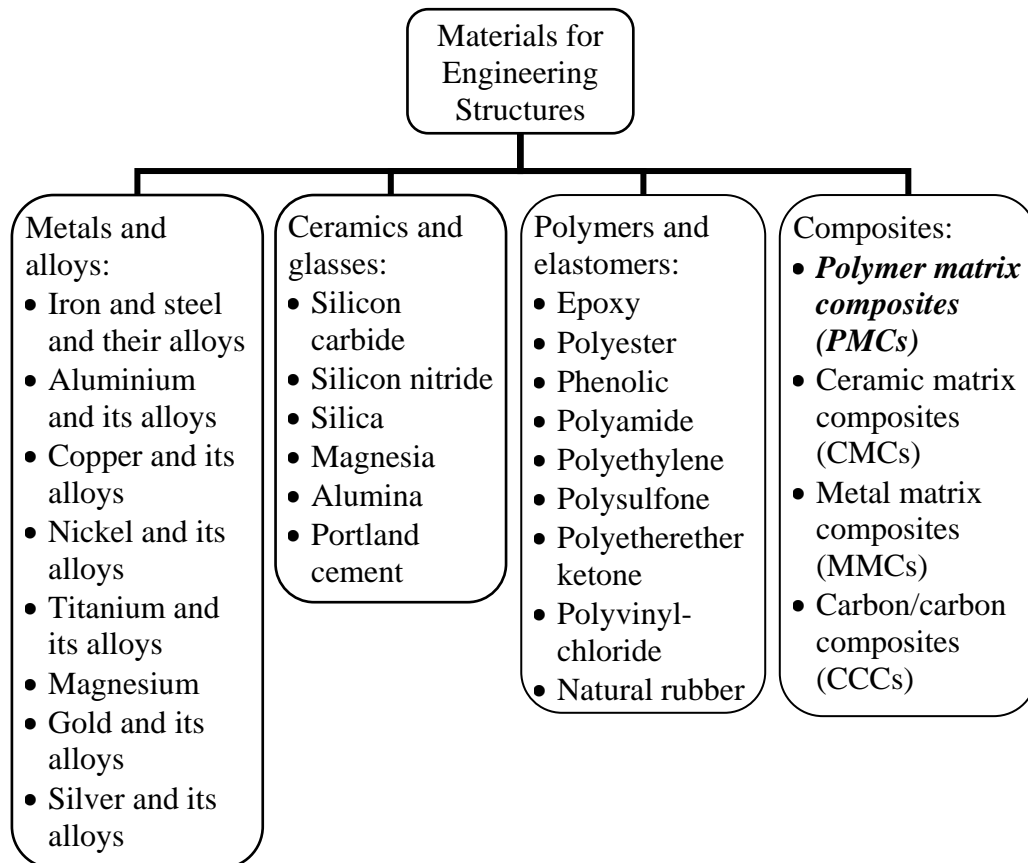


**Figure 2.1.** Classification of materials for engineering structures (Summarised from references [4], [1] (pp. 21-22), [5] (p. 5), and [6] (pp. 1-4)).

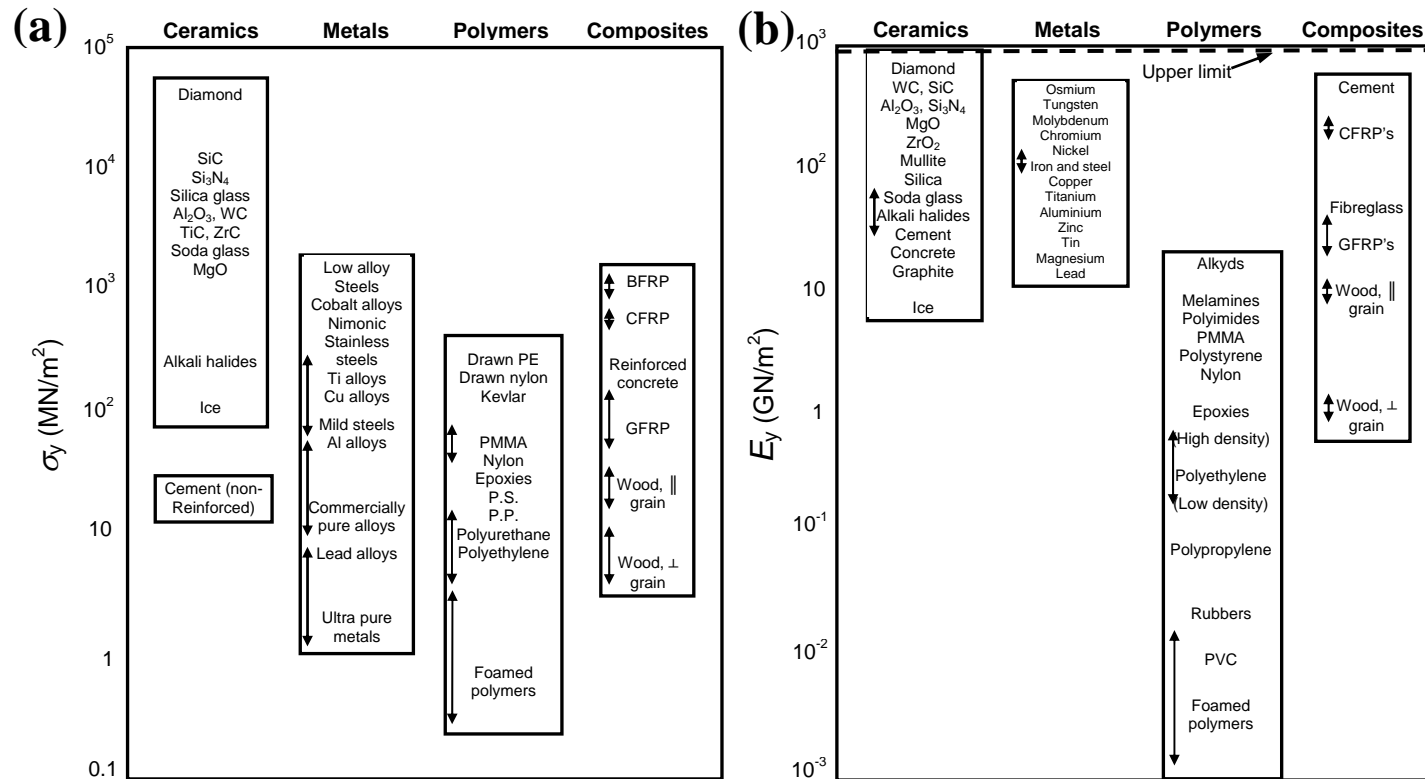


**Figure 2.2.** Strengths and moduli of typical structural materials showing that, in general, those of metallic materials are superior, redrawn from Ref. [5]. (a) Yield strength (p. 85), (b) Young's modulus (p. 35)

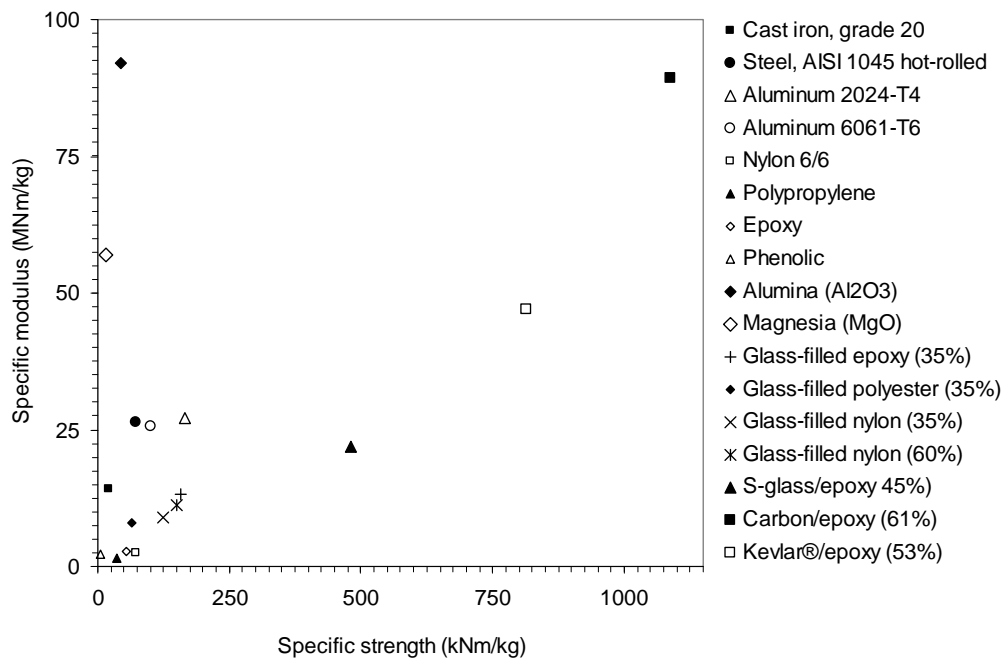


**Figure 2.3.** Specific strength and specific modulus of typical structural materials showing that, in terms of specific strength and specific modulus, a typical carbon fibre-reinforced epoxy (CFRP) composite (appears close to top-right corner) is the most superior materials compared to the other. Alumina (Al<sub>2</sub>O<sub>3</sub>, appears close to top-left corner) ceramic although it possesses high specific modulus its specific strength is very low, while materials appear close to bottom-left corner (phenolic, polypropylene, epoxy, and nylon), which are, except magnesia, polymer, possess low specific both strength and modulus (Plotted from numerical values cited from Ref. [6] (p. 2))

The utilisation of metallic materials continued to increase and reached a peak during the early 1960s [1] (p. 4) due to its relatively high strength and modulus, as presented in Figure 2.2, whereas the utilisation of other materials, such as polymers and elastomers, ceramics and glasses, and composites generally declined due to their relatively poor performance using the rudimentary manufacturing techniques available at that time. Composite materials have been used for aircraft structures since the first generation of powered aircraft in the early twentieth century [7] with airframes and stressed-skins being comprised of wood, which is a natural composite material, in addition to woven fabric stretched over wing-frames and then embedded in resin. The fuselage of the Monocaque Deperdussin monoplane produced in 1912 [8] (pp. 163-164) and Lockheed Vega radial engine passenger aircraft build in 1927 even used wood for their fuselage

and wings [8] (p. 184). During World War II, several European countries and Japan experienced a shortage of metal and were driven to use wood in different forms in order to produce aircraft. For example, laminated composite materials were used in the De Havilland Mosquito bomber aircraft of the British Royal Air Force, with wood being used for the frame and laminated plywood for the stressed-skin [7, 9]. Russian bomber aircraft also extensively utilised plywood, bakelite ply, balinit and delta wood for wing spars of the I1-4, as well as for the outer skin and fuselage of the I1-2 [10]. In Japan, wood was also used for the substitution of metal components for aircraft structures [11]. However, it was in the beginning of the 1960s that the development of modern composites started to increase significantly [12] (p. 3) as a result of the requirement for materials simultaneously possessing high specific strength and high specific stiffness (see Figure 2.3 ) in various structural applications embracing civil, military, aerospace and space, marine, and automotive engineering.

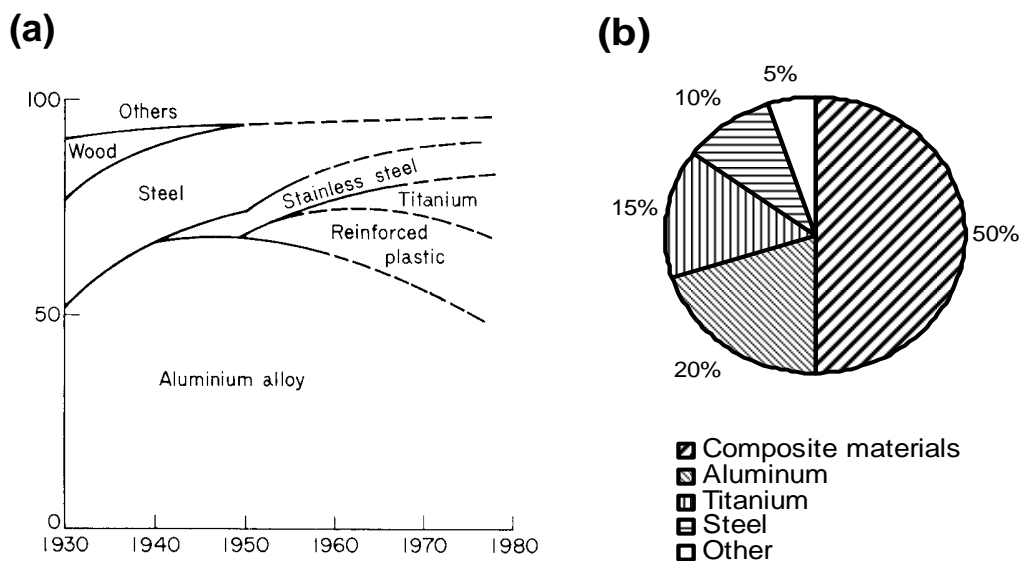


**Figure 2.4.** The utilisation of composite materials in aircraft structures from the 1930s – current. (a) Weight proportion of materials used in aircrafts manufactured from 1930 – 1980 [7], (b) Proportion of materials in modern aircraft, the Boeing 787 – Dreamliner [13].

A brief survey of materials meeting these requirements has been shown in Figure 2.3 - whilst ceramics are shown to possess the optimum combination of

specific strength and specific stiffness, their relatively poor fracture toughness behaviour rules them out for many applications. Figure 2.4(a) shows the proportion of various materials utilised in aircraft structures from 1930 to 1980, indicating that the replacement of wood with reinforced plastic materials occurred between the late 1940s and early 1950s, while those of a modern aircraft (Boeing 787 Dreamliner) have been presented in Figure 2.4(b), illustrating that composite materials are the primary structural materials for this aircraft.

The importance of composite materials in engineering structures throughout the ages can be seen in Figure 2.5. The first man-made composite was produced from bricks reinforced with wheat straw as long ago as 1,300 B.C. [14] (p. 3). Data for stone and bronze ages were obtained from archaeologists, those for 1960s were based on allocated teaching hours in the U.K. and U.S. universities, and those for 2020s were predicted utilisation in automotive industries. It can be seen from Figure 2.5 that the relative importance of composites in 2020 is expected to be similar to that of ceramics or polymers and greater than that of metals.

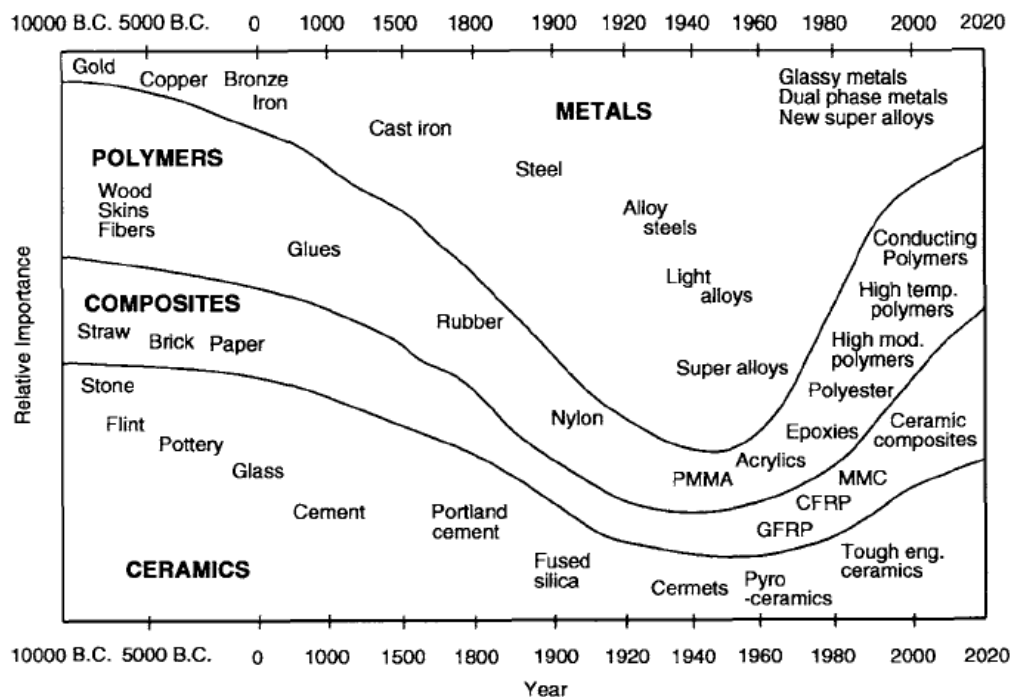


**Figure 2.5.** Engineering materials evolution through the ages showing, in the second layer from the bottom of the figure, the relative importance of composite materials [1] (p. 4)

### ***2.1.1. Definition***

A composite material can be defined as a material that comprises of two or more constituents, namely the reinforcement and matrix, which possess distinct characteristics ([15] (p. 1) and [16] (p. 6)), macroscopically combined with a recognisable interface [17], and identifiable [18]. Simple examples of composites include bamboo as a natural composite, glass fibre-reinforced polypropylene and carbon fibre-reinforced epoxy as fibrous composites, silicon carbide (SiC) or titanium carbide (TiC) particles dispersed in an aluminium matrix to produce silicon carbide particle-reinforced aluminium matrix or titanium particle-reinforced aluminium matrix composites, as well as reinforced concrete. The first feature, namely distinct characteristics, can be obtained by tailoring fibre arrangement and controlling fibre content to meet the intended in-service properties and behaviour requirements, so that a typical composite component is typically designed for that application alone and often may need to be redesigned for even relatively small changes in the application – a relatively small shift in the loading direction for unidirectional fibre-reinforced composites will generate shear stresses due to coupling effects and may significantly decrease the composite strength. The second and the third features, namely recognisable interface and identifiable, imply that the mixture of the constituents is of a physical nature where each constituent can still be identified and that there exists a distinct interface separating the two constituents as shown in Figure 2.6, such that they can be separated by means of physical methods.



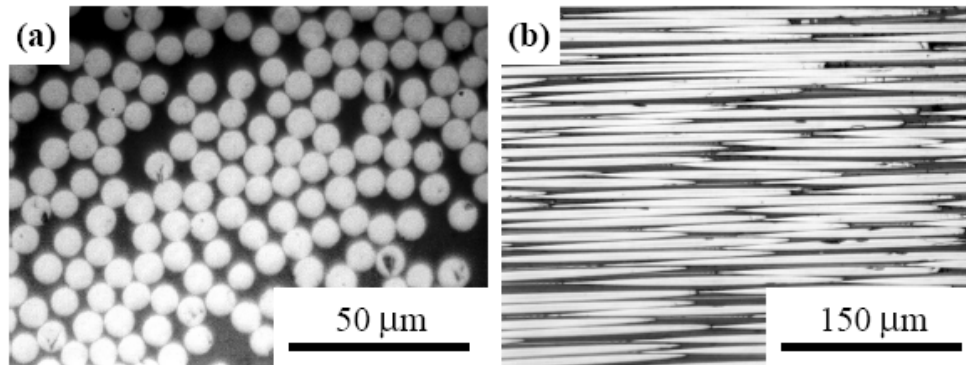


**Figure 2.6.** Carbon fibre-reinforced epoxy composite showing distinct phases between fibres (bright colour) and matrix (dark colour). (a) Transverse to fibre direction, (b) Parallel with fibre direction.

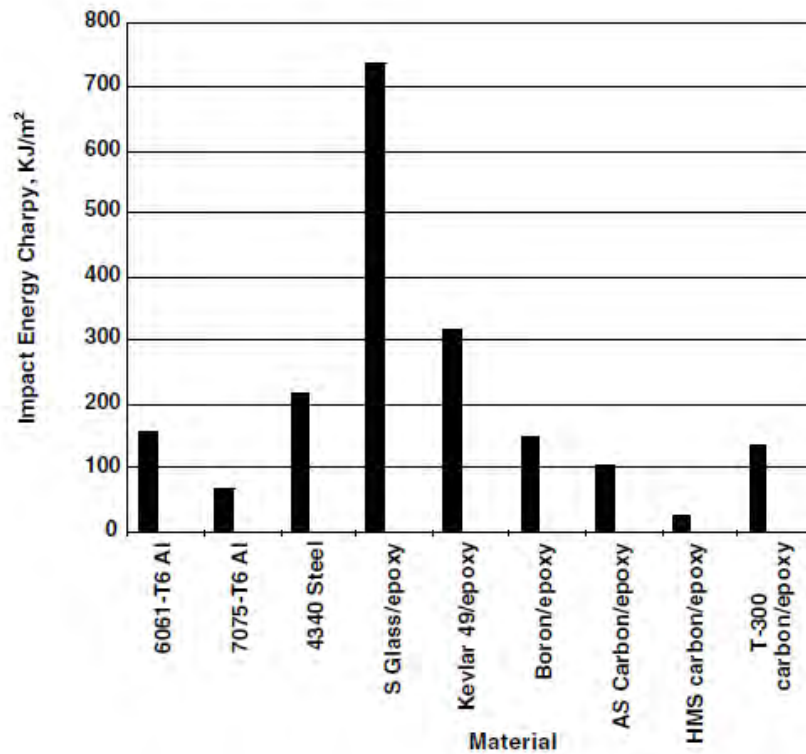


**Figure 2.7.** Impact properties of various engineering materials. Unidirectional fibre-reinforced polymer composite materials with approximately 60% fibre volume fraction (Data adapted from Mallick as cited in Ref. [6] (p. 8))

Composite materials have been utilised in various applications due to their superiority in many regards, *e.g.*, excellent mechanical properties, such as high yield strength and Young modulus (as presented in Figure 2.2.), light weight and

high corrosion resistance [19, 20] as well as impact resistance (as shown Figure 2.7.), lower tooling cost for manufacturing complex shapes [21], and outstanding fatigue strength. For example, the fatigue strength of steel and aluminium alloys is approximately 50% of their ultimate static strength whereas that of CFRP composites is up to almost 90% of their ultimate static strength [6] (p. 7) – the fatigue strength of other selected structural materials has been presented in Table 2.1. Composite materials have been utilised in applications ranging from automotive ([19, 22] and [6] (pp. 17-18)) such as in the Porsche Carrera GT all-carbon chassis [23], aircraft industries [19, 24] such as aircraft engine components in the General Electric F-404 [25] and wing elements of the Sukhoi S-27 Berkut aircraft [26], aerospace engineering [6] (pp. 14-17) such as the SuDerbird SCS Kevlar dual-shell reflector [27], marine structures [28, 29] such as boat hulls [30, 31], bulkheads, deck plates and mast systems [32], high speed ships and ferries [29], civil engineering applications such as the deck of the Wick Wire Run bridge in Taylor County, West Virginia [33], GFRP structural profile blocks [12] (p. 98), and longitudinal beams for Tom's Creek Bridge in Blacksburg, Virginia [34], electrical and electronic appliances such as switch housings, circuit boards, insulation components, and computers, telescoping composite tubes for antenna and screen monitor casings [35], as well as sporting goods [6] (pp. 18) such as graphite/epoxy and carbon/epoxy tennis and badminton racquets [36] and CFRP Fight Weapon bicycle frames from Asia Seiko [37].

**Table 2.1.** Properties of typical structural materials

Materials	Density (g/cm <sup>3</sup> )	Impact resistance (J/m) <sup>a)</sup>	Fatigue limit (MPa) <sup>b)</sup>
Metals and alloys: Al 7075 T6 Al 6005 T6 FeC, 021%C, annealed Ti alloy, 99.2% Ti Ti-6Al-4V standard Ti-6Al-4V condensate	2.81 <sup>1)</sup>  7.86 <sup>2)</sup> 4.51 <sup>3)</sup>	   43 <sup>8)</sup>	96 <sup>12)</sup> 31 <sup>13)</sup> 220 <sup>14)</sup>  400 <sup>15)</sup> 524 <sup>15)</sup>
Ceramics and glasses: Al <sub>2</sub> O <sub>3</sub> , 99.5% dense Si <sub>3</sub> N <sub>4</sub>	3.89 <sup>4)</sup>		530 <sup>16)</sup>
Polymer and elastomers: Epoxy resin Polysulfone Polyacetal PMMA	1.12 – 1.30 <sup>5)</sup>	10 – 50 <sup>5)</sup>  24 <sup>9)</sup>	18 <sup>17)</sup> 22 <sup>18)</sup>
Composites: CFRP GFRP	1.26 <sup>6)</sup> 1.99 <sup>7)</sup>	31 <sup>10)</sup> 107 <sup>11)</sup>	70 <sup>19)</sup> 46 <sup>20)</sup>

<sup>a)</sup>Izod impact unless stated other method.

<sup>b)</sup>At  $N = 10^6$  unless stated other value.

<sup>1)</sup>Reference [38], p.47.

<sup>2)</sup>Reference [39], Table 25.

<sup>3)</sup>Reference [39], Table 35.

<sup>4)</sup>Reference [40], p. 80.

<sup>5)</sup>Reference [41], pp. 90-96.

<sup>6)</sup>Reference [42], carbon fibre/polyamide,  
 $V_f = 50\%$ ,

<sup>7)</sup>Reference [43], E-glass/epoxy  
composites,  $V_f = 60\%$ .

<sup>8)</sup>Reference [39], Table 212, Charpy  
impact, notched specimen.

<sup>9)</sup>Reference [40], p. 158.

<sup>10)</sup>Reference [44, 45], pp. 396-406.

<sup>11)</sup>Reference [39], Table 215.1, glass fibre/  
polycarbonate,  $V_f = 30\%$ .

<sup>12)</sup>Reference [38].

<sup>13)</sup>Reference [45],  $f = 5$  Hz.

<sup>14)</sup>Reference [46],  $N = 10^7$ ,  $f = 22$  Hz

<sup>15)</sup>Reference [47].

<sup>16)</sup>Reference [48],  $R = -1$ .

<sup>17)</sup>Reference [48], p. 365.

<sup>18)</sup>Reference [48], p. 364,  $f = 1.67$  Hz.

<sup>19)</sup>Reference [48], p. 365, short carbon fibre/  
polysulfone,  $V_f = 40\%$ .

<sup>20)</sup>Reference [48], p. 365, short glass fibre/  
polysulfone,  $V_f = 40\%$ .

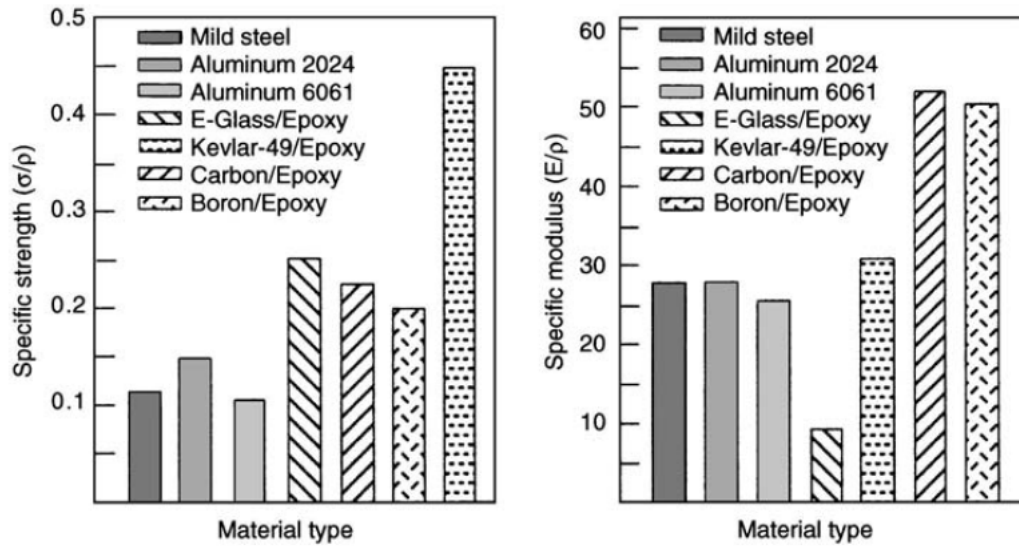


**Figure 2.8.** Specific strengths and specific modulus of typical structural materials showing that, in general, those of composite materials are superior in comparison with those of conventional metals [49] (p. 11).

The superior mechanical properties of composites, such as their excellent fatigue resistance [50], tensile strength (for a typical S-glass fibre-reinforced epoxy composite is 1136.2 MPa at 61.2% volume fraction fibre [51] compared to 525 MPa for that of Al 7075 aluminium alloy [39] (Table 139)), combined with their light weight (the density of the above GFRP is 2.06 g/cm<sup>3</sup> [51] compared to 2.80 g/cm<sup>3</sup> for that of the Al 7075 aluminium [39] (Table 139)), results in excellent specific strength and specific stiffness [20, 29, 32, 50] as presented in Figure 2.8, leading to improved application performance, whether it be lower weight as in the case of the replacement of a graphite/epoxy composite structure for the existing aluminium structure in the Boeing 777 which resulted in a weight saving of 20% or more [52], increased stiffness and load-carrying capacity [53]. In addition, the structure of composite materials can be designed to meet the specific properties of in-service loading and environmental conditions [30, 32]. For mobile structures, the use of composite materials has tended to increase load-carrying capacity and/or reduce fuel consumption, resulting in a less polluting product and safer environment, as well as prolonging the availability of natural resources. For example, the use of CFRP composite materials in the Boeing 787 fuselage [54] and other main structures is predicted to reduce labour cost and the

number of stress raiser points due to a reduction in the number of parts, improve aerodynamic performance, and furthermore, reduce fuel consumption [13], whereas the use of glass-reinforced aluminium laminate (GLARE) composites in the Airbus A380 is envisaged to increase the strength and fatigue resistance of the structure [55] compared to those of conventional titanium alloy structures.

Another key advantage of composite materials is their excellent corrosion resistance [32, 56]. It has been estimated that approximately US\$ 276 billion or 3.1% of the Gross Domestic Product (GDP) of the United States of America (U.S.A.) is lost due to corrosion and associated failures [57]. Composite materials have been used in many applications due to their improved corrosion resistance, such as one layer of unidirectional GFRP composite placed surrounding the CFRP composite core of the Aluminium Conductive Composite Core (ACCC) high voltage mains grid cables produced by CTC (Irvine, CA, U.S.A.) to separate the CFRP core from aluminium wires in order to prevent galvanic corrosion, and the use of GFRP composite for piping, walkways, stairways, hand-rails, ladders, support structures and decks of offshore oil platforms to replace those of metals that are more corrosive [56].

### ***2.1.2. Classification of Composite Materials***

Composite materials can be classified into different groups based on several criteria and this will be considered in the present section.

#### **2.1.2.1. Relative dimensions of reinforcement**

Based on the relative dimensions of the reinforcing materials, composite materials can be categorised as follows:

*Macro-composites* – such as reinforced concrete beams where concrete possessing high compressive strength but poor tensile strength is reinforced with steel [58, 59] or composite [58-60] bars in its tension sides [58] in order to improve its performance.

*Micro-composites* or simply known as *composites* – such as various types of fibrous composites, for examples CFRPs, GFRPs, and silicon carbide fibre-reinforced titanium alloy matrix [59]; and particulate composites of different reinforcement and different matrices [59-64], where their reinforcement are in the order of microns in dimension. The introduction of reinforcement into a particular matrix can improve the properties of the resulting composite in comparison with that of the matrix, the reinforcement or both.

*Nano-composites* – such as nano-sized silicon carbide (SiC) particles dispersed in epoxy [60], fine yttria ( $Y_2O_3$ ) particles dispersed in magnesium [61], and carbon nano-tubes dispersed in epoxy [62], where the nano-sized fibres or very fine particles of clay or other materials are dispersed in polymeric or other parent materials in order to improve particular properties of the parent materials. For example, in order to improve the tensile strength and modulus, flexural strength and modulus, and thermal stability of satin weave preformed CFRP nano-composite, Chisholm *et al* [60] dispersed micro- and nano-sized SiC particles in epoxy before being used as matrix to produce the CFRP nano-composite. Tun and Gupta [61] blended  $Y_2O_3$  particles with magnesium (Mg) powder, compacted it, then sintered the mixture to produce nano-composite possessing improved hardness and tensile strength in comparison with the pure Mg parent material. Kim and Lee [62] used carbon nano-tubes (CNT) to reinforce epoxy that, further, was used as a matrix in E-glass fabric/epoxy nano-composite with improved electromagnetic wave absorption capability for the complete GFRP/CFRP/PVC foam/CFRP sandwich structure.

#### 2.1.2.2. Geometry of reinforcement

Based on the geometry of the reinforcing material, composite materials can be classified into three main groups as discussed in page 2 of reference [63], *i.e.*:

*Particulate composites*, Figure 2.9(a) – composite materials where the reinforcing materials are in the form of particles, for example dispersing tungsten particles in copper (used as high-current electrical contact materials [66-68], heat sinks [64,

65], and spot-welding electrodes [64] which results in improved erosion resistance [66] and tensile strength of the Cu matrix [67]. Other commonly utilised particle reinforcements include alumina tri-hydrate ( $\text{AlH}_6\text{O}_3$ ), also known as ATH, for silicon polymer-based rubber reinforcement [68], calcium carbonate ( $\text{CaCO}_3$ ) for high density polyethylene (HDPE) [69], kaolin  $\text{Al}_2\text{Si}_2\text{O}_5(\text{OH})_4$  for polyethylene [70], mica ( $\text{KAl}_2(\text{AlSi}_3\text{O}_{10}(\text{OH})_2)$ ) for nickel-coating material [71] and silicas  $\text{SiO}_2$  for polyacrylate, polyimide and polypropylene [72], and epoxy [73].

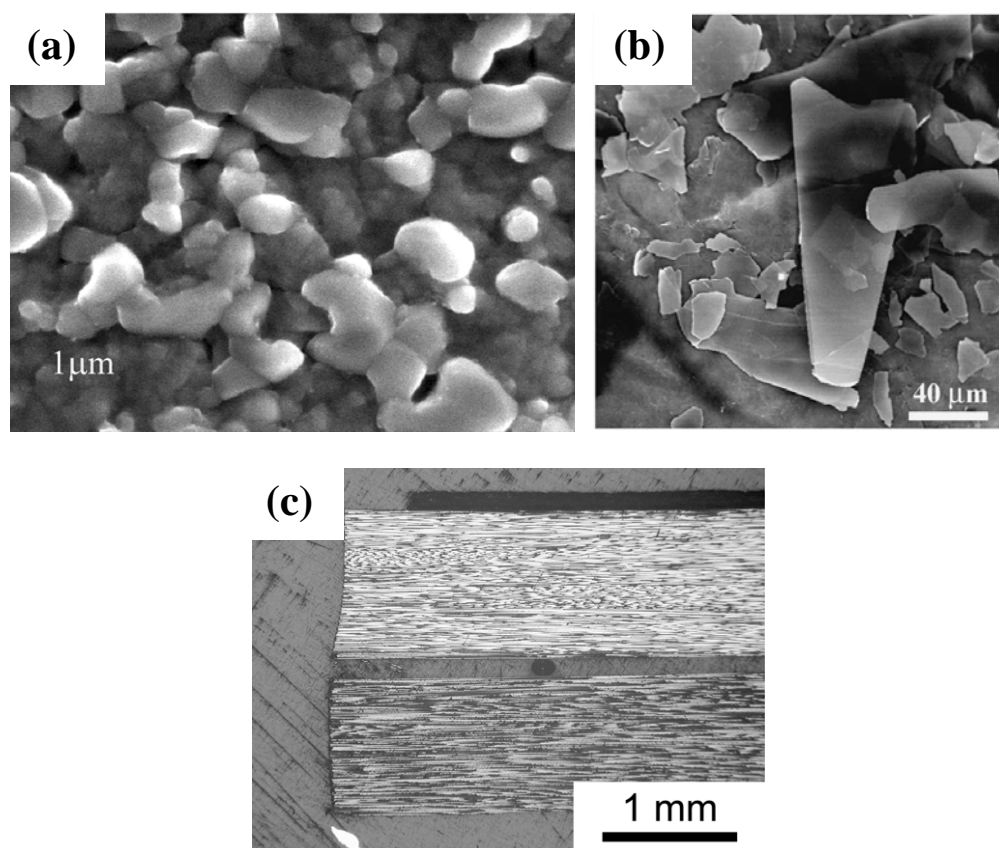


**Figure 2.9.** Three main types of composite system based on the reinforcing material geometry: (a) SEM photo micrographs of a typical nickel-based particle-reinforced lead-based matrix particulate composite with 0.3 mol fraction of  $\text{Ni}_{0.93}\text{Co}_{0.02}\text{Mn}_{0.5}\text{Fe}_{1.95}\text{O}_{4-\delta}$  and 0.7 mol fraction of  $\text{PbZr}_{0.52}\text{Ti}_{0.48}\text{O}_3$  [76], (b) Mica flake-reinforced poly-dimethylsiloxane [74], and (c) Unidirectional continuous carbon-silicon carbide fibres hybrid-reinforced polymer matrix composite containing four layers of carbon fibre prepreg in the lower part and four layers of silicon carbide fibres in the upper parts showing shear failure along its neutral plane after being loaded in bending [75].

*Flake composites*, Figure 2.9(b) – the reinforcements are commonly distributed in their matrices in a randomly oriented manner, such that the properties of these composites tend to be more isotropic rather than anisotropic. Vu-Khanh [76] dispersed mica and glass flakes in order to improve the mechanical properties of poly-propylene whereas Osman and colleagues [74] used mica flakes to improve the strength and elastic modulus of poly(dimethylsiloxane). Wang *et al* [77] embedded graphite flakes in a polyester matrix to produce a material possessing sufficient electrical properties, whilst Okumura and co-workers [78] utilised titanium flakes to reinforce aluminium matrix resulting in an improvement of tensile and flexural strength in the flake direction. Flake-reinforced composites have been widely used, ranging from coatings for decorative and protective purposes, such as the inner lining of chemical containers [79, 80] and outer coating of sub-sea pipe-lines [79, 80]; electromagnetic noise suppression material [81]; to load-bearing structural components, such as turbine blades [80].

*Fibre composites* - these reinforcing materials are in the form of fibres as illustrated in Figure 2.9(c). As the fibre component is generally significantly stronger and stiffer compared to the matrix phase – for example, tensile strength and modulus of a typical E-glass fibre are, respectively, 3.5 GPa and 73 GPa [82] (p. 58), whilst those of a typical Derakane<sup>®</sup> 8084 vinylester matrix are only 0.076 GPa and 2.9 GPa [83] – fibre properties and fibre content will strongly determine the properties of these composites. More detail concerning the properties and behaviour of fibre composites upon loading will be discussed in the next chapter. From the point of view of aspect ratio, *i.e.*, length-to-diameter ratio, fibre composites can be further divided into two sub-groups, namely, chopped fibre- (or short fibre- or whiskers-reinforced) composites and continuous fibre-reinforced composites. Chopped fibres possess aspect ratios between 5 and approximately 1000 [49] (p. 5), whilst those of continuous fibres are typically 1000 and higher [84] (p. 92). The orientation of continuous fibres can be tailored according to the required in-service loading conditions in order to optimise the contribution due to the fibres whereas that of short fibres can also be controlled, albeit to a lesser



degree, into a preferred orientation ([15] (p. 137) and [85] (p. 20)) during composite manufacture [86].

#### 2.1.2.3. Fibre architecture

Fibre orientation can be tailored into a one-dimension (1-D) form to produce unidirectional FRP composites, two-dimensions (2-D) to produce multidirectional laminated FRP composites, as well as three-dimensions (3-D) by weaving, braiding, knitting or stitching. As most of the composite properties are primarily depended upon fibre architecture [87], fibre architecture selection is crucial to meet in-service loading configurations [88]. The one-directional fibre arrangement is selected if the structures are mainly subjected to a unidirectional loading with the magnitude of the loading in the other two directions being considerably smaller [15] (p. 9), such as would be the case for simply supported beams, struts, and frame members. The 2-D fibre architecture is generally considered for more complex loading configurations where a part of a structure experiences two-dimensional loading, such as a bridge deck, whilst 3-D fibre arrangements are utilised when through the thickness loading is present in addition to in-plane loading [84] (p. 105), such as would be the case for impact loading [89] (p. 45).

The 1-D fibre arrangement can be found in the form of rovings or tows (Figures 2.9, 2.11, and 2.12), yarns, unidirectional plain weaves (Figures 2.11) where the transverse yarn is a very light minor fill that alternately crosses under and over each longitudinal heavy main tow or roving, and unidirectional pre-impregnated tapes. In the case of 2-D fibre arrangements, fibre orientation can be tailored after they are embedded within the matrix such as in laminated composites manufactured using prepregs, or before they are impregnated in the matrix by using woven fabrics. The difference between 1-D and 2-D weaves is that in 1-D plain weaves the minor transverse fill is much lighter in size compared to that of the major longitudinal main tow or roving, called the warp. 3-D fibre performs can be produced by various procedures, *i.e.*, weaving, braiding, knitting and stitching as summarised from Tong [89] (pp. 13-45). In 3-D *weaving*, there are a number of layers of warp yarn, contrary to the case of a single layer of warp yarn in 2-D

weaving. *Braiding* is a textile manufacturing technique utilised to produce tapes or 3-D structures with  $\pm\theta^\circ$  fibre orientations such as hose and shaft reinforcement and rocket casings. The main advantages of braided products are their high structural integrity and high torsional rigidity [84] (p. 106). In contrast to this, there are two main knitting techniques used to produce fibre performs, *i.e.*, warp and weft knitting. In warp knitting, a number of yarns are fed into the machine in the longitudinal product direction where each of these yarns produces a line of knit loops in this direction. In weft knitting, only one yarn is fed into the machine in the direction transverse to the longitudinal product direction – in this case the yarn produces a row of knit loops through the width of the product. Finally, fibre *stitching* is a process of inserting needles through the thickness of a stack of fabric layers in order to create stitched threads that can be used to produce 3-D fibre performs.

#### 2.1.2.4. Matrix Type

From the point of view of the matrix constituent, composite materials can be categorised into four groups ([12] (p. 58 and 151), [15] (pp. 36-52) and [85] (p. 20)), namely:

*Ceramic-matrix composites (CMCs)* - despite the superiority of ceramics with respect to their hardness [12] (p. 74), such as partially stabilised zirconia ( $\text{ZrO}_2$ ) which possesses a Vickers hardness value between  $1019 \text{ kg/mm}^2$  and  $1121 \text{ kg/mm}^2$  [39] (Table 203-5/6) (which are equivalent to approximately 77.1 and 79.6 on the 100 kg scale of Rockwell hardness number) in comparison with up to 187 HB for ASME SA395 ductile iron [39] (Table 194) which is equivalent to an approximate Rockwell hardness of 40.6, their low fracture toughness [19] is known to severely limit their utilisation as structural materials. Another common ceramic material, alumina ( $\text{Al}_2\text{O}_3$ ), is known to possess an even higher Vickers hardness of  $2720 \text{ kg/mm}^2$  [39] (Table 203-4/6). In addition, ceramics are generally high temperature resistant [12] (p. 74), for example, FPH Ceramic high temperature heater manufactured by Temcraft, Winston-Salem, North Carolina,

U.S.A., which possesses a service temperature of up to 1204 °C [90], and TemSeal Cement, a silica-based ceramic cement, produced by Sauereisen, Pittsburg, Pennsylvania, U.S.A., which possesses a service temperature of up to 1650 °C [91] in comparison with super alloy metals utilised in jet engines that are resistant to temperature up to approximately 1000 °C [12] (p. 74). A common disadvantage of CMCs is their low strain to failure, for example, ~0.15% for alumina ( $\text{Al}_2\text{O}_3$ ) obtained from a sintering process at 1300 °C [92] in comparison with 11% for that of Al 7075-T651 metal [40] (p. 282) – this results in poor fracture toughness, *i.e.*,  $5 \text{ MPa}\sqrt{\text{m}}$  for pure  $\text{Al}_2\text{O}_3$  ceramic compared to  $21 \text{ MPa}\sqrt{\text{m}}$  for bulk aluminium (Al) [93].

The main reason behind the initial development of CMCs was to improve upon the poor ductility and toughness of unreinforced (*i.e.*, monolithic) ceramics. Silicon carbide (SiC) whisker-reinforced alumina ( $\text{Al}_2\text{O}_3$ ) matrix and silicon-nitride ( $\text{Si}_3\text{N}_4$ ) whisker-reinforced alumina matrix are other examples of CMCs. Tekeli and his colleagues [94] reported that the addition of up to 10 wt% of  $\text{SiO}_2$  into c- $\text{ZrO}_2$  to produce  $\text{SiO}_2$  particulate-reinforced c- $\text{ZrO}_2$  matrix composite improved the flexural strength and fracture toughness of the matrix. Furthermore, they reported that, for pure c- $\text{ZrO}_2$  and its resulting particulate composite containing 10 wt% of  $\text{SiO}_2$ , the flexural strength increased from 275 MPa to 292 MPa, respectively, due to refinement of the matrix grains and the generation of residual stresses in the matrix upon cooling, whereas the fracture toughness increased by more than 160%.

*Carbon-carbon composites (CCCs)* - these are mostly utilised for high temperature in-service environments, for example: thermal protection for re-entry space vehicles, aircraft brakes, and engine turbine components [15] (pp. 51-52). The advantages of CCCs over CMCs are mainly related to their relatively high creep resistance, and improved strength with an increase of temperature up to 2200°C (after which their strength starts to decrease), high thermal shock resistance, and wider range of cyclic temperatures [15] (p. 52).

*Metal-matrix composites (MMCs)* - these are commonly found in the form of fibrous and particle composites. Different types of fibre materials exist, such as stainless steel [95] and tungsten [96] fibres as reinforcement for aluminium and titanium alloy matrices, respectively, ceramics ( $\text{Al}_2\text{O}_3$ , B, and SiC fibres) [97] as well as metal- or ceramic-coated graphite and carbon [98], have been used to reinforce low density metals. The primary objectives of producing MMCs are to improve their specific strength and stiffness [98], in addition to lowering their coefficient of thermal expansion (CTE), such as carbon fibre-reinforced aluminium utilised for boom antennas in NASA space telescope which can be tailored to possess a CTE close to zero without sacrificing weight in comparison to aluminium antennas [12] (p. 125). This reduction in CTE is particularly advantageous for structures experiencing severe in-service temperature fluctuations, such as aeroplane structure in which the temperature at 25,000 feet or ~7620 meter altitude is approximately  $-34.5^\circ\text{C}$  whereas that at sea-level is typically  $15^\circ\text{C}$  [99].

*Polymer-matrix composites (PMCs)* - polymers utilised as the matrix phase for PMCs can be broadly classified into two groups, namely thermosetting and thermoplastic [100]. Unlike elastomers which are highly elastic, polymers may be brittle, especially at room temperature, or else undergo plastic deformation under loading [101] (pp. 24-27) and possess low service temperatures [6] (p. 11), low strength and elastic modulus, and lower density when compared to metals [101] (pp. A3-A15). The reinforcement of polymers with other materials has the potential to significantly improve their potential to meet the design requirements. Glass fibres are the most commonly utilised reinforcement for polymer matrix composites due to their low cost whereas higher cost carbon and aramid fibres are generally reserved for situations where higher performance is required [12] (p. 6).

## 2.2. CONSTITUENT MATERIALS

### 2.2.1. Fibres

The main function of fibres within composite structures is as the load-bearing component and, as such, they are generally significantly stiffer and stronger when compared to the matrix component. For example, the elastic modulus of the polymer matrix in a PMC may be typically 3.0 GPa [102] whereas that of the reinforcing glass fibre may be 86.9 GPa [103]. Various types of fibres are available in the global commercial market, including glass, carbon, graphite, aramid, boron, silicon carbide, polyethylene, and natural fibres derived from plants or animals ([104], [15] (p. 8), [101] (p. 596) and [12] (p. 54)). The relative importance of these fibres in the global composite industry can be seen in Table 2.2.

**Table 2.2.** Global market for advanced composite fibres in 2006<sup>a)</sup>

Fibre type	Amount		Value	
	Tonnes ( $\times 10^3$ )	%	US\$ ( $\times 10^6$ )	%
E-glass fibre	2400	97	244	13.9
Carbon fibre	27	1.1	1300	74.1
Other fibres <sup>b)</sup>	46	1.9	211	12.0

<sup>a)</sup>Rearranged after Ref. [105].

<sup>b)</sup>Includes: aramid, boron, R-, S- and T-glass, as well as HMPE and quartz fibres

Geometrically, fibres can be further classified into two main groups, namely short fibres (also known as chopped or discontinuous fibres) and continuous fibres. As mentioned earlier, fibres can be categorised as continuous if they possess an aspect ratio, *i.e.*, the length to diameter ratio, of 1000 or greater. With regards to this, continuous fibre-reinforced composites (CFRCs) generally possess improved mechanical properties when compared to discontinuous fibre-reinforced composites (DFRCs) [6] (p. 5); for example, the flexural modulus and

flexural strength of chopped E-glass FRP composite containing 20 % fibre volume fraction are, respectively, 7 GPa and 140 MPa compared to 35 GPa and 840 MPa (*i.e.*, more than three times higher) for a unidirectional E-glass FRP composite with 60% fibre volume fraction [12] (p. 93); the lower production costs and ease of manufacture of complex shapes for DFRCs ([106] and [15] (p. 121)) has led to a wider variety of applications.

In the following sections, detail discussion concerning the different types of fibres will be limited to those utilised in this work, *i.e.*, glass fibre and carbon fibre.

#### 2.2.1.1. Glass fibres

Amongst the reinforcing materials used in fibre-reinforced polymer (FRP) composites, glass fibres are the most widely utilised mainly due to their relatively low price, availability and reliability [107], as well as their reasonably high strength when compared to carbon fibres [108]. Comparison between these two types of fibres in terms of cost and properties has been presented in Table 2.3 below. The table shows standard modulus continuous carbon fibre to be approximately ten times more expensive when compared to continuous E-glass fibre whilst the former is just slightly stronger in tension than the latter.

**Table 2.3.** Cost and properties of E-glass and standard modulus carbon fibre

Fibre type	Cost <sup>a)</sup> (US\$/kg)	Properties		
		Density <sup>b)</sup> (g/cm <sup>3</sup> )	Tensile strength <sup>c)</sup> (MPa)	Elastic modulus <sup>d)</sup> (GPa)
E-glass, continuous	1.90 – 3.30	2.58	3450	72.5
Carbon, continuous	31.50 – 41.50	1.78	3800 – 4200	230

<sup>a)</sup>[101] (p. A35)

<sup>c)</sup>[101] (p. A9)

<sup>b)</sup>[101] (p. A6)

<sup>d)</sup>[101] (p. A15)

Glass fibre filaments are produced by forcing a molten glass through holes in the bottom of a platinum bushing. Following this, the glass filaments are collected, quenched by passing through a light water spray, coated with a protective binder, gathered to form a bundle (also known as a tow or strand), and finally wound onto a spool as shown in Figure 2.10. This complete manufacturing process has been illustrated in Figure 2.11. In addition to protecting the surface of the fibres, the binder has additional functions including holding individual fibres together for ease of processing, lubricating the fibre surface in order to reduce abrasion when in contact with equipment during composite manufacture, impart anti-septic agent for softening and to improve chopability, and provide chemical links for improved interface bonding between the fibre surface and matrix ([109, 110], [109: pp. 18-19, and 110]).

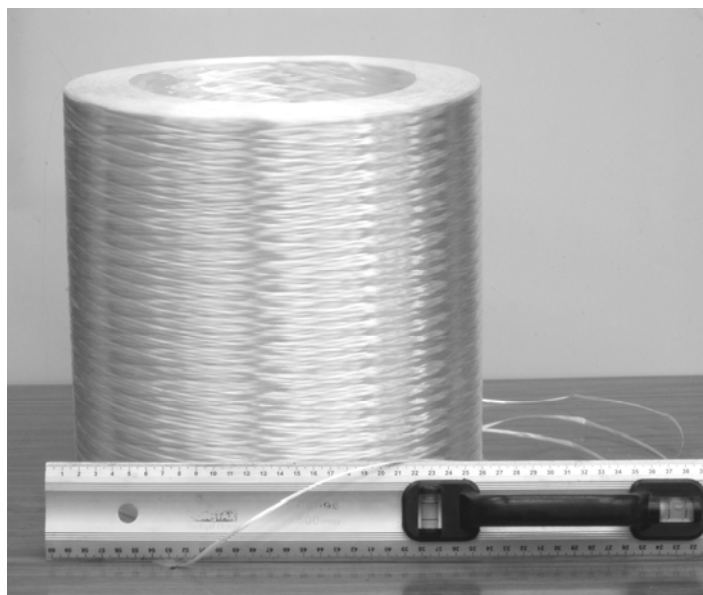


**Figure 2.10.** Spool of E-glass fibre E2350-11 supplied by Owens Corning Asia-Pacific. Net weight of the spool is 17 kgs.

The various types of glass fibres may be classified based on their chemical composition that, furthermore, determines their properties and usages. There are four types of commonly used glass fibres [110], *i.e.* A-glass fibre with high alkali content leading to good chemical resistance; C-glass fibre produced from soda borosilicate, possessing excellent chemical resistance, E-glass fibre produced from

aluminium borosilicate-based materials, possessing good electrical resistance, and S-glass fibres consisting of S- and S2-glass fibres which contain compounding elements such as aluminium silicate and magnesium which make them much stronger than E-glass fibres. Typical chemical compositions of these types of glass fibres are presented in Table 2.4.

**Table 2.4.** Typical chemical composition of E- and S-glass fibres (%wt)

Element	E-glass	S-glass
Silicon oxide, SiO <sub>2</sub>	54.3 <sup>b,c)</sup> 55.2 <sup>a)</sup>	64.2 <sup>b,c)</sup> 65.0 <sup>a)</sup>
Aluminium oxide, Al <sub>2</sub> O <sub>3</sub>	8.0 <sup>a)</sup> 15.2 <sup>b,c)</sup>	24.8 <sup>b,c)</sup> 25.0 <sup>a)</sup>
Calcium oxide, CaO	17.2 <sup>b,c)</sup> 18.7 <sup>a)</sup>	— <sup>a)</sup> 0.01 <sup>b,c)</sup>
Magnesium oxide, MgO	4.6 <sup>a)</sup> 4.7 <sup>b,c)</sup>	10.0 <sup>a)</sup> 10.27 <sup>b,c)</sup>
Sodium oxide, Na <sub>2</sub> O	0.3 <sup>a)</sup> 0.6 <sup>b,c)</sup>	0.27 <sup>b,c)</sup> 0.3 <sup>a)</sup>
Boron oxide, B <sub>2</sub> O <sub>3</sub>	7.3 <sup>a)</sup> 8.0 <sup>b,c)</sup>	— <sup>a)</sup> 0.01 <sup>b,c)</sup>

<sup>a)</sup>[12] (p. 8)

<sup>b)</sup>[15] (p. 15)

<sup>c)</sup>[110] (p. 134)

In general, glass is an amorphous material. Polyhendrons, that are each composed of oxygen atoms covalently bonded to silicon, form long three-dimensional networks within the glass structure. Glass fibres are fairly isotropic [12] (p. 11) which is a consequence of its three-dimensional network structure. Glass fibres are generally inexpensive, very strong in tension, possessing high fracture toughness, as well as being relatively insensitive to chemical environments, moisture, and elevated temperature. Some important physical and mechanical properties of glass fibres have been presented in Table 2.5.

The tensile strength of both E and S grades of glass fibre is very sensitive to temperature, although S-glass fibre is slightly less sensitive. The tensile strength of E-glass fibre degrades by approximately 24% and 50% as the temperature is increased from 22 °C to 371 °C and 538 °C, respectively, while that of S-glass



fibre degrades by approximately 18% and 47% for the same temperature increase [110] (p. 135) and [111].

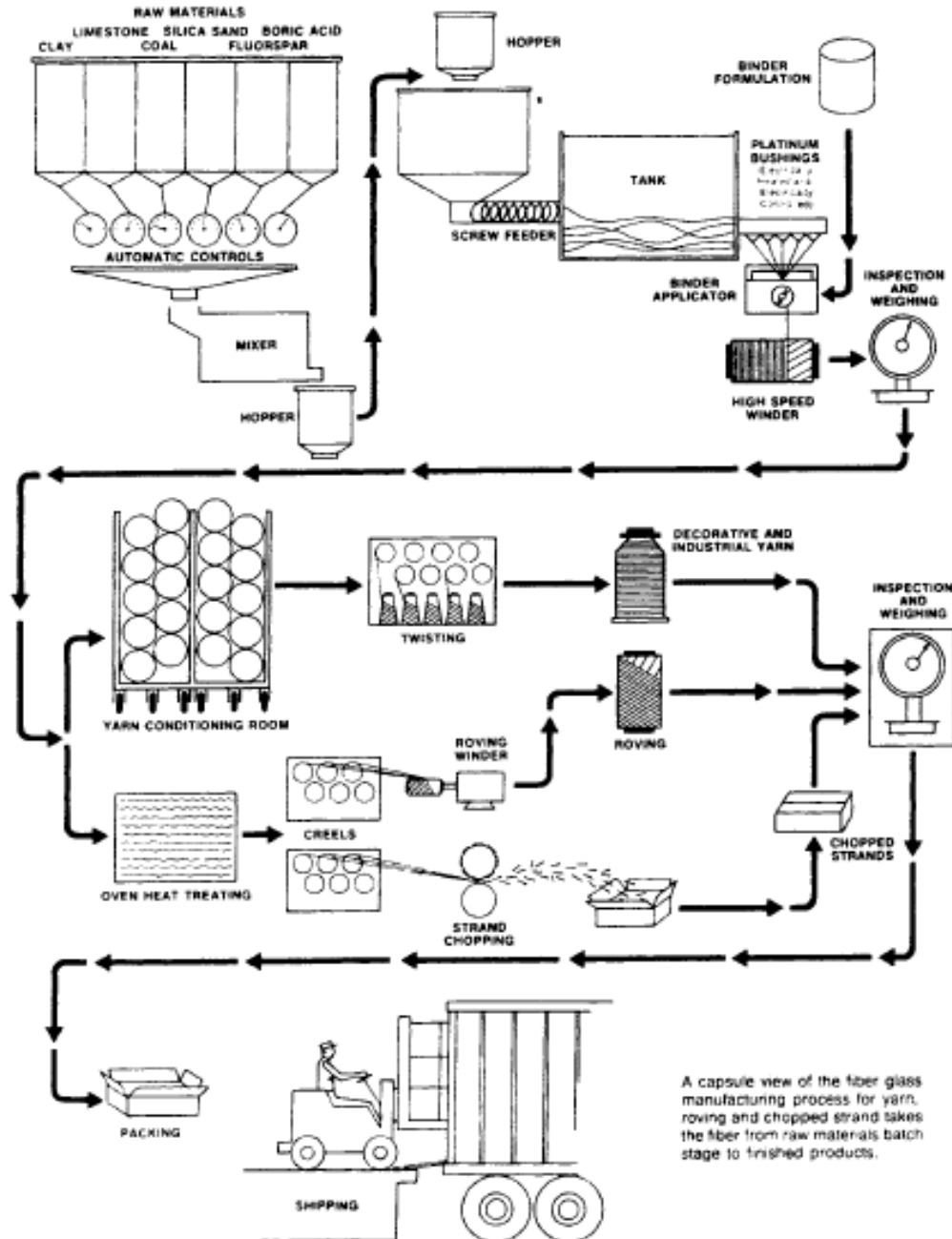


**Figure 2.11.** Direct-melt glass fibre manufacturing process [110]

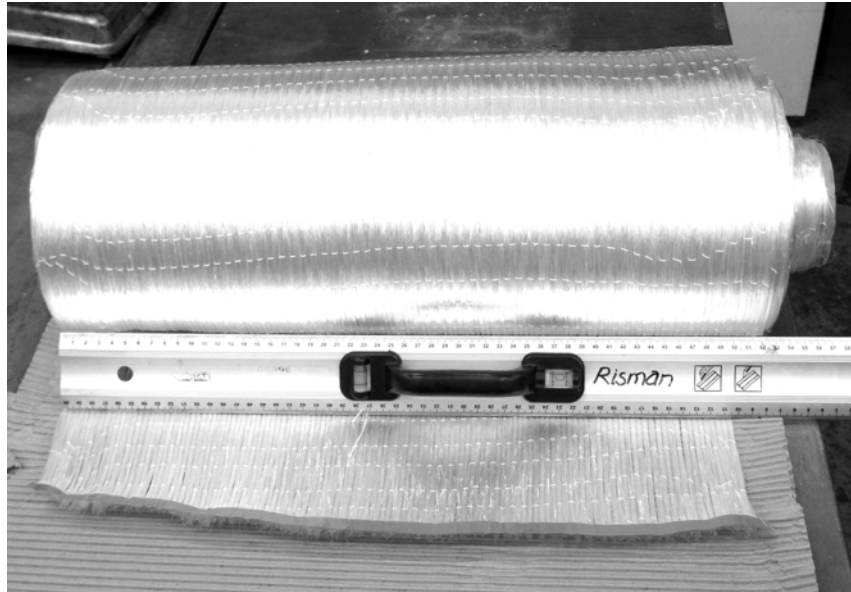


**Figure 2.12.** A roll of S2-glass fibre mat Unitex UT-S500 supplied by SP System, Newport, Isle of Wight, UK

Table 2.5. Typical properties of E- and S-glass fibres<sup>a)</sup>

Properties	E-glass	S-glass
Density ( $\text{g}\cdot\text{cm}^{-3}$ )	2.54	2.48
Coefficient of linear thermal expansion ( $\times 10^{-6} \text{ }^{\circ}\text{C}^{-1}$ )	4.7	5.6
Tensile strength at 22 $^{\circ}\text{C}$ (MPa)	3348	4585
Tensile modulus at 22 $^{\circ}\text{C}$ (GPa)	72.4	85.5
Yield elongation (%)	4.8	5.7

<sup>a)</sup>[110] (p. 135)

#### 2.2.1.2. Carbon and graphite fibres

These days, carbon fibre has been widely used in applications including sport and leisure, civil structures, ground, marine and air transportations, military equipment, as well as high performance aerospace structures. Among the advantageous of carbon and graphite fibres are their low density combined with

high strength, high modulus and high temperature resistance in non-oxidising environments [112]. When being embedded in polymer matrices, which also possess low density, they produce high specific strength and high specific stiffness fibre-reinforced polymer matrix composites. The most recent commercial passenger aircraft such as the Boeing 787, contain approximately 50 wt% of composite materials, most of which is carbon fibre reinforced polymer (CFRP) [113], whilst high performance bicycles, canoes, fishing rods, golf clubs, hockey sticks, snowboards, and tennis racquets are additional examples of sporting goods made from CFRP composite [114].

Both carbon and graphite fibres are composed of carbon atoms arranged in a specific structure. The carbon content of carbon fibres is 80% to 95% while that of graphite fibres is much higher at 99% or more [15] (p. 21). Three types of organic precursors are commonly used to produce carbon and graphite fibres, *i.e.*, rayon fibres, pitch, and polyacrilonytrile (PAN) [15] (p. 21), [82] (p. 64), [12] (p. 20), and [115]. Carbon and graphite fibres are generally produced by the so-called thermal decomposition process. The strength and modulus of carbon and graphite fibres are spread over a wide range (Table 2.6) depending upon their precursor, processing procedure and parameters. Compared to glass and silicon carbide fibres, carbon fibres possess much lower density (see Tables 2.5, 2.6 and 2.8) leading to superior specific strength and specific stiffness.

Precursors. Continuous rayon fibres are extracted from wood pulp and processed by wet spinning. Rayon fibres are a natural thermosetting polymer [12] (p. 23). Pitch precursor can be obtained from inexpensive sources such as asphalt, polyvinyl chloride (PVC), and tar [12] (p. 23), [115], while PAN fibre precursors are apparently those used in textile industries [115].

Thermal decomposition process. Prior to thermal decomposition processing, the precursors generally undergo particulate removal and spinning for pitch precursor; and spinning, extraction, and stretching to improve longitudinal alignment of polymer molecules for PAN fibre precursor. There are three important stages

generally involved in thermal decomposition process to produce carbon fibres [116] and [12] (p. 20), *i.e.*

1. *Stabilisation.* This stage is carried out at 200–260 °C [115] for a few hours in air. After being stabilised, precursors will reduce their tendency to melt in the further higher temperature processes.
2. *Carbonisation.* During this process, most of the non-carbon elements that may contaminate the precursor are removed, resulting in a higher purity of carbon fibre. The required temperature for carbonisation is approximately 1000–1500 °C [115], and it must be within an inert atmosphere such as nitrogen. In order to avoid any distortion of the precursor structure, the heating rate must be kept low.
3. *Graphitisation.* In this stage, the properties of the carbon fibres yielded in the previous stage are improved by holding the fibre at above 1800 °C [15] (p. 22), up to 3000 °C for PAN-based carbon fibre, for a very short time, *e.g.*, one minute, in an inert atmosphere such as argon [117].

The degree of alignment and order of atomic structure of the carbon fibre along the fibre axis direction, leading to higher stiffness and lower linear thermal expansion coefficient in this direction [115] and [12] (pp. 27-29), strongly depends upon the graphitisation temperature. Although carbon (graphite) possesses relatively high strength and high modulus, it is brittle in nature without any plastic deformation prior to fracture. As a consequence, the presence of any defect such as micro-cracks and fibre diameter inconsistencies will generate a very high local stress.

Hawthorne and Teghtsoonian [118] studied the compressive behaviour of carbon fibres by embedding single carbon fibres in epoxy resin and applying a compressive load onto the specimens. They found that the higher the degree of anisotropy of fibre structure the more likely that micro-buckling and kinking failure modes occurred, in which failure started at the outer surface and propagated into the fibre centre. Compressive strength was found to vary from less than 1 GPa for high modulus carbon fibre to ~2.2 GPa for moderately oriented carbon fibre, while the failure strain decreased from ~2.5% to less than 1% as the modulus

increased. In addition, Oya and Hamada [119] reported that the compressive strength of several different carbon fibre types varied from ~15.6% (M50J) to ~30.8% (T700S) of their respective tensile strengths.

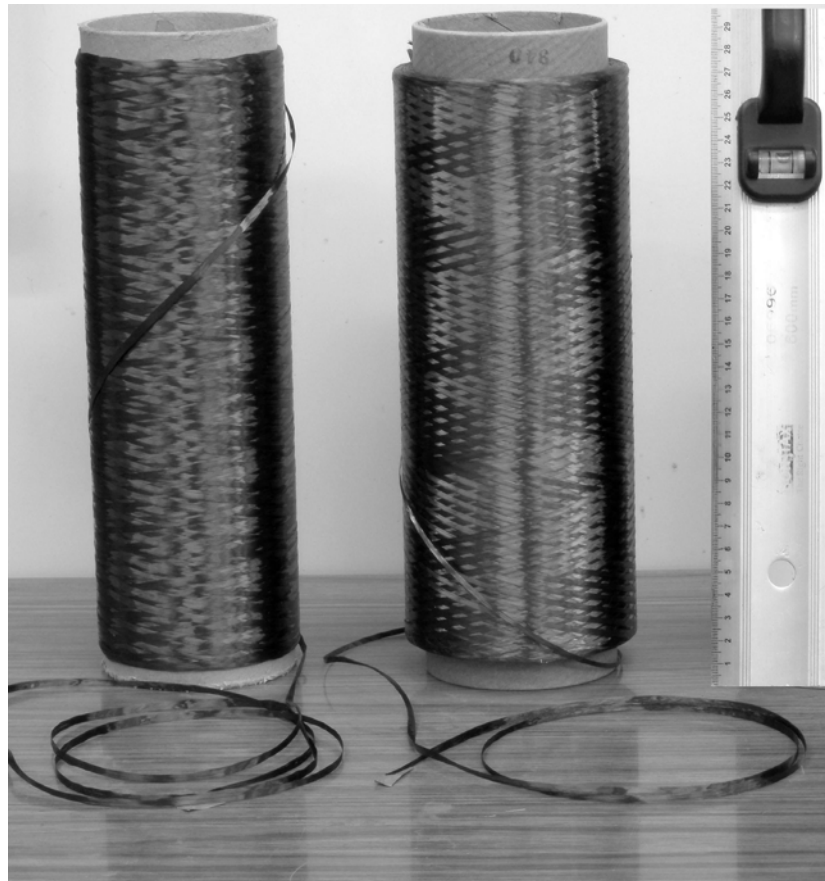


**Figure 2.13.** Two rolls of 12k tow size PAN-based carbon fibre from two different manufacturers

The wide variety of properties, which depend upon their precursor type and fabrication parameters, for several carbon fibres can be seen in Table 2.6.

**Table 2.6.** Typical properties of carbon fibres of different precursors

Carbon fibre type	Diameter ( $\mu\text{m}$ )	Density ( $\text{g}\cdot\text{cm}^{-3}$ )	Tensile strength (MPa)	Tensile modulus (GPa)
IM7 12K (PAN-based) <sup>a)</sup>	5.2	1.78	5570	276
P-30X 2K (pitch-based) <sup>b)</sup>	11	1.99	2760	201
Ural-LO (rayon-based) <sup>c)</sup>	$\sim 6 - 11$	1.4	1200 – 1500	100 – 120

<sup>a)</sup>[120]<sup>b)</sup>[121]<sup>c)</sup>[122]

### 2.2.2. Epoxy Matrix

Different matrix materials can be found in the field of composite materials. The particular matrix type for any given application may be selected based on in-service requirements and environmental considerations. Matrix materials can be based on polymers, ceramics, metals, or carbon depending upon the required performance and in-service environmental conditions of the resulting composites. The main function of the matrix is [88] and [101] (pp. 96-97), firstly, to hold the fibres in place in order to allow them to perform as designed and to ensure the structural integrity of the product. Secondly, the matrix also plays an important role as a load-transfer media from one fibre to the other surrounding fibres via the fibre-matrix interface and matrix. Thirdly, the matrix also protects fibres from physical damage and chemical attack. In addition, the matrix content within a particular composite also contributes to the determination of composite properties. Finally, in laminated composites, the shear strength of the matrix predominantly controls the interlaminar shear strength of the composites.

It has been discussed in Section 2.1.2.3 that the fibre architecture may be selected mainly based on the applied in-service loads. In order to ensure that the fibres function as designed, they must be kept in their initial state as they are designed to be held by the matrix. As the load-transfer media, the matrix will mostly bear shear loading. Fibres are very fine filaments, for example: glass fibre diameters may range from 3.8  $\mu\text{m}$  [110] to 22  $\mu\text{m}$  [123] whilst those of carbon fibre may range from 4.7  $\mu\text{m}$  to 15  $\mu\text{m}$  [124] (p. 8), so that they are very sensitive

to any physical or chemical contact during service. The matrix provides protection to fibres from any possible damage that will degrade their properties.

Polymer matrices possess some advantages, when compared to other matrices, such as low density, good chemical resistance, low cost, and ease of manufacturing process and, as such, are the most commonly used matrix materials for fibrous composites [15] (p. 26). On the other hand, disadvantages include their relatively low service temperature (*e.g.*, 200 – 250 °C), degraded mechanical properties and change of physical properties due to moisture absorption, high sensitivity of ageing to ultra-violet light, high thermal expansion coefficient, production of large amounts of smoke upon burning, and being poisonous in its uncured state [88].

Polymer matrices can be classified into *thermoplastics* that soften and melt upon heating and *thermosets* that decompose upon heating. Polyethylene, polystyrene and polymethyl methacrylate [12] (p. 60), nylon, polyvinyl chloride, and polysulfone [100] are examples of thermoplastic, whilst epoxy, polyester, vinylester, bismaleimide, polyimide, phenolic triazine and cyanate ester are examples of thermoset polymers ([100] and [12] (p. 61)). The most common matrices used with glass fibre reinforcement in order to produce GFRP composites are polyester and vinyl ester due to their low cost, whereas epoxies, which are more expensive and possess superior mechanical properties when compared to polyester and vinyl ester, are generally selected for the manufacture of high performance PMCs such as those utilised in the aerospace industries [101] (p. 600) when incorporated with high performance carbon fibres [107, 116, 129]. Compared to other polymeric matrices, epoxy possesses several advantages. The most important advantages of epoxy are its low curing shrinkage and strong adhesion with various types of fibres [125] that results in accurate dimensional stability of the products leading to its extensive usage in FRP composite materials. Other advantages of epoxy are its low swelling coefficient [12] (p. 65), high resistance to severe environments, and a curing reaction that does not produce volatile by-products so that entrapped air bubble can be minimised [125].

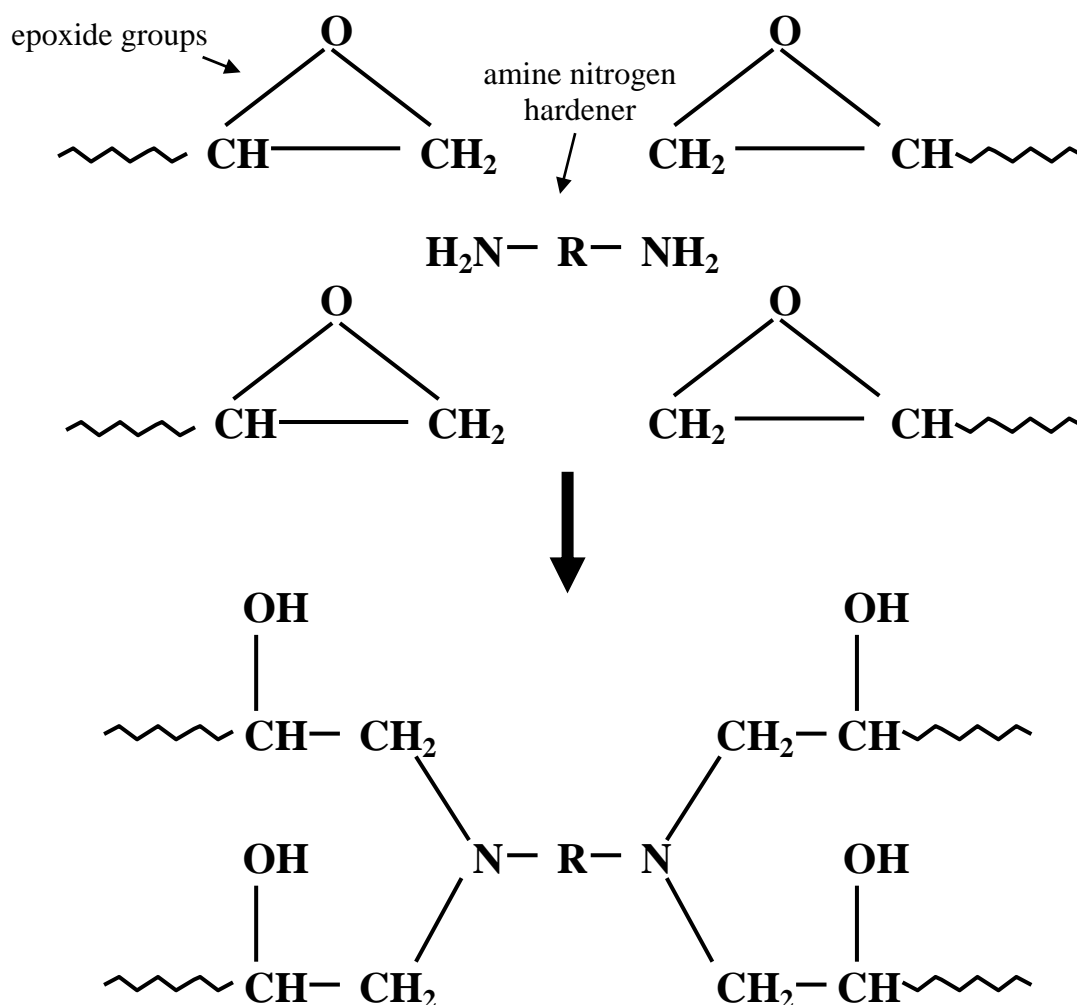


**Figure 2.14.** Amine curing reaction illustration of epoxide and amine hardener showing that each of the hydrogen of the amine curing agent reacts with each of the epoxide groups to form a strong covalent bond (Redrawn from Ref. [125])

During curing, the chemical reaction between the epoxy resin and curing agent, also known as a *hardener*, takes place to form extended crosslinked networks of monomers forming large molecular structures [125]. The chemical reaction illustrated in Figure 2.14 suggests that the epoxy resin-to-hardener ratio must be precisely controlled for optimum performance. Any imbalance will produce an excess portion of unreacted resin or hardener, furthermore, complete network structures and optimum properties of the resultant product will not be achieved. Kim *et al.* [126] reported that, unlike tensile strength, tensile modulus and ultimate strain were not sensitive to any imbalance of the resin-to-hardener



ratio, whereas impact strength, work of fracture and fracture toughness were found to be sensitive. A lack of hardener may result in a relatively high elastic modulus associated with low tensile strength and brittle cured epoxy, whereas too much hardener will result in a low elastic modulus together with relatively high tensile strength and a large deformation capability of the cured epoxy [127].

After being mixed with hardener, the epoxy resin will remain in a liquid state for a certain length of time until the gelation process begins, in which the viscosity sharply increases. This time period is called the *gel time* or more familiarly, the *pot life*, which varies from the order of minutes to more than 24 hour depending upon the type of amine curing agent being used. Aliphatic amine type curing agents produce epoxy systems with gel time of minutes up to a few hours, whilst those based on aromatic types produce epoxy systems with up to 24 hours and more of gel time [125]. When gelation has begun, the epoxy system can no longer be used to wet fibres. The time required for complete curing is strongly dependent upon the curing temperature with a higher curing temperature requiring a shorter time for curing.

In contrast to that of fibres, the compressive strength of epoxy matrices is generally higher than their tensile strength [128]. Some practically representative properties related to design considerations for epoxy matrix materials have been presented in Table 2.7.

**Table 2.7.** Typical properties of cured epoxy resin

Density ( $\text{g}\cdot\text{cm}^{-3}$ )	1.2 – 1.3 <sup>a)</sup>
Linear thermal expansion coefficient ( $\times 10^{-5} \text{ }^{\circ}\text{C}^{-1}$ )	8 – 11 <sup>b)</sup>
Continuous service temperature ( $^{\circ}\text{C}$ )	25 – 85 <sup>b)</sup>
Tensile strength (MPa)	55 – 130 <sup>a)</sup>
Tensile modulus (GPa)	2.75 – 4.10 <sup>a)</sup>
Compressive strength, Epikote 828/Epokure (MPa)	104 – 125 <sup>c)</sup>

<sup>a)</sup> [15] (p. 33)

<sup>b)</sup> [12] (p. 65)

<sup>c)</sup> [128]

### 2.3. FIBRE-MATRIX INTERFACE

The interface between any two phases in contact, such as that of fibre and matrix, is characterised by the presence of discontinuity (p. 79)[12, 15, 129]. It implies that there is a change of properties, *i.e.* physical, mechanical, thermal and/or electrical, from one side to the other (from the fibre side to matrix side or *vice versa*) across this region. Although the properties of a typical composite material are strongly controlled by the inherent properties of its constituent materials (refer to the discussion on the rule of mixtures in Section 3.2), load transfer effectiveness from one particular fibre to its surrounding matrix, and further to other surrounding fibres, is also greatly influenced by the properties of the interface (p. 69)[15, 137-139], and further characterises the mechanical properties of the resultant composites [107].

The strength of the interfacial bond of an interface for CFRP composites depends upon the degree of wetting of the fibre by the matrix [129], resin shrinkage stress [130, 131] and the length of the embedded fibre [130]. Interfacial bond strength can be improved by coating. Zhu and co-workers [132] revealed that the tensile strength of silicon carbide fibre-reinforced aluminium matrix composites can be improved by up to 45% from sizing the SiC fibre with SiO<sub>2</sub>. Furthermore, interface characteristics dictate the stress redistribution upon fibre breakage [133].

*Strong Interface Bond* – From the mechanics of materials standpoint, if strong interface bonding exists in composite structures subjected to tensile loading, for low fibre volume fractions (such that the magnitude of load that can be supported by the fibre portion is smaller than that of the matrix portion), then, due to the ultimate strain of the fibre being generally lower than that of the matrix, the fibre will be broken prior to matrix crack initiation and thus lead to brittle fracture of the composite, creating a single-surface fracture. On the other hand, if the fibre volume fraction is relatively high (such that the strength of the fibre portion is larger than that of the matrix portion), with the existence of strong interfacial bonding, the matrix will experience shear failure along the fibre length and lead to

brittle fracture creating multiple-surface fractures [15] (pp. 91-92), [134]. Interfacial debonding initiates when the difference in values of strain between fibre and matrix reaches a critical value [135]. Bader and Bowyer [136, 137] reported that the strength of interface bonding is limited by the strength of the matrix. Selby and Miller [128] found that the interfacial strength is slightly higher than the shear strength of the matrix, supporting Bader and Bowyer. With advanced experimental methods available, fourteen years later, Netravali and Schwartz working on glass fibre/epoxy [138] and graphite fibre/epoxy [139] composites observed that it was not the interface that failed but, instead, the matrix in the proximity of the interface underwent shear failure – the interfacial shear strength could thus be several times higher than the shear yield strength of the matrix. When a matrix that possesses a low elastic modulus undergoes excessive deformation and starts cracking, large portions of the load may be transferred to its surrounding fibres.

*Weak Interface Bond* – If weak bonding exists at the interface then debonding will start to occur in the interface [131], forming multiple-plane failures [15] (p. 91). Weak interfacial bonds are necessary in improving the toughness of CMCs as the toughening mechanism for CMCs is closely related to interface debonding, fibre bridging and fibre pullout [131]. Zhou and Wagner [140] observed that upon the breakage of E-glass fibre/epoxy composites, weak interface bonding was characterised by longer saturated fibre fragment lengths compared to that of strong interface bonds.

## **2.4. FABRICATION TECHNIQUES OF FIBRE-REINFORCED POLYMER (FRP) COMPOSITES**

The discussion in this section is limited to fabrication techniques related to PMCs only with more specific details being presented for those techniques employed in this research project. Various fabrication processes are available for composite product manufacturing. The properties of constituent materials need to be considered when selecting a particular processing technique in order to meet product requirements related to both performance and cost. A selection of

commonly utilised fabrication techniques for polymer matrix composites is presented in Figure 2.15 below.

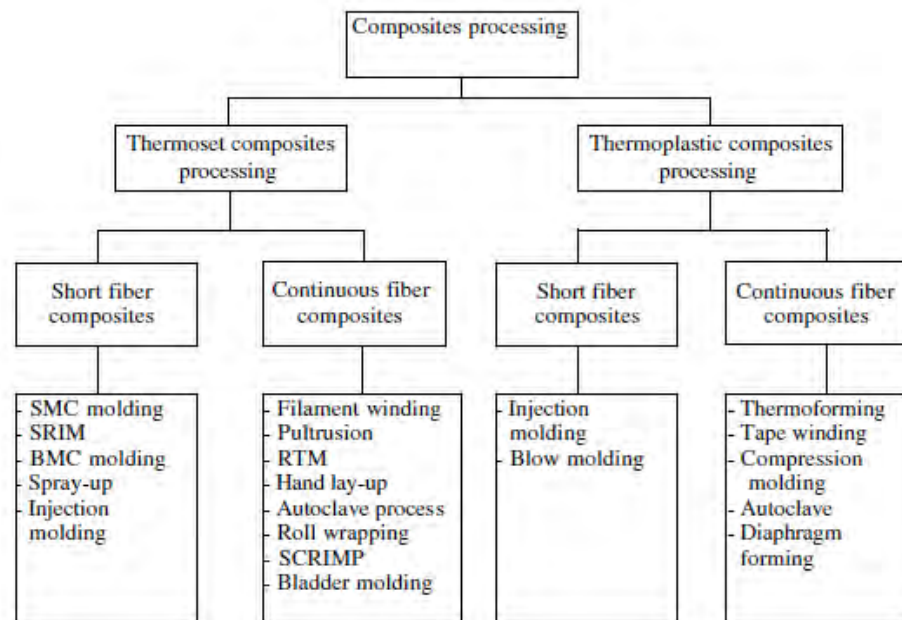


**Figure 2.15.** Classification of polymer matrix composite fabrication techniques [6] (p. 12).

Notes to Figure 2.15:

SMC – sheet moulding compound

SRIM – structural reaction injection moulding

BMC – bulk moulding compound

RTM – resin transfer moulding

SCRIMP – Seemann Composites Resin Infusion Moulding Process

The following paragraphs are brief descriptions of common processing techniques for continuous fibre-reinforced thermosetting matrix composites.

#### **2.4.1. Hand Lay-up**

Flat and curved surfaces can be manufactured using this traditional technique. If a typical geometry is required then a mould, which can be made from different

materials, can be utilised with the mould cavity being coated with release agent prior to fibre placement. As is suggested by its name, the fibres are manually placed in the mould cavity. Fibre impregnation can be performed by brushing or spraying the resin into the fibre arrangement. A roller is then applied for fibre compaction and removal of air bubbles whilst curing may take place at room or elevated temperature. More detail about this technique will be discussed in the following section [100].

Compared to other manufacturing techniques, hand lay-up is probably the simplest composite manufacturing technique, with this method being the most commonly utilised for the manufacturing of small-sized and large-sized parts [15] (p. 37). The fibres or preforms are manually laid up onto the surface of a base plate or mould. The hand lay-up technique can be further divided into two main methods, *i.e.*, wet lay-up and prepreg lay-up [6] (p. 126).

#### 2.4.1.1. Wet lay-up

Different surface geometries can be produced using this technique, both flat and curved surfaces. In manufacturing flat surfaces, base plates are used whilst for curved surfaces, moulds are generally used. Prior to fibre placement, a release system is applied onto the surface where direct contact with the moulded product occurs. Various types of release systems are available in the market, such as fluorocarbon, polyvinyl alcohol (PVA), release films, release papers, silicon, wax, as well as gel coat and liquid release agent [15] (p. 37). Release films or release papers can best be used in the production of flat surfaces. The fibres are carefully placed onto the pre-coated base plate or mould with fibre wetting being carried out by brushing or spraying a pre-mixed resin-hardener into the fibre arrangement. A roller is then applied for fibre compaction and air bubble removal. This is the first layer of the composite product.

If additional layers are required to produce a thicker product then the following fibre layers must be laid-up while the first layer is still in its tacky stage before it has completely cured, and again followed by fibre wetting and roller application. This step can be repeatedly performed until the desired thickness of

product is achieved. A simple lay-up mould for making a channel has been illustrated in Figure 2.16.

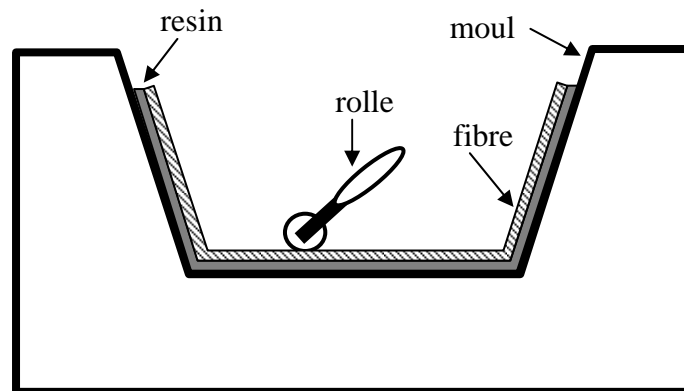


**Figure 2.16.** Schematic illustration of a simple wet lay-up moulding (Redrawn after Ref. [12] (p. 127))

Curing may be carried out at room or elevated temperature. Some examples of composites produced using this methods include racing yachts [100], boat and boat hulls, ducts, furniture, radomes, flat sheets [15] (p. 37), storage tanks, swimming pools, wind turbine blades [6] (p. 124), and wavy composite sheets for roofing.

#### 2.4.1.2. Dry Lay-up or prepreg lay-up

This method is also known as autoclave processing or vacuum bagging processing [84] (p. 215). Unlike wet lay-up where unimpregnated fibres are used as materials, in this method preimpregnated fibres or prepreps are used. Other differences with wet lay-up include that curing is carried out under vacuum atmosphere and that a compressive pressure for compaction is applied onto the part being cured. By applying pressure and curing under vacuum, it is possible to fabricate high quality products with very low void contents combined with high fibre volume fractions.

*Prepregs* – Prepreg or preimpregnated fibre is fibre that has been wetted with matrix, and can be thermoset (in its partially cured stage [15] (p. 46)) or thermoplastic [141, 142]. As mentioned, thermoset matrix prepregs are partially cured [143] with the precise determination of this stage being crucial as it is directly related to tack level which is the adhesion characteristic of the prepregs. Tack strongly influences the handling and lay-up operations, such as the levels of ease of handling, excess resin and entrapped air bubble removal, and interlayer consolidation of the final composite products. Excessive tack will lead to handling and lay-up difficulties and excessive resin removal during subsequent processing. On the other hand, prepregs with a lack of tack will not be able to produce optimum cured properties of the final products [100]. After being produced, prepregs must be stored in a freezer at sub-zero temperatures in order to decrease the curing rate of the thermoset matrix. The main disadvantage of fibre/thermoset prepregs in comparison with fibre/thermoplastic prepreg is the delivery and storage requirements for the former, due to the continued curing process of the matrix being significantly more complex than the latter. Thus, the shelf life of thermoset prepregs is much shorter compared to thermoplastic prepregs.

*Autoclave* – An autoclave is essentially a pressure vessel where heat and vacuum pressure can be simultaneously applied, in addition to compressive pressure (*via* external loading) that can be applied into the preform being processed inside the chamber [144]. These requirements imply that an autoclave must be equipped with heating elements; hose fittings, hose and vacuum pump for applying vacuum pressure; and a means for applying a compressive pressure into the preform being consolidated and cured. A small-sized, simple autoclave used in this project has been presented in Figure 2.17. The autoclave shown in Figure 2.17 is specially designed to produce flat plates of continuous fibre-reinforced composite. Its maximum effective internal size is approximately  $310 \times 185 \times 3.5 \text{ mm}^3$ . The heat is supplied by a pair of electric heater elements of 2400 watts total power. To ensure homogeneous temperature distribution over the area, the heating element geometry is designed as shown in the inset of Figure 2.17 with the temperature being controlled using a thermocouple. A PIAB vacuum pump type L28 [145] and

a vacuum gauge were installed. This mini pump can generate vacuum levels up to  $-70$  kPa. Compressive pressure onto the lay-ups was applied by means of a 30-ton loading capacity *via* a hydraulic pump – this pump can generate compressive pressures in excess of 5 MPa over the largest plates that can be accommodated by the autoclave.

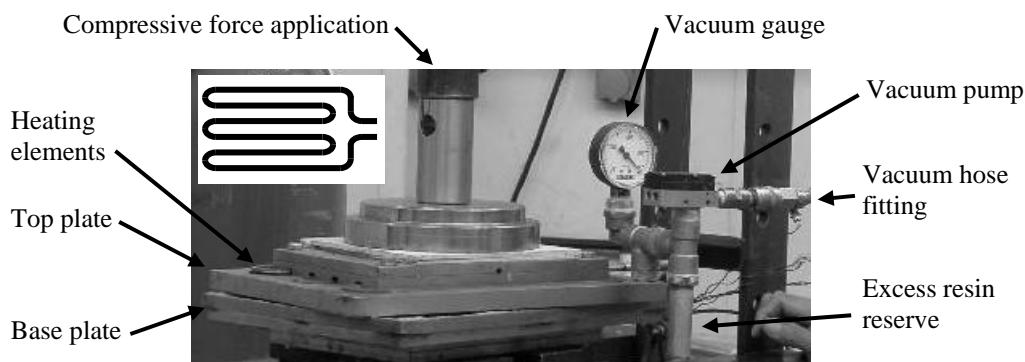


**Figure 2.17.** A small-sized autoclave showing its important elements. Thermostat that is installed to control its temperature is not shown. Element geometry is shown in the inset. (Basic design by Nick Jensen , improvement and instrumentation by Sudarisman)

*Curing Process* – Release agent or release paper can be applied onto the contact surface with the prepreg preform. Prepregs should be taken out of the storage and the release papers being immediately removed and then stacked together to form the required number of layers. The preform is then cut along its edges to trim the resin-rich area and to conform to the size of the autoclave. Prepregs that have been stacked together, usually called a *preform* or *lay-up*, are then carefully placed into the air tight autoclave chamber. Simultaneously with the increase of temperature to its dwell temperature, the air inside the chamber is pumped out in order to generate the required vacuum pressure inside the chamber. The curing temperature for thermoset matrix composites is known to generally vary from  $120^{\circ}\text{C}$  to  $200^{\circ}\text{C}$  [146] (p. 2-53).

Different vacuum level and magnitude of compressive pressure have been applied and reported in previous work. In 2005, Gustin and colleagues [44]



applied  $\sim 0.077$  MPa (600 mm Hg) autoclave vacuum pressure to produce carbon fibre-reinforced epoxy, Kevlar fibre-reinforced epoxy and carbon-glass hybrid fibre-reinforced epoxy composites, while, for producing GLARE using glass fibre-reinforced epoxy as reinforcement, Botelho and co-workers [147] applied an autoclave vacuum pressure of  $\sim 0.083$  MPa. More recently, Sudarisman and Davies [143] reported that they utilised an autoclave vacuum pressure ranging from 0.085 MPa to 0.035 MPa in order to produce CFRP composites with the void content decreasing from  $\sim 4.2$  vol.% to  $\sim 1.5$  vol.% as the vacuum level increased from 0.085 MPa to 0.035 MPa.

In 1992, Boey and Lye [148] applied up to 7 MPa of external compressive pressure in order to reduce void content during the vacuum-bagged curing of E-glass/epoxy composites. They reported that the void content started to reduce when the applied compressive pressure reached 0.4 MPa, with a sharp drop being observed for an applied compressive pressure of 5 MPa or higher. They further reported that the lowest void content obtained was  $\sim 4$  vol.%. Park and Jang [149] also applied 7 MPa of compressive pressure whereas other researchers such as Davies and colleagues [79, 161, 162] and Sudarisman and colleagues [150], applied a lower compressive pressure,  $\sim 2.5$  MPa, during the vacuum-bagged curing of FRP composites. Olivier *et al.* [151] in 1995 and Liu *et al.* [152] in 2006 applied compressive pressures of 0.1 to 1.0 MPa and 0.0 to 0.6 MPa, respectively, to cure carbon fibre reinforced epoxy composites. Both groups revealed that higher applied compressive pressures resulted in lower void content, however, Sudarisman and Davies [143] reported that excessive compressive pressure can result in fibre misalignment.

It should be noted that applying a vacuum into the chamber atmosphere immediately after shielding the chamber is crucial, as the viscosity level of the matrix will increase in accordance with the increase of temperature prior to undergoing cross-linking [100], in order to be able to remove as much air as possible. In addition, for the same reason it should also be performed prior to applying any compressive pressure.

*Advantages and disadvantages* – In comparison with other available techniques, hand lay-up possesses some advantages and disadvantages. The following are its main advantages and disadvantages [100].

*Advantages:*

- a. Flexible design capability.
- b. Accommodates small- and large-sized products.
- c. Low investment on equipment and tooling.
- d. Minimum start-up lead time and cost.
- e. Designs can easily be modified.
- f. Cores and reinforcing structures can be employed.
- g. Sandwich structures can be produced.
- h. Low cost for prototyping and pre-production process.
- i. The required intermediate level skilled workers can easily be trained.

*Disadvantages:*

- a. Needs more workers.
- b. Good quality surface can only be attained on one side.
- c. Product quality relies on the skill of the worker.
- d. Can not handle large volume production.
- e. Curing time can be longer.
- f. Waste product relatively high.

#### **2.4.2. Other Fabrication Techniques**

*Filament winding* [15] (pp. 42-44) – In filament winding, a continuous fibre tow or tows are passed through a resin impregnation bath and embedded into the resin. The tows, which have already been wetted with resin, are then helically wound onto a rotating mandrel. The helical angle depends upon the linear velocity of the rotating mandrel and the relative longitudinal velocity of the mandrel with respect to the resin bath. The number of layers depends on the thickness of the product, filament diameter, and the number of filaments within the tow. After being cured

at elevated temperature, the product is removed from the mandrel. The resulting products are in the form of cylindrical- or spherical-shapes, such as pipes, tubes, and fuel tanks.

*Pultrusion* [12] (pp. 89-90) – This technique is fully automatic controlled. Various shapes of continuous composite profiles, such as channels and I-sections, as well as flat-sections and solid cylindrical bars, can be produced utilising this technique. Continuous fibre tows or mats are first passed through a resin impregnation bath and then pulled through a pre-forming die for the removal of excess resin and air bubbles. Next, they pass through a heated die for final shaping and curing. The continuous product is then cut into certain lengths as required.

*Resin Transfer Moulding (RTM)* [6] (p. 155) – In this technique, a pair of moulds with a cavity in the shape of the required product are utilised. Before being used, the mould cavity surfaces are coated with release agent to ease product removal. Fibres, generally as perform, are carefully placed into the mould cavity after which the mating mould is placed and clamped together. Prior to being injected into the mould cavity, the resin is mixed with hardener or catalyst, as well as reinforcing particles and colouring pigment if required. A high surface quality for the product can be attained depending on the surface quality of the mould cavity. A vast variety of products can be produced, such as bicycle frames, doors, helmets, hockey sticks, wind turbine blades, as well as complex geometry products such as automotive panels, sports car bodies, and aircraft components (bulkheads, fairings, ribs, stiffeners, and spars).

*Autoclave process* [82] (pp. 126-128) – An autoclave is principally an air-sealed chamber whose pressure and temperature can be controlled. Prior to product preform placement on the mould base plate, the surface of the base plate needs to be coated with release agent or release film. The pressure of the atmosphere in which the product is cured is then decreased to a required vacuum in order to help remove any entrapped air bubbles and thus improve the quality of the product. In addition, compressive pressure may be applied onto the product preform in order

to assist air bubble removal and to compact fibre arrangement. Elevated temperature helps to accelerate the curing process. More detail concerning the autoclave process was previously presented in Sub-Section 2.4.1.2.

*Roll wrapping* [6] (pp. 190-193) – Roll wrapping is basically prepreg lay-up where the mould is in the form of a mandrel, either cylindrical or tapered. Prepregs are cut into the required geometry and dimensions and then wrapped onto a mandrel which has been coated with wax or other release agent. The mandrel which has been wrapped with prepreg is then rolled on a table. During the rolling, force is applied into the mandrel to provide compressive pressure exerted from the mandrel and also table surface into the prepreg in order to produce prepreg compaction and to ensure thorough contact between the mandrel surface and the prepreg for obtaining a precise geometry of the final product. For small-sized products, rolling is usually performed manually while for large-sized products this is accomplished by machine. Golf shafts and fishing rods are some examples of products manufactured using this method.

*Seemann Composite Resin Infusion Moulding Process (SCRIMP)* [6](pp. 166-168) – SCRIMP is a typical variant of RTM where a one-sided open mould is utilised. A number of fibre layers are put onto a mould cavity which has been coated with release agent. If a core, usually for stiffening purposes, is needed, it is put on the existing fibre layers. Other layers of fibre are then put into the existing arrangement. All the reinforcing arrangement within the mould cavity is then covered with a layer of plastic sheet and air-sealed tightened with the mould. Vacuum pressure is applied onto the arrangement for fibre compaction and to suck the resin system into the mould passing through the fibre arrangement. The vacuum level should be kept high in order to ensure that adequate resin wetting of the fibre occurs and thoroughly fills the entire cavity. Various products, such as boat hulls, car bodies, satellite dishes, and wind turbine blades, can be made using this method.

*Bladder moulding* [153] – Bladder moulding is, principally, a typical application of a pressure-bag moulding technique whose products are mostly tubular structures. Unlike pressure-bag moulding [15] (p. 40) where a pressure-bag is constructed between a flexible air-sealed sheet covering the bagged lay-up, and a pressure plate, a bladder is placed between prepreg layers. The moulding process is started by coating the surface of the cavity with release agent. Next, the prepreg arrangement with an uninflated bladder is placed into the cavity. The mould is then securely closed with the mated mould, and the bladder is inflated by being blown with compressed air (up to ~2 MPa [154]) in order to generate pressure that is required for preform densification. Curing and part consolidation can be carried out at elevated temperature. After completion of the curing process, the compressed air is released and the bladder is taken out from the moulded part for finishing processing if necessary.

## 2.5. FIBRE-REINFORCED POLYMER (FRP) COMPOSITES

Polymers are the most widely utilised matrix to produce composite materials [49] (p. 8). They can be reinforced with a wide variety of reinforcing materials in terms of their geometry, *e.g.*, particles [68-79], flakes [80, 82-87], discontinuous and continuous fibres [42, 44, 51, 54, 60, 61, 81, 108, 109, 156, 163, 165, 168-170], as well as other types of materials, *e.g.* polymers [155], carbon, graphite and aramid [107, 116, 160-162], metals [156, 157], ceramics and glasses [177-181], as well as natural fibres [167, 172, 173]. Deng [107] used the difference between theoretical and experimental values of  $V_f$  to calculate void volume fraction,  $V_v$ , and further predicted tensile and flexural properties of GFRP composites. Unlike  $V_f$  and density,  $\rho$ , the thermal expansion coefficient,  $\alpha$ , of FRP composites may be altered by the presence of residual stresses upon curing and the fibre-matrix interfacial strength, and thus it is not as accurate as  $V_f$  and  $\rho$  predictions.

The discussion on PMCs in the following sub-sections will be limited to those being the objects of this investigation, namely glass fibre-reinforced polymer (GFRP), carbon fibre-reinforced polymer (CFRP), and their hybrid fibre-reinforced polymer (hFRP) composites. The properties being discussed will also

be limited only to those directly related to the subject of the current research project, *i.e.* tension, compression and flexure.

### ***2.5.1. Glass Fibre-Reinforced Polymer (GFRP) Composites***

Glass fibres are the most widely used polymer reinforcement [158], such that GFRP composites are the most widely utilised composite materials. Different polymer matrices, such as nylon 6.6 [159, 160], polypropylene [112, 187-189], polycarbonate [161], polyester [21, 29, 191-193], vinylester [85, 167-171], polyurethane [162, 163], and epoxies [19, 162, 164-168], have also been reinforced with glass fibre using various fibre architectures, *e.g.*, randomly distributed discontinuous [160, 163, 169], unidirectional [168, 177], unidirectional stitched [162], cross ply [169], plain weave [168], woven roving [29], woven fabric [165], knitted fabric [83], and 3D braided [87].

Different mechanical properties of GFRP composites, *e.g.*, tension [20, 89, 113, 145, 185, 186, 200, 202], compression [20, 89, 145, 194, 196, 201, 203-205], flexure [20, 28, 197, 198, 206], torsion or shear [28, 93, 195, 197, 199], impact [28, 29, 83, 160, 170], and hardness [163, 171], have been investigated and reported. Various methods and/or standards and specimen geometries were utilised to study a particular mechanical property aforementioned above.

#### **2.5.1.1. Tensile properties**

Hamada and co-workers (1992) [134] investigated woven cloth E-glass/epoxy composite subjected to tensile loading. Gripped areas of the specimens were reinforced with aluminium tabs. They found that the tensile modulus of amino-silane coated glass fibre/epoxy samples was slightly higher than those of acryl-silane coated, but the tensile strength of the former was higher than that of the latter.

In 1999, Deng and colleagues [107] utilised three different cross-sectional geometries, and thus cross-sectional aspect ratios, *i.e.*, circular, ‘peanut’-shaped, and oval, of glass fibre to produce glass fibre-reinforced epoxy composite plates.

Specimens were cut from unidirectional GFRP composite panels containing a particular fibre cross-sectional geometry produced using an autoclave at 0.6 MPa compressive pressure and 120 °C in vacuum atmosphere for 16 hours. To prevent damage in the gripped areas, cross ply CFRP composite tabs were glued onto this area. The fibre volume fraction,  $V_f$ , was relatively high and varied between  $(62.0 \pm 1.9)\%$  to  $(69.8 \pm 0.4)\%$ . Tensile testing in both the longitudinal and transverse directions were carried out according to ASTM D3039 [172]. They revealed that longitudinal tensile strength,  $\sigma_{L-t}$ , and modulus,  $E_{L-t}$  were not sensitive to fibre cross-sectional aspect ratio, whereas transverse tensile strength,  $\sigma_{T-t}$ , and modulus,  $E_{T-t}$ , are sensitive to fibre cross-sectional aspect ratio with the ‘peanut’-shaped fibre cross-section FRP composites exhibiting the lowest  $\sigma_{T-t}$  and  $E_{T-t}$ . The circular fibre cross-section FRP composite specimens subjected to longitudinal tensile loading underwent catastrophic failure due to multiple fibre breakage and transverse matrix cracking, indicating strong fibre-matrix interfacial bonding, immediately after the linear load-displacement plot reached its peak load – the fracture surfaces indicated brittle failure. Such a failure mode has also been reported in other literatures [173, 174] resulting in fibre bundle pull-out [169] because the interfacial bond characteristics control the interlaminar shear and tensile strength [175]. The other two types of fibres experienced progressive fibre breakage and longitudinal matrix cracking producing splitting, as has been previously observed by Hayashi [176], because of poor structural integrity due to a lack of matrix surrounding the fibres induced by the applied compressive pressure during autoclave curing. Such a failure mechanism resulted in ‘broom-like’ failure. Different topographic views were observed on the failure surfaces on the specimens subjected to transverse tensile loading. The circular fibre cross-section FRP specimens exhibited flat fracture surfaces with some matrix stuck on the fibre indicating strong fibre-matrix interfacial bonding producing matrix cracking in the fibre longitudinal direction. Unlike the aforementioned FRP specimens, the other two types of specimens showed matrix channels on the fracture surfaces indicating debonding along the fibre-matrix interface.

Thomason [160] investigated the effect of fibre diameter and fibre aspect ratio on the properties of discontinuous E-glass fibre-reinforced polyamide 6,6

(PA6,6) produced by injection moulding. E-glass fibres of four different diameters, *i.e.*, 10, 11, 14 and 17  $\mu\text{m}$ , were chopped into  $\sim 3.8$  mm lengths. Pre-dried PA6,6 pellets were dry-blended with chopped E-glass prior to being fed into an extruder for injection moulding. Thomason observed that increasing the fibre diameter resulted in slight decreases in elastic modulus, strength and strain to failure.

Wonderly *et al.* [83], in 2005, investigated the mechanical properties of knitted E-glass fabric/vinylester composites. Longitudinal tensile testing was carried out in accordance with ASTM D3039 [172] and open hole longitudinal tensile testing was according to ASTM D5766 standards, while ASTM C297 was employed for transverse tensile tests. All specimens contained end tabs of  $\pm 45^\circ$  glass fibre-reinforced vinyl ester composites glued onto their gripped areas, with ‘brooming’ being observed during failure, which represents longitudinal matrix cracking and possibly fibre-matrix debonding, failure similar to those reported by Deng and colleagues [107], with the average failure stress being presented in Table 2.11. They also found that the longitudinal tensile strength of the GFRP specimens, for both the solid and open hole cases, is lower than that of the CFRP specimens, whereas the transverse tensile strength of the GFRP specimens is higher than that of CFRP specimens. This phenomenon may be attributed to the fact that longitudinal properties are fibre-dominated [162] whilst transverse properties are matrix-dominated [177].

Thomason [159] recently reported that the tensile modulus of chopped glass fibre/polyamide 6.6 composite containing between 0-50 wt.% of glass fibre of various diameters, *i.e.*, 10, 14 and 17  $\mu\text{m}$  (similar to the case mentioned earlier), is higher than its flexural modulus, with the fabrication and testing procedure being identical to that outlined in reference [160]. In addition to finding that the tensile modulus, which is fibre-dominated [162], is higher than the flexural modulus, Thomason also noted both properties to be more sensitive to fibre content in comparison to fibre length or fibre diameter. In addition, shorter fibre composites lost more of their elastic modulus with a decrease of matrix modulus compared to longer fibre composites. Thomason also observed that, for injection moulded thermoplastic matrix composites, fibre content can be increased by increasing



moulding die diameter while keeping fibre diameter constant, whilst the residual fibre length decreased, which led to a decrease in mechanical properties [170, 178], with increasing fibre content.

The discussion in the previous paragraphs can be summarised as follows. There are some factors that control the tensile properties of GFRP composites, *i.e.*, fibre coating that leads to fibre-matrix interfacial characteristics [134], fibre diameter [159, 160], length and content [159]. Unlike the longitudinal tensile properties of GFRP composites, transverse tensile properties are sensitive to fibre cross-sectional aspect ratio [107]. Deng also pointed out that the longitudinal tensile failure mode is also influenced by fibre cross-sectional aspect ratio and he observed that GFRP specimens underwent catastrophic failure showing fibre breakage and transverse matrix cracking [107], whereas Wonderly [83] observed that longitudinally tensile loaded specimens failed by longitudinal matrix cracking leading to splitting. Inline with transverse tensile properties, the transverse tensile failure mode is also influenced by fibre cross-sectional aspect ratio and GFRP specimens were noted to transversely fail due to matrix failure in the fibre direction [107].

#### 2.5.1.2. Compressive properties

Sigley and colleagues [179] reported their work on unidirectional E-glass fibre-reinforced talc-filled or calcium carbide-filled polyester composites, containing 52% of fibre, under hydrostatic pressure subjected to axial compressive loading. They observed that failure initiated with kinking of fibre bundles, instead of individual fibre failure due to the inhomogeneous distribution of fibres, followed by debonding of fibre bundles controlled by the resin transverse tensile strain. Material debris and pieces of fibres were found at the fracture surfaces. Fibre-matrix interfacial debonding, as indicated by clean surfaces of broken fibres, was also noticed at the edges of kink bands. Up to a certain limit, atmospheric hydrostatic pressure increased the stress at both the proportional limit and failure, but a change of failure mode with the increase of hydrostatic pressure was not observed.

In 1992, Hamada and co-workers [134] reported their work on woven cloth E-glass/epoxy composite tubes subjected to compressive loading. Aluminium tabs were glued onto the gripped areas of the specimens. They found that the compressive strength varies from ~27% to ~29% of tensile strength depending on the fibre surface treatment. Compressive properties were influenced by the fibre surface coating, with the properties of amino-silane coated glass fibre/epoxy samples being higher than those of acryl-silane coated. Both groups of samples exhibited similar load-displacement plots, with the load increasing with the increase of displacement up to a certain displacement and then fluctuating within a certain range indicating fracture propagation. The amino-silane treated fibre/epoxy samples failed by splaying crushing with fronds being generated inward and outward of the wall, while the acryl-silane treated samples failed by fragmentation crushing with rings of failure being generated at the failure area.

Budiansky and his colleagues pointed out that FRP composites subjected to compressive loading mainly failed by plastic kinking which is strongly controlled by initial fibre misalignment [180, 181] and the shear yield strength of the composites [181].

Lee and colleagues [166, 182] reported that low volume fraction,  $V_f \leq 30\%$ , unidirectional GFRP composites under compressive loading failed by splitting, and by combined failure modes of splitting and kinking for higher  $V_f$ . Later, a study on the splitting failure mode of E-glass fibre/vinyl ester composites under combined compressive and shear loading was carried out by Yerramalli and Waas in 2003 [183]. Specimens of  $d \times l = 6.7 \text{ mm} \times 63.5 \text{ mm}$  with a compressive gauge length of  $l_g = 12.7 \text{ mm}$  were loaded under proportionally combined compressive and shear loading. They observed that under high cross-head translation speed-to-rotational speed ratios, the specimens failed by combined splitting and kinking, with extensive fibre brooming being more profound in the splitting region. Another finding was that compressive strength decreased with the increase of shear stress.

The compressive strength of knitted glass fabric-reinforced vinyl ester composites have been reported by Wonderly *et al.* [83]. The compressive tests

were carried out according to ASTM D6641, while open hole compressive specimens were tested in accordance with the Northrop Grumman standard due to its more consistent results. All specimens contained end tabs of  $\pm 45^\circ$  glass fibre-reinforced vinyl ester composites glued onto their gripped areas. They found that compressive strength was significantly lower than tensile strength, *i.e.*  $\sim 73\%$  of tensile strength for solid specimens, and  $\sim 66\%$  for open hole specimens. Contrary to the trend noted for tensile strength, the compressive strength of GFRP specimens was higher than that of CFRP specimens,  $396.2 \pm 20.3$  MPa compared to  $328.0 \pm 37.9$  MPa for GFRP and CFRP specimens, respectively. The data also showed the strengths of GFRP specimens to be spread over a narrower range in comparison to those of CFRP specimens.

Wong *et al.* [184] investigated the behaviour of E-glass fibre-reinforced polyester C-shaped composite short columns at elevated temperature. The temperatures were 20 °C, 60 °C, 90 °C, 120 °C, 150 °C, 200 °C, and 250 °C, while the size of the C-channel was 100 mm flange  $\times$  30mm web  $\times$  4mm wall thickness, and the column high being 30 mm. They found that compressive mechanical properties of the specimens dropped sharply at the heat distortion temperature of the resin. Above the heat distortion temperature, these properties were resin dominated due to resin softening effects at high temperature. At room temperature up to approximately the heat distortion temperature, specimens showed local buckling then failed in an explosive manner, which may indicate crushing, while at higher temperature they showed a combination of local crushing and local buckling and bending.

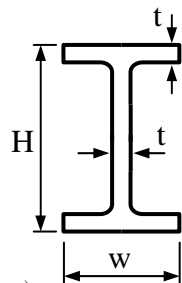
**Table 2.8.** Average compressive mechanical properties of E-glass/polyester C-channel composites at elevated temperatures [184]<sup>\*)</sup>

Compressive properties	Temperature (°C)						
	20	60	90	120	150	200	250
Strength (MPa)	282.20	177.72	87.49	45.61	31.68	30.39	22.58
Modulus (GPa)	22.25	12.90	15.60	10.00	7.50	6.70	6.60

<sup>\*)</sup>Summarised from Tables 2 and 3.

Khalid and colleagues [19] reported an investigation on woven fabric E-glass/epoxy composite I-beams of different flange and web thicknesses, *i.e.* 3.5, 4.5, 5.5 and 6.5 mm, with a constant flange width (77 mm), beam depth (125 mm), and specimen length of 250 mm subjected to compressive loading. They reported that the first crushing load and amount of absorbed energy increased with the increase of both flange and web thicknesses of the beam. Significant increases of the cross-sectional area, as presented in Table 2.9 below, may be responsible for the increase of the first crushing load, although it is in a linear relationship. The increase of compressive strength, the last column of Table 2.9, may be caused by an increase of fibre volume fraction as also reported by Algood and his colleagues [163]. It can be seen in the third column that the increase of flange and web thicknesses were not as linear as the increase of the number of prepreg layers, *i.e.*, 4, 6, 8 and 10, while the increase of flange and web thicknesses did not significantly influence the minimum first moment of inertia of the cross sectional area (fourth column of Table 2.9).

**Table 2.9.** Compressive strength calculation for Khalid *et al.*, 2005 [19]



Dimensions (mm)			Area, $A$ (mm <sup>2</sup> )	$I_{min}$ (mm <sup>4</sup> )	Crushing load (kN)	Compress- ive strength, $\sigma_c$ (MPa)
$H$	$w$	$t$				
125	77	3.5	952	3,604,889	36.9565	38.82
125	77	4.5	1,215	3,663,260	66.6667	54.87
125	77	5.5	1,474	3,705,019	142.3913	96.60
125	77	6.5	1,729	3,773,117	230.4348	133.28

<sup>a)</sup>Fillet areas are neglected

<sup>b)</sup>Approximated from Figure 4 of Ref. [19].

It can be concluded from the previously reported findings that the compressive strength of a typical GFRP composite is significantly lower than its respective tensile strength [83, 134]. Compressive properties of GFRP composites are influenced by matrix properties [179, 181], the degree of fibre misalignment [180, 181], fibre-matrix interfacial characteristics [134], fibre volume fraction [20,

195, 196] and temperature [184]. The compressive failure mode is mostly kinking [204, 214, 215] initiated by local buckling, and then followed by fibre crushing [134, 184]. Lee and colleagues [166, 182] and Yerramalli and colleagues [185] further revealed that this is valid for high  $V_f$ , while a splitting mode is more dominant for low  $V_f$ .

#### 2.5.1.3. Flexural properties

In addition to tensile and compressive moduli and strengths, Hamada and co-workers [134] investigated three-point bend loaded properties of woven cloth E-glass/epoxy composite plates employing a span-to-depth ratio,  $S/d$ , of 16. They found that the tensile and compressive strength of the composites being tested were significantly lower than the flexural strength, while the tensile modulus was much higher than the flexural modulus. Flexural modulus and flexural strength were influenced by the fibre surface coating, with those of amino-silane coated glass fibre/epoxy samples being 27% and 44%, respectively, higher than those of acryl-silane coated, see Table 2.10. The specimens showed fibre-matrix debonding failure at both the compressive and tensile sides of the beams.

Chen *et al.* (1994) [186] reported their work on flexural failure mechanisms of unidirectional E-glass fibre-reinforced soft thermoplastic matrix composites, where they utilised three different thermoplastic matrices possessing three distinct different elastic moduli, *i.e.*, 48 MPa, 207 MPa and 516 MPa. Testing was carried out under four-point bend (FPB) loading configuration with loading spans equal to one-third of the support span. They found that a stiffer matrix produces significantly higher flexural strength (Table 2.10), and concluded that flexural strength was mainly controlled by composite shear strength and fibre-matrix interfacial characteristics. All failures were initiated at the compressive sides producing in-plane and out-of-plane fibre microbuckling and then followed by local buckling. Significant differences of matrix stiffness also lead to different failure modes, where the most flexible matrix produced catastrophic failure with fibre microbuckling while the stiffest matrix produced gradual failure due to the accumulation of fibre microbuckling, surface delamination and fibre breakage.

Gilchrist *et al.* (1996) [108, 187] working on different lay-ups of E-glass/epoxy composite I-beams, notched with circular cut-out and unnotched, loaded under FPB reported that the presence of circular cut-out in the webs reduced the maximum load by approximately 25% and changed the failure initiation point. Failure of unnotched beams was initiated at the compressive sides, as had been reported by Chen *et al.* [186] for GFRP composite beams, at approximately 50% of maximum load, while that of the notched beams was initiated from a shear-loaded circular cut-out in the web [108] showing matrix cracking due to local tensile stresses [187]. The damaged compressive flange exhibited local buckling and delamination [187] while the tension flange damage was very minor [108]. In addition, upon calculation of the flexural modulus and strength, it was found that flexural modulus was higher than tensile modulus, but flexural strength was lower than tensile strength. Such lower flexural strength may be caused by the fact that failure was initiated at the compression side, with the compressive strength generally being much lower than tensile strength.

Deng and colleagues (1999) [107] studied the longitudinal and transverse flexural properties of GFRP composites whose physical description is as given in the first paragraph of sub-section 2.5.1.1. Flexural characterisation was carried out in three-point bending (TPB) tests in accordance with ASTM D790 [188]. A fixed support span of 40 mm was used, such that specimens contained different fibre cross-sectional geometries due to the different thickness from specimen to specimen. They reported that longitudinal and transverse flexural strength,  $\sigma_{L-fl}$  and  $\sigma_{T-fl}$ , and modulus,  $E_{L-fl}$  and  $E_{T-fl}$ , are slightly affected by fibre cross-sectional aspect ratio. Larger cross-sectional aspect ratios resulted in lower  $\sigma_{L-fl}$  and  $E_{L-fl}$ , while  $\sigma_{T-fl}$  and  $E_{T-fl}$  are the lowest in comparison with the respective values of those of the circular and ‘peanut’-shaped fibre cross-sections. Stress distributions in a beam which linearly varies along the span of the beam may be responsible for the higher flexural strength and strain-to-failure in comparison to their respective transverse tensile and strain-to-failure. The top surfaces of the specimens subjected to longitudinal flexural loading experienced compressive loading while the other surfaces underwent tensile loading. Apart from the oval fibre cross section, the compression sides failed by local buckling followed by kink band formations as

have been discussed in sub-section 2.5.1.2, while the other side failed by tension, exhibiting fibre-matrix debonding or splitting and fibre breakage as have been discussed in sub-section 2.5.1.1. The ‘peanut’-shaped fibre cross-section specimens suffered much less compressive failure at their top surfaces but more tensile failure at their bottom surfaces in comparison with the circular fibre cross-section specimens. Perhaps surprisingly, the oval fibre cross-section specimens showed only very minor, even negligible, compressive failure at their top surfaces accompanied by excessive fibre-matrix interface splitting at their bottom surfaces. The transverse flexural failure surfaces exhibited transverse matrix cracking, inferring that the transverse modulus, strength and strain to failure are strongly influenced by matrix properties and fibre-matrix interfacial strength. For all the cross-sectional geometries, they found that the flexural strength was higher than tensile strength, but apart from the circular fibre cross-section composites, the composite flexural modulus was lower than tensile modulus as had been reported by Hamada *et al.* [134].

The effect of fibre pre-stressing on flexural properties, evaluated under FPB loading configuration, for unidirectional [189] E-glass fibre-reinforced epoxy composites was reported by Motahhari and Cameron (1999) [190]. The prestressing was applied during the whole cycle of fabrication processing. They reported that there is an optimum value, at which exists an optimum synergetic effect of the degree of ‘loose’ fibre and curing residual stress, of pre-stressing level, and flexural modulus and flexural can be increased by up to 33%. These increases can be attributed to the fact that upon prestressing, the fibres simultaneously react to external loading such that they also tend to break simultaneously resulting in lower strain on complete fracture as shown by the force-deflection curve.

Srivastava [28] investigated the effect of water immersion on interlaminar shear strength (ILSS), flexural strength under TPB loading, and impact resistance of E-glass fabric reinforced particle-filled vinyl ester composites. Polyethylene (PE) particles of 40- $\mu\text{m}$  size and 10- $\mu\text{m}$  size aluminium tri-hydrate (ATH) particles have been utilised to improve matrix properties prior to fibre embedment. He reported that, before being immersed in water, ATH-filled matrix composite

specimens exhibited increase of up to 40% of flexural strength and up to 33% of ILSS, while PE-filled matrix composite specimens produced only insignificant increase in both flexural strength and ILSS in comparison with un-filled matrix composite specimens. In addition, both flexural strength and ILSS increased with the increase of immerse time because water intake increases the formation of sub-microcracking and energy absorption.

Thomason (2000) observed that elastic modulus, strength and strain to failure of discontinuous E-glass fibre-reinforced polyamide 6,6 decreased with the increase of fibre diameter [160].

O'Brien and Krueger (2003) [167] carried out finite element analysis on unidirectional GFRP composite beams of various span-to-depth ratios subjected to TPB and FPB loading and compared the results with those calculated based on beam theory. They reported that the 2D plain-strain and plain-stress models under TPB loading configuration for both linear and geometric non-linear analyses as well as under FPB loading configuration for 2D geometric non-linear analysis gave slightly lower maximum tensile stresses right under the loading nose when compared to those predicted by beam theory. Smaller span-to-depth ratios resulted in larger discrepancies. For the FPB loading configuration for 2D geometric non-linear analysis, the result was considerably close to each other apart from those right under the loading nose. This may due to the Saint-Venant effect [191, 192] (pp. 240 and 34, respectively). They also revealed that the beam theory prediction on maximum tensile stress in bending was more accurate compared to 2D finite element analysis, and for 3D finite element analysis, the larger span-to-depth ratio as well as larger beam width results in more accurate predictions of beam theory.

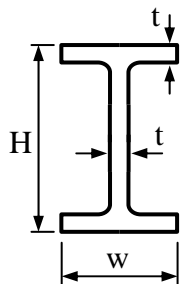
Hagstrand *et al.* (2005) [193] studying unidirectional glass fibre-reinforced polypropylene thermoplastic composites found that the presence of voids in composite materials decreases flexural modulus and flexural strength, but it increases beam stiffness. In addition, flexural failure loads also increase slightly with the increase of void content up to 14%. The composites were produced by compression moulding, and the specimens were tested in FPB loading according to ASTM D790 [188] with a loading span of 16 mm, support span of 48 mm, and span-to-depth ratio of 19.92 to 23.08 depending upon the depth of the beam.



Specimens mostly failed between the two loading noses and showing compressive buckling and interlaminar shear delamination.

Khalid and colleagues [19] reported an investigation concerning GFRP composite I-beams subjected to three- and four-point bend loading. The physical description of the beams is as given in sub-section 2.5.1.2, except that the length of the beams was 500 mm with a constant support span of 450 mm. Instead of in terms of stress-strain, the results were presented as load-displacement and bending moment-rotation angle terms. They reported that the first crushing loads of four-point bend (FPB) tests are higher than those of three-point bend (TPB) tests, however, apart from the specimens containing 8-layer thick flange and webs, the respective flexural strengths of FPB tests are lower than those of TPB tests. Such lower flexural strength may be caused by the fact that in FPB cases, there were two loading noses, and that the first failure, which often happened at the compressive side right under the loading noses [108], were in two separate places compared to only one single area for the TPB cases. Therefore, failure was initiated in two different places.

**Table 2.10.** Flexural strength calculation from Khalid *et al.*, 2005 [19]



Dimensions (mm)			$I_y$ (mm <sup>4</sup> ) <sup>a)</sup>	TPB test		FPB test	
$H$	$w$	$t$		Max load, $F$ (kN) <sup>b)</sup>	Strength, $\sigma_f$ (MPa)	Max load, $F$ (kN) <sup>b)</sup>	Strength, $\sigma_f$ (MPa)
125	77	3.5	2,468,981	7.108	20.24	7.941	15.08
125	77	4.5	3,102,139	12.530	28.40	17.353	26.22
125	77	5.5	3,705,019	16.747	31.78	27.500	34.79
125	77	6.5	4,278,600	27.470	45.14	35.000	38.34

<sup>a)</sup>Fillet areas are neglected

<sup>b)</sup>Approximated from Figures 6 and 7 of Ref. [19].

Flexural properties of GFRP composites were also investigated by Cao and Cameron [164]. Untreated and treated E-glass fibre was utilised to reinforce epoxy matrix material. Three different treatments, *i.e.* prestressing, silica particle modification and combination of prestressing and silica particle modification,

were applied onto the fibre surface prior to embedment into epoxy matrix. Flexural characterisation was carried out in TPB loading in accordance with ASTM D790 [188]. They revealed that the flexural properties can be improved by prestressing, silica particle coating of glass fibres, and the combination of both treatments. As presented in Table 2.10, prestressing can improve the flexural modulus and flexural strength by ~29.4% and ~34.7%, respectively, while silica particle coating can improve these properties by ~27.8% and ~11.4%, respectively. Both treatments, when combined, can improve flexural modulus and flexural strength by ~74.7% and ~87.5%, respectively.

The following conclusions can be drawn from the above discussion. Hamada *et al.* [134] for fibre cloth, Deng *et al.* [107] for unidirectional fibre and Thomason [160] for discontinuous fibre reinforced polymer composites independently reported that their composites exhibited higher tensile modulus with lower tensile strength in comparison with flexural modulus and flexural strength, respectively. Hagstrand *et al.* [193] found the same phenomenon for modulus but the opposite effect for strength, while Gilchrist *et al.* [108] revealed in the contrary for both tensile and modulus. Compressive strength is much lower than flexural strength [134]. In addition to fibre content, flexural strength and flexural modulus of GFRP composites are influenced by fibre diameter [160], fibre-matrix interfacial properties [134, 164], matrix properties and composite shear strength [28, 186], fibre prestressing level [164, 190], fabrication parameters [190] which influence composite microstructure, moisture content [28], void content [193], span-to-depth ratio and specimen width [167], and loading configuration [19] where FPB shows a higher crushing load but, in fact, lower flexural modulus and flexural strength compared to TPB. Failure was initiated at the compressive side of the beams with the failure mode being influenced by matrix properties [186]. Fibre-matrix debonding may be observed at both the compressive and tensile sides of the failed specimens [134, 186], fibre microbuckling [186], interlaminar delamination or splitting [193].

**Table 2.11.** Typical properties of GFRP composites

First author, year	Fibre characteristics	Matrix type	$V_f$ (%)	Elastic modulus, $E$ (GPa)			Strength, $\sigma$ (MPa)			Strain to failure, $\epsilon$ (%) <sup>a)</sup>	Dominant failure mode		
				$E_t$	$E_c$	$E_{fl}$	$\sigma_t$	$\sigma_c$	$\sigma_{fl}$		Tension	Compression	Flexure
Deng, 1999	UD, 0°, ØC	Epoxy	69.20	49.9		50.2	1,056.8		1,653.7	2.18, 3.34	FB, T-MC, Db		K / FB, T-MC
	UD, 0°, ØP	Epoxy	68.20	51.0		48.1	1,089.4		1,564.7	2.36, 3.55	Db, L-MC, SR		Less K / Db, FB
	UD, 0°, ØO	Epoxy	69.30	49.7		47.0	1,080.6		1,354.5	2.33, 3.66	Db, L-MC, SR		--- / Db, L-MC
	UD, 90°, ØC	Epoxy	69.80	18.3		17.0	40.7		92.9	0.26, 0.57	Db, T-MC, SF		T-MC
	UD, 90°, ØP	Epoxy	64.20	11.8		12.8	37.3		84.2	0.38, 0.66	Db, T-MC, SR		T-MC
	UD, 90°, ØO	Epoxy	62.00	15.5		13.2	45.4		92.2	0.32, 0.81	Db, T-MC, SR		T-MC
Thomason, 2000 <sup>a)</sup>	Dc, d10	PP6,6	15.90	9.7		9.2	184.1		286.5	2.83, N/A	N/A		N/A
	Dc, d11	PP6,6	15.90	9.8		9.2	182.9		285.4	2.80, N/A	N/A		N/A
	Dc, d14	PP6,6	15.90	9.6		9.3	173.7		269.8	2.70, N/A	N/A		N/A
	Dc, d17	PP6,6	15.90	9.5		9.0	164.0		249.3	2.49, N/A	N/A		N/A
Wonderly, 2005, OH: d/w = 6/38	E-g, UD, 0°	VE	N/A				544.0	396.2			Db, T-MC	Db, K	
	E-g, UD, 0°, OH	VE	N/A				367.4	238.9			Db, T-MC	Db, K	
	E-g, UD, 90°	VE	N/A				23.6				T-MC		
Khalid, 2005 <sup>b)</sup>	UD, I-beam, 4 layers	Epoxy	N/A					38.8	20.2		N/A	N/A	
	6 layers	Epoxy	N/A					54.9	28.4		N/A	N/A	
	8 layers	Epoxy	N/A					96.6	31.8		N/A	N/A	
	10 layers	Epoxy	N/A					133.3	45.1		N/A	N/A	

*Continued*

**Table 2.11. *Continued***

First author, year	Fibre characteristics	Matrix type	$V_f$ (%)	Elastic modulus, $E$ (GPa)			Strength, $\sigma$ (MPa)			Strain to failure, $\epsilon$ (%) <sup>a</sup>	Dominant failure mode		
				$E_t$	$E_c$	$E_{fl}$	$\sigma_t$	$\sigma_c$	$\sigma_{fl}$		Tension	Compression	Flexure
Sigley, 1992	E-g 28x2400, UD, 0°	talc PE	52.00					780.0				K in & out, SF	
	E-g 18x2400, UD, 0°	cc PE	52.00					380.0				K in & out, SF	
	E-g 9x4800, UD, 0°	cc PE	52.00					450.0				K in & out, SF	
Hamada, 1992	Ac-s E-g cloth	Epoxy	42.00	20.5		11.5	315.6	90.2	422.0			Fragmentation	Db in both sides
	Am-s E-g cloth	Epoxy	42.00	21.2		14.6	403.1	108.4	608.1			Splaying	Db in both sides
Lee, 1999	E-g, UD, 0°	VE	0.00		3.7							Dd or splitting	
	E-g, UD, 0°	VE	10-30									Dd or splitting	
	E-g, UD, 0°	VE	40-60									Db and K	
Yerramalli, 2003	E-g, UD, 0°	VE	50.00									Db then K	
Wong, 2004	E-g, UD, 0°, C-shaped,	20 °C PE	N/A		22.3			282.2					
		60 °C PE	N/A		12.9			177.7					
		90 °C PE	N/A		15.6			87.5					
		120 °C PE	N/A		10.0			45.6					
		150 °C PE	N/A		7.5			31.7					
		200 °C PE	N/A		6.7			30.4					
		250 °C PE	N/A		6.6			22.6					
	90°, 20 °C	PE	N/A		7.4								

***Continued***

**Table 2.11. *Continued***

First author, year	Fibre characteristics	Matrix type	$V_f$ (%)	Elastic modulus, $E$ (GPa)			Strength, $\sigma$ (MPa)			Strain to failure, $\epsilon$ (%) <sup>a</sup>	Dominant failure mode		
				$E_t$	$E_c$	$E_{fl}$	$\sigma_t$	$\sigma_c$	$\sigma_{fl}$		Tension	Compression	Flexure
Chen, 1994	E-g, UD, 0°/Thrplast	H4056 H5526 H7246	44.60 45.00 43.20						41.0 247.0 355.0				MB, K MB, K, FB MB, K, Db, DI
Gilchrist, 1996 <sup>c</sup>  notched:	E-g, UD, 0°	Epoxy	N/A	45.4			1,049.0			1.27/-1.38			Compr FBu, DI
	E-g, UD, 90°	Epoxy	N/A	15.2			46.5						Compr FBu, DI
	E-g, UD, 0°, ±45°	Epoxy	N/A	26.7		38.6	432.8		278.8				Compr FBu, DI
	E-g, UD, 0°	Epoxy	N/A										Compr FBu, DI
	E-g, UD, 90°	Epoxy	N/A										Compr FBu, DI
	E-g, UD, 0°, ±45°	Epoxy	N/A							1.40/-1.38			Compr FBu, DI
Srivastava, 1999 <sup>d</sup>	E-g, farbic	VE	N/A						320.0				
		VE-ATH	N/A						451.0				
		VE-PE	N/A						330.0				
O'Brein, 2003	S2-g, UD, 0°	Epoxy	N/A	47.7									
	S2-g, UD, 90°	Epoxy	N/A	12.3									
Hagstrand, 2005	UD, 0°	PP	N/A	28.0		24.0	700.0		470.0				comp, int lam DI
Cao, 2006 <sup>e</sup>	E-g, UD, 0°	Epoxy	20.00			13.0			283.5				comp, int lam DI
	E-g prestr15, UD, 0°	Epoxy	20.00			16.8			382.0				comp, int lam DI
	E-g-Sil mod, UD, 0°	Epoxy	20.00			16.6			315.8				comp, int lam DI

*Continued*

**Table 2.11.** *Continued*

First author, year	Fibre characteristics	Matrix type	$V_f$ (%)	Elastic modulus, $E$ (GPa)			Strength, $\sigma$ (MPa)			Strain to failure, $\epsilon$ (%) <sup>a)</sup>	Dominant failure mode		
				$E_t$	$E_c$	$E_{fl}$	$\sigma_t$	$\sigma_c$	$\sigma_{fl}$		Tension	Compression	Flexure
Cao, 2006 ( <i>Continued</i> )	E-g prestr-Sil,UD,0°	Epoxy	20.00			22.6			531.7				comp, int lam DI
	E-g, UD, 0°	Epoxy	30.00			19.0			468.8				comp, int lam DI
	E-g-SiO <sub>2</sub> mod,UD,0°	Epoxy	30.00			24.6			502.8				comp, int lam DI
	E-g prestr-Sil,UD,0°	Epoxy	25.00			28.7			657.7				comp, int lam DI

**Notes:**

Subscripts: t = tension, c = compression, fl = flexural.

Fibre characteristics: Ac-s = acrylo-silane coated, Am-s = amino-silane coated, Dc = randomly oriented discontinuous fibre, KF = knitted fabric, UD = unidirectional, 0° = longitudinal direction, 90° = transverse direction,  $\delta$  = fibre diameter ( $\mu\text{m}$ ), L = fibre length (mm), OH = open hole,  $\varnothing$ C = circular fibre cross section,  $\varnothing$ P = 'peanut'-shaped fibre cross section,  $\varnothing$ O = oval fibre cross section.

Matrix type: cc = calcium carbonate-filled, PA = polyamide, PC = polycarbonate, PE = polyester, PEt = polyethylene, PP = polypropylene, PU = polyurethane, talc = talc-filled, VE = vinylester.

Strain to failure: <sup>a)</sup> respective values of the utilised test methods.

Dominant failure mode: comp = compressive, Db = fibre-matrix interfacial debonding or splitting, DI = delamination, FB = fibre breakage, Fbu = flange buckling, FP = fibre pull-out, int lam DI = interlaminar delamination, K = kinking, L = longitudinal direction, MB = microbuckling, MC = matrix cracking, SF = surface is flat, SR = surface is rough, T = transverse direction.

<sup>a)</sup> Considering  $\rho_E = 2.58$  (g/cm<sup>3</sup>) [103],  $\rho_{S2} = 2.46$  (g/cm<sup>3</sup>) [103], and  $\rho_{PA6,6} = 1.14$  [106] (p. A5), fibre content of 30 wt.% is equivalent to  $V_f = 15.92$  %.

<sup>b)</sup> Compressive properties calculated based the available load, geometry and dimension data. Flexural strength for TPB test.

<sup>c)</sup>Moduli were calculated from Figure 11, and strength were calculated from Table 2 of Ref. [108].

<sup>d)</sup>Approximated from Figure 2 of Ref. [28].

<sup>e)</sup>Numerical values were approximated from Figures 3, 4, 6, 7, 9, and 10 of Ref. [164].

#### 2.5.1.4. GFRP summary

The compressive strength of GFRP composites is commonly much lower than their tensile strength [83, 134], which is a drawback of their utilisation for structural materials. Some typical GFRP composites exhibit lower flexural modulus combined with higher flexural strength [110, 140, 169], some others possess both lower flexural modulus and strength [193], and some others exhibit higher flexural modulus with lower flexural strength [108].

*Mechanical properties* of GFRP composites are influenced by a number of factors related to their micro- and macro-structures. Tensile properties are sensitive to fibre-matrix interfacial properties [134], as well as fibre diameter [159, 160], length and content [159], while transverse tensile properties are also influenced by fibre cross-sectional aspect ratio [107]. In addition to fibre content [19, 163, 183] and temperature [184], compressive properties are controlled by matrix properties [179, 181], degree of fibre misalignment [180, 181], fibre-matrix interfacial properties [134]. Flexural modulus and strength are influenced by fibre diameter [160], fibre prestressing level [164, 190], fabrication parameters [190], fibre-matrix interfacial properties [134, 164], matrix properties and composite shear strength [28, 186], moisture content [28], void content [193], span-to-depth ratio and specimen width [167], and loading configuration [19].

Different longitudinal failure modes have been reported for GFRP composites subjected to tensile loading, *i.e.*, catastrophic failure exhibits fibre breakage and transverse matrix cracking [107], and longitudinal matrix cracking leading to splitting [83], while transverse tensile failure shows matrix failure in the fibre direction [107]. Compressive failure modes can be divided into two categories, *i.e.*, fibre kinking [204, 214, 215] initiated by fibre local buckling and followed by crushing [145, 205] for high  $V_f$  [179, 188, 200], and longitudinal splitting for  $V_f \leq 30\%$  [179, 188, 200]. Flexural failure modes of GFRP composites subjected to flexural loading can be fibre-matrix debonding at both the tension and compression sides [143, 202], fibre micro buckling at the compression side [186], and combined with delamination or splitting following buckling [193]. Mechanical behaviour discussed in this section, 2.5.1, have been summarised in Table 2.11.



### 2.5.2. Carbon Fibre-Reinforced Polymer (CFRP) Composites

Amongst the reasons of superiority of CFRP composites over other structural materials for aerospace applications is their high specific strength and stiffness [194]. Most matrices incorporated with carbon fibres to produce CFRP composites have tended to be epoxies [151, 177, 195-201] and other thermosetting resins, *i.e.*, polyester [185, 202], vinylester [89, 114, 194, 203, 232, 233], phenolic [196], and bismaleimide [203]. Carbon fibres have also been utilised to reinforce thermoplastic matrices, such as polyphenylene sulphide (PPS) [204], nylons 6 [42, 204] and 6,6 [42], and polyetherether ketone (PEEK) [205]. For high-temperature applications, carbon fibres have been embedded in carbon [206] and graphite [83, 108, 167, 207] matrices. Different fibre architectures of continuous carbon fibres have been employed in producing CFRP composites, *e.g.*, unidirectional [86, 111, 172, 178, 181, 193, 203, 204, 206, 207, 209, 211, 215, 218], discontinuous [197], unidirectional stitched, cross ply, plain weave, woven roving, woven fabric [42, 196], knitted fabric [83], and 3D braided [208].

Different mechanical properties of CFRP composites, *e.g.*, tension [42, 159, 208, 209, 211, 214, 218], compression [42, 181, 204, 207, 210, 214, 215, 217-220], flexure [108, 119, 151, 167, 177, 196, 197, 199], torsion or shear [42, 151], and impact [206, 210], have been investigated and reported. Various methods and/or standards and specimen geometries were utilised to study a particular mechanical property.

#### 2.5.2.1. Tensile properties

Transverse properties of unidirectional CFRP composites have been reported by Rezaifard *et al.* [177]. They reported that transverse modulus and strength increased with an increase of fibre surface treatment up to a certain level, but not sensitive to fibre properties because they are fibre-dominated [162] as was also reported by Wonderly *et al.* [83] for glass fibre/vinylester composites.

Olivier and colleagues [151] investigated the effect of cure cycle pressure on void content, longitudinal and transverse tensile, and flexural properties of carbon

fibre/epoxy composites. They reported that void content decreased with the increase of cure pressure. In addition to this, they observed that longitudinal tensile modulus was not affected by void content, longitudinal tensile strength slightly decreased with an increase of void content, and both the transverse modulus and strength were severely affected by void content. As the matrix macro-structure is more severely impacted by the presence of voids when compared to the fibre, this result confirms that transverse properties are matrix-dominated [177] whereas longitudinal properties are fibre-dominated [162].

Wonderly *et al.* [83] investigated the mechanical properties of knitted E-glass fabric/vinyl ester composites. Tensile tests were carried out in accordance with ASTM D3039 [172], while open hole tensile specimens were tested according to ASTM D5766; all specimens contained end tabs of  $\pm 45^\circ$  glass fibre-reinforced vinyl ester composites glued onto their gripped areas. It was observed that CFRP specimens exhibited lateral failure close to the tabs, while the average tensile strength has been presented in Table 2.11. They also reported that longitudinal tensile strength for solid CFRP specimens is  $\sim 76\%$  higher than that of solid GFRP specimens, and that of open hole CFRP specimens is  $\sim 69\%$  higher than that of open hole GFRP specimens, whereas the transverse tensile strength of CFRP specimens is lower than that of GFRP specimens. This phenomenon may be attributed to the fact that the longitudinal tensile strength is fibre-dominated while transverse tensile strength is matrix-dominated, with the longitudinal tensile strength of carbon fibre, 4.9 GPa, being more than double compared to that of glass fibres, 2.4 GPa [83, 162, 177].

Oya and Hamada [119] reported that the lower the modulus, 410.6 GPa to 226.9 GPa, of CFRP composites, the higher their strain to failure, 0.32% to 0.98%. High tensile strength CFRP composites failed at even higher tensile strains, 1.78%. Most of their failed samples showed brooming failure incorporated with transverse matrix failure for lower strength specimens, and longitudinal matrix failure for higher strength specimens. Failure initiated in fibres due to the lower strain-to-failure of CF compared to that of the matrix. Strong fibre-matrix interfacial bonds will result in brittle fracture for low strength CF and brooming

for high strength CF, while weak interfacial bonds will lead to a brooming failure mode. Tensile mechanical properties have been presented in Table 2.12.

Oya and Hamada [204] also reported their work on carbon fibre-reinforced nylon6 and poly propylene sulphide (PPS). Although nylon6 is much tougher than PPS, both resultant composites exhibited very similar *axial* tensile behaviour showing slight slope increase of their stress-strain plots with an increase of strain. The nylon6 specimens showed a slightly lower axial tensile strength, but with wider scatter than PPS specimens. Such a lower axial tensile strength may be caused by lower tensile strength of the matrix. The scatter of mechanical properties was inline with the variation of fracture mode, *i.e.*, nylon6 specimens showing wider scatter exhibited a combination of transverse matrix failure with fibre breakage indicating the presence of strong fibre-matrix interfacial bonding and the brooming mode indicating weaker interface bonding, while the PPS specimens showed only a brooming failure mode. Unlike the *transversally*-loaded PPS specimens which failed in a brittle manner, the nylon6 specimens underwent plastic deformation prior to failure. Fracture surfaces of the nylon6 specimens exhibited matrix-covered fibres indicating strong fibre-matrix interfacial bonding leading to higher transverse strength, while those of PPS specimens are in the contrary. Such behaviour reveals that axial properties are matrix dominated, while transverse properties are also matrix dominated as have been reported in other work [83, 162, 177].

Fragmentation tests to investigate fibre fracture and fibre-matrix interfacial debonding of AS4 carbon fibre embedded in Shell Epon 828 epoxy resin has been reported by Kim and Nairn [201]. The behaviour of fibres embedded in a matrix is primarily influenced by inherent properties of the fibre, curing parameters, and fibre-matrix interface characteristics. At a certain strain level, the fibre starts to break leaving a gap between the two pieces and creating a debonding region in the surrounding breakage. Further increases of strain will generate other breakages along with their own new gaps and debonding regions until reaching saturation.

Tensile properties of carbon fibre reinforced polyamide6 and 6,6 thermoplastics of two different fibre architectures have been reported by Botelho

*et al.* [42]. They observed that damage development was primarily caused by fibre-matrix interface failure due to shear loading. Tensile mechanical properties of their specimens have been presented in Table 2.12. At the same fibre volume fraction, carbon fibre fabric/PA6,6 specimens were ~13% – ~38% stronger than carbon fibre fabric/PA6 specimens. There was no trend observed for tensile modulus in comparison between carbon fibre fabric/PA6,6 and carbon fibre fabric/PA6 specimens, as well as for the axial modulus of unidirectional fibre composite specimens, whereas the transverse tensile modulus of unidirectional carbon fibre/PA6,6 specimens were ~27% – ~36% higher than those of unidirectional carbon fibre/PA6 specimens. This might be caused by the existing stronger interfacial bond in PA6,6 composite specimens as confirmed by the micrographs of their fracture surface showing shorter fibre pull-out length in the PA6,6 composite specimen. Both groups of specimens showed linear axial tensile stress-axial tensile strain relationships to failure, whereas the transverse tensile stress-transverse tensile strain relationships showed a slightly decreasing slope with respect to the increase of strain. Matrix softening might be responsible for such a phenomenon [101] (p. 527). Most of the specimens, for both axial transverse tests, exhibited fibre pull-out modes upon failure, indicating that only weak fibre-matrix interfacial bonding existed at the interface. Their results on axial and transverse testings also confirmed that axial properties are fibre-dominated while transverse properties are matrix-dominated as has been reported in other work [204, 209].

The following conclusions can be drawn from the above findings and discussion. Comparing the axial and transverse test results leads to confirmation that axial properties are fibre-dominated while transverse properties are matrix-dominated [42, 204], as has been reported in elsewhere [83, 162, 177]. Following an initial breakage of a fibre, on the increase of strain level, new breakages will be generated along the fibre creating gaps between fibre pieces and fibre-matrix debonding regions in the surrounding gaps until reaching saturation [201]. Shear failure along the fibre-matrix interface indicates that loading is transferred from matrix into fibres via the interface in the form of shear loading [42]. The strength is closely related to fracture modes. Transverse matrix failure combined with fibre

breakage indicating excessively strong interface bonding leading to lower tensile strength, while brooming failure with longitudinal fibre-matrix debonding indicates weaker interfacial bonding leading higher tensile strength [177].

#### 2.5.2.2. Compressive properties

Jelf and Fleck [210] reported that the compressive strength of carbon fibre-reinforced epoxy composite tubes,  $V_f = 65\%$ , linearly decreased with an increase of applied combined shear stresses. This finding was later supported by finding of Vogler and Kyriakides [211] for AS4 carbon fibre-reinforced PEEK composites.

Axial compressive properties of unidirectional carbon fibre-reinforced epoxy composites has been reported by Oya and Hamada [119]. They found that the higher the compressive modulus the lower the compressive strength and strain to failure. Stress-strain relationships of the samples exhibited linearity almost up to failure, only small portions of the curve underwent ‘softening’. In comparison with tensile properties, compressive moduli were found to vary from 78.54% to 93.36% of the tensile modulus, while the compressive strength ranged from 28.34% to 53.38% of tensile strength. Two different failure modes were observed, *i.e.*, shear mode showing a fracture surface at a  $45^\circ$  angle to the fibre direction and mostly associated with low strength CFRP specimens, and transverse or crushing mode showing a fracture surface perpendicular to the fibre direction and associated with higher strength CFRP specimens.

In another paper [204] Oya and Hamada reported their work on carbon fibre-reinforced thermoplastics, *i.e.*, nylon6 and PPS. They observed that, for both groups of specimens subjected to compressive loading, the stress-strain relationship was linear up to failure, and both failed at almost the same magnitudes of strain-to-failure, strength, as well as exhibited very close magnitudes of modulus, presented in Table 2.12. Whilst strain-to-failure of the nylon6 matrix, 57.4%, is much higher than that of PPS matrix, 1.6%, it showed that the compressive properties are more fibre-dominated than matrix-dominated. They observed that most of the nylon6 specimens, 83.3%, failed in a shear mode, while almost half, 55.2%, of the PPS specimens failed in a transverse mode. They also

noticed that specimens which failed in a shear mode resulted in lower compressive strength in their group in comparison with those that failed in a transverse mode.

Experimental observation of Moran and Shih [205] confirmed that kink band formation in ductile matrix composites, in this particular case, an IM7 carbon fibre-reinforced PEEK composite, consist of three stages, *i.e.*, initial kinking, transitory kinking and band broadening. In the first stage, at a certain level of loading, fibres with micro-structure imperfections, such as curved or disoriented, will start to rotate and generate shear deformation of the matrix leading to non-linear stress-strain relationships up to its peak load. Further loading in the next step will drive kink band propagation across the specimen in combinations with a significant drop of load. Due to fibre rotation, its surrounding matrix experiences extreme shear straining, until it reaches its rotation limit. This will then be followed by a softer deformation mode of band broadening at considerably constant load until complete failure. They also predicted the magnitude of kink band angle between  $10^\circ - 35^\circ$ , and the magnitude of steady-state driving stress to be between 3 and 7 times the shear yield strength of the composite.

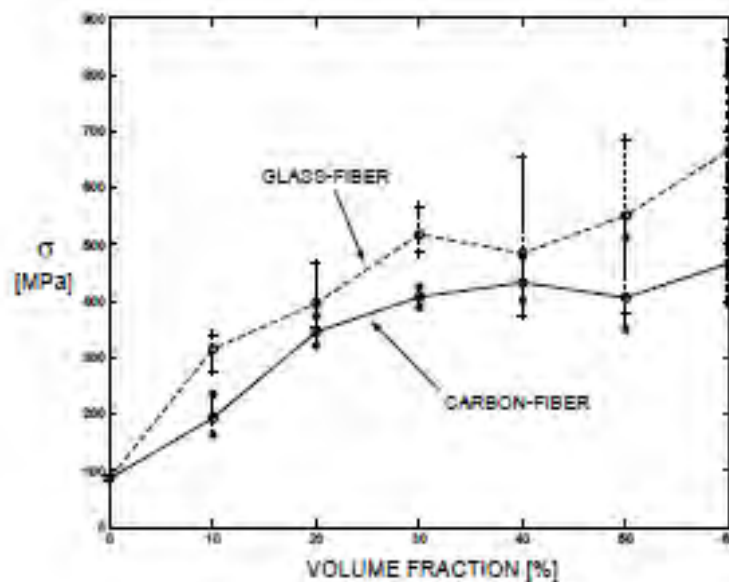


**Figure 2.18.** Compressive strength comparison between E-glass fibre/vinylester and IM7-12k carbon fibre/vinylester composites showing, within the range of given fibre volume fraction, that of the GFRP composite is higher than that of the CFRP composites [166].

Lee and colleagues (1999, 2000) [166, 182] observed that unidirectional carbon/epoxy composites subjected to compressive loading failed by kinking irrespective of  $V_f$ . Lee and Waas [166] concluded that compression test results with these specimens show that carbon fibre composites have lower compressive strengths than glass fibre composites, as presented in Figure 2.18.

Compressive properties in comparison with tensile properties of carbon fibre reinforced polyamide6 and 6,6 thermoplastics of two different fibre architectures have been reported by Botelho *et al.* [42]. They revealed that the carbon fabric-reinforced PA6,6 composite specimens presented ~7% – ~9% higher compressive strength compared to PA6 composite specimens of the same reinforcing materials. The compressive strength of woven fabric-reinforced polymer composites is significantly lower than their tensile strength which is later supported by Kawai and Koizumi [212] for multidirectional fibre-reinforced polymer composites. On the other hand, PA6,6 composite specimens exhibited compressive strengths that are only ~71.1% – ~79.5% of their respective tensile strength in comparison to ~82.2% – ~91.6% for the PA6 composite specimens. Regarding failure mechanisms and modes, they observed that matrix cracking initiated at loads ranging from 40% to 50% of failure load within a matrix-rich area. Further loading leads to local rotation, similar to kink band formation, and interlaminar delamination. Finally, specimens under loading failed in a shear mode at an angle of greater than 60°. Comparing these compressive strength results with those of Oya and Hamada [119, 204], presented in Table 2.11, one can confirmed what has been previously reported [119, 204], *i.e.*, that shear failure is related to lower compressive strength.

Yerramalli and Waas (2003) [183] investigated the effect of shear stress on the compressive strength of IM7-12k carbon fibre/vinylester composites. Specimen dimensions and loading configurations are as described in sub-section 2.5.1.2 in paragraph four. Unlike GFRP specimens that failed by combined mode splitting and kinking, CFRP specimens failed by a single mode of kinking irrespective of cross-head translation speed-to-rotational speed ratio. A decrease of compressive strength with the increase of shear stress was also noticed.

The compressive strength of knitted glass fabric-reinforced vinyl ester composites has been reported by Wonderly *et al.* [83]. Compressive tests were carried out according to ASTM D6641 while open hole compressive specimens were tested in accordance with the Northrop Grumman standard due to its more consistent results. All specimens contained end tabs of  $\pm 45^\circ$  glass fibre-reinforced vinyl ester composites glued onto their gripped areas. They observed that the compressive strength of solid CFRP specimens is  $\sim 17\%$  lower than that of GFRP specimens, and those of CFRP specimens showed a broader spread of values in comparison to those of GFRP specimens. Perhaps surprisingly, the compressive strength of open hole CFRP composite specimens is only slightly,  $\sim 2\%$ , lower than that of open hole GFRP specimens. The compressive strength of FRP composites mainly depends upon shear yield strength and fibre misalignment of the composites [181].

The discussion above leads to the following conclusion. Compressive strength decreases with the increase of combined shear stress [213, 214]. Compressive strength is significantly lower than tensile strength, the higher the compressive modulus the lower the compressive strength [42, 119]. Although the tensile strength of CFRP composites is significantly higher than that of GFRP composites, the compressive strength of CFRP composites is considerably lower than that of GFRP composites [166]. Shear failure is related to lower compressive strength whereas transverse failure is related to higher compressive strength [119, 204]. Compressive failure modes for unidirectional fibre-reinforced composites are dominantly kinking [166, 182, 205, 213] regardless of their fibre volume fraction [166], as well as for multidirectional fibre-reinforced polymer composites [42, 212]. The kink band formation process is identified as initial kinking, transitory kinking and band broadening [205].

#### 2.5.2.3. Flexural properties

Parry and Wronski [199] in 1981 reported their work on Grafil A-S type III carbon fibre-reinforced epoxy composites beams of various span-to-depth ratios,  $S/d$ , subjected to TPB and FPB flexural loading. They revealed that flexural



strength was significantly lower than tensile strength and that kinking initiated in contact with the loading nose at the compressive side of the beam, producing a non-linear stress-strain relationship, followed by kink growth propagation towards the neutral axis in a decreasing pattern of load magnitude, and eventually, failure in either a flexural mode, for  $S/d = 15$  and  $S/d = 40$ , or interlaminar delamination mode due to the presence of matrix rich areas between two adjacent plies for  $S/d = 5$ . Flexural failure surfaces showing tension and compression failure in their fracture surface separated approximately at the neutral axis. The failure mechanism at the compressive side has later been confirmed by Moran and Shih from their compressive tests of unidirectional IM7 carbon fibre/PEEK composites [205]. In the later failure mode, kink band formation was followed by longitudinal delamination through matrix rich region.

A typical CFRP prepreg fabrication method was employed by Kim and Mai [197]. Prior to being impregnated with the matrix to produce CFRP prepregs, either continuous carbon fibre bundles or discontinuous carbon fibre was impregnated with either polycarbonate or epoxy solution in order to ensure thorough wetting of the fibre. Specimens with  $S/d = 30$  were subjected to TPB loading at a constant crosshead speed of 0.5 mm/min in order to determine their flexural strength. Although there was only a slight increase in flexural strength when compared to those commonly produced prepreg, the increase in fracture toughness for both with discontinuous and continuous fibre reinforcement was significant, up to 100%.

Transverse flexural properties of unidirectional CFRP composites subjected to TPB loading has been reported by Rezaifard *et al.* [177]. They reported that the pattern of transverse flexural modulus and strength with respect to fibre surface treatment level is similar to those for the respective tensile properties. They observed the an increase of up to more than 100% of flexural strength for 100%-level surface-treated fibre composites in comparison with that of untreated carbon fibre/epoxy composites, and further treatment exhibited a declining trend of flexural strength. They found that the flexural strength was up to ~70% higher than tensile strength.

The effect of compressive cure pressure on void content, and flexural properties of carbon fibre/epoxy composites has been studied by Olivier *et al.* [151]. They pointed out that void content decreases with an increase of compressive curing pressure. Void content along with void shape and distribution must be considered in determining the effect of void on the flexural properties of composites. The decrease of flexural strength may be closely related to the decrease of ILSS with any increase of void content, as flexural strength decreases with an increase of shear stress as reported in reference [183].

Gilchrist *et al.* (1996) [108, 187] working on different lay-ups of T300 carbon fibre/epoxy composite I-beams, notched with circular cut-outs and unnotched, loaded under FPB, reported that the presence of a circular cut-out in the webs reduced the maximum load by approximately 25% and changed the failure initiation point. In comparison with its GFRP counterpart, the T300 carbon/epoxy I-beams are approximately 33% stronger. Failure of the unnotched beams was initiated at the compressive sides, as has been reported by Chen *et al.* [186] for GFRP composite beams, with the most severe damage being in the fillet resulting from a stress raiser due to geometric discontinuity, while that of the notched beams was initiated from a shear-loaded circular cut-out in the web [108] exhibited matrix cracking due to local tensile stresses [187]. Compressive flange damage exhibited delamination [108] following local buckling [187], while the damage at the tension side was barely visible [108]. Axial flexural strength of both unnotched and notched CFRP composite I-beams is higher than that of their respective GFRP counterparts.

Oya and Hamada [119] observed that the higher the flexural modulus of the composites, the lower the flexural strength. Flexural mechanical properties were higher than their respective compressive mechanical properties, but lower than their respective tensile properties. Linear stress-deflection relationships up to the point of initial failure were observed for all four different grades of CFRP composites, and failure was initiated at the compression side, as has been reported in [214] for carbon-fibre-reinforced thermoplastic composite I-beams tested under three-point bending, advancing into the tension side, passing through the neutral plane, and producing interlaminar debonding adjacent to the neutral plane.

Oya and Hamada [204] also reported their work on carbon fibre-reinforced nylon6 and poly propylene sulphide (PPS). Although nylon6 is much tougher than PPS, both resultant composites showed very similar axial tensile behaviour. The scatter of mechanical properties was in line with the variation of fracture mode. In order to obtain considerably high strength composites, the matrix must possess high fracture toughness and proportional properties of the fibre, matrix and interface.

Finite element analysis on unidirectional CFRP and GFRP composite beams of various span-to-depth ratios subjected to transverse TPB and FPB loading to identify its accuracy compared to beam theory prediction has been reported by O'Brien and Krueger (2003) [167]. They pointed out that the 2D plain-strain and plain-stress models under TPB loading configurations for both linear and geometric non-linear analyses, as well as under FPB loading configuration for 2D geometric non-linear analysis, gave slightly lower maximum tensile stress right under the loading nose when compared to those predicted by beam theory. Smaller span-to-depth ratios resulted in larger discrepancies. For the FPB loading configuration and 2D geometric non-linear analysis, the results were close to each other apart from those right under the loading nose. This may due to the Saint-Venant effect [191, 192] (pp. 240 and 34, respectively). They also revealed that beam theory prediction for maximum tensile stress in bending was in very good agreement with the result of their model for the 2D finite element analysis, and for 3D finite element analysis, the larger span-to-depth ratio as well as larger beam width results in better agreement with that of beam theory.

The following are conclusions drawn from the previously reported work on the mechanical behaviour of CFRP composites. Whilst short beams,  $S/d = 5$ , failed by interlaminar shear, longer beams,  $S/d = 15$  and  $S/d = 40$ , failed in a flexural mode with fracture surfaces showing tensile and compressive failure separated approximately at the neutral axis [199]. Failure initiated at the compression side [119, 214] with a lower flexural modulus being associated with higher flexural strength. Whilst the failure of solid laminated CFRP I-beams subjected to FPB loading initiated in their compressive flanges [108, 187], producing local buckling and delamination [187], those of the beams with circular cut-outs in their webs

initiated in these stress raisers, producing matrix cracking [108, 191] due to local tensile stresses [187]. Individually impregnated fibre bundles prior to prepreg fabrication can improve fracture toughness up to 100% in comparison to previously unimpregnated fibre bundle preregs [197]. The scatter of flexural properties are reflected by the diversity of failure modes [204] whilst the flexural strength of CFRP composites can be increase by fibre surface treatments [177]. It is not only the quantity of voids that influences CFRP flexural properties but also their shapes and distribution [151]. Flexural mechanical properties were higher than their respective compressive mechanical properties, but they may be lower [119] or higher [177] than their respective tensile properties. Axial flexural properties of CFRP composites are not sensitive to matrix properties [204]. The axial flexural strength of CFRP I-beams is approximately 33% higher than those of GFRP I-beams [108, 187]. O'Brien and Krueger reported that their finite element results that predict transverse flexural properties of CFRP and GFRP composites were in good agreement with that of beam theory predictions.

**Table 2.12.** Typical properties of CFRP composites

First author, year	Fibre characteristics	Matrix type	$V_f$ (%)	Elastic modulus, $E$ (GPa)			Strength, $\sigma$ (MPa)			Strain to failure, $\varepsilon$ (%) <sup>1</sup>	Dominant failure mode		
				$E_t$	$E_c$	$E_{fl}$	$\sigma_t$	$\sigma_c$	$\sigma_{fl}$		Tension	Compression	Flexure
Rezaifard, 1994	HTA513X, Ud, 90°	Epoxy	N/A	10.0			64.6		110.7	0.71, N/A			
Oya, 1996	T700S, Ud	Epoxy	N/A	143.0	133.5	128.8	2304.1	1058.3	1521.8	1.78, 0.81, 0.12	Br, L-MC	shear	comp, mds
	M40J, Ud, 0°	Epoxy	N/A	226.9	194.0	202.5	2126.1	1135.0	1323.0	0.98, 0.60, 0.10	Br, L-MC	transverse	comp, mds
	M50J, Ud, 0°	Epoxy	N/A	313.8	259.9	254.1	2085.5	843.2	1183.4	0.66, 0.36, 0.06	Br, L-MC	transverse	comp, mds
	M60J, Ud, 0°	Epoxy	N/A	410.6	322.5	346.7	2248.3	637.1	1086.5	0.32, 0.20, 0.05	Br, L-MC	shear	comp, mds
Oya, 1997	AT400, Ud, 0°	Nylon6	N/A	113.6	104.3		1511.3	813.2		1.28, 0.78	T-MC, FB, Db		
	AT400, Ud, 0°	PPS	N/A	115.9	100.7		1559.8	819.8		1.28, 0.80	L-MC, Db		
	AT400, Ud, 90°	Nylon6	N/A	7.3			71.2			1.54	matrix failure		
	AT400, Ud, 90°	PPS	N/A	7.9			20.2			0.25	interface failure		
Botelho, 2003	plain weave fabric	PA6	40.00	28.3			296.0	271.0					
			50.00	48.1			393.0	323.0					
			60.00	50.2			410.0	367.0					
	Hexcel CF, Ud, 0°	PA6	40.00	68.3									
			50.00	91.2									
			60.00	110.4									
	Hexcel CF, Ud, 90°	PA6	40.00	1.9									
			50.00	2.4									
			60.00	3.1									

*Continued*

Table 2.12. *Continued*

First author, year	Fibre characteristics	Matrix type	$V_f$ (%)	Elastic modulus, $E$ (GPa)			Strength, $\sigma$ (MPa)			Strain to failure, $\varepsilon$ (%) <sup>a</sup>	Dominant failure mode		
				$E_t$	$E_c$	$E_{fl}$	$\sigma_t$	$\sigma_c$	$\sigma_{fl}$		Tension	Compression	Flexure
Botelho, 2003 (Continued)	plain weave fabric	PA6,6	40.00	35.4			408.0	290.0					
			50.00	39.0			43.0	352.0					
			60.00	51.1			512.0	391.0					
	Hexcel CF, Ud, 0°	PA6,6	40.00	71.4									
			50.00	88.2									
			60.00	112.1									
	Hexcel CF, Ud, 0°	PA6,6	40.00	2.4									
			50.00	3.3									
			60.00	4.2									
Moran, 1998	IM7, Ud	PEEK	60.00					660.0				fibre	
Wonderly, 2005,	T700SC, UD, 0°	VE	N/A				958.0	328.0			FB, T-MC, SF	Db	
OH: d/w = 6/38	T700SC, UD, 0°	VE	N/A				621.2	234.6			Db, T-MC	N/A	
	T700SC, UD, 90°	VE	N/A				17.8				N/A		
Lee, 1999	IM7-12k, UD, 0°	VE	0.00									Db/splitting	
	IM7-12k, UD, 0°	VE	10-30									Db/splitting	
	IM7-12k, UD, 0°	VE	40-60									Db and K	

*Continued*

Table 2.12. *Continued*

First author, year	Fibre characteristics	Matrix type	$V_f$ (%)	Elastic modulus, $E$ (GPa)			Strength, $\sigma$ (MPa)			Strain to failure, $\varepsilon$ (%) <sup>a</sup>	Dominant failure mode		
				$E_t$	$E_c$	$E_{fl}$	$\sigma_t$	$\sigma_c$	$\sigma_{fl}$		Tension	Compression	Flexure
Lee, 2000	IM7-12k, UD, 0°	VE	0.00									Db/splitting	
	IM7-12k, UD, 0°	VE	10-30									Db/splitting	
	IM7-12k, UD, 0°	VE	40-60									Db and K	
Yerramalli, 2003	IM7-12k, UD, 0°	VE	50.00									K (+ torsion)	
Gilchrist, 1996  notched:	T300, UD, 0°	Epoxy	N/A	134.8			1563.0						Compr FBu, DI
	T300, UD, 90°	Epoxy	N/A	8.2			44.8						Compr FBu, DI
	T300, UD, 0°, ±45°	Epoxy	N/A	54.8		69.3	534.2		357.8	0.75/-0.84			Compr FBu, DI
	E-g, UD, 0°	Epoxy	N/A										Compr FBu, DI
	E-g, UD, 90°	Epoxy	N/A										Compr FBu, DI
	E-g, UD, 0°, ±45°	Epoxy	N/A							0.94/-0.99			Compr FBu, DI
O'Brein, 2003	IM7, UD, 0°	Epoxy	N/A	161.0									
	IM7, UD, 90°	Epoxy	N/A	11.4									
Parry, 1981	Type III, Ud	Epoxy	60.00			110.0	1,750.0		1,570.0				catastrophic

**Notes:**

Subscripts: t = tension, c = compression, fl = flexural.

Fibre architecture: Ac-s = acrylo-silane coated, Am-s = amino-silane coated, Dc = randomly oriented discontinuous fibre, KF = knitted fabric, UD = unidirectional, 0° = longitudinal direction, 90° = transverse direction,  $\delta$  = fibre diameter ( $\mu\text{m}$ ), L = fibre length (mm), OH = open hole,  $\emptyset\text{C}$  = circular fibre cross section,  $\emptyset\text{P}$  = 'peanut'-shaped fibre cross section,  $\emptyset\text{O}$  = oval fibre cross section.

Matrix type: cc = calcium carbonate-filled, PA = polyamide, PC = polycarbonate, PE = polyester, PEt = polyethylene, PP = polypropylene, PU = polyurethane, talc = talc-filled, VE = vinylester.

Strain to failure: \*) respective values of the utilised test methods.

Dominant failure mode: comp = compressive, Db = fibre-matrix interfacial debonding or splitting, Dl = delamination, FB = fibre breakage, Fbu = flange buckling, FP = fibre pull-out, int lam Dl = interlaminar delamination, GC = global crushing, K = kinking, L = longitudinal direction, MB = microbuckling, MC = matrix cracking, Mds = mid-depth splitting, SF = surface is flat, SR = surface is rough, T = transverse direction.



#### 2.5.2.4. CFRP Summary

Tables 2.12 and 2.13 show that the axial tensile strength of CFRP composites is generally higher than that of their GFRP counterparts. Whilst axial properties of CFRP composites are fibre-dominated, transverse properties are more sensitive to matrix properties [42, 83, 166, 181, 208]. In addition, their transverse tensile properties are more sensitive to the presence of voids compared to longitudinal tensile properties [151]. The data in Table 2.11 shows that the axial compressive strength of unidirectional CFRP composites is significantly lower than their tensile strength, and the higher is the compressive modulus the lower is the compressive strength [42, 119]. The increase in magnitude of combined shear loading significantly decreases compressive strength [213, 214]. Whilst fracture toughness can be improved by embedment of individual fibre bundle into polymer in order to increase their wetting prior to prepreg fabrication [197], flexural strength can be increased by fibre surface treatment [177]. T300 carbon/epoxy I-beams are approximately 33% stronger than E-glass fibre/epoxy I-beams of the same geometry and dimensions [108]. The presence of discontinuities, such as holes [108, 187] as well as the quantity, shape and distribution of voids [151], alters flexural strength and failure mechanisms.

Fibre-matrix interfacial bonding influences the tensile behaviour of CFRP composites, *i.e.*, failure mode and tensile strength. Load transfer from matrix to fibres takes places via shear loading in the fibre-matrix interface [42]. A weak interface produces brooming tensile failure accompanied by longitudinal fibre-matrix debonding leading to relatively higher tensile strength in comparison with excessively strong interfaces that produce transverse matrix failure combined with fibre breakage leading to lower tensile strength [177]. Therefore, moderately strong interfaces are required in order to produce considerably higher tensile strength CFRP composites. Different failure modes of CFRP composites subjected to compressive loading have been reported, *i.e.*, shear failure producing lower compressive strength, transverse failure associated with comparatively higher compressive strength [119, 204], and fibre kinking leading to crushing regardless of their  $V_f$  [42, 166, 212]. Kink band formation consists of three distinct steps, *i.e.*

initial kinking, transitory kinking, and band broadening characterised by non-linear stress-strain curves, significant load decrease, and steady load, respectively [205]. Flexural failure modes of CFRP composite beams depend upon their span-to-depth ratios,  $S/d$ . Small  $S/d$ ,  $S/d = 5$ , fails by shear showing interply delamination initiated under the loading nose at the neutral axis, while  $S/d \geq 15$  flexural failure exhibited tensile and compressive fracture surfaces with border line approximately at the neutral axis [199]. For solid rectangular beams, failure initiates at the compression side [119, 214], and in the compressive flange [108, 191] producing local buckling and delamination for solid CFRP composite I-beams [187]. The presence of geometric discontinuities as stress raisers in CFRP composite I-beams changes the failure mode to matrix cracking [108, 187] due to local tensile stresses [187]. The variation in failure modes indicates the spread of their respective flexural mechanical property data [204].

In addition, by comparing Tables 2.12 and 2.13 it can be concluded that the compressive strength of CFRP composites is lower than that of GFRP composites, as has been reported by O'Brien and Krueger [166].

### ***2.5.3. Hybrid Fibre-Reinforced Polymer (HFRP) Composites***

The use of glass fibre in various fibre architectures to improve the various properties of structural materials [147, 215-222], *e.g.*, natural fibre composites [216, 217, 221, 222], metal structures [147, 218], and synthetic fibre-reinforced composites [215, 219, 220], has been studied. Carbon or graphite fibre has also been incorporated with other fibres or metal structures, such as Kevlar [44, 223-225], E-glass [223], polyvinyl alcohol [223], polyethylene [226-228], natural fibre [226], and metal structure [229, 230], to produce hybrid FRP composites or hybrid structures. Another type of fibre being studied for improving FRP composite properties by producing hybrid FRP composites is silicon carbide fibre [75, 231-234]. Basically, FRP composites can be said to be hybrid even if the fibres differ only in their the geometries [235].

#### 2.5.4.1. Hybrid effect

The hybrid effect can be defined as the synergistic effect resulting from combining two or more types of fibre embedded in a common matrix. The hybrid effect can be said to exist if any properties of hybrid FRP composites deviate from those predicted by the rule of mixtures [236]. If the observed value is higher than that predicted by the rule of mixture then a positive hybrid effect will be said to exist, and *vice versa* [235]. It should be noted that the rule of mixtures must be applied on a relative volume fraction basis, as opposed to weight fraction or layer fraction [237]. Whether the hybrid effect exists or not is still debatable amongst many composite researchers.

By comparing the failure strains of unbonded and bonded layer specimens, Bunsell and Harris indicated that the hybrid effect exists, provided that the fibre-matrix interfacial bond is sufficiently strong [173]. Thomason [160] was reported to observe a hybrid effect by substitution of 5 wt.% up to 20 wt.% of S2-glass fibre for E-glass fibre in chopped E-glass/S2-glass hybrid fibre-reinforced polyamide 6,6 composite strength. Reid *et al.* [220] observed a positive hybrid effect in interlaminar shear strength with glass fibre substitution for 75% and 50 % for polypropylene fibres for their hybrid FRP composites. You *et al.* [238] reported that the hybrid effect was evident for the tensile properties of carbon-glass hybrid FRP composites. According to Kretsis [239], the hybrid effect would be more obvious with the decrease in proportion of the lower elongation fibre. The incorporation of short glass fibre into short carbon fibre-reinforced polypropylene composites to produce short glass-short carbon fibre hybrid FRP composites was also found to exhibit a positive hybrid effect in terms of their fracture toughness [240].

Although their silicon carbide-carbon hybrid FRP composite specimens did not show any hybrid effect in compressive strength and flexural strength, just followed the rule of mixtures, Wang *et al.* [234] observed a positive hybrid effect in terms of compressive strength and flexural strength in their boron-carbon fibre hybrid FRP composite specimens. In contrast to this, a negative hybrid effect in tensile strength was reported by Kang *et al.* [241], but they observed a positive

hybrid effect for tensile modulus and flexural strength. Marom *et al.* [235] also reported to observe a small negative hybrid effect in flexural strength whereas the modulus was just obeying the rule of mixtures of their glass-carbon hybrid FRP composite specimens.

Whilst negative hybrid effects were observed in some particular properties of hybrid FRP composites, some other properties of the respective specimens exhibited a positive hybrid effect. Thus, there may be some conditions that need to be met in order to produce a positive hybrid effect.

#### 2.5.4.2. Tensile properties

Jones and DiBenedetto [242] studied hybrid FRP composites containing E-glass fibres coated with two different seizing agents resulting in different fibre-matrix interfacial and load transfer characteristics. They found that the critical fragmentation length of both fibres of the hybrid system slightly decreased in comparison with GFRP composites containing a single-type of the fibre. They observed that the weaker fibre-matrix interface acted as a crack propagation arrester that prevents the adjacent fibres from further breaking; instead, the crack would propagate along the fibre and produced multiple fracture planes and fibre brooming.

Incorporation of glass fibre to improve the properties of natural FRP composites by producing hybrid FRP composites has been studied. Thwe and Liao [222] investigated bamboo-glass fibre hybrid FRP composites subjected to immersion on water at 25 °C and 75 °C for different periods of time. They reported that partial substitution of short glass fibre for short bamboo fibre in bamboo/polypropylene FRP composites improved their tensile strength and stiffness retention to environmental aging. In addition, they observed that the polypropylene matrix degraded by dissolution. Hariharan and Khalil [243] studied a hybrid of randomly oriented oil palm fibre (OPF) and E-glass chopped strand mat embedded in an epoxy subjected to tensile loading. Hybrid FRP composites possessing a range of hybrid weight ratios (wt% of GF relative to total wt% of

fibres), given in Table 2.12, were produced and tested in accordance with ASTM D638-76. They reported that a non-symmetrical stacking configuration, *i.e.*, GF on one side and OPF in the other, resulted in un-symmetrical deformation because of large differences of elastic modulus between the two fibres. A negative hybrid effect for tensile properties may be attributed to the fact that the coefficient of thermal expansion of GF is much higher than that of OPF leading to tensile residual stresses in the OPF upon curing. In addition, the hybrid ratio was presented based on weight while the composite strength is given per unit area – the density of GF ( $2.56 \text{ g}\cdot\text{cm}^{-3}$ ) is much higher than that of the OPF ( $0.7 - 1.55 \text{ g}\cdot\text{cm}^{-3}$ ) leading to a decrease in hybrid ratio if it was presented in terms of volume. Another combination of natural fibre, *i.e.*, flax fibre, and glass fibre to produce hybrid FRP composites was studied by Arbelaiz *et al.* [215]. Various hybrid ratios were employed, see Table 2.13. It was reported that there was no hybrid effect observed with the substitution of glass fibre for flax fibre in the untreated hybrid FRP composites resulting in improved properties obeying the rule of mixtures. Poor wetting of the fibre by the matrix leading to weak fibre-matrix interfacial bonding, as was obvious from the SEM micrographs, may be responsible for the absence of a hybrid effect as has been reported by Li *et al.* [227].

Reid *et al.* [220] investigated the use of polypropylene fibres for the warp, and glass fibre for the weft, to produce plain weave hybrid fabric of various hybrid ratios,  $V_{fG}/V_f$ , with polyester resin being used as the matrix. Although a negative hybrid effect was noted for tensile strength, which may be caused by the use of GF as the weft that did not significantly contribute to the strength in the warp, a positive hybrid effect was more obvious for interlaminar shear strength.

Kang *et al.* [241] studied the combination of high tensile and flexural strength continuous carbon fibre and spun fabric carbon fibre hybrid-reinforced phenolic composites. CF hybrid reinforced polymer specimens with a hybrid ratio,  $V_{f-Ud}/V_f$ , of 0.25 were fabricated for tensile specimens and tested in accordance with ASTM D3039-76. Different tensile failure modes, a small negative hybrid effect for tensile strength that can be caused by weak fibre-matrix interfacial bonding, as confirmed by their respective SEM micrographs, and a positive hybrid effect for tensile modulus were observed. Spun fabric CFRP/phenolic specimens

failed predominantly by fibre pull-out whereas unidirectional CFRP/phenolic specimens failed by a combination of delamination, fibre-matrix interfacial debonding and fibre breakage, while the CF hybrid/phenolic composite failed mainly due to fibre breakage and delamination combined with a small amount of fibre pull-out. Jones and DiBenedetto [242] working on AS4-IM6G hybrid FRP composites found out that the fragmentation length of the hybrid increased in comparison with even the longer fragmentation length of single fibre composites, *i.e.*, AS4 CFRP composites.

A number of papers dealing with the tensile behaviour of glass-carbon hybrid FRP composites can be found, such as that of Bunsell and Harris, Dickson *et al.*, Jones and DiBenedetto and You *et al.* [173, 238, 242, 244]. Bunsell and Harris [173] reported that there was no significant effect of fibre placement, *i.e.*, whether the CFRP layers or the GFRP layers were placed as the outer layers, on tensile behaviour of the carbon-glass hybrid FRP composites. The CFRP layers failed in a brittle mode, while the GFRP layers failed due to extensive splitting or brooming. You *et al.* [238] studied tensile properties of carbon-glass hybrid FRP composite rods with one single hybrid ratio of  $\sim 0.47$  but with two different matrices, *i.e.*, vinylester and polyester, and various fibre placements, *i.e.*, CFRP as the core, GFRP as the core and CF dispersed within the GFRP. They reported that a hybrid effect was evident, while the effect of matrix type on composite properties was insignificant. Unlike that previously reported by Bunsell and Harris [173], they revealed that, for both matrix types, rods with CFRP cores exhibited higher tensile strength, tensile modulus and ultimate tensile strain compared to those with GFRP cores. The increase in tensile strength is due to the decrease of failure probability of the carbon fibre with the presence of a higher strain-to-failure glass fibre as has been explained by Jones and DiBenedetto [242]. The highest failure strength exhibited by the CFRP core rod can be attributed to the packing geometry of the carbon-glass hybrid FRP system as has also been reported by Jones and DiBenedetto [242]. Stress-strain curves of carbon-glass hybrid fibre-reinforced vinylester composite rods showed gradual fibre breakage that most probably was initiated by the lower elongation fibre, *i.e.* carbon fibre. Dickson *et al.* [244] revealed that there was no hybrid effect observed in both tensile strength

and tensile modulus, but they found an increase in strain-to-failure for the CFRP layers.

The tensile behaviour of hybrid FRP composites containing different combinations of fibres, *i.e.*, two different types of glass fibre [242], natural fibre and glass fibre [215, 222, 243], synthetic fibre and glass fibre [220], two different grades of carbon fibre [241, 242], and glass fibre and carbon fibre [173, 238, 242, 244], has been studied. No hybrid effect was observed if poor fibre wetting of the hybrid FRP composites was present [215]. In contrast to this, a negative hybrid effect can be caused by incorrect placement of stronger fibres [220], coefficient of thermal expansion mismatch resulting in residual tensile stresses [243], or poor fibre-matrix interfacial bonding [241]. Positive hybrid effects were reported in other references, *i.e.*, improved retention to environmental aging [222], increase in elastic modulus [241], and increase in tensile strength and tensile modulus [238, 242], and increased strain-to-failure [238, 244].

#### 2.5.4.3. Compressive properties

Different hybrid combinations have been reported, *e.g.*, chopped short sisal and chopped strand glass fibre mats [217], polyethylene and carbon fibres [227], carbon and glass fibres [185, 245], carbon and silicon carbide fibres [231, 233, 234], as well as boron and carbon fibres [234].

John and Naidu reported that weak fibre-matrix interfacial bonding due to the presence of voids, and fibre-to-fibre contact may cause poor load transfer among fibres leading to a decrease in compressive strength [220] of their sisal-glass hybrid FRP composites. Li *et al.* [227] studied the compressive strength of ultra-high-modulus polyethylene (UHMPE)-carbon hybrid FRP composites of various hybrid ratios as presented in Table 2.13. They reported that substitution of carbon fibre for UHMPE fibre at moderate amounts, up to ~46%, showed a positive hybrid effect for strain at ultimate strength and significantly increased compressive strength of the composite but no hybrid effect in compressive strength was observed. The lower compressive strength of the UHMPE fibre in comparison with the epoxy matrix, which was considered constant for all the

hybrid ratios, may be responsible for the absence of a hybrid effect in compressive strength. The increase in strain at ultimate strength can be the result of synergistic effects of the stiffer fibre as the load bearing phase and the less stiff fibre as a crack propagation arrester. The failure of the UHMPE/epoxy specimens was initiated by matrix cracking followed by a combination of debonding and fibre buckling at lower stress levels, then delamination and kinking prior to failure. That of the CFRP specimens was dominated by fibre micro-buckling followed by matrix cracking and fibre breakage.

Chaudhuri and Garala [245] reported that fibre misalignment due to poor composite fabrication processing induced fibre kinking under compressive loading leading to shear crippling failure of CFRP samples. A significant positive hybrid effect was observed for fracture toughness, *i.e.*, 15% substitution of S-glass fibre for carbon fibre resulted in an increase of fracture toughness of approximately 100%. Although compressive strength and modulus were observed to increase with the incorporation of S-glass fibres in CFRP composite samples, a positive hybrid effect was not observed. In addition, unlike the dominant failure mode of the baseline CFRP samples, which was fibre kinking as later supported by the finding of Yerramalli and Waas [185], that of the hybrid samples was mostly multiple fibre fracture.

Sudarisman *et al.* [233] revealed that there was no significant increase in compressive strength, modulus, and work of fracture of SiCF-CF/epoxy hybrid composites with different hybrid ratios. Each of their specimens consisted of eight layers of SiCF/epoxy and/or CF/epoxy prepregs, with CF/epoxy prepreg layers being placed on the inner side while SiC/epoxy prepreg layers were placed in the outer side as has been described in the work of Davies *et al.* [231]. Their failure modes were dominated by shear failure, except for the SiC-FRP specimens which was global crushing, with the presence of longitudinal interlaminar delamination due to interlaminar shear stress for both cases.

The following is the summary that can be drawn from the above discussion on the compressive properties of hybrid FRP composites. A positive hybrid effect



has been noted in compressive strain at ultimate strength that can be attributed to the synergistic effect of the stiffer fibre as load bearing phase and the less stiff fibre as crack propagation arrester [220], and also for the work of fracture [245]. The presence of voids, and fibre-to-fibre contact leading to poor load transfer among fibres [220], as well as fibre misalignment due to poor composite fabrication processing induced fibre kinking and shear crippling [245] may cause strength degradation and result in the absence of any positive hybrid effect. The failure mode of hybrid FRP composites is closely related to those of their single-fibre-type composites [217, 233, 234, 245].

#### 2.5.4.4. Flexural properties

Positive hybrid effects have been reported for some flexural properties, *i.e.*, strain at ultimate strength [227], flexural strength [241], and fracture toughness [245]. The increase in flexural fracture toughness may be attributed to the increase in flexural failure strain of the hybrid specimens. Although some researchers [215, 227, 245] did not observe a positive hybrid effect in some flexural properties of their samples, they still reported significant increases in those particular properties, *i.e.*, as expected from the rule of mixtures.

Wang *et al.* [234] reported that the flexural strengths of their carbon-boron and carbon-silicon carbide hybrid FRP samples, 1788 MPa and 1855 MPa, were ~120% and ~150% higher than those of their respective compressive strengths. The flexural strength of the carbon-boron hybrid FRP samples were ~8% and ~58% higher than those of the BFRP and CFRP samples, respectively, but this may be credited to the increase of fibre volume fraction of the hybrid system, 75%, in comparison with those of the CFRP and BFRP samples that are 53.1% and 50.0%, respectively. The flexural strength of carbon-silicon carbide hybrid FRP samples, 1788 MPa, was approximately 52% higher than that of CFRP samples, but ~15% lower than that of SiC-FRP samples. Stress-strain relationships for both hybrids were essentially linear until the initiation of failure. Their load-displacement plots showed a sharp drop of load after reaching their peak that may

be associated with the initiation of kink band formation in their compressive side [205] and followed by delamination or splitting at relatively constant load.

Arbelaiz *et al.* [215] reported that the flexural strength and flexural modulus of untreated flax fibre-reinforced polypropylene composites increased with the incorporation of glass fibre at various hybrid ratios. That poor fibre wetting was obviously observed in their SEM micrographs due to weak fibre-matrix interfacial bonding (and thus reducing the ultimate strength) may be responsible for limiting further increases in flexural properties of their hybrid system and led to the absence of positive hybrid effect. Another cause may be related to fibre architecture and placement as has been revealed by Park and Jang [228] that placing higher strength fibres in the outer layers of carbon-polyethylene hybrid FRP composite beams resulted in higher flexural strength. Li *et al.* [227] revealed that substitution of carbon fibre for ultra-high modulus polyethylene (UHMPE) fibre up to ~46% showed a significant increase in flexural strength. The failure of low carbon fibre content, up to ~46%, specimens was initiated with debonding and delamination at the compressive side propagating to the tensile side. Extensive fibre fracture, marked by a sharp load drop, and followed by delamination was the predominant failure mode of higher carbon fibre content specimens. Chaudhuri and Garala [245] observed significant increases in flexural strength and modulus with the incorporation of S-glass fibres in CFRP composite samples. In addition, the flexural strength was observed to be higher than the compressive strength of the same hybrid specimens as has been presented in Table 2.13.

Davies and his colleagues [75, 232] reported that a hybrid ratio of 1:8 produces flexural strength increases in comparison to those of the reference CFRP composites. However, there was a slight decrease in flexural modulus for this case which was attributed to the fact that the SiC fibre possesses a slightly lower elastic modulus than C fibre. Although further increases in hybrid ratio up to 4:8 did not show significant increases in flexural modulus and flexural strength for  $S/d = 32$ , a maximum increase of 35% in flexural strength was obtained for a hybrid ratio of 4:8 and  $S/d = 64$ . It was also noted that a significant increase in fracture energy was apparent that may be credited to the increase in strain to failure. The failure mode of the SiC-C hybrid FRP composites subjected to a three-point bending load

predominantly appeared to be kinking and out of plane buckling at the compressive surface underneath the loading nose and propagated towards the neutral plane.

The discussion on flexural properties of hybrid FRP composites can be summarised below. Although previously published research do not have a common agreement on the existence of a hybrid effect for flexural properties, most reports noted that the incorporation of higher strength fibre in the baseline FRP composites results in a significant increase in particular flexural properties, *i.e.* strain at ultimate strength [227], flexural strength [75, 215, 227, 232, 241, 245], flexural modulus [215, 245], strain-to-failure [75, 232], fracture toughness [245], and fracture energy [75, 232]. The flexural strength of hybrid FRP composite beams is mainly controlled by the properties of fibres in the outer layer, whilst the flexural modulus is more dependent upon properties at the compressive side [228]. Flexural strength was observed to be higher than compressive strength for the same hybrid specimens [245]. Failure are initiated at the compressive side and propagated toward the neutral axis. Li *et al.* [227] observed failure in the form of debonding and delamination for lower carbon fibre content, and fibre fracture and delamination for higher carbon fibre content with respect to their carbon-UHMPE hybrid FRP composite specimens. Davies and colleagues [75] noticed out of plane buckling of fibres followed by kinking at the compressive side at maximum flexural stress point.

**Table 2.13.** Typical properties of hybrid FRP composites

First author, year	Fibre		Matrix type	$V_f$ (%)	Elastic modulus, $E$ (GPa)			Strength, $\sigma$ (MPa)			Strain to failure, $\epsilon$ (%) <sup>a</sup>	Dominant failure mode		
	Fibre characteristic	$r_h = V_{f2}/V_f$			$E_t$	$E_c$	$E_{fl}$	$\sigma_t$	$\sigma_c$	$\sigma_{fl}$		Tension	Compression	Flexure
Thwe, 2003	Mixture of short bamboo fibre and short E-glass fibre	0.00	Pp	20 %wt	2.15			20.4						
		0.25			2.45			21.1						
		0.50			3.30			23.3						
Reid, 2004	Plain weave fabric with polypropylene fibre warp and glass fibre weft	0.00	Polyester resin	N/A				39						
		0.28						67						
		0.52						93						
		0.78						136						
		1.00						179						
Hariharan, 2005 Note: $\rho_{OPF} = 1.12$ $\rho_{GF} = 2.56$ $\rho_{Ep} = 1.15$	Non-symmetric layer-wise configuration of oil palm fibre and glass fibre	0.00	Epoxy	N/A	0.912			24.0						
		0.08			1.007			26.0						
		0.20			1.007			37.5						
		0.40			1.265			40.5						
		0.49			1.588			47.5						
		0.80			2.206			89.5						
		1.00			4.265			111.0						
Kang, 2006	Layer-wise configuration of spun fabric and unidirectional CF	0.00	Phenolic	N/A	36.8			176		248		FP		
		0.25			45.1			227		289		FB, DI, FP		$Sl d = 16$
		1.00			56.2			436		332		FB, DI, Db		

*Continued*

Table 2.13. Continuation

First author, year	Fibre		Matrix type	$V_f$ (%)	Elastic modulus, $E$ (GPa)			Strength, $\sigma$ (MPa)			Strain to failure, $\varepsilon$ (%) <sup>a</sup>	Dominant failure mode			
	Fibre characteristic	$r_h = V_{f2}/V_f$			$E_t$	$E_c$	$E_{fl}$	$\sigma_t$	$\sigma_c$	$\sigma_{fl}$		Tension	Compression	Flexure	
Arbelaiz, 2005 Note: $\rho_{FF} = 1.4$ $\rho_{GF} = 2.6$ $\rho_{PP} = 0.934$	Mixture of short flax fibre and short E-glass fibre	0.00	MAPP-modified polypropylene	30wt%	1.61		3.69	27.4		43.2					
		0.15			1.90		3.90	32.7		50.1					
		0.35			1.97		4.27	35.4		55.2					
		0.62			2.00		4.39	39.2		65.7					
		1.00			2.17		5.15	48.6		84.0					
Bunsell, 1974	Layer-wise CF-GF, Ud	0.50	Epoxy	0.5	89						1.25	CF: FB, MC GF: Db, Br			
Dickson, 1989	Symmetric structures of Ud XAS CF - E-GF hybrid	0.00	Epoxy	0.60	42.1			1300			3.74				
		0.25			70.4			1056			1.52				
		0.50			85.8			1330			1.52				
		0.75			114.2			1511			1.26				
		1.00			136.6			1952			1.43				
You, 2007 Note: $\rho_{CF} = 1.80$ $\rho_{GF} = 2.56$ $\rho_{PE} = 1.40$ $\rho_{VE} = 1.23$ $r_h = V_{ICF}/V_{IGF}$	GFRP compose rods	0.00	Polyester	~34.4	47.8			972			2.03				
			Vinylester	~31.6	48.3			983			2.03				
	CFRP core in GFRP composite rods	0.47	Polyester	~48.8	83.1			1331			1.60				
			Vinylester	~45.6	80.4			1281			1.59				
	GFRP core in CFRP composite rods		Polyester	~48.8	79.5			1128			1.42				
Vinylester			~45.6	78.9			1083			1.37					

Continued

Table 2.13. Continuation

First author, year	Fibre		Matrix type	$V_f$ (%)	Elastic modulus, $E$ (GPa)			Strength, $\sigma$ (MPa)			Strain to failure, $\epsilon$ (%)	Dominant failure mode		
	Fibre characteristic	$r_h = V_{f2}/V_f$			$E_t$	$E_c$	$E_{fl}$	$\sigma_t$	$\sigma_c$	$\sigma_{fl}$		Tension	Compression	Flexure
You, 2007 (continuation)	CFRP core in GFRP composite rods	0.47	Polyester	~48.8	84.0			1213			1.44			
			Vinylester	~45.6	92.4			1045			1.68			
	CFRP composite rods	1.00	Polyester	~33.2	114.6			1431			1.25			
			Vinylester	~30.4	114.8			1454			1.27			
Li, 1999	Layer-wise UHMPE-carbon fibre	0.00	Epoxy	55			21.7		54.4	137	3.0, N/A		MC, Db, FBu, DI, K	FB, DI
		0.14					30.6		105.6	191	4.0, N/A			
		0.46					50.4		196.8	269	7.5, N/A			
		0.80					86.0		379.6	620	12.5, N/A			
		1.00					96.5		451.3	716	1.5, N/A			
Chaudhuri, 1994 Note: $\rho_{CF} = 1.76$ $\rho_{GF} = 2.49$ $\rho_{Ep} = 1.10$	Commingled T300 6K carbon - IK S-glass fibres, Ud	0.00	Rubber toughened-epoxy	~34.2		8.0	7.4		86.5	107.8				
		0.15				8.1	6.8		98.1	121.7				
Sudarisman, 2007	Layer-wise SiC-C hybrid FRP, Ud.	0.00	Epikote® 828 poxy	~70.0 – 74.0		177.6			1028				SF, K, DI	
		0.25				163.2			933				SF, K, DI	
		0.50				167.4			1016				SF, K, DI	
		0.75				156.7			1075				SF, K, DI	
		1.00				149.1			1333				GC, K, DI	

Continued

**Table 2.13.** Continuation

First author, year	Fibre		Matrix type	$V_f$ (%)	Elastic modulus, $E$ (GPa)			Strength, $\sigma$ (MPa)			Strain to failure, $\varepsilon$ (%) <sup>a</sup>	Dominant failure mode		
	Fibre characteristic	$r_h =$ $V_{f2}/V_f$			$E_t$	$E_c$	$E_{fl}$	$\sigma_t$	$\sigma_c$	$\sigma_{fl}$		Tension	Compression	Flexure
Wang, 2009	Layer-wise carbon- boron hybrid FRP, Ud.	0.00	Epoxy	53.1			101.0		557	1174				
		0.47		75.0			139.8		742	1855				
		1.00		50.0			161.4		680	1717				
	Layer-wise carbon- silicon carbide hybrid FRP, Ud.	0.00	Epoxy	53.1			101.0		557	1174				
		46.3		75.2			161.2		806	1788				
		1.00		51.0			221.3		991	2096				
Park, 1999	PEth <sub>8</sub>	0.00	vinylester	N/A			1.2			33.0				
	[PEth/C] <sub>4</sub>	0.50					4.2			124.1				
	[PEth <sub>2</sub> /C <sub>2</sub> ] <sub>5</sub>	0.50					5.8			126.0				
	[PEth <sub>2</sub> /C <sub>2</sub> ] <sub>2</sub>	0.50					6.1			131.2				
	[C/PEth] <sub>4</sub>	0.50					5.9			133.2				
	[C <sub>2</sub> /PEth <sub>2</sub> ] <sub>2</sub>	0.50					6.3			136.8				
	PEth <sub>4</sub> /C <sub>4</sub>	0.50					4.6			141.7				
	C <sub>4</sub> /PEth <sub>4</sub>	0.50					6.6			188.3				
	[C <sub>2</sub> /PEth <sub>2</sub> ] <sub>5</sub>	0.50					7.0			205.1				
	C <sub>8</sub>	1.00					31.2			467.9				

*Continued*

**Table 2.13.** Continuation

First author, year	Fibre		Matrix type	$V_f$ (%)	Elastic modulus, $E$ (GPa)			Strength, $\sigma$ (MPa)			Strain to failure, $\epsilon$ (%) <sup>*)</sup>	Dominant failure mode		
	Fibre characteristic	$r_h = V_{f2}/V_f$			$E_t$	$E_c$	$E_{fl}$	$\sigma_t$	$\sigma_c$	$\sigma_{fl}$		Tension	Compression	Flexure
Davies, 1999, 2001	C <sub>8</sub>	0.00	Epoxy	~70			141.0			1745				S/d≤32: Out of plane FBu/K. S/d=64: DI, FPo
	SiC/C <sub>7</sub>	~0.14		~71.2			~132.0			1942				
	SiC <sub>2</sub> /C <sub>6</sub>	~0.27		~72			~128.0			~1945				
	SiC <sub>3</sub> /C <sub>5</sub>	~0.40		~73.1			~130.0			~1910				
	SiC <sub>4</sub> /C <sub>4</sub>	~0.53		~74			~122.0			2090				Shear, DI
	SiC <sub>8</sub>	1.00		~78			115.1			~2100				

**Notes:**

<sup>\*)</sup>Single fibre, dual fibre or fibre bundle FRP specimens, hence the given values are for SiC fibre properties irrespective of their matrices or interlaminar shear strength.

Subscripts: t = tension, c = compression, fl = flexural.

Fibre architecture: Ud = unidirectional, 0° = longitudinal direction, 90° = transverse direction.

Strain to failure: respective values of the utilised test methods.

Dominant failure mode: Br = brooming, comp = compressive, Db = fibre-matrix interfacial debonding or splitting, DI = delamination, FB = fibre breakage, FBu = fibre buckling, FP = fibre pull-out, GC = global crushing, K = kinking, L = longitudinal direction, MB = microbuckling, MC = matrix cracking, SF = surface is flat, SR = surface is rough, T = transverse direction.



#### 2.5.4.5. Hybrid FRP summary

Hybrid FRP composites can be defined as FRP composites containing two or more types of fibre even if the fibres differ only in their geometries [235]. The hybrid effect can be defined as the synergistic effect resulted from combining two or more types of fibre embedded in a common matrix. The hybrid effect as the synergistic effect can be said to exist if any properties of hybrid FRP composites either positively or negatively deviate from those predicted by the rule of mixtures [235, 236]. Certain conditions may be required in order to produce positive hybrid effect.

The tensile properties of different hybrid FRP composites have been studied. No hybrid effect was observed if poor fibre wetting of the hybrid FRP composites was present [215]. A negative hybrid effect can be caused by incorrect placement of stronger fibres [220], coefficient of thermal expansion mismatch resulting in tensile residual stresses [243], or poor fibre-matrix interfacial bonding [241]. Positive hybrid effects were reported in other references, *i.e.*, improved retention to environmental aging [222], increased elastic modulus [241], and increased tensile strength and tensile modulus [238, 242], and increased strain-to-failure [238, 244].

Investigations on the compressive properties of hybrid FRP composites have been published in a number of papers. Positive hybrid effects have been noted for compressive strain at ultimate strength that can be attributed to the synergistic effect of the stiffer fibre as load bearing phase and the less stiff fibre as crack propagation arrester [220], and also for the work of fracture [245]. The presence of voids, and fibre-to-fibre contact leading to poor load transfer among fibres [220], as well as fibre misalignment due to poor composite fabrication processing inducing fibre kinking and shear crippling [245] may cause strength degradation and result in the absence of a positive hybrid effect. The failure mode of hybrid FRP composites is closely related to those of their single-fibre-type composites [217, 233, 234, 245].

Although previously published researchers do not have a common agreement on the existence of hybrid effect for flexural properties, most reports

noted that the incorporation of higher strength fibre in the baseline FRP composites results in a significant increase in particular flexural properties, *i.e.*, strain at ultimate strength [227], flexural strength [75, 215, 227, 232, 241, 245], flexural modulus [215, 245], strain-to-failure [75, 232], fracture toughness [245], and fracture energy [75, 232]. The flexural strength of hybrid FRP composite beams is mainly controlled by the properties of fibres in the outer layer, while flexural modulus is more dependent on properties at the compressive side [228]. Flexural strength was observed to be higher than compressive strength for the same hybrid specimens [245]. Failure are initiated at the compressive side and propagated towards the neutral axis. Li *et al.* [227] observed failure in the forms of debonding and delamination for lower carbon fibre content, and fibre fracture and delamination for higher carbon fibre content in their carbon-UHMPE hybrid FRP composite specimens. Davies and colleagues [75] noticed out of plane buckling of fibres followed by kinking at the compressive side at maximum flexural stress point.

## REFERENCES

- [1] M. F. Ashby, *Materials selection in mechanical design*, Second ed. Oxford: Pergamon Press, 1999.
- [2] T. K. Derry and T. I. Williams, "The extraction and working of metals," in *A Short History of Technology* Oxford: Oxford University Press, 1970, pp. 114-156.
- [3] A. F. Tylecote, *A history of metallurgy*, Second ed. London: The Institute of Materials, 1992.
- [4] "Aircraft Fundamentals: Aircraft Materials," RV-Groovin.com, <http://www.rv-grovin.com/fundamaterials.html>, Accessed date: 04 September 2008.
- [5] M. F. Ashby and D. R. H. Jones, "Engineering materials and their properties," in *Engineering Materials 1: An Introduction to Their Properties and Applications* Oxford: Butterworth-Heinemann, 2000, pp. 3-14.
- [6] S. K. Mazumdar, *Composites Manufacturing: Materials, Product, and Process Engineering*. Boca Raton: CRC Press, 2002.

- [7] T. H. G. Megson, "Chapter 7. Principles of stressed-skin construction," in *Aircraft Structures for Engineering Students* London: Edward Arnold, 1972, pp. 197-224.
- [8] C. H. Gibbs-Smith, "Aviation: An Historical Survey from Its Origins to the End of World War II," London: Her Majesty's Stationery Office, 1970.
- [9] J. M. Seng, "30. Laminate design," in *Handbook of Composites*, Second ed, S. T. Peters, Ed. London: Chapman and Hall, 1998, pp. 686-708.
- [10] J. Alexander, "The Soviet aircraft industry since 1940," in *Russian Aircraft Since 1940* London: Putman and Company Ltd., 1975, pp. 1-21.
- [11] H. Fukuda, "Professor Hayashi's brilliant activities in composites research," *Advanced Composite Materials*, vol. 8, pp. 207-215, 1999.
- [12] K. K. Chawla, *Composite Materials: Science and Engineering*. New York: Springer-Verlag, 1987.
- [13] "Boeing Commercial Airplanes - 787 Dreamliner," The Boeing Company, <http://www.boeing.com/commercial/787family/programfacts.html>, Accessed date: 14/09/2008.
- [14] E. G. Wolff, *Introduction to the dimensional stability of composite materials*. Lancaster: DEStech Pub. Inc., 2004.
- [15] B. D. Agarwal and L. J. Broutman, *Analysis and Performance of Fiber Composites*, 2nd ed. New York: John Wiley and Sons, Inc., 1990.
- [16] F. L. Matthews, "Part 1. Overview and review of composite materials," in *Finite Element Modelling of composite materials and structures*, 1 ed, F. L. Matthews, G. A. O. Davies, D. Hitchings, and C. Soutis, Eds. Boca Raton: CRC Press, 2000, pp. 1-40.
- [17] T. J. Reinhardt and L. L. Clements, "Introduction to composites," in *Engineered Materials Handbook*. vol. 1. Composites Conshohoken: ASM International, 1989, pp. 28-34.
- [18] J. W. Weeton, D. M. Peters, and K. L. Thomas, "Engineers' guide to composite materials," Metal Park: ASM International, 1990, pp. 1.1 - 1.16.
- [19] Y. A. Khalid, F. A. Ali, B. B. Sahari, and E. M. A. Saad, "Performance of composite I-beams under axial compression and bending load modes," *Materials & Design*, vol. 26(2), pp. 127-135, 2005.
- [20] T. Ogasawara, S. Aizawa, T. Ogawa, and T. Ishikawa, "Sensitive strain monitoring of SiC fiber/epoxy composite using electrical resistance changes," *Composites Science and Technology*, vol. 67, pp. 955-962, 2007.
- [21] Y. Baillargeon and T. Vu-Khanh, "Prediction of fiber orientation and microstructure of woven fabric composites after forming," *Composite Structures*, vol. 52, pp. 475-481, 2001.

- [22] D. L. Denton, "Land transportation application," in *Handbook of Composites*, Second ed, S. T. Peters, Ed. London: Chapman and Hall, 1998, pp. 905-915.
- [23] N. Pottish, "Carbon fiber race car technology hits the streets," in *High Performance Composites*: 7 January 2005. <http://www.composites-world.com/articles/carbon-fiber-race-car-technology-hits-the-streets.aspx>. Accessed date: 15/09/2008., 2005.
- [24] R. N. Hadcock, "Aircraft applications," in *Handbook of Composites*, Second ed, S. T. Peters, Ed. London: Chapman and Hall, 1998, pp. 1044-1052.
- [25] "Composite Materials for Aircraft Industry," <http://www.key-to-nonferrous.com/default.aspx?ID=CheckArticle&NM=103>, Accessed date: 03 September 2008.
- [26] "Composite and Advanced Materials in Aircraft," <http://www.century-of-flight.net/Aviation%20history/evolution%20of%20technology/Composites%20and%20Advanced%20Materials.html>, Accessed date: 03 September 2008.
- [27] G. C. Krumweide and E. A. derby, "67. Aerospace equipment and instrument structure," in *Handbook of Composites*, Second ed, S. T. Peters, Ed. London: Chapman and Hall, 1998, pp. 1004-1043.
- [28] V. K. Srivastava, "Influence of water immersion on mechanical properties of quasi-isotropic glass fibre reinforced epoxy vinylester resin composites," *Materials Science and Engineering A*, vol. 263, pp. 56-63, 1999.
- [29] L. S. Sutherland and C. Guedes Soares, "Effect of laminate thickness and of matrix resin on the impact of low fibre-volume, woven roving E-glass composites," *Composites Science and Technology*, vol. 64, pp. 1691-1700, 2004.
- [30] G. Marsh, "Patching it up," *Reinforced Plastics*, vol. 48, pp. 42-45, 2004.
- [31] W. C. Tucker and T. Juska, "62. Marine application," in *Handbook of Composites*, Second ed, S. T. Peters, Ed. London: Chapman and Hall, 1998, pp. 916-930.
- [32] J. O. Barton and S. Mouring, "On the moisture-related buckling of marine composite panels using approximate analysis," *Ocean Engineering*, vol. 34, pp. 1778-1780, 2007.
- [33] E. J. Barbero, "46. Construction," in *Handbook of Composites*, Second ed, S. T. Peters, Ed. London: Chapman and Hall, 1998, pp. 982-1003.
- [34] J. L. Senne, "Fatigue Life of Hybrid FRP Composite Beams," in *M.S. Thesis, Engineering Mechanics*, Blacksburg, Virginia: Virginia Polytechnic Institute and State University, 2000.
- [35] S. N. Loud, "63. Commercial and industrial application of composites," in *Handbook of Composites*, Second ed, S. T. Peters, Ed. London: Chapman and Hall, 1998, pp. 931-956.

- [36] B. E. Spencer, "Composites in the sporting goods industry," in *Handbook of Composites*, Second ed, S. T. Peters, Ed. London: Chapman and Hall, 1998, pp. 1044-1052.
- [37] "Ultra lightweight bike frame features Oxeon carbon fiber," in *Composites World*: 9 August 2008. <http://www.compositesworld.com/news/ultralightweight-bike-frame-features-oxeon-carbon-fiber.aspx>. Accessed date: September 15, 2008.
- [38] J. W. Bray, "Aluminum mill and engineered wrought product," in *ASM Handbook*. vol. 2. Properties and Selection: Non-ferro alloys and special purpose materials, S. R. Lampman, T. B. Zorc, S. D. Henry, J. Daquila, A. W. Ronkie, J. Jakel, K. L. O'Keefe, L. A. Abel, R. T. Kiepora, P. T. Heather, F. Lampman, and N. D. Weaton, Eds. Materials Park: ASM International, 1996, pp. 29-61.
- [39] J. F. Shackelford and W. Alexander, *Materials Science and Engineering Handbook*. Boca Raton: CRC Press, 2001.
- [40] N. E. Dowling, *Mechanical Behavior of Materials*. Englewood Cliff: Prentice Hall, 1993.
- [41] M. Y. Sheeley, "Epoxy resins," in *Polymer Data Handbook*, J. E. Mark, Ed. New York: Oxford University Press, 1999, pp. 90-96.
- [42] E. C. Botelho, L. Figiel, M. C. Rezende, and B. Lauke, "Mechanical behavior of carbon fiber reinforced polyamide composites," *Composites Science and Technology*, vol. 63, pp. 1843-1855, 2003.
- [43] C. Zweben, "Composite materials," in *Mechanical Engineers Handbook*, 3rd ed, M. Kutz, Ed. Hoboken: John Wiley and Sons, 2006, pp. 380-417.
- [44] J. Gustin, A. Joneson, M. Mahinfalah, and J. Stone, "Low velocity impact of combination Kevlar/carbon fiber sandwich composites," *Composite Structures*, vol. 69, pp. 396-406, 2005.
- [45] S. I. Seo, C. S. Park, K. H. Kim, B. C. Sin, and A. K. Min, "Fatigue strength evaluation of the aluminum carbody of urban transit unit by large scale dynamic load test," *JMSE International Journal Series A*, vol. 48, pp. 27-34, 2005.
- [46] A. D. Wilson, "Fracture and fatigue properties of structural steel," in *ASM Handbook*. vol. 19: Fatigue and Fracture, S. R. Lampman, G. M. Davidson, F. Reidenbach, R. R. Boring, A. Hammel, S. D. Henry, W. W. Scott, N. D. Matteo, K. S. Dragolich, K. Ferjutz, H. Lampman, K. Mills, and M. J. Reiddelbangh, Eds. Materials Park: ASM International, 1996, pp. 591-602.
- [47] O. M. Gerasimchuk, G. A. Sergienko, V. I. Bondarchuk, A. V. Terukov, Y. S. Nalimov, and B. A. Gryaznov, "Fatigue strength of an ( $\alpha+\beta$ )-type titanium alloy Ti-6Al-4V produced by the electron beam physical vapor deposition method," *Strength of Materials*, vol. 38, pp. 651-658, 2006.
- [48] J. Rosler, H. Harders, and M. Baker, *Mechanical Behaviour of Engineering Materials*. New York: Springer-Verlag, 2007.

- [49] G. H. Staab, *Laminar Composites*. Boston: Butterworth Heinemann, 1999.
- [50] M. de Freitas and R. de Carvalho, "Residual strength of a damaged laminated CFRP under compressive fatigue stresses," *Composites Science and Technology*, vol. 66, pp. 373-378, 2006.
- [51] Y.-P. Zheng, R. C. Ning, and Y. Zheng, "Glass fibre-reinforced composites of high compressive strength.," *Journal of Reinforced Plastics and Composites*, vol. 23, pp. 1729-1740, 2004.
- [52] "Composite Materials," <http://www.aviation-history.com/theory/composite.htm>, Accessed date: 21 July 2008.
- [53] A. J. Aref, Y. Kitane, and G. C. Lee, "Analysis of hybrid FRP-concrete multi-cell bridge superstructure," *Composite Structures*, vol. 69(3), pp. 346-359, 2005.
- [54] C. Caneva, S. Olivieri, C. Santulli, and G. Bonifazi, "Impact damage evaluation on advanced stitched composites by means of acoustic emission and image analysis," *Composite Structures*, vol. 25, pp. 121-128, 1993.
- [55] G. Wu and J.-M. Yang, "The mechanical behavior of glare laminates for aircraft structures," *Journal of Materials Science*, vol. 57, pp. 72-79, 2005.
- [56] D. Dawson, "Composite connect with the world of cabling," in *Composites Technology*. vol. February, 2006, pp. 24-29.
- [57] G. H. Koch, M. P. H. Brongers, N. G. Thompson, Y. P. Virmani, and J. H. Payer, "Corrosion Cost and Preventive Strategies in the United States," NACE International, Houston, Research Report 2002.
- [58] R. Capozucca, "Analysis of the experimental flexural behaviour of a concrete beam grid reinforced with C-FRP bars," *Composite Structures*, vol. 79, pp. 517-526, 2007.
- [59] S. Mall and S. R. Cunningham, "Fatigue behavior of integrally fabricated joints between titanium matrix composite and titanium alloy," *Composite Structures*, vol. 80, pp. 65-72, 2007.
- [60] N. Chisholm, H. Mahfuz, V. K. Rangari, A. Ashfaq, and S. Jeelani, "Fabrication and mechanical characterisation of carbon/SiC-epoxy nanocomposites," *Composite Structures*, vol. 67, pp. 115-124, 2005.
- [61] K. S. Tun and M. Gupta, "Effect of heating rate during hybrid microwave sintering on the tensile properties of magnesium and Mg/Y2O3 nanocomposite," *Journal of Alloys and Compounds*, vol. 466, pp. 140-145, 2008.
- [62] P. C. Kim and D. G. Lee, "Composite sandwich constructions for absorbing the electromagnetic waves," *Composite Structures*, vol. 87, pp. 161-167, 2009.
- [63] J. R. Vinson and R. L. Sierakowski, *The Behavior of Structures Composed of Composite Materials*, 2nd ed. New York: Springer, 2002.
- [64] "Tungsten Copper, W-Cu Composite Powders: A Substitute for Infiltration ": in *SYLVANIA Business Product*, <http://www.sylvania.com/>

BusinessProducts/MaterialsandComponents/ElectronicsDisplayProducts/TungstenCopper/, Accessed: October 18, 2008.

- [65] Z. J. Zhou and Y. S. Kwon, "Fabrication of W-Cu composite by resistance sintering under ultra-high pressure," *Journal of Materials Processing Technology*, vol. 168, pp. 107-111, 2005.
- [66] A. P. Gavrilenko, M. S. Koval'chenko, A. A. Kravchenko, V. V. Skorokhod, Y. M. Solonin, N. I. Filippov, and I. I. Karpikov, "Influence of structure on the resistance of tungsten-copper pseudoalloys in electroerosion machining of a sintered carbide," *Powder Metallurgy and Metal Ceramics*, vol. 25, pp. 838-841, 1986.
- [67] E. K. Ohriner and B. Bryskin, "Thermomechanical processing of tungsten-copper composites," Metals and Ceramics Division, Oak Ridge National Laboratory, Oak Ridge 1996.
- [68] E. Tuncer and S. M. Gubanski, "Filler concentration effects on losses in silicone based polymeric composites," in *1999 Conference on Electrical Insulation and Dielectric Phenomena, Austin, Texas, the U.S.A., 17-20 October 1999*, Vol. 2, pp. 687-690: IEEE Press, 1999.
- [69] P. Nerikar, A. Dasari, and R. D. K. Misra, "Microstructural surface damage evolution during tensile straining of calcium carbonate containing high density polyethylene," *Microscopy and Microanalysis*, vol. 10, pp. 668-669, 2004.
- [70] F. H. J. Maurer, R. Kosfeld, and T. Uhlenbroich, "Interfacial interaction in kaolin-filled polyethylene composites," *Colloid and Polymer Science*, vol. 263, pp. 624-630, 1985.
- [71] A. John Rethinam, G. N. K. Ramesh Bapu, and R. M. Krishnan, "Deposition of nickel-mica electrocomposites and characterisation," *Materials Chemistry and Physics*, vol. 85, pp. 251-256, 2004.
- [72] J.-C. Lin, "Investigation of impact behavior of various silica-reinforced polymeric matrix nanocomposites," *Composite Structures*, vol. 84, pp. 125-131, 2008.
- [73] S.-C. Kwon, T. Adachi, and W. Araki, "Temperature dependence of fracture toughness of silica/epoxy composites: Related to microstructure of nano- and micro-particles packing," *Composites Part B: Engineering*, vol. 39, pp. 773-781, 2008.
- [74] M. A. Osman, A. Atallah, M. Müller, and U. W. Suter, "Reinforcement of poly(dimethylsiloxane) networks by mica flakes," *Polymer*, vol. 42, pp. 6545-6556, 2001.
- [75] I. J. Davies and H. Hamada, "Flexural properties of a hybrid composite containing carbon and silicon carbide fibres," *Advanced Composite Materials*, vol. 10, pp. 77-96, 2001.
- [76] T. Vu-Khanh, "Toughness of flake-reinforced polypropylene," *Journal of Thermoplastic Composite Materials*, vol. 46, pp. 46-58, 1991.

- [77] H. Wang, H. Zhang, and G. Chen, "Preparation of unsaturated polyester/graphite nanosheet conducting composite under electric field," *Composites Part A: Applied Science and Manufacturing*, vol. 38, pp. 2116-2120, 2007.
- [78] Y. Okumura, S. Saji, and H. Anada, "Titanium-flake reinforced aluminum-matrix composite prepared from multilayered foils by cold pressure welding," *Advanced Engineering Materials*, vol. 2, pp. 818-821, 2000.
- [79] K.-J. Jeon, A. Theodore, and C.-Y. Wu, "Enhanced hydrogen absorption kinetics for hydrogen storage using Mg flakes as compared to conventional spherical powders," *Journal of Power Sources*, vol. 183, pp. 693-700, 2008.
- [80] J. Rexer and E. Anderson, "Composites with planar reinforcements (flakes, ribbons) - A Review," *Polymer Engineering and Science*, vol. 19, pp. 1-11, 1979.
- [81] S. Yoshida, H. Ono, S. Ando, F. Tsuda, T. Ito, Y. Shimada, M. Yamaguchi, K.-I. Arai, S. Ohnuma, and T. Masumoto, "High-frequency noise suppression in downsized circuits using magnetic granular films," *IEEE Transactions on Magnetics*, vol. 37, pp. 2401-2403, 2001.
- [82] A. Baker, S. Dutton, and D. Kelly, *Composite Materials for Aircraft Structures*, 2nd ed. Reston: AIAA, 2004.
- [83] C. Wonderly, J. Grenestedt, G. Fernlund, and E. Cetus, "Comparison of mechanical properties of glass fiber/vinyl ester and carbon fiber/vinyl ester composites," *Composites Part B: Engineering*, vol. 36, pp. 417-426, 2005.
- [84] B. T. Astrom, *Manufacturing of Polymer Composites*, First ed. London: Chapman Hall, 1997.
- [85] I. M. Daniel and O. Ishai, *Engineering Mechanics of Composite Materials*, First ed. New York: Oxford University Press, 1994.
- [86] K. Waschitschek, A. Kech, and J. d. Christiansen, "Influence of push-pull injection moulding on fibres and matrix of fibre reinforced polypropylene," *Composites Part A: Applied Science and Manufacturing*, vol. 33, pp. 735-744, 2002.
- [87] S. R. Malkan and F. K. Ko, "Effect of fibre reinforcement geometry on single shear and fracture behavior of three dimensionally braided glass/epoxy composite pins," *Journal of Composite Materials*, vol. 23, pp. 798-818, 1989.
- [88] S. T. Peters, "Introduction, composite basics and road map," in *Handbook of Composites*, Second ed, S. T. Peters, Ed. London: Chapman and Hall, 1998, pp. 1-20.
- [89] L. Tong, A. P. Mauritz, and M. K. Bannister, *3D Fibre Reinforced Polymer Composites*, 1st ed. Amsterdam: Elsevier, 2002.
- [90] "Thermcraft High Temperature Ceramic Electric Heaters," Winston-Salem, NC: Thermcraft, <http://www.thermcraftinc.com/high-temperature-heaters.html>, Accessed date: November 11<sup>th</sup>, 2008.



- [91] "High Temperature Ceramic Cements, Engineered for performance," Pittsburg, PA: Sauereisen, <http://www.sauereisen.com/pdf/hightemp.pdf>, Accessed date: November 11<sup>th</sup>, 2008.
- [92] Z. Y. Deng, T. Fukasawa, M. Ando, G. J. Zhang, and T. Ohji, "Bulk alumina support with high tolerant strain and its reinforcing mechanisms," *Acta Materialia*, vol. 49, pp. 1939-1946, 2001.
- [93] J. M. McNaney, R. M. Cannon, and R. O. Ritchie, "Fracture and fatigue-crack growth along aluminum-alumina interfaces," *Acta Materialia*, vol. 44, pp. 4713-4728, 1996.
- [94] S. Tekeli, T. Boyacıoglu, and A. Güral, "The effect of silica doping on the microstructure and mechanical properties of c-ZrO<sub>2</sub>/SiO<sub>2</sub> composites," *Ceramics International*, vol. 34(8), pp. 1959-1964, 2008.
- [95] M. R. Pinnel and A. Lawley, "Correlation of uniaxial yielding and substructure in aluminum-stainless steel composites " *Journal Metallurgical and Materials Transactions B* vol. 1(5), pp. 1337-1348, 1970.
- [96] K. K. Chawla and M. Metzger, "Initial dislocation distributions in tungsten fibre-copper composites," *Journal of Materials Science*, vol. 7, pp. 34-39, 1972.
- [97] C. M. Ward-Close and P. G. Partridge, "A fibre coating process for advanced metal-matrix composites," *Journal of Materials Science*, vol. 25, pp. 4315-4323, 1990.
- [98] V. I. Kostikov and V. S. Kilin, "13. Metal matrix composites," in *Handbook of Composites*, Second ed, S. T. Peters, Ed. London: Chapman and Hall, 1998, pp. 291-306.
- [99] C. E. Wakayama, "V-22 Osprey: High Altitude Flight," <http://www.dtic.mil/ndia/2002training/wakayama3.pdf>, Accessed date: November 11<sup>th</sup>, 2008., 2002.
- [100] D. R. Sidwell, "16. Hand lay-up and bag molding," in *Handbook of Composites*, Second ed, S. T. Peters, Ed. London: Chapman and Hall, 1998, pp. 352-377.
- [101] W. D. Callister, *Materials Science and Engineering: An Introduction*, 7th ed. Danvers, MA, U.S.A.: John Wiley and Sons, 2007.
- [102] Sudarisman and I. J. Davies, "The effect of processing parameters on the flexural properties of unidirectional CFRP composites," *Materials Science and Engineering: A*, vol. 498, pp. 65-68, 2008.
- [103] Sudarisman and I. J. Davies, "Flexural failure of unidirectional hybrid fibre-reinforced polymer FRP) composites containing different grades of glass fibre," *Advanced Materials Research*, vol. 41-42, pp. 357-362, 2008.
- [104] "Global Composites Market 2004-2010 : Opportunities, Market and Technologies," Dublin 8, Ireland.: Research and Markets, Guinness Centre, Taylors Lane, Dublin 8, Ireland, <http://www.researchandmarkets.com/reports/295860/>. Accessed date: November 17<sup>th</sup>, 2008, 2004.

- [105] T. Roberts, "Rapid growth forecast for carbon fibre market," *Reinforced Plastics*, vol. 51, pp. 10-13, 2007.
- [106] J. L. Thomason, "The influence of fibre length and concentration on the properties of glass fibre reinforced polypropylene: 7. Interface strength and fibre strain in injection moulded long fibre PP at high fibre content," *Composites Part A: Applied Science and Manufacturing*, vol. 38, pp. 210-216, 2007.
- [107] S. Deng, L. Ye, and Y.-W. Mai, "Influence of fibre cross-sectional aspect ratio on mechanical properties of glass fibre/epoxy composites I. Tensile and flexure behaviour," *Composites Science and Technology*, vol. 59, pp. 1331-1339, 1999.
- [108] M. D. Gilchrist, A. J. Kinloch, F. L. Matthews, and S. O. Osiyemi, "Mechanical performance of carbon-fibre- and glass-fibre-reinforced epoxy I-beams: I. Mechanical behaviour," *Composites Science and Technology*, vol. 56(1), pp. 37-53, 1996.
- [109] D. Hull and T. W. Clyne, *An Introduction to Composite Materials*, 2nd ed. Cambridge: Cambridge University Press, 2002.
- [110] D. J. Vaughan, "7. Fiberglass reinforcement," in *Handbook of Composites*, Second ed, S. T. Peters, Ed. London: Chapman and Hall, 1998, pp. 131-155.
- [111] "Glass fibers," in *Composite World*. vol. January 11<sup>th</sup>, 2006, pp. <http://www.compositesworld.com/articles/glass-fibers.aspx>. Accessed: October 11, 2007.
- [112] C. Reder, D. Loidl, S. Puchegger, D. Gitchthaler, H. Paterlik, K. Kromp, G. Khatibi, A. Betzwar, P. Zimprich, and B. Weiss, "Non-contacting strain measurement of ceramic and carbon single fibres by using the laser speckle method," *Composites Part A: Applied Science and Manufacturing*, vol. 34, pp. 1029-1033, 2003.
- [113] "Program Fact Sheet BOEING 787 Dreamliner," Seattle: The Boeing Company, <http://www.boeing.com/commercial/787family/programfacts.html>, Accessed date: 14<sup>th</sup> September 2008.
- [114] A. Jacob, "The popularity of carbon fibre," *Reinforced Plastics*, vol. 50, pp. 22-24, 2006.
- [115] K. Lafdi and M. A. Wright, "9. Carbon fibers," in *Handbook of Composites*, Second ed, S. T. Peters, Ed. London: Chapman and Hall, 1998, pp. 169-201.
- [116] R. J. Diefendorf and E. Tokarsky, "High-performance carbon fibers," *Polymer Engineering and Science*, vol. 15, pp. 150-159, 1975.
- [117] Singer, "US patent 4 005 183," 1977.
- [118] H. M. Hawthorne and E. Teghtsoonian, "Axial compression fracture in carbon fibre," *Journal of Materials Science*, vol. 10, pp. 41-51, 1975.

- [119] N. Oya and H. Hamada, "Effect of reinforcing fibre properties on various mechanical behavior of unidirectional carbon/epoxy laminates," *Sci. Eng. Compos. Mater.*, vol. 5, pp. 105-129, 1996.
- [120] *Hexcel Tow<sup>TM</sup> IM7 (5000) Carbon Fiber Product Data*. Stamford, CT, U.S.A.: Hexcel Corporation, [http://www.hexcel.com/NR/rdonlyres/BD219725-D46D-4884-A3B3-AFC86020EFDA/0/HexTow\\_IM7\\_5000.pdf](http://www.hexcel.com/NR/rdonlyres/BD219725-D46D-4884-A3B3-AFC86020EFDA/0/HexTow_IM7_5000.pdf), Accessed date: November 10<sup>th</sup>, 2008.
- [121] *Typical Properties for Thornel<sup>(R)</sup> Carbon Fibers - Standard Products*. Alpharetta, GA, U.S.A.: BP Amoco Chemicals, <http://www.cyttec.com/engineered-materials/downloads/ThornelTP.pdf>, Accessed date: November 10<sup>th</sup>, 2008.
- [122] *Unidirectional Carbon Fabric 'Ural-LO'*. Zavodskaya, Belarus: Svetlogorsk 'Khimvolokno', [http://www.sohim.by/\\_modules/\\_cfiles/files/unidirectional\\_96.pdf](http://www.sohim.by/_modules/_cfiles/files/unidirectional_96.pdf), Accessed date: November 10<sup>th</sup>, 2008.
- [123] "Product Information: OC<sup>®</sup> SE 2350 Single-end Continuous Rovings (Type 30<sup>®</sup>)," Toledo, OH, U.S.A.: OWENS CORNING: <http://www.owenscorningchina.com/upload/File/748226345.pdf>. Accessed date: November 22<sup>th</sup>, 2008.
- [124] D. D. L. Chung, *Carbon fibre composites*. Boston: Butterworth-Heinemann, 1994.
- [125] L. S. Penn and H. Wang, "3. Epoxy resins," in *Handbook of Composites*, Second ed, S. T. Peters, Ed. London: Chapman and Hall, 1998, pp. 48-74.
- [126] S. L. Kim, M. D. Skibo, J. A. Manson, R. W. Hertzberg, and J. Janiszewski, "Tensile, impact and fatigue behavior of an amine-cured epoxy resin," *Polymer Engineering & Science*, vol. 18, pp. 1093-1100, 1978.
- [127] J. R. M. d'Almeida and S. N. Monteiro, "The influence of the amount of hardener on the tensile mechanical behavior of an epoxy system," *Polymers for Advanced Technologies*, vol. 9, pp. 216-221, 1998.
- [128] K. Selby and L. E. Miller, "Fracture toughness and mechanical behaviour of an epoxy resin," *Journal of Materials Science*, vol. 10, pp. 12-24, 1975.
- [129] L. T. Drzal, "Interfaces and interphases," in *ASM Handbook, vol. 21: Composites*, D. B. Miracle, A. I. H. Committee, and S. L. Donaldson, Eds. Materials Parks, OH, U.S.A.: AM International, 2001, pp. 169-179.
- [130] M. R. Piggott and D. Andison, "The carbon fibre-epoxy interface," *Journal of Reinforced Plastics and Composites*, vol. 6, pp. 290-302, 1987.
- [131] Y. Sun and R. N. Singh, "A technique for the determination of interfacial properties from debond length measurement," *Journal of Materials Science*, vol. 35, pp. 5681 – 5690, 2000.
- [132] Z. Zhu, Y. Guo, and N. Shi, "Effect of surface modification of SiC fiber on acoustic emission behaviors and interface strength of SiC<sub>f</sub>/Al composite," in *Progress in Acoustic Emission IX*. Kamuela, Hawaii, U.S.A., 1998, pp. 9-14.

- [133] M. S. Amer and L. S. Schadler, "Stress concentration phenomenon in graphite/epoxy composites: Tension/compression effects," *Composites Science and Technology*, vol. 57(8), pp. 1129-1137, 1997.
- [134] H. Hamada, J. C. Coppola, and D. Hull, "Effect of surface treatment on crushing behaviour of glass cloth/epoxy composite tubes," *Composites*, vol. 23(2), pp. 93-99, 1992.
- [135] C.-H. Hsueh, "Crack-wake interfacial debonding criteria for fiber-reinforced ceramic composites," *Acta Materialia*, vol. 44, pp. 2211-2216, 1996.
- [136] M. G. Bader and W. H. Bowyer, "An improved method of production for high strength fibre-reinforced thermoplastics," *Composites*, vol. 4(4), pp. 150-156, 1973.
- [137] W. H. Bowyer and M. G. Bader, "On the reinforcement of thermoplastics by imperfectly aligned discontinuous fibres," *Journal of Materials Science*, vol. 7(11), pp. 1315-1321, 1972.
- [138] A. N. Netravali, P. Schwartz, and S. L. Phoenix, "*Study of interfaces of high performance glass fibres and DGEBA based epoxy resins using single-fibre-composite test*," *Polymer Compos.*, vol. 10, pp. 385-388, 1989.
- [139] A. N. Netravali, R. B. Henstenburg, S. L. Phoenix, and P. Schwartz, "Interfacial shear strength studies using the single filament composite test. I: Experiment on graphite fiber in epoxy," *Polymer Composites*, vol. 10, pp. 226-241, 1989.
- [140] X.-F. Zhou and H. D. Wagner, "Fragmentation of two-fiber hybrid microcomposites: stress concentration factors and interfacial adhesion," *Composites Science and Technology*, vol. 60, pp. 367-377, 2000.
- [141] S. Miziarski, A. McGratha, N. Milby, D. E. Brosius, and M. J. v. Bertouch, "A new look for Gemini: rapid-cured composites for an exchangeable top-end," Anglo-Australian Observatory, <http://www.aao.gov.au/local/www/ajm/cfrp-spie6273-121-06.pdf>, Epping, NSW, Australia, Accessed date: November 26th, 2008.
- [142] A. Salomi, A. Greco, F. Feline, O. Manni, and A. Maffezzoli, "A preliminary study on bladder-assisted rotomolding of thermoplastic polymer composites," *Advances in Polymer Technology*, vol. 26(1), pp. 21-32, 2007.
- [143] Sudarisman and I. J. Davies, "Influence of compressive pressure, vacuum pressure, and holding temperature applied during autoclave curing on the microstructure of unidirectional CFRP composites," *Advanced Materials Research*, vol. 41-42, pp. 323-328, 2008.
- [144] Z. Cai and T. Gutowsky, "26. Consolidation Techniques and consolidation control," in *Handbook of Composites*, Second ed, S. T. Peters, Ed. London: Chapman and Hall, 1998, pp. 576-595.

- [145] *Vacuum Pump Mini L28 - Brochure*. Täby, Sweden: PIAB AB, <http://www.piab.com/upload/6317/2e8f813c-21c1-470f-a6b1-68a5ada54632/11604.pdf>, Accessed date: September 4<sup>th</sup>, 2007.
- [146] Anonymus, *Composite Materials Handbook* vol. 3. Polymer Matrix Composites: Material Usage, Design, and Analysis: Department of Defence, U.S.A., 2002.
- [147] E. C. Botelho, L. C. Pardini, and M. C. Rezende, "Hygrothermal effects on damping behavior of metal/glass fiber/epoxy hybrid composites," *Materials Science and Engineering: A, Measurement and Interpretation of Internal/Residual Stresses*, vol. 399, pp. 190-198, 2005.
- [148] F. Y. C. Boey and S. W. Lye, "Void reduction in autoclave processing of thermoset composites: Part 1: High pressure effects on void reduction," *Composites*, vol. 23, pp. 261-265, 1992.
- [149] R. Park and J. Jang, "Effect of stacking sequence on the compressive performance of impacted aramid fiber/glass fiber hybrid composite," *Polymer Composites*, vol. 21, pp. 231-237, 2000.
- [150] Sudarisman, I. J. Davies, and H. Hamada, "Compressive failure of unidirectional hybrid fibre-reinforced composites containing carbon and silicon carbide fibres," *Composite Part A: Applied Science and Manufacturing*, 2007.
- [151] P. Olivier, J. P. Cottu, and B. Ferret, "Effects of cure cycle pressure and voids on some mechanical properties of carbon/epoxy laminates," *Composites*, vol. 26, pp. 509-515, 1995.
- [152] L. Liu, B.-M. Zhang, D.-F. Wang, and Z.-J. Wu, "Effects of cure cycles on void content and mechanical properties of composite laminates," *Composite Structures*, vol. 73, p. 303, 2006.
- [153] M. Deleglise, C. Binetruy, and P. Krawczak, "Simulation of LCM processes involving induced or forced deformations," *Composites Part A: Applied Science and Manufacturing*, vol. 37, pp. 874-880, 2006.
- [154] "High Pressure Bladder Molding System," Oceanside, CA, U.S.A.: [http://www.carbonbydesign.com/features/features\\_bladder.asp](http://www.carbonbydesign.com/features/features_bladder.asp), Accessed date: July 27<sup>th</sup>, 2008.
- [155] T. N. Abraham and K. E. George, "Short nylon fibre reinforced PP: Melt rheology," *Polymer-Plastics Technology and Engineering*, 46: 321-325, 2007, vol. 46, pp. 321-325, 2007.
- [156] U. Esendemir and A. Ondurucu, "An elasto-plastic analysis of thermoplastic composite cantilever beam loaded by a single force at its free end," *Journal of Reinforced Plastic and Composites*, vol. 23, pp. 761-775, 2004.
- [157] O. Sayman, M. Uyaner, and N. Tarakcioglu, "Elastic-plastic stress analysis in a thermoplastic composite cantilever beam loaded by bending moment," *Journal of Reinforced Plastics and Composites*, vol. 21, pp. 175-192, 2002.

- [158] T. Lenau, "Composites," Lyngby, Denmark: DesigninSite, <http://www.designinsite.dk/>, 2005, Accessed date: May 23<sup>th</sup>, 2006.
- [159] J. L. Thomason, "The influence of fibre length, diameter and concentration on the modulus of glass fibre reinforced polyamide 6,6," *Composites Part A: Applied Science and Manufacturing*, vol. 39, pp. 1732-1738, 2008.
- [160] J. L. Thomason, "The influence of fibre properties on the properties of glass fibre-reinforced polyamide 6,6," *Journal of Composite Materials*, vol. 34, pp. 158-172, 2000.
- [161] J. Jancar, "Hydrolytic stability of PC/GF composites with engineered interphase of varying elastic modulus," *Composites Science and Technology*, vol. 66(16), pp. 3144-3152, 2006.
- [162] J. F. Mandell, D. D. Samborsky, M. Li, R. Orozco, and D. S. Cairns, "Selection of fibreglass matrix resins for increased toughness and environmental resistance in wind turbine blades," AIAA - ASTM: AIAA-2000-0057, Reston, VA 20191-4344, U.S.A., Presentation Paper 1999.
- [163] R. Algood, S. C. Sharma, A. A. Syed, A. V. Rajulu, and M. Krishna, "Compression properties of E-glass/polyurethane composites," *Journal of Reinforced Plastic and Composites*, vol. 25(14), pp. 1445-1447, 2006.
- [164] Y. Cao and J. Cameron, "Flexural and shear properties of silica particle modified glass fiber reinforced epoxy composite," *Journal of Reinforced Plastics and Composites*, vol. 25, pp. 347-359, 2006.
- [165] A. M. A. El-Habak, "Mechanical behaviour of woven glass fibre-reinforced composites under impact compression load," *Composites*, vol. 22, pp. 129-134, 1991.
- [166] S. H. Lee, and A. M. Waas, "Compressive response and failure of fiber reinforced unidirectional composites," *International Journal of Fracture*, vol. 100(3), pp. 275-306, 1999.
- [167] K. O'Brien and R. Krueger, "Analysis of flexural test for transverse tensile strength characterization of unidirectional composites," *Journal of Composites, Technology and Research*, vol. 25, pp. 50-68, 2003.
- [168] J. R. Xiao, B. A. Gama, and J. W. G. Jr, "Progressive damage and delamination o in plain wave S-2 glass/SC-15 composites under quasi-static punch-shear loading," *Composite Structures*, vol. 78, pp. 182-196, 2007.
- [169] O. I. Okoli and G. F. Smith, "The effect of strain rate and fibre content on the Poisson's ratio of glass/epoxy composites," *Composite Structures*, vol. 48, pp. 157-161, 2000.
- [170] R. S. Bailey, M. Davies, and D. R. Moore, "Processing property characteristics for long glass fibre reinforced polyamide," *Composites*, vol. 20, pp. 453-460, 1989.
- [171] B. J. Briscoe and P. D. Evans, "Scratch hardness as an evaluation of cure temperature for glass fibre reinforced polyester: Composites Science and

- Technology Vol 34 No 1 (1989) pp 73-90," *Composites*, vol. 20, p. 497, 1989.
- [172] "ASTM D3039 Standard test method for tensile properties of polymer matrix composite materials," in *Annual Book of ASTM Standard*. vol. Vol. 03.01? West Conshohocken, PA, USA: ASTM Int., 2005, pp. 105-117.
  - [173] A. R. Bunsell and B. Harris, "Hybrid carbon and glass fibre composites," *Composites*, vol. 5, pp. 157-164, 1974.
  - [174] B. Harris and A. R. Bunsell, "Impact properties of glass fibre/carbon fibre hybrid composites," *Composites*, vol. 6, pp. 197-201, 1975.
  - [175] P. Yeung and L. J. Broutman, "The effect of glass-resin interface on the impact strength of fibre-reinforced plastics," *Polymer Engineering and Science*, vol. 18(2), pp. 62-72, 1978.
  - [176] T. Hayashi, "On the improvement of mechanical properties of composites by hybrid composition," in *Proceedings of the 8th International Reinforced Plastics Conference, Paper No. 22*, Brighton, U.K., October 1972, pp. 149-152.
  - [177] A. H. Rezaifard, M. G. Bader, and P. A. Smith, "Investigation of the transverse properties of a unidirectional carbon/epoxy laminate: Part 2- Laminate properties," *Composites Science and Technology*, vol. 52, pp. 287-295, 1994.
  - [178] J. L. Thomason, "The influence of fibre length and concentration on the properties of glass fibre reinforced polypropylene: 5. Injection moulded long and short fibre PP," *Composites Part A: Applied Science and Manufacturing*, vol. 33, pp. 1641-1652, 2002.
  - [179] R. H. Singley, A. S. Wronski, and T. V. Parry, "Axial compressive failure of glass-fibre polyester composites under superposed hydrostatic pressure: influence of fibre bundle size : Singley, R.H., Wronski, A.S. and Parry, T.V. *Composites Science and Technology* Vol 43 No 2 (1992) pp 171-183," *Composites*, vol. 23, p. 375, 1992.
  - [180] B. Budiansky and N. A. Fleck, "Compressive failure of fibre composites," *Journal of the Mechanics and Physics of Solids*, vol. 41, pp. 183-211, 1993.
  - [181] B. Budiansky, N. A. Fleck, and J. C. Amazigo, "On kink-band propagation in fiber composites," *Journal of the Mechanics and Physics of Solids*, vol. 46, pp. 1637-1653, 1998.
  - [182] S. H. Lee, C. S. Yerramalli, and A. M. Waas, "Compressive splitting response of glass-fiber reinforced unidirectional composites," *Composites Science and Technology*, vol. 60, pp. 2957-2966, 2000.
  - [183] C. S. Yerramalli and A. M. Waas, "A failure criterion for fiber reinforced polymer composites under combined compression-torsion loading," *International Journal of Solids and Structures*, vol. 40, pp. 1139-1164, 2003.

- [184] P. M. H. Wong, J. M. Davies, and Y. C. Wang, "An experimental and numerical study of the behaviour of glass fibre reinforced plastics (GRP) short columns at elevated temperatures," *Composite Structures*, vol. 63, pp. 33-43, 2004.
- [185] C. S. Yerramalli and A. M. Waas, "Compressive behavior of hybrid composites," in *44th AIAA/ASME/ASCE/AHS/ASC Structures, Structural Dynamics, and Materials Conference, Apr 7-10 2003*, Norfolk, VA, United States, 2003, pp. 979-987.
- [186] F. Chen, S. Bazhenov, A. Hiltner, and E. Baer, "Flexural failure mechanisms in unidirectional glass fibre-reinforced thermoplastics," *Composites*, vol. 25, pp. 11-20, 1994.
- [187] M. D. Gilchrist, A. J. Kinloch, and F. L. Matthews, "Mechanical performance of carbon-fibre and glass-fibre-reinforced epoxy I-beams: II. Fractographic failure observations," *Composites Science and Technology*, vol. 56(9), pp. 1031-1045, 1996.
- [188] "ASTM D790-07 Standard test method for flexural properties of unreinforced and reinforced plastic and electrical insulating materials by three-point bending," in *Annual Book of ASTM Standard*. vol. Vol. 08.01 West Conshohocken, PA, USA: ASTM Int., 2005.
- [189] S. Motahhari and J. Cameron, "Measurement of Micro-Residual Stresses in Fiber-Prestressed Composites," *Journal of Reinforced Plastics and Composites*, vol. 16, pp. 1129-1137, 1997.
- [190] S. Motahhari and J. Cameron, "Fibre prestressed composites: Improvement of flexural properties through fibre prestressing," *Journal of Reinforced Plastics and Composites*, vol. 18, pp. 279-288, 1999.
- [191] A. P. Boresi, R. J. Schmidt, and O. M. Sidebottom, *Advanced Mechanics of Materials*. New York: John Wiley and Sons, Inc., 1993.
- [192] J. R. Barber, *Elasticity*. Dordrecht: Kluwer Academic Publishers, 1992.
- [193] P.-O. Hagstrand, F. Bonjour, and J.-A. E. Manson, "The influence of void content on the structural flexural performance of unidirectional glass fibre reinforced polypropylene composites," *Composites Part A: Applied Science and Manufacturing*, vol. 36, pp. 705-714, 2005.
- [194] T. Yokozeki, T. Ogasawara, and, and T. Ishikawa, "Effect of fiber nonlinear properties on the compressive strength prediction on unidirectional carbon-fiber composites." *Compos Sci and Technol*, vol. 65, pp. 2140-2147, 2005.
- [195] Q. Bing and C. T. Sun, "Modeling and testing strain rate-dependent compressive strength of carbon/epoxy composites," *Composites Science and Technology, 20th Anniversary Special Issue*, vol. 65, pp. 2481-2491, 2005.
- [196] P. Jongvisuttisun, W. Tanthapanichakoon, and S. Rimdusit, "Development of high performance carbon fiber based prepreps for honeycomb structure," in *MaDParT 2005*, 2005.



- [197] J.-K. Kim and Y.-W. Mai, "Fracture of CFRP containing impregnated fibre bundles," *Composites Science and Technology*, vol. 49(1), pp. 51-60, 1993.
- [198] J. Lee and C. Soutis, "Thickness effect on the compressive strength of T800.24C carbon fibre-epoxy laminates," *Composites Part A: Applied Science and Manufacturing*, vol. 36(2), pp. 213-227, 2005.
- [199] T. V. Parry and A. S. Wronski, "Kinking and tensile, compressive and interlaminar shear failure in carbon-fibre-reinforced plastic beams tested in flexure," *Journal Materials Science*, vol. 16(2), pp. 439-450, 1981.
- [200] D. D. R. Cartié and P. E. Irving, "Effect of resin and fibre properties on impact and compression after impact performance of CFRP," *Composites Part A: Applied Science and Manufacturing*, vol. 33, pp. 483-493, 2002.
- [201] B. W. Kim and J. A. Nairn, "Observations of Fiber Fracture and Interfacial Debonding Phenomena Using the Fragmentation Test in Single Fiber Composites," *Journal of Composite Materials*, vol. 36, pp. 1825-1858, 2002.
- [202] P. W. R. Beaumont and P. D. Anstice, "A failure analysis of the micromechanisms of fracture of carbon fibre and glass fibre composites in monotonic loading," *Journal of Materials Science*, vol. 15(10), pp. 2619-2635, 1980.
- [203] T. Shimokawa, Y. Kakuta, Y. Hamaguchi, and T. Aiyama, "Static and Fatigue Strengths of a G40-800/5260 Carbon Fiber/Bismaleimide Composite Material at Room Temperature and 150{degrees}C," *Journal of Composite Materials*, vol. 42(7), pp. 655-679, 2008.
- [204] N. Oya and H. Hamada, "Mechanical properties and failure mechanism of carbon fibre reinforced thermoplastic laminates," *Composites Part A: Applied Science and Manufacturing*, vol. 28A, pp. 823-832, 1997.
- [205] P. M. Moran and C. F. Shih, "Kink band propagation and broadening in ductile matrix fiber composites: Experiments and analysis," *International Journal of Solids and Structures*, vol. 35(15), pp. 1709-1722, 1998.
- [206] I. J. Davies and R. D. Rawlings, "Mechanical properties in flexure and tension of low density carbon-carbon composites," *Carbon*, vol. 32, pp. 1449-1456, 1994.
- [207] A. G. Evans and W. F. Adler, "Kinking as a mode of structural degradation in carbon fibre composites," *Acta Metallurgica*, vol. 26, pp. 725-738, 1978.
- [208] Y. Z. Wan, J. J. Lian, Y. Huang, Y. L. Wang, and G. C. Chen, "Two-step surface treatment of 3D braided carbon/Kevlar hybrid fabric and influence on mechanical performance of its composites," *Materials Science and Engineering: A*, vol. 429, pp. 304-311, 2006.
- [209] L. A. Berglund, "6. Thermoplastic resins," in *Handbook of Composites*, Second ed, S. T. Peters, Ed. London: Chapman and Hall, 1998, pp. 115-130.

- [210] P. M. Jelf and N. A. Fleck, "Compression Failure Mechanisms in Unidirectional Composites," *Journal of Composite Materials*, vol. 26, pp. 2706-2726, 1992.
- [211] T. J. Vogler and S. Kyriakides, "Inelastic behavior of an AS4/PEEK composite under combined transverse compression and shear. Part I: experiments," *International Journal of Plasticity*, vol. 15, pp. 783-806, 1999.
- [212] M. Kawai and M. Koizumi, "Nonlinear constant fatigue life diagrams for carbon/epoxy laminates at room temperature," *Composites Part A: Applied Science and Manufacturing*, vol. 38, pp. 2342-2353, 2007.
- [213] P. M. Moran, X. H. Liu, and C. F. Shih, "Kink band formation and band broadening in fiber composites under compressive loading," *Acta Metallurgica et Materialia*, vol. 43(8), pp. 2943-2958, 1995.
- [214] E. S. Greenhalgh, "Mechanical evaluation of carbon fibre reinforced thermoplastic I-beams," DRA TR 92071, Farnborough, U.K. 1993.
- [215] A. Arbelaiz, B. Fernandez, G. Cantero, R. Llano-Ponte, A. Valea, and I. Mondragon, "Mechanical properties of flax fibre/polypropylene composites. Influence of fibre/matrix modification and glass fibre hybridization," *Composites Part A: Applied Science and Manufacturing*, vol. 36(12), pp. 1637-1644, 2005.
- [216] R. Burgueno, M. J. Quagliata, A. K. Mohanty, G. Mehta, L. T. Drzal, and M. Misra, "Hybrid biofiber-based composites for structural cellular plates," *Composites Part A: Applied Science and Manufacturing*, vol. 36, pp. 581-593, 2005.
- [217] K. John and S. V. Naidu, "Sisal fiber/glass fiber hybrid composites: The impact and compressive properties," *Journal of Reinforced Plastics and Composites*, vol. 23, pp. 1253-1258, 2004.
- [218] Y. A. Khalid, S. A. Mutasher, B. B. Sahari, and A. M. S. Hamouda, "Bending fatigue behavior of hybrid aluminum/composite drive shafts," *Materials & Design*, vol. 28, pp. 329-334, 2007.
- [219] R. Park and J. Jang, "Impact behavior of aramid fiber/glass fiber hybrid composite: Evaluation of four-layer hybrid composites," *Journal of Materials Science*, vol. 36, pp. 2359-2367, 2001.
- [220] R. G. Reid, T. A. I'Ons, and R. Paskaramoorthy, "The mechanical properties of oxyfluorinated hybrids of glass fibre and polypropylene fibre," *Composite Structures*, vol. 66, pp. 611-616, 2004.
- [221] A. K. Srivastav, M. K. Behera, and B. C. Ray, "Loading rate sensitivity of jute/glass hybrid reinforced epoxy composites: effect of surface modification," *Journal of Reinforced Plastic and Composites*, vol. 26, pp. 851-860, 2007.
- [222] M. M. Thwe and K. Liao, "Durability of bamboo-glass fiber reinforced polymer matrix hybrid composites," *Composites Science and Technology*, vol. 63, pp. 375-387, 2003.

- [223] C. E. Bakis, A. Nanni, J. A. Torosky, and S. W. Koehler, "Self-monitoring, pseudo-ductile, hybrid FRP reinforcement rods for concrete applications," *Composites Science and Technology*, vol. 61, pp. 815-823, 2001.
- [224] Y. Z. Wan, G. C. Chen, Y. Huang, Q. Y. Li, F. G. Zhou, J. Y. Xin, and Y. L. Wang, "Characterization of three-dimensional braided carbon/Kevlar hybrid composites for orthopedic usage," *Materials Science and Engineering A*, vol. 398, pp. 227-232, 2005.
- [225] Y. Z. Wan, Y. L. Wang, Y. Huang, H. L. Luo, F. He, and G. C. Chen, "Moisture absorption in a three-dimensional braided carbon/Kevlar/epoxy hybrid composite for orthopaedic usage and its influence on mechanical performance," *Composites Part A: Applied Science and Manufacturing*, vol. 37, pp. 1480-1484, 2006.
- [226] F. Larsson and L. Svensson, "Carbon, polyethylene and PBO hybrid fibre composites for structural lightweight armour," *Composites Part A: Applied Science and Manufacturing*, vol. 33, pp. 221-231, 2002.
- [227] Y. Li, X. J. Xian, C. L. Choy, M. Guo, and Z. Zhang, "Compressive and flexural behavior of ultra-high-modulus polyethylene fiber and carbon fiber hybrid composites," *Composites Science and Technology*, vol. 59, pp. 13-18, 1999.
- [228] R. Park and J. Jang, "Performance improvement of carbon fiber/polyethylene fiber hybrid composites," *Journal of Materials Science*, vol. 34, pp. 2903-2910, 1999.
- [229] D. A. Burianek and S. M. Spearing, "Delamination growth from face sheet seams in cross-ply titanium/graphite hybrid laminates," *Composites Science and Technology*, vol. 61, pp. 261-269, 2001.
- [230] D. A. Burianek and S. M. Spearing, "Fatigue damage in titanium-graphite hybrid laminates," *Composites Science and Technology*, vol. 62, pp. 607-617, 2002.
- [231] I. J. Davies, H. Hamada, and M. Shibuya, "Flexural and compressive properties of polymer matrix composites containing a mixture of carbon and silicon carbide fibres: Part 2 - Compression," in *H. Fukuda, T. Ishikawa, Y. Kogo (editors): Proceedings of the 9th US-Japan conference on composite materials*, Mishima, Shizuoka, Japan, July 3-4, 2000, pp. 373-374, Japan Society for Composite Materials, Tokyo, Japan.
- [232] I. J. Davies, H. Hamada, and M. Shibuya, "Compressive and flexural strength of polymer composites containing a mixture of carbon and silicon carbide fibres: Part 1 - Flexural properties," in *T. Tanimoto and T. Morii (editors): Proceedings of the 6th Japan International SAMPE Symposium*, Tokyo, Japan, October 26-29, 1999, pp. 571-574, Japan Chapter of SAMPE, Tokyo, Japan.
- [233] Sudarisman, I. J. Davies, and H. Hamada, "Compressive failure of unidirectional hybrid fibre-reinforced epoxy composites containing carbon

- and silicon carbide fibres," *Composites Part A: Applied Science and Manufacturing*, vol. 38, pp. 1070-1074, 2007.
- [234] M. Wang, Z. Zhang, and Z. Sun, "The Hybrid Model and Mechanical Properties of Hybrid Composites Reinforced with Different Diameter Fibers," *Journal of Reinforced Plastics and Composites*, vol. 28, pp. 257-264, 2009.
  - [235] G. Marom, S. Fischer, F. R. Tuler, and H. D. Wagner, "Hybrid effects in composites: conditions for positive or negative effects versus rule-of-mixtures behaviour," *Journal of Materials Science (Historical Archive)*, vol. 13, pp. 1419-1426, 1978.
  - [236] T. Hayashi, "On the improvement of mechanical properties of composites by hybrid composition," in *Proceedings of the 8th International Reinforced Plastics Conference, Paper No. 22*, Brighton, U.K., 10-12 October 1972, pp. 149-152.
  - [237] M. G. Phillips, "Composition parameters for hybrid composite materials," *Composites*, vol. 12, pp. 113-116, 1981.
  - [238] Y. J. You, Y. H. Park, H. Y. Kim, and J. S. Park, "Hybrid effect in tensile properties rods with various material compositions," *Composite Structures*, vol. 80, pp. 117-122, 2007.
  - [239] G. Kretsis, "A review of the tensile, compressive, flexural and shear properties of hybrid fibre-reinforced plastics," *Composites*, vol. 18, pp. 13-23, 1987.
  - [240] S.-Y. Fu, Y.-W. Mai, B. Lauke, and C.-Y. Yue, "Synergistic effect on the fracture toughness of hybrid short glass fibre and short carbon fibre reinforced polypropylene composites," *Materials Science and Engineering: A*, vol. 323, pp. 326-335, 2002.
  - [241] T. J. Kang, S. J. Shin, K. Jung, and J. K. Park, "Mechanical, thermal and ablative properties of interply continuous/spun hybrid carbon composites," *Carbon*, vol. 44, pp. 833-839, 2006.
  - [242] K. D. Jones and A. T. DiBenedetto, "Fiber fracture in hybrid composite systems," *Composites Science and Technology*, vol. 51, pp. 53-62, 1994.
  - [243] A. B. A. Hariharan and H. P. S. A. Khalil, "Lignocellulose-based hybrid bilayer laminate composite: Part I - Studies on tensile and impact behavior of oil palm fiber-reinforced epoxy resin," *Journal of Composite Materials*, vol. 39, pp. 663-684, 2005.
  - [244] R. F. Dickson, G. Fernando, T. Adam, H. Reiter, and B. Harris, "Fatigue behaviour of hybrid composites," *Journal of Materials Science (Historical Archive)*, vol. 24, pp. 227-233, 1989.
  - [245] R. A. Chaudhuri and H. J. Garala, "Analytical/experimental evaluation of hybrid commingled carbon/glass/epoxy thick-section composites under compression," *Journal of Composite Materials*, vol. 29, pp. 1695-1718, 1995.

Every reasonable effort has been made to acknowledge the owners of copyright materials. I would be pleased to hear from any copyright owner who has been omitted or incorrectly acknowledged.

## CHAPTER 3

# MECHANICS OF MATERIALS

### 3.1. CLASSICAL BEAM THEORY

The Euler beam theory solution is an approximate solution that, generally, gives results in good agreement with the elasticity solution that is an exact solution. The strength of materials solution of beams, according to the classical beam theory, is based on the following assumptions [1] pp. 221-222.

1. The span of the beam is much larger than the other two dimensions such that normal stresses generated in its cross-sectional area are much greater than those generated in the lateral directions.
2. The beam is prismatic, *i.e.*, its cross-section is constant along its span.
3. The loads are applied in the plane of symmetry of the beam.
4. Beam deformation is small, such that the beam behaves elastically.
5. The plane that is perpendicular to the longitudinal axis of the beam before deformation remains perpendicular under deformation.
6. The beam is comprised of isotropic material.

#### 3.1.1. Normal Stress and Normal Strain Distribution

Figure 3.1(b) shows that a line of length  $dx$  before deformation experiences an elongation of  $\Delta x$ . Consider two similar triangles OAB and OCD,

$$\frac{dx + \Delta x}{dx} = \frac{r + (-y)}{r} \quad (3.1)$$

Defining the normal strain as elongation per unit length,  $\varepsilon = \Delta x / dx$ , then equation (3.1) gives

$$\varepsilon = -\frac{y}{r} \quad (3.2)$$

where  $y$  is the layer ordinate and  $r$  is the curvature of radius of the beam upon deformation.

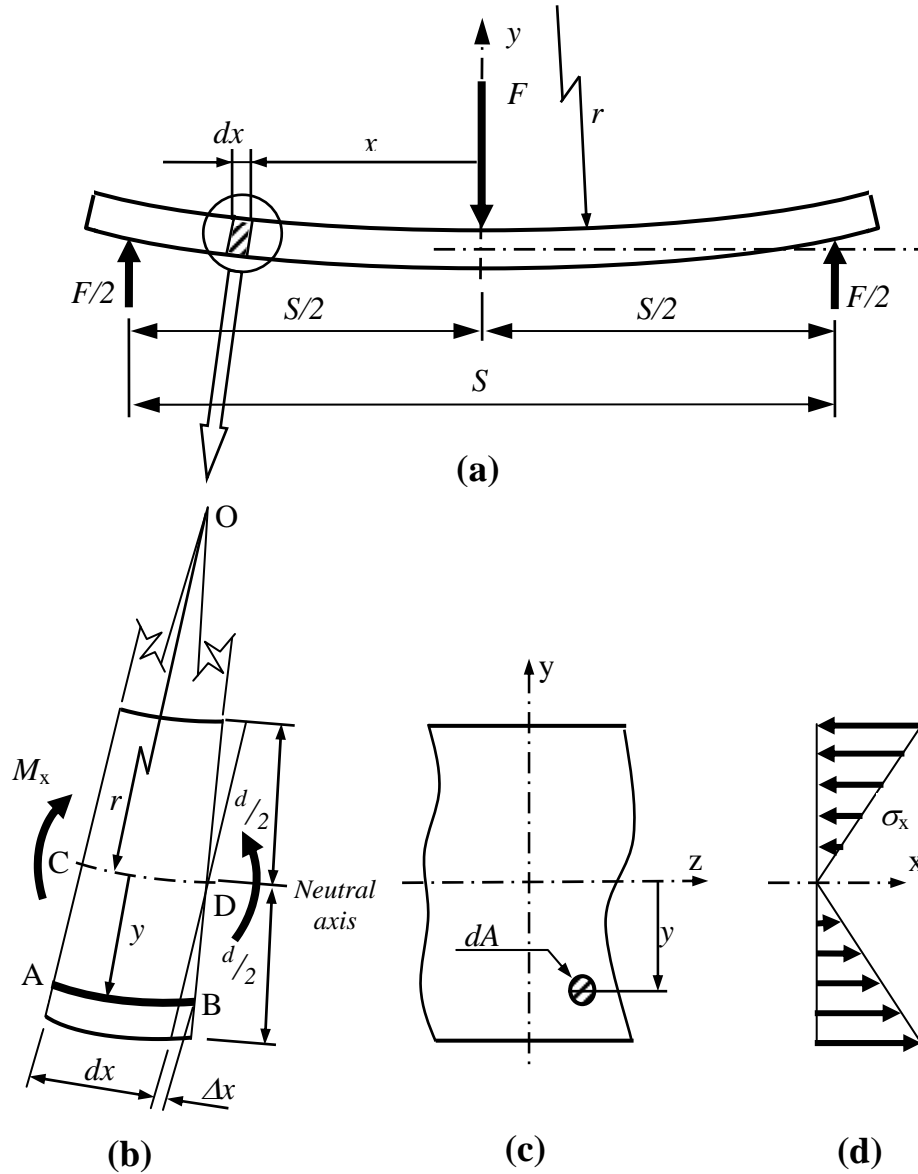


**Figure 3.1.** A beam subjected to a three-point bending: (a) A simply supported beam of span  $S$  deformed with curvature radius of  $r$  due to a shear force  $F$  acting in the mid-span, (b) Magnification of an arbitrary segment of the beam showing the deformation of a layer located in a distance of  $y$  from neutral axis, (c) Arbitrary cross section of the beam showing an elementary cross section  $dA$  experiencing normal stress of magnitude  $\sigma_x$ , (d) Schematic representation of normal stress distribution along the  $y$  axis.

Employing Hooke's law in equation (3.2) and rearranging the terms yields

$$\sigma_x = E \cdot \left( -\frac{y}{r} \right) \quad (3.3a)$$

$$\text{or} \quad \frac{E}{r} = -\frac{\sigma_x}{y} \quad (3.3b)$$

where  $E$  is the elastic modulus. The magnitude of the bending moment with respect to the neutral axis generated by  $\sigma_x$  acting over the elementary area  $dA$  is  $dM_x = -(\sigma_x \cdot dA) \cdot y$ . Thus, the magnitude of bending over the entire cross-sectional area is

$$M_x = \int -(\sigma_x \cdot dA) \cdot y = \frac{E}{r} \int y^2 \cdot dA = \frac{E \cdot I_x}{r} \quad (3.4)$$

where  $I_x = \int y^2 \cdot dA$  is the second moment of inertia. Upon the substitution of equation (3.3b) into equation (3.4) and rearranging the terms gives

$$\sigma_x = -\frac{M_x \cdot y}{I_x} \quad (3.5)$$

Equation (3.5) shows that the normal stress is linearly distributed along the y-axis as illustrated in Figure 3.1(d). For special cases as shown Figure 3.1(a) and given that the width and depth of the beam are  $w$  and  $d$ , respectively, the magnitudes of maximum and minimum normal stresses, which occur at  $y = \mp d/2$ , and will be given by equations (3.6a) and (3.6b), respectively.

$$\sigma_x = \frac{3F \cdot S}{2w \cdot d^2} \quad (3.6a)$$

$$\sigma_x = -\frac{3F \cdot S}{2w \cdot d^2} \quad (3.6b)$$



If the units of force and linear dimensions in equations (3.6a) and (3.6b) are given in Newton (N) and millimetres (mm), respectively, then the magnitude of stress will be obtained in mega-Pascal (MPa). Equation (3.6a) is the same as equation (3) given in the ASTM D790 test standard for the three-point bend testing of short beams, *i.e.*, beams with a span-to-depth ratio,  $S/d$ , of 16 or less [2]. Employing Hooke's law into equations (3.6a) and (3.6b) yields their respective strains.

### 3.1.2. Shear Stress Distribution

Consider a segment of length  $dx$  at a distance of  $x$  from the mid span of a prismatic beam subjected to a lateral load  $F$  as shown Figure 3.1(a). An enlarged view of this segment has been redrawn in Figure 3.2(a). Defining the magnitude of bending moment acted on the right face and on the left face of the segment as  $M_x$  and  $M_x + dM_x$ , respectively, results in respective normal stresses of  $\sigma_x$  and  $\sigma_x + d\sigma_x$ , such that the magnitude of forces acted upon face elements BC on the right and AD on the left are, respectively

$$F_{BC} = \int \sigma_x \cdot dA = \int \frac{M_x \cdot y}{I} \cdot dA \quad (3.7a)$$

$$F_{AD} = \int (\sigma_x + d\sigma_x) \cdot dA = \int \frac{(M_x + dM_x) \cdot y}{I} \cdot dA \quad (3.7b)$$

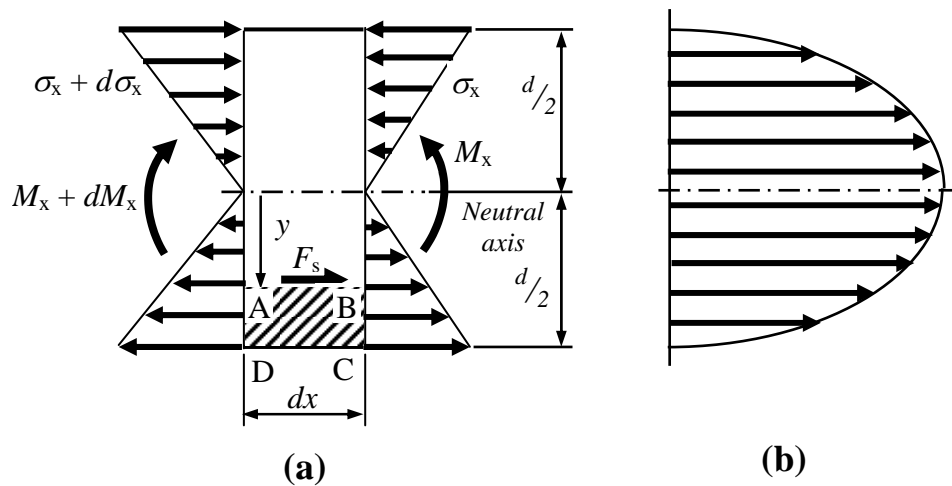


**Figure 3.2.** Enlarged view of beam segments as seen Figure 3.1(a): (a) Normal and shear stresses generated over the segment due to lateral force  $F$ , (b) Shear stress distribution over the depth of the beam.

Denoting  $\tau$  as the shear stress generated on the surface AB, and given the width of a rectangular cross-section beam being  $w$ , not shown on the figure, then the magnitude of shear force  $F_s$  generated on the surface AB is

$$F_s = \tau \cdot w \cdot dx \quad (3.8)$$

Applying an equilibrium equation for the shaded layers ABCD of the beam segment gives

$$F_s = F_{AD} - F_{BC} = \int \frac{(M_x + dM_x) \cdot y}{I} \cdot dA - \int \frac{M_x \cdot y}{I} \cdot dA$$

$$\tau \cdot w \cdot dx = \frac{dM_x}{I} \cdot \int y \cdot dA \quad \text{or} \quad \tau = \frac{dM_x / dx}{I \cdot w} \cdot \int_{y=y}^{y=d/2} y \cdot (w \cdot dy)$$

Recall that the lateral force acted on the respective cross section is  $F = \frac{dM_x}{dx}$ , the

second moment of inertia of the cross-section is  $I = \frac{w \cdot d^3}{12}$ , and the depth of the

beam is  $d$ , then the magnitude of shear stress generated on a layer at a distance  $y$  from the neutral axis is

$$\tau = \frac{3F}{2w \cdot d^3} (d^2 - 4y^2) \quad (3.9)$$

Unlike the normal stress distribution which is linear along the  $y$ -axis, that of shear stress is parabolic as schematically shown in Figure 3.2(b). The maximum shear stress will occur when  $4y^2 = 0$  or  $y = 0$ , which is located along the neutral axis with the magnitude being given by

$$\tau = \frac{3F}{2w \cdot d} \quad (3.10)$$

### 3.1.3. 'Composite' Cross Section of Beams

By definition, the composite cross-section of a beam is the cross-section of a beam that comprises of more than one material [3] pp. 301-302. Reinforced concrete beams, bimetallic beams, sandwich beams and hybrid composite beams are some examples of beams possessing composite cross-sections. A schematic illustration of this typical cross-section has been presented in Figure 3.3(a).

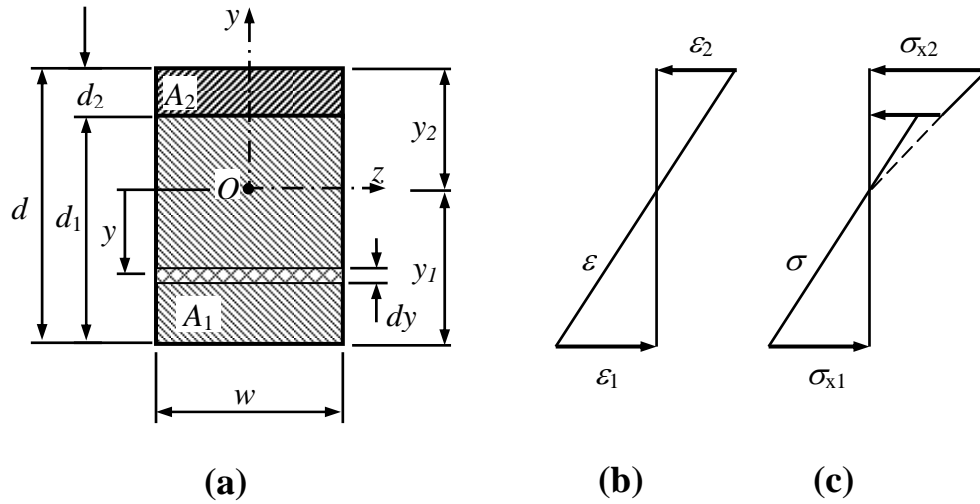


**Figure 3.3.** A typical composite cross section comprising of two different materials of rectangular shapes. (a) Cross section, (b) Normal strain distribution along  $y$ -axis is assumed to be linear, (c) Normal stress distribution along  $y$ -axis showing discontinuity on the interface of the two materials.

#### 3.1.3.1. Normal stress distribution

Given that the elastic modulus of materials 1 and 2 are  $E_1$  and  $E_2$ , respectively, the maximum normal stress at the outermost layers according to equation (3.3a) are

$$\sigma_{x1} = E_1 \cdot \left( -\frac{y}{r} \right) \quad (3.10a)$$

$$\sigma_{x2} = E_2 \cdot \left( -\frac{y}{r} \right) \quad (3.10b)$$

In addition, the magnitude of the bending moment generated over the entire cross-section according to equation (3.4) becomes

$$M_x = \int_{A1} -(\sigma_{x1} \cdot dA) \cdot y + \int_{A2} -(\sigma_{x2} \cdot dA) \cdot y = \frac{E_1}{r} \int_{A1} y^2 \cdot dA + \frac{E_2}{r} \int_{A2} y^2 \cdot dA$$

Recall that  $\int_{A1} y^2 \cdot dA = I_1$  and  $\int_{A2} y^2 \cdot dA = I_2$ , then the magnitude of bending moment becomes

$$M_x = \frac{E_1 \cdot I_1}{r} + \frac{E_2 \cdot I_2}{r}$$

$$\text{or } r = \frac{E_1 \cdot I_1 + E_2 \cdot I_2}{M_x} \quad (3.11)$$

Substitution of equation (3.11) into equations (3.10a) and (3.10b) and rearrange the terms gives

$$\sigma_{x1} = -\frac{M_x \cdot y \cdot E_1}{E_1 \cdot I_1 + E_2 \cdot I_2} \quad (3.12a)$$

$$\sigma_{x2} = -\frac{M_x \cdot y \cdot E_2}{E_1 \cdot I_1 + E_2 \cdot I_2} \quad (3.12b)$$

### 3.1.3.2. Locating the neutral axis

Considering Figure 3.3(a), a composite cross section comprising of two different types of RFP composite materials, the equilibrium equation of horizontal forces over the entire cross-sectional area is

$$\int_{A1} \sigma_{x1} \cdot dA + \int_{A2} \sigma_{x2} \cdot dA = 0 \quad (3.13)$$

Upon substitution of equations (3.10a) and (3.10b), eliminating the term  $r$  and rearranging the terms yields

$$E_1 \int_{A1} y \cdot dA + E_2 \int_{A2} y \cdot dA = 0 \quad (3.14)$$

From Figure 3.3(a)

$$\int_{A1} y \cdot dA = \int_{y_1}^{d_1 - y_1} y(w \cdot dy) = \frac{w}{2} (d_1^2 - 2d_1 y_1) \quad (3.15a)$$

$$\int_{A2} y \cdot dA = \int_{d_1 - y_1}^{d - y_1} y(w \cdot dy) = \frac{w}{2} \{d^2 - d_1^2 - 2(d - d_1)y_1\} \quad (3.15b)$$

Substitution of the above equations into equation (3.14), and noting that  $d_1 = d - d_2$  or  $d - d_1 = d_2$ , as seen in Figure 3.3a, gives the distance  $y_1$  measured from the bottom face of the beam as

$$y_1 = \frac{d^2 \cdot E_1 + (2d \cdot d_2 - d_2^2)(E_2 - E_1)}{2[d \cdot E_1 + d_2(E_2 - E_1)]} \quad (3.16)$$

If the volume fractions of the two fibre-reinforced polymer composites composing the hybrid composite beams are the same,  $V_{f1} = V_{f2}$ , then the hybrid ratio,  $r_h$ , will be

$$r_h = \frac{V_{f2}}{V_f} = \frac{d_2}{d} \quad (3.17)$$

Dividing both the numerator and denominator of equation (3.16) by  $d^2$ , and substituting equation (3.17) into equation (3.16) yields the distance of the neutral plane from the bottom surface as

$$y_1 = \frac{d \cdot [E_1 + r_h \cdot (2d \cdot d_2 - d_2^2)(E_2 - E_1)]}{2[E_1 + r_h(E_2 - E_1)]} \quad (3.18)$$

#### 3.1.4. Beam Deflection

Consider an infinitesimally small segment,  $DE = ds$ , of a beam subjected to a three-point bending load as shown in Figure 3.4. Defining  $r$  as the radius of curvature of the beam, then the magnitude of increment angle DOE is

$$d\theta = \frac{ds}{r} \quad (3.19)$$

Because  $ds$  is infinitesimally small,  $ds \approx dx$ , and equation (3.19) becomes.

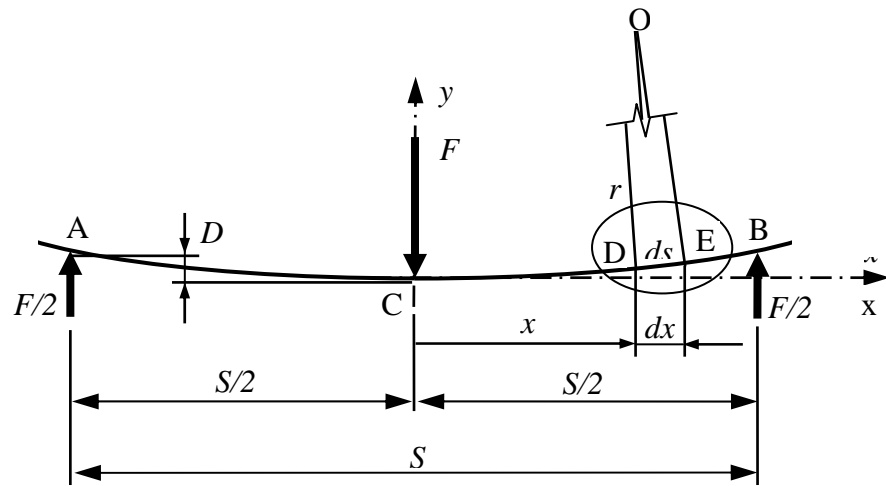
$$d\theta = \frac{dx}{r} \quad (3.20)$$

Substituting the value of  $r$  from equation (3.4), and rearranging the terms yields

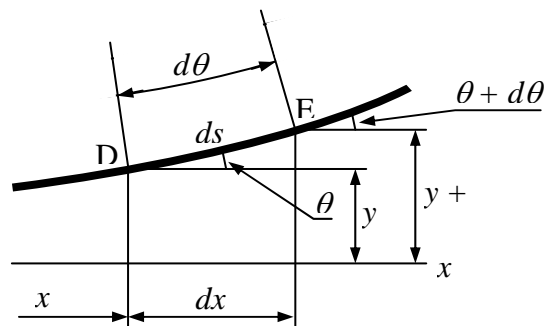
$$\frac{d\theta}{dx} = -\frac{M_x}{E \cdot I_x} \quad (3.21)$$

The slope of deflection curve at D, Figure 3.4(b), is

$$\tan \theta = \frac{dy}{dx} \quad (3.22)$$



(a)



(b)

**Figure 3.4.** Deflection of a beam: (a) A simply supported beam subjected to a lateral force  $F$  acted at the mid-span of the beam, (b) Magnified view of segment DE of the beam showing the slope and deflection  $y$  and  $\theta$ , respectively, at D, and  $\theta + d\theta$  and  $y + dy$ , respectively at E.

When  $\theta \approx 0$ ,  $\tan \theta = \theta$ , and equations (3.21) and (3.22) become

$$\tan \theta = \theta = \frac{dy}{dx} \quad (3.23)$$

$$\frac{d\theta}{dx} = \frac{d^2y}{dx^2} = -\frac{M_x}{E \cdot I_x} \quad (3.24)$$

For the special case as illustrated in Figure 3.4(a), the magnitude of bending moment at any  $0 \leq x \leq S/2$  along the  $x$  axis is  $M_x = \frac{F}{2} \cdot \left( \frac{S}{2} - x \right)$ , the boundary conditions are

$$\left. \begin{array}{l} \theta = 0 \\ y = 0 \end{array} \right\} \text{ at } x = 0 \quad (3.25)$$

Integration of equation (3.24) gives

$$\theta = \frac{dy}{dx} = \frac{F}{4E \cdot I_x} (S \cdot x - x^2) + C_1 \quad (3.26)$$

Employing the first boundary condition as given in equation (3.25) gives  $C_1 = 0$ , and equation (3.26) becomes

$$\theta = \frac{dy}{dx} = \frac{F}{4E \cdot I_x} (S \cdot x - x^2) \quad (3.27)$$

Integration of equation (3.27) then yields

$$y = \frac{F}{24E \cdot I_x} (3S \cdot x^2 - 2x^3) + C_2 \quad (3.28)$$

Applying the second boundary condition as given in equation (3.25) gives  $C_2 = 0$ , and equation (3.28) becomes

$$y = \frac{F}{24E \cdot I_x} (3S \cdot x^2 - 2x^3) \quad (3.29)$$

The deflection at point B where  $x = S/2$  is

$$D = \frac{F \cdot S^3}{48E \cdot I_x} \quad (3.30)$$

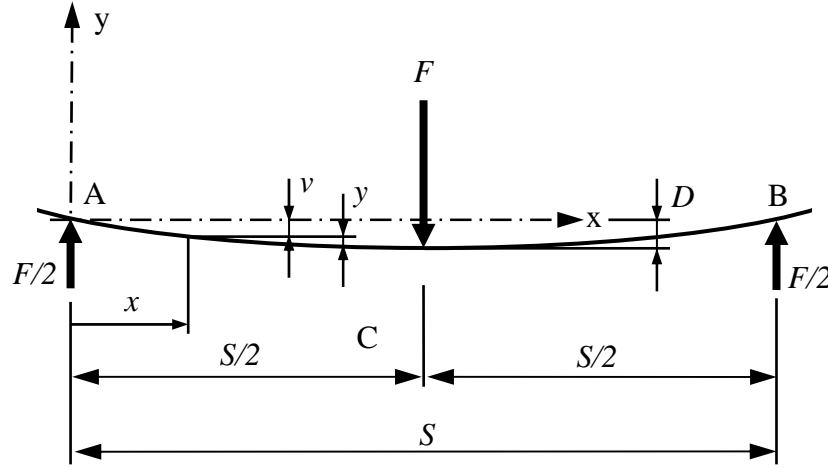


**Figure 3.5.** Deflection of a simply supported beam after the origin has been move to point A

As the beam shown in Figure 3.4(a) is symmetric about the  $y$  axis, so is its deflection. If the  $x$  axis is moved up so that it passes points A and B, and the  $y$  axis is moved to the left so that it passes point A, as illustrated in Figure 3.5, then in the new coordinate system, the  $x$  value in equation (3.29) is replaced with  $\left(\frac{S}{2} - x\right)$

and equation (3.29) becomes

$$y = \frac{F}{48E \cdot I_x} (S^3 - 3S^2x + 2x^3) \quad (3.31)$$

Deflection in the new coordinate system becomes

$$v = \frac{F \cdot x}{48E \cdot I_x} (3S^2 - 4x^2) \quad (3.32)$$

Maximum deflection,  $D$ , occurs at  $x = S/2$ , thus, equation (3.32) becomes

$$D = \frac{F \cdot S^3}{48E \cdot I_x} \quad (3.33)$$



Equation (3.33) can be found in other references [2] and [4-6] pp. (610, 314, and 192, respectively).

### 3.2. THE RULE OF MIXTURES

The properties of a unidirectional composite material can be predicted by the so called *rule of mixtures*, provided that the properties of the constituent materials are known. The principle of this rule is that composite properties are proportional to the volume fraction of its constituent properties [7, 8], pp. 57 and 177, respectively. The discussion in this section is extended to hybrid fibre composites containing two different types or grades of fibres, but is limited to unidirectional fibre arrangements.

#### 3.2.1. Volume Fraction and Composite Density

The volume fraction of the constituents of composite materials can be defined as the partial volume of their respective constituents, or mathematically can be written as

$$V_i = \frac{v_i}{v_c} \quad (3.34)$$

Where  $V_i = V_{f1}, V_{f2}, V_m$ , or  $V_v$  = volume fraction of each constituent,  $v_i = v_{f1}, v_{f2}, v_m$ , or  $v_v$  = volume of each constituent, and  $v_c$  = volume of the composite. Thus,

$$V_{f1} + V_{f2} + V_m + V_v = 1 \quad (3.35a)$$

If the total volume fraction of fibre is denoted by  $V_f$  where  $V_f = V_{f1} + V_{f2}$ , while for a high quality PMC composite  $V_v \ll V_{fi}$  and  $V_v \ll V_m$  then  $V_v$  is negligible, and Eq. (3.35a) can be rewritten as

$$V_f + V_m = 1 \quad (3.35b)$$

$$V_m = 1 - V_f \quad (3.35c)$$

Given the densities of the two types of fibre, the matrix and the voids as  $\rho_{f1}$ ,  $\rho_{f2}$ ,  $\rho_m$ , and  $\rho_v$ , respectively, the density of a hybrid composite is

$$\rho_c = V_{f1} \cdot \rho_{f1} + V_{f2} \cdot \rho_{f2} + V_m \cdot \rho_m + V_v \cdot \rho_v \quad (3.36a)$$

As voids contain entrapped gas within solid composite materials, the density of voids is much lower than those of the matrix or the fibres, so is their volume fraction, thus their product given in the last term in Eq. (3.36a) can be neglected, and Eq. (3.36a) can be rewritten as

$$\rho_c = V_{f1} \cdot \rho_{f1} + V_{f2} \cdot \rho_{f2} + V_m \cdot \rho_m \quad (3.36b)$$

Then defining the hybrid ratio,  $r_h$ , as the ratio of volume fraction of the fibre possessing higher strength,  $V_{f2}$ , to volume fraction of total fibre,  $V_f$ ,

$$r_h = \frac{V_{f2}}{V_f} \quad (3.37a)$$

or

$$V_{f2} = r_h \cdot V_f \quad (3.37b)$$

$$V_{f1} = V_f - V_{f2} = (1 - r_h) \cdot V_f \quad (3.37c)$$

Combining Eqs. (3.36b), (3.35c), (3.37b) and (3.37c) yields

$$V_f = \frac{\rho_c - \rho_m}{(1 - r_h) \cdot \rho_{f1} + r_h \cdot \rho_{f2} + \rho_m} \quad (3.38)$$

Composite density,  $\rho_c$ , can be calculated from the measured values of the mass and the volume of specimens

$$\rho_c = \frac{m_c}{V_c} \quad (3.39)$$

### 3.2.2. Longitudinal Strengths

*Longitudinal strength* – The longitudinal strength,  $\sigma_{11}$ , of unidirectional composites can be predicted using the rule of mixtures. The assumptions employed in this prediction are (i) fibre and matrix properties are uniform, (ii) fibres are continuous and parallel to one another throughout the length, and (iii) perfect bonding exists at the fibre-matrix interface [7] pp. 59-60, such that the composite under loading experiences isostrain deformation [8] p.178.

If a normal, either tensile or compressive, load of magnitude  $F$  is applied onto a unidirectional composite specimen in the longitudinal direction, and given that the cross-sectional area of the composite is  $A_c$  and fibre volume fractions are  $V_{f1}$  and  $V_{f2}$ , then each of the constituents will carry a fraction of  $F$  which is proportional to their respective volume fraction as follows

$$F = F_{f1} + F_{f2} + F_m \quad (3.40a)$$

where  $F_{f1}$ ,  $F_{f2}$ , and  $F_m$  are the portions of load carried by fibre one, fibre two and the matrix, respectively. Eq. (3.40a) can be written in terms of the longitudinal stress as

$$F = \sigma_{11} \cdot A_c = \sigma_{f1} \cdot A_{f1} + \sigma_{f2} \cdot A_{f2} + \sigma_m \cdot A_m \quad (3.40b)$$

where  $\sigma_{11}$ ,  $\sigma_{f1}$ ,  $\sigma_{f2}$ , and  $\sigma_m$  are the longitudinal stresses in the composite, in fibre one, in fibre two, and in the matrix, respectively, while  $A_{f1}$ ,  $A_{f2}$  and  $A_m$  are the cross-sectional areas of fibre one, fibre two and the matrix, respectively. Each term in Eq. (3.40b) is then multiplied with  $(l/v_c)$  where  $l$  is the length of the specimen, yielding

$$\sigma_{11} \cdot \frac{A_c \cdot l}{v_c} = \sigma_{f1} \cdot \frac{A_{f1} \cdot l}{v_c} + \sigma_{f2} \cdot \frac{A_{f2} \cdot l}{v_c} + \sigma_m \cdot \frac{A_m \cdot l}{v_c}$$

$$\sigma_{11} \cdot \frac{v_c}{v_c} = \sigma_{f1} \cdot \frac{v_{f1}}{v_c} + \sigma_{f2} \cdot \frac{v_{f2}}{v_c} + \sigma_m \cdot \frac{v_m}{v_c}$$

Considering the definition of volume fraction as given in Eq. (3.34), the above equation can be rewritten as

$$\sigma_{11} = \sigma_{f1} \cdot V_{f1} + \sigma_{f2} \cdot V_{f2} + \sigma_m \cdot V_m \quad (3.41)$$

### 3.2.3. Modulus of elasticity

The first derivative of Eq. (3.41) with respect to strain can be written as

$$\frac{d\sigma_c}{d\varepsilon} = \frac{d\sigma_{f1}}{d\varepsilon} \cdot V_{f1} + \frac{d\sigma_{f2}}{d\varepsilon} \cdot V_{f2} + \frac{d\sigma_m}{d\varepsilon} \cdot V_m$$

Referring to a standard stress-strain curve for tensile testing,  $d\sigma/d\varepsilon$  represents the slope of the curve. If this slope is taken in the initial straight line of the curve, then  $d\sigma/d\varepsilon = E$ , the modulus of elasticity. Therefore

$$E_{11} = E_{f1} \cdot V_{f1} + E_{f2} \cdot V_{f2} + E_m \cdot V_m \quad (3.42)$$

## 3.3. LAMINATED BEAM THEORY

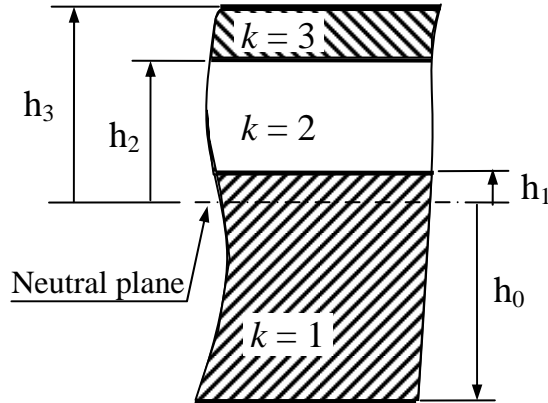


**Figure 3.6.** A representative sectional view a three-layer laminated composite beam showing the layer numbers (*i.e.*  $k = 1$ ,  $k = 2$ , and  $k = 3$ ), the number of layer (*i.e.*  $n = 3$ ), and for  $k = 1$ :  $h_k = h_1$  and  $h_{k-1} = h_0$ , for  $k = 2$ :  $h_k = h_2$  and  $h_{k-1} = h_1$ , and for  $k = 3$ :  $h_k = h_3$  and  $h_{k-1} = h_2$ .

The discussion presented in this section is limited to two dimensional cases only. The bending moment-strain relationship for a laminated composite beam is given by [7] p. 193:

$$\{M\} = [B]\{\varepsilon^0\} + [D]\{\kappa\} \quad (3.43)$$

where  $M$  is the bending moment;  $[B]$  and  $[D]$  are the coupling and bending stiffness matrices, respectively, and  $\{\varepsilon^0\}$  and  $\{\kappa\}$  are the strain and radius of beam curvature matrices at the mid-plane, respectively. The elements of  $[B]$  and  $[D]$  matrices at the  $i^{\text{th}}$  row and  $j^{\text{th}}$  column are given as

$$B_{ij} = \frac{1}{2} \sum_{k=1}^n \left\{ (\bar{Q}_{ij})_k \cdot (h_k^2 - h_{k-1}^2) \right\} \quad (3.44a)$$

$$D_{ij} = \frac{1}{3} \sum_{k=1}^n \left\{ (\bar{Q}_{ij})_k \cdot (h_k^3 - h_{k-1}^3) \right\} \quad (3.44b)$$

where  $k$ ,  $n$  and  $h$  are the layer number, the number of layers comprising the laminated beam, and the ordinates of the interface of any two adjacent layers, respectively, as illustrated in Figure 3.6 for  $n = 3$  and  $k = 1$ .  $(\bar{Q}_{ij})_k$  is the element of the stiffness matrix,  $[\bar{Q}_{ij}]$ , at  $\theta^\circ$  fibre orientation for the  $k^{\text{th}}$  material. For special cases where  $\theta^\circ = 0$ , as fabricated and utilised in this research,  $[\bar{Q}_{ij}]$  becomes [8] p. 208.

$$[\bar{Q}]_0 = [Q] = \begin{bmatrix} Q_{11} & Q_{12} & 0 \\ Q_{12} & Q_{22} & 0 \\ 0 & 0 & Q_{66} \end{bmatrix} \quad (3.45)$$

It should be noted that for orthotropic materials, the bending stiffness matrix,  $[D]$ , is always symmetric, and elements 16 and 26 are always zero. The non-zero elements of the stiffness matrix are

$$Q_{11} = \frac{E_{11}}{1 - \nu_{12}\nu_{21}} \quad (3.46a)$$

$$Q_{22} = \frac{E_{22}}{1 - \nu_{12}\nu_{21}} \quad (3.46b)$$

$$Q_{12} = \frac{\nu_{12}E_{22}}{1 - \nu_{12}\nu_{21}}, \quad E_{22} = \frac{(1 + \xi\eta V_f)E_m}{1 - \eta V_f}, \quad \eta = \frac{(E_f/E_m) - 1}{(E_f/E_m) + \xi} \quad (3.46c)$$

$$\xi = 2$$

$$Q_{66} = G_{12} = \frac{(1 + \xi\eta V_f)G_{12}}{1 - \eta V_f}, \quad \eta = \frac{(G_f/G_m) - 1}{(G_f/G_m) + \xi} \quad (3.46d)$$

$$\xi = 1$$

where  $E_{11}$  and  $E_{22}$  are the longitudinal and transverse moduli, respectively;  $\nu_{12}$  and  $\nu_{21}$  are the major and minor Poisson's ratios, respectively;  $E_f$  and  $E_m$  are the elastic moduli of fibre and matrix, respectively;  $G_{12}$ ,  $G_f$  and  $G_m$  are the in-plane shear moduli of the layer, the fibre and the matrix, respectively; and  $\xi$  is the measure of reinforcement that depends on the fibre geometry, packing geometry and loading conditions. Halpin and Tsai recommended that values of  $\xi = 2$  and  $\xi = 1$  for transverse and shear moduli, respectively, are sufficiently accurate for circular and rectangular cross-section fibres [7] p. 76. The formulas for calculating  $E_{22}$  and  $G_{12}$  as given in equations (3.46c) and (3.46d), respectively, are known as the Halpin-Tsai equations. Poisson's ratios may be calculated as follows

$$\nu_{12} = \nu_f V_f + \nu_m V_m \quad \text{and} \quad \nu_{21} = \frac{E_{22}}{E_{11}} \nu_{12} \quad (4.47)$$

where  $\nu$  and  $V$  are the Poisson's ratio and volume fraction, respectively, whilst the subscripts  $f$  and  $m$  refer to fibre and matrix, respectively. The strain and curvature components are [7] p. 208,

$$\{\varepsilon^o\} = ([A^*] - [B^*][D^{*-1}][C^*])\{N\} + [B^*][D^{*-1}]\{M\} \quad (3.48a)$$

$$\{\kappa\} = [D^{*-1}]\{M\} + [D^{*-1}][C^*]\{N\} \quad (3.48b)$$

Where  $[A]$  is the extensional stiffness matrix and it is, like  $[D]$ , always symmetric, and elements 16 and 26 are always zero for orthotropic materials. Its non-zero elements are calculated using the following expression.

$$A_{ij} = \sum_{k=1}^n \left\{ \left( \overline{Q}_{ij} \right)_k \cdot (h_k - h_{k-1}) \right\} \quad (3.49)$$

In the absence of an external normal force,  $N$ , the first term of equation (3.48a) and the second term of equation (3.48b) will disappear, and equations (3.48a) and (3.48b) then become

$$\{ \varepsilon^o \} = [B^*][D^{*-1}]\{ M \} \quad (3.50a)$$

$$\{ \kappa \} = [D^{*-1}]\{ M \} \quad (3.50b)$$

where

$$[B^*] = -[A^{-1}][B] \quad (3.51a)$$

$$[D^*] = [D] - [B][A^{-1}][B] \quad (3.51b)$$

Substitution of equation (3.45) into equations (3.49), (3.44a) and (3.44b) yields

$$[A] = \begin{bmatrix} A_{11} & A_{12} & 0 \\ A_{12} & A_{22} & 0 \\ 0 & 0 & A_{66} \end{bmatrix} \quad (3.52a)$$

$$[B] = \begin{bmatrix} B_{11} & B_{12} & 0 \\ B_{12} & B_{22} & 0 \\ 0 & 0 & B_{66} \end{bmatrix} \quad (3.52b)$$

$$[D] = \begin{bmatrix} D_{11} & D_{12} & 0 \\ D_{12} & D_{22} & 0 \\ 0 & 0 & D_{66} \end{bmatrix} \quad (3.52c)$$

The inverse of the extensional stiffness matrix, equation (3.52a), and  $[D^{*-1}]$  are

$$[A^{-1}] = \frac{1}{A_{11}A_{22} - A_{12}^2} \begin{bmatrix} A_{22} & -A_{12} & 0 \\ -A_{12} & A_{11} & 0 \\ 0 & 0 & \frac{A_{11}A_{22} - A_{12}^2}{A_{66}} \end{bmatrix} \quad (3.53a)$$

$$[D^{*-1}] = \frac{1}{D_{11}^* D_{22}^* - D_{12}^{*2}} \begin{bmatrix} D_{22}^* & -D_{12}^* & 0 \\ -D_{12}^* & D_{11}^* & 0 \\ 0 & 0 & \frac{D_{11}^* D_{22}^* - D_{12}^{*2}}{D_{66}^*} \end{bmatrix} \quad (3.53a)$$

For the current work where the only non-zero moment is  $M_x$ , equation (3.51a) will result in the following strain components at the mid-plane.

$$\varepsilon_x^0 = \left( B_{11}^* D_{11}^{*-1} + B_{12}^* D_{12}^{*-1} \right) M_x \quad (3.54a)$$

$$\varepsilon_y^0 = \left( B_{12}^* D_{11}^{*-1} + B_{22}^* D_{12}^{*-1} \right) M_x \quad (3.54b)$$

$$\varepsilon_{xy}^0 = \frac{\gamma_{xy}}{2} = 0 \quad (3.54c)$$

The radii of beam curvature at the mid-plane given by equation (3.51b) are

$$\kappa_x = D_{11}^{*-1} M_x \quad (3.55a)$$

$$\kappa_y = D_{12}^{*-1} M_x \quad (3.55b)$$

$$\kappa_{xy} = 0 \quad (3.55c)$$

The magnitude of strains at the tensile and compressive surfaces can be calculated using the following expression.

$$\begin{Bmatrix} \varepsilon_x \\ \varepsilon_y \\ \gamma_{xy} \end{Bmatrix} = \begin{Bmatrix} \varepsilon_x^0 \\ \varepsilon_y^0 \\ 0 \end{Bmatrix} + y \begin{Bmatrix} \kappa_x \\ \kappa_y \\ 0 \end{Bmatrix} \quad (3.56)$$



where  $y$  is the distance of the respective outer layer from the mid-plane (note: not from the neutral axis). Finally, the magnitude of their respective stresses may be calculated as follows.

$$\begin{Bmatrix} \sigma_x \\ \sigma_y \\ \tau_{xy} \end{Bmatrix}_k = \begin{bmatrix} \frac{E_{11}}{1-\nu_{12}\nu_{21}} & \frac{\nu_{12}E_{22}}{1-\nu_{12}\nu_{21}} & 0 \\ \frac{\nu_{12}E_{22}}{1-\nu_{12}\nu_{21}} & \frac{E_{22}}{1-\nu_{12}\nu_{21}} & 0 \\ 0 & 0 & G_{12} \end{bmatrix} \begin{Bmatrix} \varepsilon_x \\ \varepsilon_y \\ \gamma_{xy} \end{Bmatrix}_k \quad (3.57)$$

where  $E_{11}|_k = E_{fk} \cdot V_{fk} + E_m \cdot V_m$  is the longitudinal elastic modulus of the  $k^{\text{th}}$  material;  $E_{22}$  and  $G_{12}$  are as given in equations (3.46c) and (3.46d) and the major and minor Poisson's ratios has been given in equation (3.47).

Equation (3.56) shows that the applied bending moment loaded on the  $x$ -axis does not produce shear strain, but it obviously shows that it can produce normal strain transverse to the fibre direction, *i.e.*  $y$ -direction. Such strain may cause local fibre displacement that initiates local buckling and lead to kink band formation.

### 3.4. THE WORK OF FRACTURE

The work of fracture,  $\gamma_f$ , can be defined as the amount of energy required to create fracture surfaces approximately perpendicular to the loading direction [9]. Its experimental value is represented by the area underneath the load-displacement curve, such that it can be calculated as follows [10].

$$\gamma_f = \frac{1}{2wd} \sum_{i=1}^{i=n-1} \left( \frac{F_i + F_{i+1}}{2} \right) (x_{i+1} - x_i) \quad (3.58)$$

where  $wd$  is the cross-sectional area of the specimen,  $n$  is the number of points at the load-displacement curve up to failure, and  $F_i$  and  $x_i$  are the force and displacement at point  $i$ , respectively. Thus, the work of fracture of materials also represents the capacity of the materials to absorb energy [11] up to failure.

Another quantity that may be as important as the work of fracture is the energy storage capacity up to ultimate stress,  $\gamma_{\max}$ . The magnitude of this quantity can be calculated using equation with  $n$  being counted up to the maximum stress (as opposed to failure for  $\gamma_f$ ).

### 3.5. FAILURE THEORIES

Failure theories predict the strength of a structure, component or member of a structure under various loading configurations. Three failure theories exist that are commonly applied to predict the strength of composite materials, which can be anisotropic, orthotropic or quasi-isotropic depending upon their respective fibre architectures, *e.g.* maximum stress theory, maximum strain theory and maximum distortion energy or Tsai-Hill theory [7] pp. 174-181.

The maximum stress theory predicts that failure will occur if any one of the following inequalities is violated.

$$\sigma_{11} < \sigma_{11-u} \quad (3.59a)$$

$$\sigma_{22} < \sigma_{22-u} \quad (3.59b)$$

$$\tau_{12} < \tau_{12-u} \quad (3.59c)$$

where  $\sigma_{ij}$  and  $\sigma_{ij-u}$  are the applied stress and the composite strength in the principal material axis directions, respectively. Note that, in equations (3.59a) and (3.59b), the composite strength, either tensile or compressive, should be appropriately applied referring to the applied stress.

The maximum strain theory states that in order to prevent failure the following inequalities need to be satisfied

$$\varepsilon_{11} < \varepsilon_{11-u} \quad (3.60a)$$

$$\varepsilon_{22} < \varepsilon_{22-u} \quad (3.60b)$$

$$\gamma_{12} < \gamma_{12-u} \quad (3.60c)$$

where  $\varepsilon_{ij}$  and  $\varepsilon_{ij-u}$  are the applied strain and the composite allowable strain in the principal material axis directions, respectively. It should be noted that, in

equations (3.60a) and (3.60b), the composite allowable strain, either tensile or compressive, should be appropriately applied referring to the applied strain.

According to the maximum distortion energy theory, failure will occur when the following inequality is satisfied.

$$\left(\frac{\sigma_{11}}{\sigma_{11-u}}\right)^2 - \left(\frac{\sigma_{11}}{\sigma_{11-u}}\right)\left(\frac{\sigma_{22}}{\sigma_{11-u}}\right) + \left(\frac{\sigma_{22}}{\sigma_{22-u}}\right)^2 + \left(\frac{\tau_{12}}{\tau_{12-u}}\right)^2 \geq 1 \quad (3.61)$$

Note that the composite normal strength,  $\sigma_{ij-u}$ , either tensile or compressive, needs to be applied in accordance with the applied normal stress.

Let us look at the maximum stress and maximum strain theories. Inequalities (3.59)s and (3.60)s show that each of the stresses and strains are evaluated individually. It can further be deduced that the failure mode will be associated with any term of the inequality being violated. In addition to this, for brittle composite materials with linear stress-strain relationships up to failure, these two theories will result in the same prediction. In the contrary to this, the maximum distortion energy theory brings about the interaction effect between the existing stresses in the materials under consideration. Although these inequalities are applicable to two-dimensional cases, equations (3.56) and (3.57) show that multi-axial stress and strain states will be produced even if the material is subjected to one-dimensional loading. Therefore, these inequalities may also need to be applied to the three-point bend loading configuration carried out in this research.

## REFERENCES

- [1] R. K. Bansal, *A Textbook of Strength of Materials*, 4th ed. New Delhi: Laxmi Publications, 2007.
- [2] "ASTM D790-07 Standard test method for flexural properties of unreinforced and reinforced plastic and electrical insulating materials by three-point bending," in *Annual Book of ASTM Standard*. vol. Vol. 08.01 West Conshohocken, PA, USA: ASTM Int., 2005.
- [3] J. M. Gere and S. P. Timoshenko, *Mechanics of Materials*. London: Chapman and Hall, 1989.

- [4] A. P. Boresi, R. J. Schmidt, and O. M. Sidebottom, *Advanced Mechanics of Materials*. New York: John Wiley and Sons, Inc., 1993.
- [5] J. M. Gere, *Mechanics of Materials*, 2nd ed. Southbank, VIC, Australia: Thomson, 2004.
- [6] N. E. Dowling, *Mechanical Behavior of Materials*. Englewood Cliff: Prentice Hall, 1993.
- [7] B. D. Agarwal and L. J. Broutman, *Analysis and Performance of Fiber Composites*, 2nd ed. New York: John Wiley and Sons, Inc., 1990.
- [8] K. K. Chawla, *Composite Materials: Science and Engineering*. New York: Springer-Verlag, 1987.
- [9] J. E. Gordon and G. Jeronimidis, "Work of fracture of natural cellulose," *Nature*, vol. 252, pp. 116-, 1974.
- [10] Sudarisman, B. de San Miguel, and I. J. Davies, "The Effect of Partial Substitution of E-glass Fibre for Carbon Fibre on the Mechanical Properties of CFRP Composites," in *Proceedings of the International Conference on Materials and Metallurgical Engineering 2009, 24-25 June*, Surabaya, Indonesia, 2009, pp. MI 116-119.
- [11] M. Yang and R. Stevens, "Microstructure and properties of SiC whisker reinforced ceramic composites," *Journal of Materials Science*, vol. 26, pp. 726-736, 1991.

Every reasonable effort has been made to acknowledge the owners of copyright materials. I would be pleased to hear from any copyright owner who has been omitted or incorrectly acknowledged.

## CHAPTER 4

# EXPERIMENTAL PROCEDURE

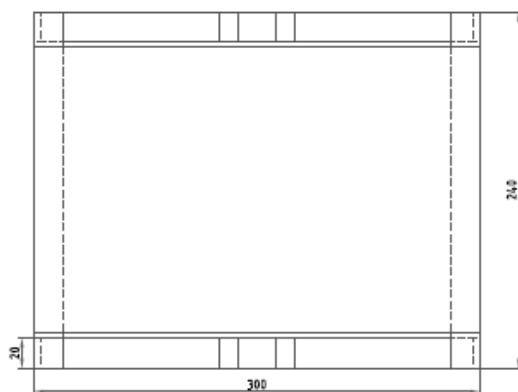
### 4.1. EQUIPMENT DESIGN AND MANUFACTURING

Prior to composite plate fabrication and testing, the required equipment was first designed and manufactured. Shop drawings of the required equipment were sent to the Faculty of Science and Engineering Workshop, Curtin University of Technology, for manufacture and assembling.

#### *4.1.1. Composite Plate Fabrication Equipment*

The main equipment for composite plate fabrication includes rectangular stainless steel frames, a frame holder and oven for prepreg manufacturing, and a hot-press for prepreg preform curing.

##### 4.1.1.1. Rectangular stainless steel frames



(a)



(b)

**Figure 4.1.** Rectangular stainless steel frames. (a) Top view, (b) Photograph.

These frames were used for winding fibre rovings or tows prior to being embedded with epoxy. The size and geometry can be seen in Figure 4.1 with details being given in Appendix 1.

#### 4.1.1.2. Frame holder

In order to ease the winding of fibre tow onto a frame, the frame was affixed into the shaft of this holder. This holder is shown in Figure 4.2.

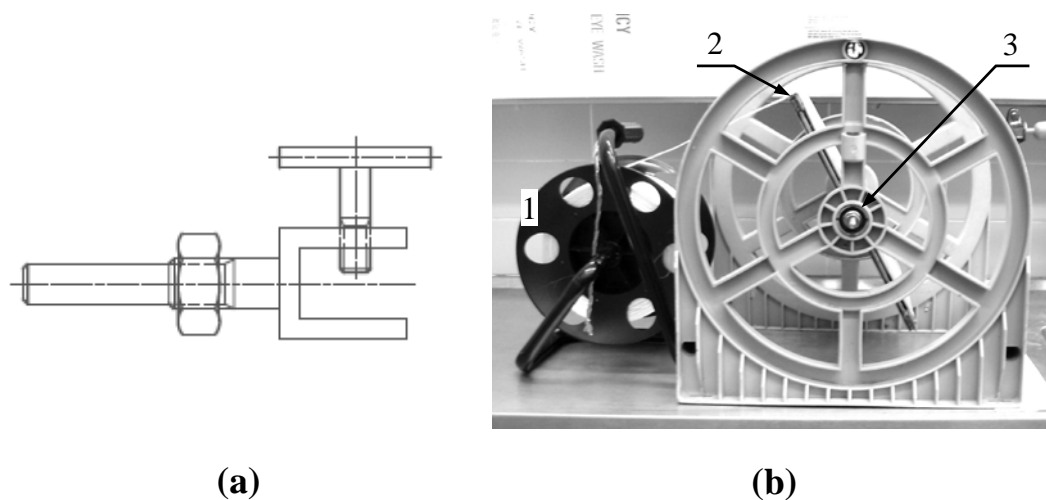
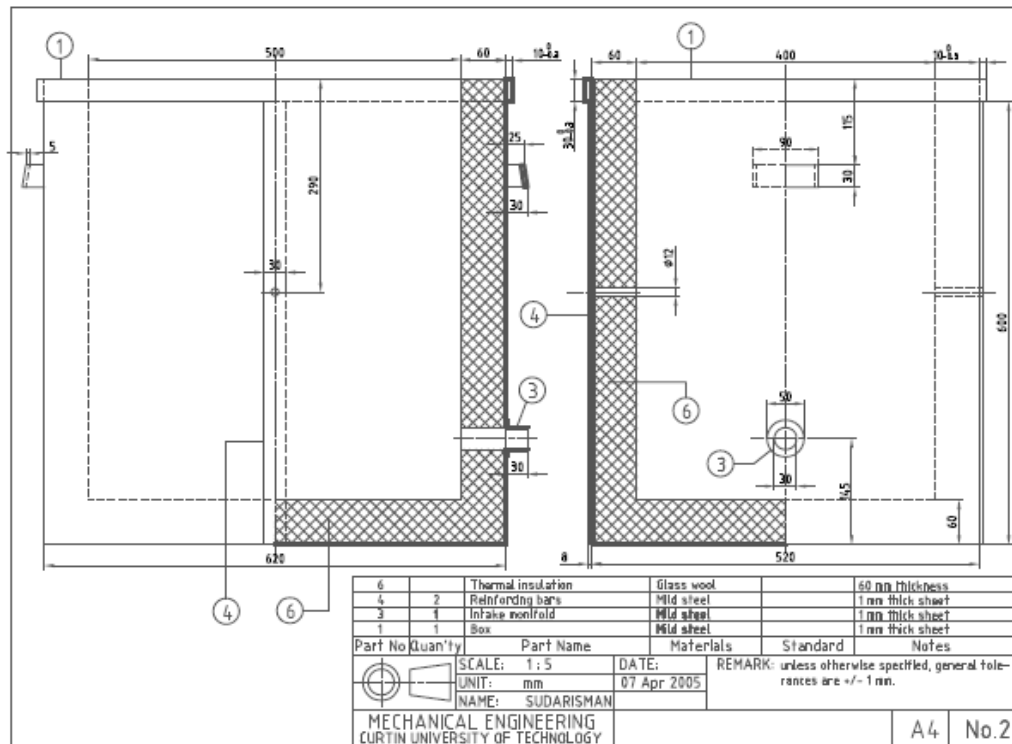


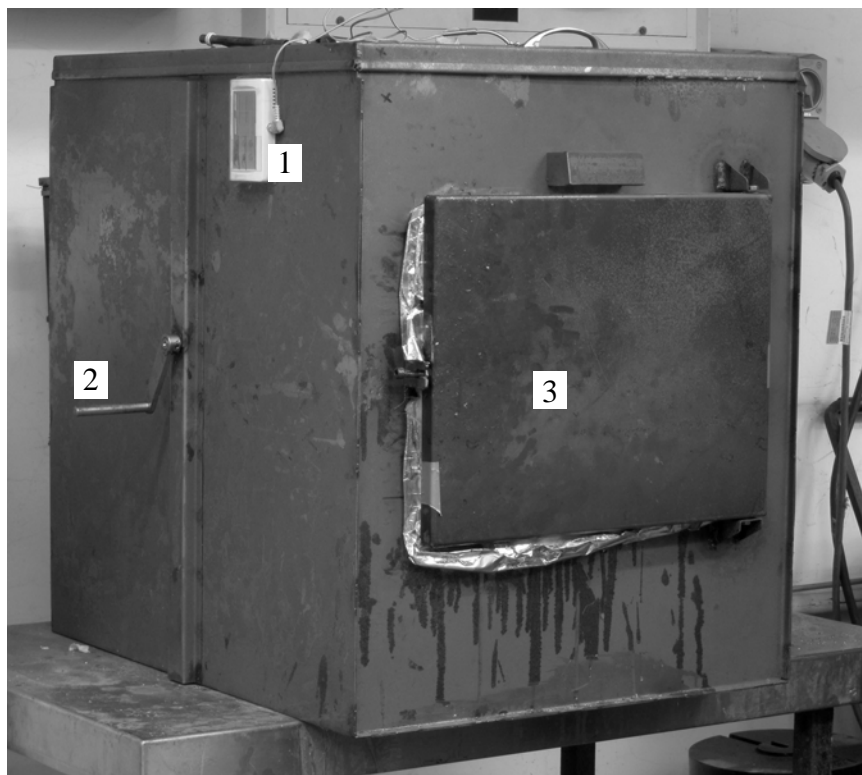
**Figure 4.2.** Frame holder. (a) Front view of the holder, (b) Photograph showing: 1. Glass fibre roll, 2. Stainless steel frame, and 3. Holder.

#### 4.1.1.3. Oven

This oven, as presented in Figure 4.3, was utilised to partially cure the embedded fibres wound onto a frame in order to produce fibre/epoxy prepregs. The oven was equipped with an adjustable temperature 2400-watt heat gun that supplies hot air into the oven, a probe thermometer and timer, and a shaft. The shaft was specially designed such that a frame with embedded fibre wound onto it can be affixed and rotated during curing in order to ensure the homogeneous evaporation of acetone and curing of the matrix over the frame. The detail of this oven has been presented in Appendix 2.



(a)



(b)

**Figure 4.3.** Oven for producing fibre/epoxy prepregs. (a) Shop drawing showing its details and dimensions, (b) Photograph showing: 1. Digital thermometer and timer, 2. Rotating handle, and 3. Door.

#### 4.1.1.4. Hot-press

The hot-press utilised in this project has been presented in Figure 2.17. Its basic design was carried out by an undergraduate student as a final year project. Some modifications, *e.g.*, installing upper plate guides, preform guides, excess resin collection chamber, and vacuum meter, had been undertaken during this project in order to improve its performance. The press was used to perform curing of prepreg preforms.

#### 4.1.2. Mechanical Test Equipment

In order to carry out mechanical testing, the required equipment for specimen preparation and testing was designed and manufactured. This equipment included a tabbing-press, an alignment jig, a compressive test fixture, and an adjustable-span specimen support equipped with a three-point bend loading nose.

##### 4.1.2.1. Tabbing-press

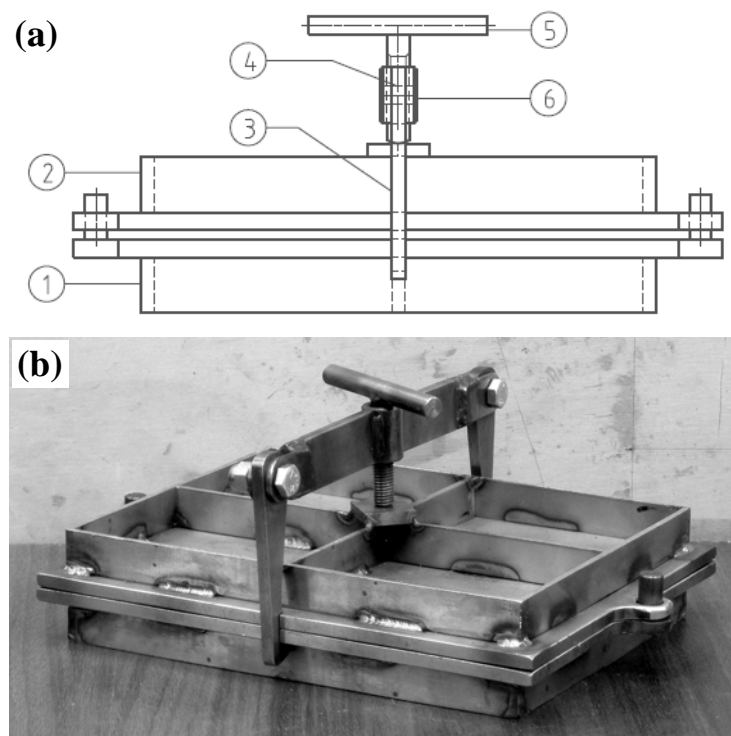


**Figure 4.4.** Tabbing press. (a) Front view showing: 1. Bottom plate, 2. Top plate, 3. Hooks, 4. Guiding Pins, 5. Bolt, and 6. Arm, (b) Photograph



A tabbing-press has been presented in Figure 4.4. It was utilised to press tensile and compressive specimens during adhesive curing when affixing end-tabs onto the ends of the specimens. By applying a compressive pressure, a thin layer of adhesive resulted in strong interface bonding between specimen and end. A shop drawing of this press has been presented in Appendix 3.

#### 4.1.2.2. Alignment jig

An alignment jig, Figure 4.5 and its detail in Appendix 4, was required for specimen alignment in compressive test grips. It was equipped with changeable gauge length spacers that enabled the production of various specimen gauge lengths in accordance with the ASTM D3410 [1] test standard. Prior to being put into the compressive test fixture, a specimen was first aligned and affixed in the fixture grips.

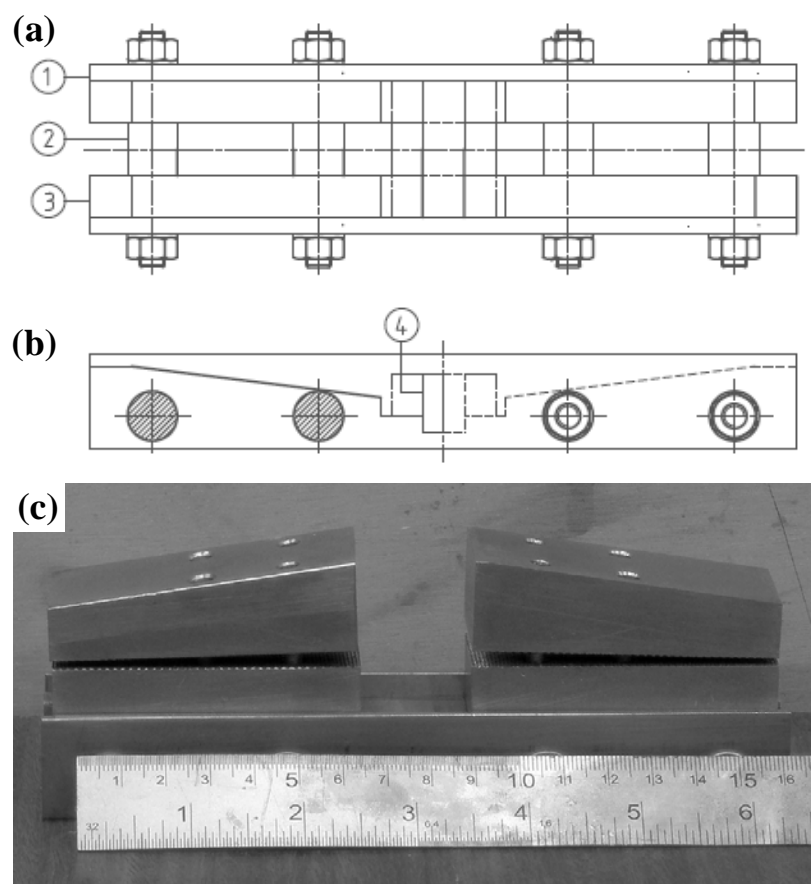


**Figure 4.5.** Alignment jig. (a) Top view showing: 1. Holding plates, 2. Parallel holders, 3. Bases, (b) Front view showing: 4. Gauge length spacers, and (c) photograph showing fixture grips separated one inch apart.

#### 4.1.2.3. Compression test fixture

Unlike the tensile test fixture, a compression test fixture as presented in Figure 4.6 needed to be manufactured due to its unavailability. This fixture was required to perform preliminary tests, *i.e.*, compressive testing. Its detail has been depicted in Appendix 5.

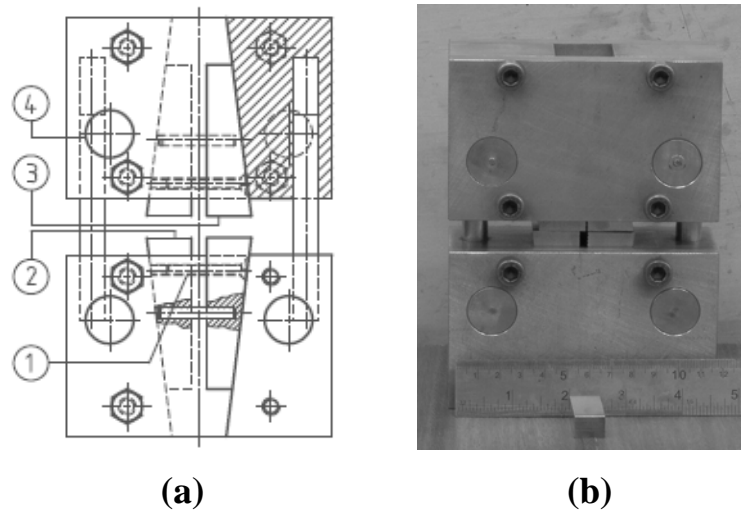


**Figure 4.6.** Compressive test fixture. (a) Front view showing: 1. Clamping screws, 2 and 3. Grips, 4. Load pins, and (b) Photograph.

#### 4.1.2.4. Flexural test fixture and loading nose

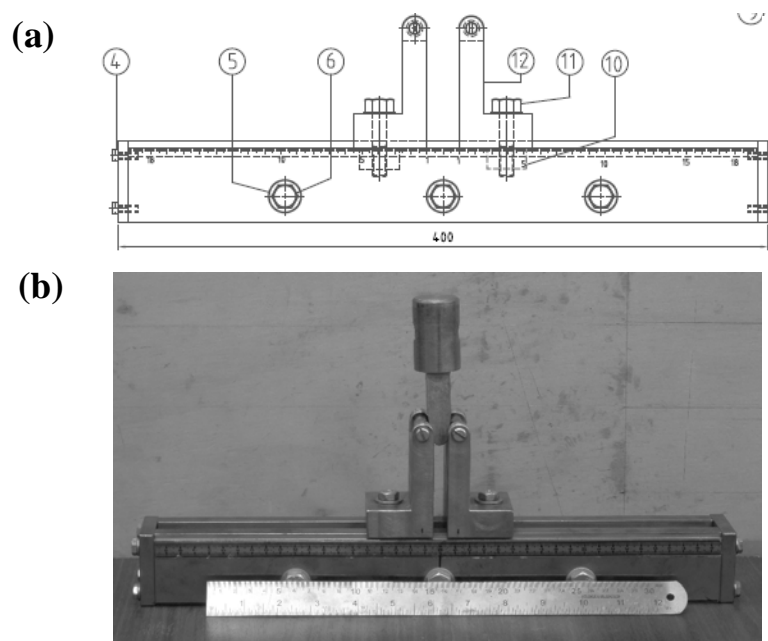


**Figure 4.7.** Flexural test fixture. (a) Front view, and (b) Photograph showing the support along with the three-point bend loading nose

Flexural tests were carried out in accordance with Procedure A of the ASTM D790 [2] test standard. The test fixture along with its loading nose, as presented in Figure 4.7, was manufactured in order to meet the requirements of the standard. It should be noted that to avoid any excessive indentation effect and to minimise stress concentration effects due to sharp edges at the loading nose and specimen supports, the standard recommends that the contact surface geometry of the loading nose and specimens supports should be cylindrical and of radius  $5 \pm 0.1$  mm. A detail shop drawing of this fixture has been presented in Appendix 6.

## **4.2. COMPOSITE PLATE FABRICATION**

### **4.2.1. Materials**

Two different grades of carbon fibre and two types of glass fibre were utilised as reinforcement, with epoxy being selected as the matrix in this project. Their primary properties have been presented in Table 4.1.

#### **4.2.1.1. Fibres**

It has been previously discussed in Section 2.5.2 that, despite their high tensile strength, compressive strengths of carbon fibres are relatively low in comparison with their respective tensile strengths. Low cost E-glass FRP composites demonstrated superior compressive strength in comparison with CFRP composite [3]. In light of this, in this research the author has attempted to improve the flexural properties of CFRP composites by replacing carbon fibres at the compressive side of beams with higher compressive strength glass fibre.

Pyrofil<sup>TM</sup> TR50S is a polyacrilonytrile-based (PAN-based) carbon fibre produced by Grafil Inc., Sacramento, CA, USA [4]. The fibre utilised in this project was supplied in the of a unidirectional tow that contained 12000 filaments [4]. This fibre is considered to be a standard modulus carbon fibre [5] combined with moderate strength (Table 4.1). The other grade of carbon fibre used was PAN-based HexTow<sup>TM</sup> IM7 (HS-CP-5000) manufactured by Hexcel Corp.,

Stamford, CT, USA [6] which combined high strength and standard modulus – this tow also contained 12000 filaments. Their production process has been discussed previously in section 2.2.1.2.

Two different types of glass fibre have been selected as a reinforcing material for the production of hybrid composites, *i.e.*, E-glass and S2-glass fibres. The SE 2350-450 E-glass fibre was supplied by Owens Corning, Toledo, OH, USA [13], while the UT-S500 S2-glass was supplied by SP System, Newport, Isle of Wight, UK [14]. The E-glass, Figure 2.10, was in the form of a single-end continuous roving with approximately 2000 filament content in its tow. The S2-glass, Figure 2.12, was received from the supplier in the form of unidirectional plain weave fabric of 500 mm width and approximately  $500 \text{ g}\cdot\text{m}^{-2}$  weight. The tow constructing the principal fabric direction was 1988 tex while that in the weft direction was an extra fine 10 tex, with both edges of the fabric being lopped [14] – their properties have been presented in Table 4.1.

#### 4.2.1.2. Matrix

Epoxy resin has been selected as the matrix material due to its compatibility with different fibres, fast wettability, ease of processing [15] and good mechanical properties [15, 16]. In addition, epoxy also possesses low shrinkage on curing in comparison with polyester and vinylester [16]. Its properties have been presented in Table 4.1.

Kinetix<sup>®</sup> R240 epoxy resin combined with Kinetix<sup>®</sup> H160 hardener were selected as the matrix in this project. This epoxy, supplied by ATL Composite Australia, Southport, QLD, Australia, possesses low viscosity resulting in excellent wettability in fibre impregnation.

**Table 4.1.** Properties of constituent materials

Material	Code	Density (g·cm <sup>-3</sup> )	Filament dia (μm)	Strength (MPa)		Tensile Modulus (GPa)	T. failure strain (%) <sup>b)</sup>
				Tensile	Other		
Unidirectional plain wave C-fibre [7, 8]	C0	1.80	N/A	2480		238	1.2
TR-50S carbon fibre [4]	C2	1.82	7	4900		240	2.0
HexTow <sup>TM</sup> IM7-12000 carbon fibre [6]	C3	1.78	5.2	5570		276	1.9
E2350-450 type 30 glass fibre [9]	Eg	2.58 <sup>a)</sup>	17	3400		72.3 <sup>a)</sup>	2.5
UT-S500 <sup>c)</sup> UD fabric S2 glass fibre [10]	S2	2.46	9	4890		86.9	5.7
Technirez <sup>®</sup> R2519/H2409 epoxy [8, 11]	Em0	1.14	N/A	96		3.00	
Kinetix <sup>®</sup> R240/H160 epoxy [12]	Em	1.09	N/A	83.3	Comp.: 98 <sup>d)</sup>	3.65	9.8

<sup>a)</sup>System Information: OC<sup>TM</sup> Advantex<sup>®</sup> 162A, Owens Corning, Toledo, OH, USA.

<sup>b)</sup>Tensile failure strain.

<sup>c)</sup>SP System, Newport, Isle of Wight, UK.

<sup>d)</sup>Compressive yield strength.

#### 4.2.1.3. Stacking configuration

Although CFRP composites are well known for their superior tensile strength, their low longitudinal compressive strength may become a limitation for their widespread utilisation [17]. This problem becomes of primary concern if the structure will be subjected to compressive or flexural loads. However, through partial substitution of another type of fibre possessing a higher compressive strength for the carbon fibres in the compressive region of a composite structural members subjected to flexural loading, such problems may be minimised. Park and Jang [18] proved that placing stronger fibres in the outer layers of laminated beams resulted in a higher failure stress for their hybrid composite beams. Considering the above mentioned reason, the average thickness of individual single prepreg layers, and the resulting plate thickness of approximately 2.00 mm, the stacking configurations presented in Table 4.2 have been investigated.

**Table 4.2.** Stacking configurations

Plate number	The number of prepreg layers of the hybrids					
	E-g/S2-g		TR50S/IM7		E-g/TR50S	
	S2-g	E-g	IM7	TR50S	E-g	TR50S
(1)	(2)	(3)	(4)	(5)	(6)	(7)
1	0	4	0	6	0	6
2	1	3	1	4	1	4
3	2	2	2	3	2	3
4	3	1	3	2	2	2
5	4	0	4	1	3	1
6	-	-	6	0	4	0

**Note:** All fibres in the even numbered columns were placed at the compressive faces of their respective hybrid composite plates.

### 4.2.2. Plate Fabrication Development

#### 4.2.2.1. Fabrication parameters

In addition to the inherent properties of their constituent materials, the properties of FRP composite materials may be influenced by a number of factors related to their microstructure characteristics, *e.g.*, void content, fibre misalignment, fibre volume fraction. Tjong *et al.* [19] have observed process-structure-property relationships in their ternary short-glass fibre-reinforced polymer (FRP) composite materials. They reported that a change in manufacturing route resulted in microstructure change leading to changes in tensile yield stress, tensile fracture stress, tensile modulus and Izod impact energy of their short-glass FRP samples due to changes in reinforcement dispersion within the matrix and reinforcement-matrix interfacial bonding. Thus, any change in processing parameters can influence mechanical properties of the resulting materials.

For FRP composites produced using the prepreg lay-up technique, these parameters include epoxy system concentration in the epoxy solution used for wetting the fibres, as well as the magnitude of the applied compressive pressure and curing chamber vacuum pressure, dwell time, and holding temperature during hot-press curing [8, 20]. Epoxy concentration in the epoxy solution will influence the viscosity of the solution resulting in changes in matrix wettability and fibre volume fraction and void content. Whilst vacuum pressure inside the curing chamber affects void content [20], minimising void content by controlling the magnitude of compressive pressure during hot-press curing has also been recommended by Olivier *et al.* [21] and Boey and Lye [22]. Sudarisman and Davies [20] also observed the influence of applied compressive pressure on fibre misalignment.

Five manufacturing parameters, *i.e.*, (i) epoxy system concentration in the epoxy solution used for wetting the fibres, (ii) magnitude of the applied compressive pressure, (iii) magnitude of vacuum pressure inside the vacuum chamber, (iv) dwell time, and (v) holding temperature during hot-press curing process, will be optimised during manufacture of the FRP composite plates. These parameters will be discussed in detail in Chapter 5.

#### 4.2.2.2. Fabrication parameter optimisation

There were five steps in optimising the fabrication parameters as had been outlined in previously published work by the author [8, 20]. In each step, only one parameter was varied whilst the other four parameters were kept constant. Five different values of the parameter being optimised were considered with the optimisation procedure being carried out as follows:

1. Epoxy system concentration,  $C_e$ , optimisation in prepreg production process.
2. Once  $C_e$  had been optimised, the second step was to vary the magnitude of the applied compressive pressure,  $p_c$ , during hot-press curing.
3. The next step was to vary the magnitude of the applied vacuum pressure,  $p_v$ , inside the curing chamber during hot-press curing.
4. Once the optimum value of  $p_v$  had been established, the next step was to vary the holding time,  $t$ , during hot-press curing.
5. Finally, the hot-press curing temperature,  $T$ , was varied in order to determine its optimum value.

In each step, the resulting composite plate was evaluated in terms of flexural properties. It should be noted that the optimum values established in each step were applied for each successive step. Physical characterisation and flexural testing procedures will be discussed in the following sections, whilst the optimisation process will be discussed in detail in Chapter 5.

#### 4.2.2.3. Composite plate fabrication procedure

Composite plate fabrication was carried using a fully manual technique as has been discussed in papers previously published by the author [20, 23], that involved prepreg manufacturing, prepreg lay-up and hot-press curing. This procedure has been illustrated in Figure 4.8.



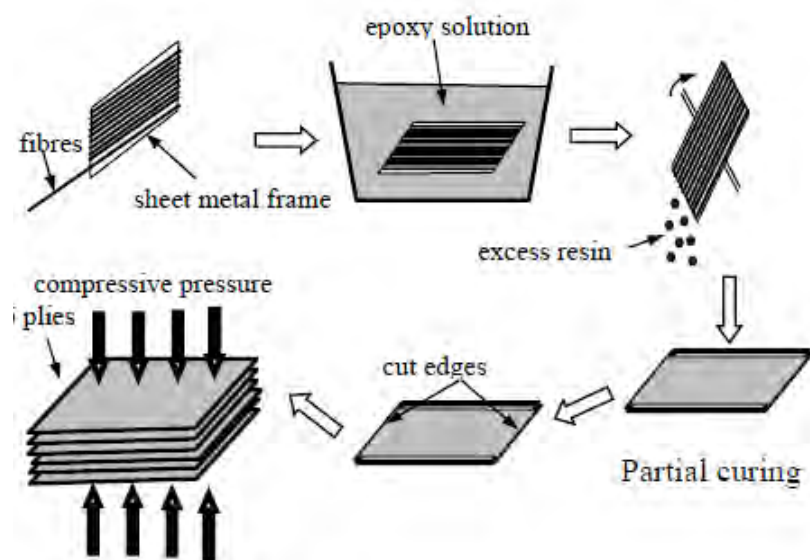


**Figure 4.8.** Schematic illustration of the composite plate manufacturing procedure [23, 24].

*Prepreg manufacturing procedure* – Firstly, either carbon, glass or silicon carbide fibre was wrapped onto a rectangular stainless steel frame. Next, epoxy resin and its hardener were diluted in acetone in two separate pots, in order to prolong their pot life time, before mixing them to produce epoxy solution. The resin-to-hardener ratio strictly followed the supplier recommendations whilst the epoxy system-to-acetone ratio was based on the values established during the fabrication optimisation procedure. The fibre arrangement was then embedded in the epoxy matrix by pouring the epoxy solution onto the fibre arrangement, compacting, and draining it by allowing excess resin to flow out. Finally, it was put into an oven that had been pre-heated to  $\sim 80\text{ }^{\circ}\text{C}$  for partial curing processing. The temperature inside the oven was increase up to  $120\text{ }^{\circ}\text{C}$  [25, 26] at the rate of  $\sim 10\text{ }^{\circ}\text{C}\cdot\text{m}^{-1}$  [27] with a total oven time of 20 minutes [25, 26] being previously employed. Upon visual observation of the resulting prepregs, this time duration was found to be adequate for producing carbon/epoxy prepregs and silicon carbide/epoxy prepregs, whilst for glass/epoxy prepregs, 23 minutes was consider to be adequate. The resulted prepreg sheets were cut into an approximate size of  $150\text{ mm} \times 290\text{ mm}$  and placed between two sheets of release paper before being stored in a freezer at  $\sim -10\text{ }^{\circ}\text{C}$  in order to prevent further curing.

*Preform curing procedure* – When a sheet of prepreg was taken out from the freezer, one piece of release paper was immediately removed and it was exposed to open air for ~5 minutes in order to adjust to room temperature. Two sheets of the required prepreg were then carefully stuck together in order to produce a two-layer preform held between two sheets of release paper. These two-layer preforms were then cooled down in the freezer in order to ease removal of the release paper. The above procedure applied to single layer preregs was applied to these two-layer preregs until the number of the required layers was obtained. The number of layers and the stacking configuration depended upon whether a hybrid or baseline composite plate was to be produced. The resulting preform was then placed into the hot-press that had been preheated up to ~80 °C, and finally, curing was carried out under ~1.0 MPa mechanical compressive pressure and ~0.035 MPa vacuum atmosphere at ~120 °C for ~30 minutes.

#### **4.3. FIBRE VOLUME FRACTION AND VOID CONTENT DETERMINATION**

Experimental values of fibre volume fraction,  $V_f$ , and void content,  $V_v$ , for each composite plate were measured using the image analysis of cross-sectional micrographs similar to the method employed by Wang *et al.* [28]. However, whilst Wang *e. al.* analysed SEM images, the current author utilised optical microscopy in order to determine  $V_f$  and  $V_v$ . For each measurement, at least five optical micrographs taken at the same magnification were captured for each of five samples carefully removed from different regions of the composite plate – details of this procedure will be discussed in detail in Sub-section 4.4.3.

To verify its accuracy, another group of samples comprising of five or more specimens taken from the same plate and selected in the same way as the previous group was prepared for  $V_f$  and  $V_v$  prediction by employing the rule of mixtures. The results of the second group were then compared with those of the first group through use of a least squares fit procedure.

Prediction of the fibre volume fraction using the rule of mixtures has been reported by Deng *et al.* [29]. In the present research, the sample dimension was

$25.4 \pm 0.2$  mm long  $\times$   $12.7 \pm 0.2$  mm width with the thickness depending on the thickness of the plate. Measurements were carried out using a Mitutoyo vernier calliper with a 0.02 mm resolution. Knowing the individual dimensions of the samples, their respective volumes could be calculated, whilst their individual weights were measured using an AL-3K digital scale, Denver Instrumentation Company, Denver, CO, USA. The bulk density of the samples was calculated as follows

$$\rho_c = \frac{m_c}{v_c} = \frac{m_c}{l \cdot w \cdot t} \quad (4.1)$$

where  $\rho_c$ ,  $m_c$  and  $v_c$  are the density ( $\text{g}\cdot\text{cm}^{-3}$ ), mass (g) and volume ( $\text{m}^3$ ) of the sample, respectively; whilst  $l$ ,  $w$  and  $t$  are the length, width, and thickness of the sample (cm), respectively, as illustrated in Figure 4.9. Finally, for single fibre-type composites the predicted values of fibre volume fraction were calculated based on this volume and weight data using equation (4.2).

$$V_f = \frac{\rho_c - \rho_m}{\rho_f - \rho_m} \quad (4.2)$$

where  $\rho$  is density ( $\text{g}\cdot\text{cm}^{-3}$ ), and the indices  $c$ ,  $m$  and  $f$  refer to composite, fibre and matrix, respectively.

For unidirectional hybrid FRP composites, consider Figure 4.9 which illustrates a unidirectional hybrid FRP composite containing two types of fibre embedded in a common matrix and arranged in a layer-wise pattern.

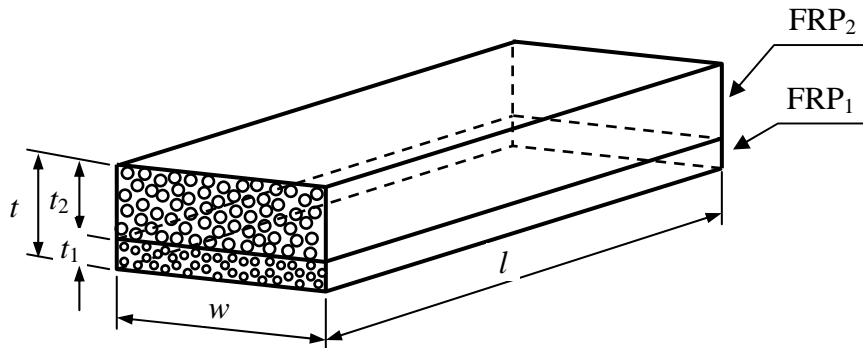


**Figure 4.9.** Schematic illustration of hybrid FRP composites containing two types of fibres in a common matrix

We should start by defining  $V_{f1}$  and  $V_{f2}$  as the fibre volume fraction of the single fibre-type FRP composite containing fibre 1 and fibre 2, respectively. The volumes of fibre 1, fibre 2 and their total volume are given in equations (4.3a), (4.3b) and (4.3c), respectively.

$$v_{f1} = V_{f1} \cdot v_1 = V_{f1} \cdot (l \cdot w \cdot t_1) \quad (4.3a)$$

$$v_{f2} = V_{f2} \cdot v_2 = V_{f2} \cdot (l \cdot w \cdot t_2) \quad (4.3b)$$

$$v_f = v_{f1} + v_{f2} \quad (4.3c)$$

where  $v$  and  $V$  are the volume and volume fraction, respectively; and the indices 1 and 2 refer to fibre 1 and fibre 2, respectively. Substitution of equations (4.3a) and (4.3b) into equation (4.3c) gives

$$v_f = (V_{f1} \cdot t_1 + V_{f2} \cdot t_2)(l \cdot w) \quad (4.4)$$

Dividing both side of equation (4.4) with  $v_c = l \cdot w \cdot t$ , and recall that  $V_f = \frac{v_f}{v_c}$  yields the fibre volume fraction of the hybrid FRP composite as

$$V_f = \frac{t_1}{t} V_{f1} + \frac{t_2}{t} V_{f2} \quad (4.6)$$

The values of  $t_1$  and  $t_2$  as well as  $V_{f1}$  and  $V_{f2}$  can be determined using image analysis that will be discussed in Sub-section 4.4.3, whilst  $t$  can be determined by direct measurement. Any discrepancy in  $V_f$  values obtained using these two methods can be attributed to the presence of voids [30].

## 4.4. MECHANICAL TESTING

### 4.4.1. Compressive Test

In order to provide compressive strength data of the single fibre-type, *i.e.* E-glass, S2-glass, TR50S carbon, and IM7 carbon polymer composites to be used

for the manufacture of hybrid FRP composites, compressive test was carried out for these four single fibre-type polymer composites. The compressive strength of Tyranno<sup>®</sup> silicon carbide/epoxy composite was obtained from the previous work of Davies and Hamada [25] as presented in Table 4.1. The compressive tests were conducted in accordance with ASTM D3410-03 [1], using rectangular wedge grips (Figure 4.6) in order to accommodate variations in specimen thickness.

#### 4.4.1.1. Specimen preparation

The specimen geometry according to ASTM D3410 has been depicted in Figure 4.10. The specimens were cut from composite plates under investigation using a diamond-tipped circular blade saw. In order to minimise edge effects due to damage produced by cutting, their longitudinal edges were polished using 600-grit abrasive paper. Aluminium end-tabs [31-33] were utilised in order to prevent damage within the gripped areas during loading.

The gripped areas of the specimens and one face of each tab were lightly abraded using a 1000-grit abrasive paper prior to affixing the aluminium end-tabs onto the gripped areas. The thickness of the tabs was 0.8 mm with four tabs being glued using the same type of epoxy as the composite matrix materials onto four gripped areas of each specimen. In order to obtain as thin a layer of adhesive as possible, the glued tabs on each specimen were cured at room temperature under mechanical compressive pressure using the tabbing-press shown in Figure 4.4. The specimen geometry according to ASTM D3410 has been presented in Figure 4.10. Two C2A-06-125LW-120 strain gauges were installed on opposite surfaces of each specimen at the mid-length of the gauge length as shown in Figure 4.10. The grid length of the gauges was 3.18 mm with a  $120.0 \pm 0.6\%$  Ohm grid resistance and  $2.080 \pm 0.5\%$  gauge factor supplied by Vishay Micro Measurement and SR-4 [34]. The compressive strain was recorded using a 4-channel strain indicator and recorder, the P3 Strain Indicator and Recorder, manufactured by Micro Measurement, Inc., Raleigh, North Carolina, the USA.

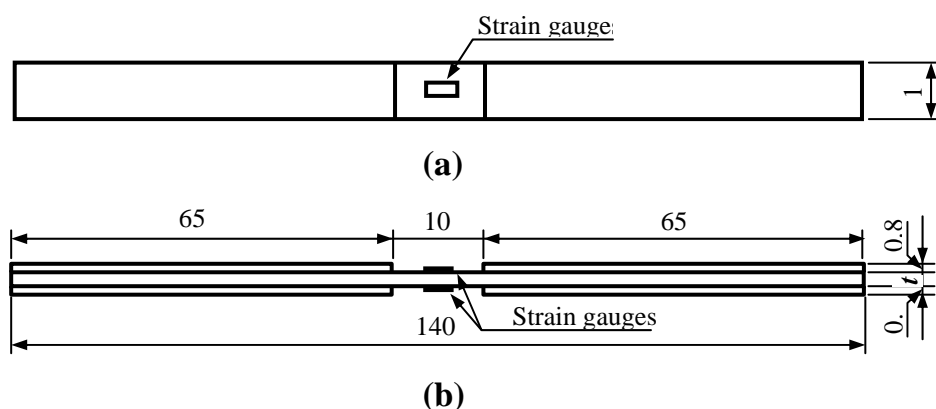


**Figure 4.10.** Compressive test specimen showing nominal dimensions. (a) Top view, (b) Front view, note that  $t$  is specimen thickness which depends on the thickness of composite plate panel.

#### 4.4.1.2. Testing

Compressive loading was introduced into the specimen through shear at the roughened wedge grip interfaces. Due to there being a high sensitivity of compressive properties to specimen alignment, care was taken when affixing the wedge grips onto each specimen as well as when placing this pre-gripped specimen into the test fixture. The tests were carried out in a computer-controlled Instron<sup>®</sup> 5500R universal testing machine at a constant crosshead speed of  $1.5 \text{ mm} \cdot \text{sec}^{-1}$  with the results being using a Microsoft Excel spreadsheet.

#### 4.4.2. Flexural Test

Flexural tests were carried out in accordance with Procedure B of the ASTM D790-07 Standard [2] in a computer-controlled Instron<sup>®</sup> 5500R universal testing machine equipped with an adjustable-span flexural test fixture (Figure 4.7). At least five specimens were tested for each case with the specimens being subjected to three-point bend loading up to failure.

#### 4.4.2.1. Specimen preparation

According to ASTM D790-07, the specimen geometry should be rectangular with a 12.7 mm width. The specimen thicknesses in the present work were determined by the respective composite plate thickness, whilst their length depended upon their respective thickness and span-to-depth ratio,  $S/d$ . A diamond-tipped circular blade saw was used to cut the specimens from the composite plates. After being cut, the longitudinal edges of the specimens were polished using 600-grit abrasive paper in order to remove any possible edge damage due to cutting that may affect the flexural properties. For each case, at least five specimens were prepared and tested.

ASTM D790-07 recommends that  $S/d$  be chosen in order to ensure that specimens fail in their outer layers and due to flexural loading rather than by shear loading. In accordance with this, three different  $S/d$  ratios, *i.e.*, 16, 32 and 64 [25], were selected for testing. Two of the  $S/d = 64$  specimens for each stacking configuration were equipped with strain gauges in order to directly measure the strain. One gauge was installed at the compressive face (close to the loading nose, approximately 5 mm from the mid-span) whilst the other was located at the tensile face directly below the compressive face gauge – the gauge type was identical to that utilised for the compressive test specimens.

#### 4.4.2.2. Testing

The layers of the hybrid FRP specimens containing higher compressive strength were placed at the compressive side of the beam for testing – this was done in order to enhance any positive hybrid effect. Crosshead speeds were set equivalent to a  $10^{-2} \text{ mm} \cdot \text{mm}^{-1} \text{sec}^{-1}$  strain rate as recommended by the ASTM D790-07 standard. Direct strain measurement for the specimens installed with strain gauges was carried out by means of a four channel P3 Strain Indicator and Recorder (Micro Measurement, Inc., Raleigh, North Carolina, USA). The data acquisition setup for specimens instrumented with strain gauges has been depicted in Figure 4.11. The values of flexural strain at maximum stress were calculated

from their respective recorded crosshead displacement using the following equation [2].

$$\varepsilon_{\max} = \frac{6Dd}{S^2} \quad (4.7)$$

where  $\varepsilon_{\max}$  is the strain at maximum stress,  $D$  is the crosshead displacement,  $d$  is the depth of the beam, and  $S$  is the span of the beam.

The ASTM D790-07 standard dictated that for shorter beam, *i.e.*,  $S/d \leq 16$ , flexural strength,  $\sigma_f$ , can be calculated using equation (3.6a) where flexural strength is the normal stress at maximum load. For  $S/d > 16$ , due to excessive deflection experienced by the beam, the flexural strength should be calculated using the following modified equation.

$$\sigma_f = \frac{3F_{\max} \cdot S}{2wd^2} \left[ 1 + 6\left(\frac{D}{S}\right)^2 - 4\left(\frac{d}{S}\right)\left(\frac{D}{S}\right) \right] \quad (4.8)$$

where  $F_{\max}$  and  $w$  are the maximum applied force and the width of the specimen, respectively.

The flexural modulus,  $E_f$ , should be determined at the initial straight line of each individual force-displacement curve [2]. In this research, it was determined at a strain,  $\varepsilon$ , of  $2.5 \times 10^{-3}$  [25] and calculated using equation (4.9) which was obtained from rearranging equation (3.34) and substitutions of  $E_f$  for  $E$  and  $\left(\frac{1}{12}\right) w \cdot d^3$  for  $I_x$ .

$$E_f = \frac{S^3}{4w \cdot d^3} \times \frac{\Delta F}{\Delta x} \quad (4.9)$$

where  $\Delta F / \Delta x$  (unit:  $\text{N} \cdot \text{mm}^{-1}$ ) is the slope of the load-displacement curve at the range being calculated.



The specific energy storage capacity for each specimen was calculated using equation (4.10) from the individual load-displacement curves produced by the Instron testing machine [35].

$$\gamma = \frac{1}{2wd} \sum_{i=0}^{i=n-1} \left( \frac{F_i + F_{i+1}}{2} \right) (D_{i+1} - D_i) \quad (4.10)$$

where  $wd$  is the cross-sectional area,  $n$  is the number of points of the load-displacement curve up to  $F_{\max}$ ,  $F_i$  is the force at point  $i$ , and  $D_i$  is the displacement at point  $i$ .

Unless otherwise stated, all data presented in this work was the average value of at least five specimens. After being tested up to failure, the fracture regions of specimens were removed for failure mode examination with details of this procedure being discussed in the following section.

#### 4.4. OPTICAL MICROGRAPHY

##### 4.4.1. Specimen Preparation

Samples for microstructural analysis were carefully removed from either the composite plates or fractured specimens using a diamond-tipped circular blade saw. Samples removed from composite plates were utilised for fibre volume fraction and void content determination, whilst those taken from fractured specimens were utilised for failure mode analysis. First of all, each sample was mounted into a polyester block using standard procedures and then cured at room temperature. The specimens were then gradually polished, starting with 120 grade silicon carbide-coated polishing paper and finally a suspension of 0.3  $\mu\text{m}$  grain size alpha alumina polishing powder produced by Leco Corp., St Joseph, Michigan, USA [36].

##### 4.4.2. Image Capturing

The samples that have been mounted into polyester blocks and mirror-surface polished were observed under a Nikon Eclipse ME600 optical microscope with their images being captured using a colour digital camera, the Spot Insight™ 2MP, that had been installed on the microscope. These micrographs were used for the determination of fibre volume fraction, void content and fibre misalignment. In addition to these samples, a micrograph of a scale bar was also captured at each magnification for the purpose of scaling the resulting micrographs.

#### 4.4.3. Image Analysis

All image analyses were carried out using an open source image analysis software, ImageJ, developed by the National Institutes of Health, USA [37] apart from fibre misalignment that was determined through direct measurement of the micrographs [38].

*Fibre volume fraction determination* - The first step in predicting fibre volume fraction was to calculate the average diameter,  $\delta_f$ , (unit: pixels = px) of the fibre images to be analysed following the method of Ogasawara and colleagues [39]. At least one hundred fibre images of each type of fibre were randomly selected with the resulting average diameters being used to predict the fibre volume fractions from optical micrographs of the composite specimens. Next, after calculating the number of fibre images within each micrograph and calculating their area, the fibre volume fraction can be determined as follows

$$V_f = \frac{A_f}{A_i} = \frac{n_f (\pi / 4) \delta_f^2}{l_i \cdot w_i} \quad (4.11)$$

where  $V_f$  is the fibre volume fraction,  $A_f$  is the fibre image area (px<sup>2</sup>),  $A_i$  is the image area (px<sup>2</sup>),  $n_f$  is the number of fibres,  $\delta_f$  is the average fibre image diameter (px),  $l_i$  is the length of the image (px), and  $w_i$  is the width of the image (px).

*Void content determination* - Unlike those of fibre images, the boundaries of void images are especially obvious. Kim and Nairn pointed out that images of empty spaces, holes, and air bubbles inside an epoxy matrix appear dark [40]. Considering this fact and the irregular geometrical nature of the voids, void

content was predicted using the ImageJ software as previously reported by the author [8]. Firstly, each colour image captured using an optical microscope was transferred into an 8-bit gray scale image. Next, the intensity threshold of the image was set to such a level that the voids appeared as one colour with the fibres and matrix appearing as another colour. The third step was to run a particle analysis procedure which calculated the void image fraction of the image.

*Layer thickness determination* – This procedure started by calculating the scaling factor of the sample images through comparing the known fibre diameter (unit:  $\mu\text{m}$ ) provided by the supplier with the average values (unit: px) obtained in the fibre volume fraction determination. The scaling factor was calculated as

$$f_s = \frac{\delta(\mu\text{m})}{\bar{\delta}(\text{px})} \times 1000 \quad (\mu\text{m}/\text{px}) \quad (4.12)$$

where  $\delta(\mu\text{m})$  and  $\bar{\delta}(\text{px})$  are the diameter of the fibre provided by the supplier and the average values calculated from image analysis, respectively. The next step was to measure the distances (unit: pixels) from the outer surface of the layer under observation to the interface between the two layers at a minimum of ten points. The thickness of the layer could then be calculated as the average value of these distances using equation (4.13).

$$t_i = \bar{t}_i \times f_s \quad (\text{mm}) \quad (4.12)$$

where  $t_i$  and  $\bar{t}_i$  are the thickness of the layer and the average value calculated from image analysis, respectively.

## REFERENCES

- [1] "ASTM D3410 Standard test method for compressive properties of polymer matrix composite materials with unsupported gage section by shear loading," in *Annual Book of ASTM Standard*. vol. Vol. 03.01? West Conshohocken, PA, USA: ASTM Int., 2005, pp. 128-144.
- [2] "ASTM D790-07 Standard test method for flexural properties of unreinforced and reinforced plastic and electrical insulating materials by

- three-point bending*," in *Annual Book of ASTM Standard*. vol. Vol. 08.01 West Conshohocken, PA, USA: ASTM Int., 2005.
- [3] S. H. Lee, and A. M. Waas, "Compressive response and failure of fiber reinforced unidirectional composites," *International Journal of Fracture*, vol. 100(3), pp. 275-306, 1999.
  - [4] "PYROFIL<sup>TM</sup> - Typical Properties of Carbon Fibre," Sacramento, CA, USA: Grafil, Inc., 2008.
  - [5] "GRAFIL: Worldwide leader in carbon fiber manufacturing," Sacramento, CA, USA: Grafil, Inc.
  - [6] "HexTow<sup>TM</sup> IM7 (5000) Carbon Fibre," Stamford, CT, USA: Hexcel Corp., 2007.
  - [7] "Composite Reinforcement - Product Range," Huntingwood, NSW, Australia: Colan Australia Pty. Ltd., Accessed date: 20/10/2006.
  - [8] Sudarisman and I. J. Davies, "The effect of processing parameters on the flexural properties of unidirectional carbon fibre-reinforced polymer (CFRP) composites," *Materials Science and Engineering: A*, vol. 498, pp. 65-68, 2008.
  - [9] "Product Information: OC(R) SE 2350 Single-End Continuous Roving (Type30(R))," Toledo, OH, USA: Owens Corning, 2005.
  - [10] "Product Information: S2-glass(R) fibre yarn," Aiken, SC, USA: AGY, 2004.
  - [11] "Technirez(R) Engineering Data / R2519," Southport, QLD, Australia: ATL Composites Pty. Ltd., 2004.
  - [12] "Kinetix(R) Engineering Data / R240 wet preg," Southport, QLD, Australia: ATL Composites Pty. Ltd., 2004.
  - [13] "Product Information: OC<sup>®</sup> SE 2350 Single-end Continuous Rovings (Type 30<sup>®</sup>)," Toledo, OH, U.S.A.: OWENS CORNING: <http://www.owenscorningchina.com/upload/File/748226345.pdf>. Accessed date: November 22<sup>th</sup>, 2008.
  - [14] "Unidirectional fabrics," Newport, Isle of Wight, UK: SP System Pty. Ltd.
  - [15] S. R. Malkan and F. K. Ko, "Effect of fibre reinforcement geometry on single shear and fracture behavior of three dimensionally braided glass/epoxy composite pins," *Journal of Composite Materials*, vol. 23, pp. 798-818, 1989.
  - [16] A. M. A. El-Habak, "Mechanical behaviour of woven glass fibre-reinforced composites under impact compression load," *Composites*, vol. 22, pp. 129-134, 1991.
  - [17] I. J. Davies, H. Hamada, and M. Shibuya, "Flexural and compressive properties of polymer matrix composites containing a mixture of carbon and silicon carbide fibres: Part 2 - Compression," in *H. Fukuda, T. Ishikawa, Y. Kogo (editors): Proceedings of the 9th US-Japan conference*

on composite materials, Mishima, Shizuoka, Japan, July 3-4, 2000, pp. 373-374, Japan Society for Composite Materials, Tokyo, Japan.

- [18] R. Park and J. Jang, "Performance improvement of carbon fiber/polyethylene fiber hybrid composites," *Journal of Materials Science*, vol. 34, pp. 2903-2910, 1999.
- [19] S. C. Tjong, S. A. Xu, and Y. W. Mai, "Process-structure-property relationship in ternary short-glass-fiber/elastomer/polypropylene composites," *Journal of Applied Polymer Science*, vol. 88, pp. 1384-1392, 2003.
- [20] Sudarisman and I. J. Davies, "Influence of compressive pressure, vacuum pressure, and holding temperature applied during autoclave curing on the microstructure of unidirectional CFRP composites," *Advanced Materials Research*, vol. 41-42, pp. 323-328, 2008.
- [21] P. Olivier, J. P. Cottu, and B. Ferret, "Effects of cure cycle pressure and voids on some mechanical properties of carbon/epoxy laminates," *Composites*, vol. 26, pp. 509-515, 1995.
- [22] F. Y. C. Boey and S. W. Lye, "Void reduction in autoclave processing of thermoset composites: Part 1: High pressure effects on void reduction," *Composites*, vol. 23, pp. 261-265, 1992.
- [23] Sudarisman and I. J. Davies, "Flexural failure of unidirectional hybrid fibre-reinforced polymer FRP) composites containing different grades of glass fibre," *Advanced Materials Research*, vol. 41-42, pp. 357-362, 2008.
- [24] Sudarisman, B. de San Miguel, and I. J. Davies, "Failure mechanism of unidirectional hybrid FRP composites containing carbon and E-glass fibres subjected to three-point bend loading," in *Proceedings of the International Conference on Materials and Metallurgical Engineering 2009*, 24-25 June, Surabaya, Indonesia, 2009, pp. FA 5-8.
- [25] I. J. Davies and H. Hamada, "Flexural properties of a hybrid composite containing carbon and silicon carbide fibres," *Advanced Composite Materials*, vol. 10, pp. 77-96, 2001.
- [26] Sudarisman, I. J. Davies, and H. Hamada, "Compressive failure of unidirectional hybrid fibre-reinforced epoxy composites containing carbon and silicon carbide fibres," *Composites Part A: Applied Science and Manufacturing*, vol. 38, pp. 1070-1074, 2007.
- [27] P. Jongvisuttisun, W. Tanthapanichakoon, and S. Rimdusit, "Development of high performance carbon fiber based prepregs for honeycomb structure," in *MaDParT 2005*, 2005.
- [28] M. Wang, Z. Zhang, and Z. Sun, "The Hybrid Model and Mechanical Properties of Hybrid Composites Reinforced with Different Diameter Fibers," *Journal of Reinforced Plastics and Composites*, vol. 28, pp. 257-264, 2009.
- [29] S. Deng, L. Ye, and Y.-W. Mai, "Influence of fibre cross-sectional aspect ratio on mechanical properties of glass fibre/epoxy composites I. Tensile

- and flexure behaviour," *Composites Science and Technology*, vol. 59, pp. 1331-1339, 1999.
- [30] P.-O. Hagstrand, F. Bonjour, and J.-A. E. Manson, "The influence of void content on the structural flexural performance of unidirectional glass fibre reinforced polypropylene composites," *Composites Part A: Applied Science and Manufacturing*, vol. 36, pp. 705-714, 2005.
  - [31] A. R. Bunsell and B. Harris, "Hybrid carbon and glass fibre composites," *Composites*, vol. 5, pp. 157-164, 1974.
  - [32] R. F. Dickson, G. Fernando, T. Adam, H. Reiter, and B. Harris, "Fatigue behaviour of hybrid composites," *Journal of Materials Science (Historical Archive)*, vol. 24, pp. 227-233, 1989.
  - [33] S. Sivashanker, N. A. Fleck, and M. P. F. Sutcliffe, "Microbuckle propagation in a unidirectional carbon fibre-epoxy matrix composites," *Acta Materials*, vol. 44, pp. 2581-2590, 1996.
  - [34] "C2A-Series Strain Gages," Raleigh, NC, USA: Vishay Micro-Measurements, Inc., 2004.
  - [35] Sudarisman, B. de San Miguel, and I. J. Davies, "The Effect of Partial Substitution of E-glass Fibre for Carbon Fibre on the Mechanical Properties of CFRP Composites," in *Proceedings of the International Conference on Materials and Metallurgical Engineering 2009, 24-25 June*, Surabaya, Indonesia, 2009, pp. MI 116-119.
  - [36] "Supplies for Microstructural Analysis," St. Joseph, MI, USA: Leco Corp.
  - [37] "ImageJ, Image Processing and Analysis in Java," Bethesda, MD, U.S.A., National Institute of Health: <http://rsb.info.nih.gov/ij/>, Accessed date: November 12<sup>th</sup>, 2005.
  - [38] S. H. Lee, and A. M. Waas, "Compressive response and failure of fiber reinforced unidirectional composites," *International Journal of Fracture*, vol. 100(3), pp. 275-306, Dec 1999.
  - [39] T. Ogasawara, S. Aizawa, T. Ogawa, and T. Ishikawa, "Sensitive strain monitoring of SiC fiber/epoxy composite using electrical resistance changes," *Composites Science and Technology*, vol. 67, pp. 955-962, 2007.
  - [40] B. W. Kim and J. A. Nairn, "Observations of Fiber Fracture and Interfacial Debonding Phenomena Using the Fragmentation Test in Single Fiber Composites," *Journal of Composite Materials*, vol. 36, pp. 1825-1858, 2002.

Every reasonable effort has been made to acknowledge the owners of copyright materials. I would be pleased to hear from any copyright owner who has been omitted or incorrectly acknowledged.

## CHAPTER 5

# FABRICATION PARAMETER OPTIMISATION

### 5.1. FABRICATION PARAMETERS

In addition to the inherent flexural properties of the constituent materials, other parameters that will greatly influence the resulting mechanical properties of unidirectional carbon fibre-reinforced polymer (CFRP) composites include the microstructural characteristics, *e.g.*, the degree of void content [1, 2], the degree of fibre misalignment, and the fibre volume fraction [3, 4]. Furthermore, the microstructural characteristics of CFRP composites may also be influenced by their processing conditions during manufacture. Important processing parameters for consideration in this research include: (i) the concentration of matrix precursor,  $C_e$ , within the solvent solution utilised to wet the fibres, (ii) the compressive pressure,  $p_c$ , applied during hot-press curing, (iii) the vacuum pressure,  $p_v$ , of the atmosphere inside the curing chamber, (iv) the dwell time,  $t$ , during hot-press curing, and (v) the holding temperature,  $T$ , during hot-press curing. In this chapter, the optimisation procedure of these five processing parameters will be discussed.

The concentration of matrix precursor (*e.g.*, epoxy resin) within the solvent solution (*e.g.*, acetone) is known to significantly influence the viscosity of the resulting solution. Although smaller concentrations of epoxy matrix will tend to produce lower viscosity solutions which are more easily able to infiltrate and wet the fibre bundles, if the volume fraction of the epoxy matrix becomes too small then this will result in insufficient matrix surrounding the fibres, resulting in poor structural integrity of the composite [3, 4]. Therefore, although an optimum packing density of 82%-83% would be expected for unidirectional composites

based on 2D packing models [5], with values close to this being observed from experimental work, the structural integrity of the composite should also be considered in order to achieve optimum mechanical properties. In this research, the epoxy content within the epoxy solution was varied from 45% to 65% in increments of 5% – this range covering typical values used for CFRP composites.

Another related parameter that influences microstructural characteristics is the magnitude of the applied compressive pressure on the preform during autoclave curing in order to minimise the void content [1, 2]. The presence of voids within a CFRP composite is known to significantly decrease the performance of structures [1, 2, 6, 7], in particular the compressive and flexural strengths due to the increased chance of local fibre buckling and eventual failure of the component. In addition, compressive pressure may also affect the degree of fibre volume fraction and fibre alignment due to matrix overflow from the prepreg lay-up together with fibre displacement during curing [4]. Whilst Boey and Lye [1] utilised a compressive pressure as high as 7 MPa in order to reduce the void content, when taking into account considerations such as ease of manufacture, other researchers [2, 8] have tended to utilise relatively low compressive pressures, ranging from 0.1~1.0 MPa and 0.0~0.6 MPa, respectively. In between these two extremes, Davies and Hamada [9] have successfully utilised compressive pressures in the region of 2.5 MPa. Considering these factors, the magnitude of compressive pressure in the present work was varied from 0.25 MPa to 1.25 MPa in steps of 0.25 MPa.

Another parameter that may influence microstructural characteristics is the dwell time, with a longer dwell time being known to result in lower void contents [10]. Whilst the matrix precursor manufacturer supplied a recommended curing time at room temperature under the absence of compressive pressure, in this research, a compressive pressure, vacuum pressure and elevated curing temperature were applied in order to accelerate the curing process. Thus, an optimum dwell time needed to be determined. A typical dwell time of 30 minutes has been reported in previously published work [11, 12] and thus the dwell time in the present research was varied within the range  $30 \pm 10$  minutes in 5 minute steps, *i.e.*, 20, 25, 30, 35 and 40 minutes.



In addition to controlling the magnitude of compressive pressure, Boey and Lye [1] also applied a vacuum pressure inside the curing chamber ranging from 0.00 to 0.03 MPa during curing. They reported that the void content asymptotically decreases with an increase of vacuum. In the current work, the author hence employed five different magnitudes of vacuum pressure, *i.e.*, 0.085 MPa, 0.080 MPa, 0.070 MPa, 0.055 MPa and 0.035 MPa.

Another parameter that may influence microstructural characteristics of FRP composites is the holding temperature during curing. At the beginning of the curing process, the viscosity of the resin decreases due to the temperature increase, then, when the cross-linking process begins, the viscosity increases [8]. Varying the viscosity of the resin during curing by varying the holding temperature may result in controlled void removal from the resin system as void removal depends upon the resin viscosity (in addition to the applied compressive pressure and vacuum pressure). A lower viscosity of the resin during curing may ease the removal of voids from the resin. However, if the viscosity of the resin is too low then excessive resin may also flow out of the composite (aided by the vacuum) and cause a lack of resin in the resulted FRP composites. In addition, too high a holding temperature may result in higher resin flows that may displace the fibres from their initial positions, resulting in fibre misalignment. Opposite to this, too low a holding temperature may result in the viscosity of the resin being too high which, when combined with a high compressive pressure, may lead to similar consequences due to the matrix (containing the fibres) being deformed. Davies and Hamada [9] previously applied a 120 °C holding temperature and, in light of this, the present research utilised holding temperatures of  $120 \pm 20$  °C in steps of 10 °C, *i.e.* 100 °C, 110 °C, 120 °C, 130 °C, and 140 °C.

The selected values of the five processing parameters have been summarised in Table 5.1.

**Table 5.1.** Selected values of the processing parameters

Processing parameters	Values				
Epoxy concentration, $C_e$ (%)	<b>45</b>	<b>50</b>	<b>55</b>	<b>60</b>	<b>65</b>
Compressive pressure, $p_c$ (MPa)	0.25	0.50	<b>0.75</b>	01.00	1.25
Vacuum pressure, $p_v$ (MPa)	0.085	0.080	<b>0.070</b>	0.055	0.035
Dwelling time, $t$ (minutes)	20	25	<b>30</b>	35	40
Holding temperature, $T$ (°C)	100	110	<b>120</b>	130	140

**Note:** the values printed in bold were used in the first step of the optimisation procedure.

## 5.2. EXPERIMENTAL PROCEDURE

### 5.2.1. Materials

Unidirectional plain woven carbon fibre tape supplied by Colan Products Pty. Ltd., Huntingwood, NSW, Australia, was selected as reinforcement in developing this fabrication procedure. The nominal width of the tape is 300 mm, the nominal thickness is 0.25 mm, and the specific area weight is 200 g·cm<sup>-2</sup>. The warp contains approximately 98% of the total fibre with the remaining 2% comprising the weft fibre [13]. Due to its compatibility with different fibres, fast wettability, ease of processing [14], low shrinkage upon curing [15], and good mechanical properties [14, 15], an epoxy resin was selected for the matrix. The epoxy, comprising of Technirez<sup>®</sup> R2519 resin and Technirez<sup>®</sup> R2419 hardener, was supplied by ATL Composites, Southport, Australia. A 70-to-30 by weight mixing ratio [16] was recommended by the manufacturer for this particular epoxy system. Properties of the constituent materials have been presented in Table 4.1.

### 5.2.2. Optimisation Procedure

The optimisation procedure consists of five steps with one parameter being optimised in each step. An optimum value that had been obtained in a particular

step was then applied in all following steps. In each step, the plates that had been produced were cut into specimens according to the adopted flexural test standard, ASTM D790-05 [17], and subjected to three-point bend loading until failure or else underwent 5% strain, whichever occurred first. Another five samples were also carefully removed from the plate, cast into polyester blocks, polished, and subjected to optical microscopy for later microstructural analysis. The composite fabrication and parameter optimisation procedures have previously been discussed in Sub-section 4.2.2. Mechanical testing and optical micrography have been discussed in sections 4.4 and 4.5, respectively.

First, in order to determine the optimum value of epoxy content,  $C_e$ , within the epoxy solution utilised for embedding the carbon fibre (that had been wrapped onto a steel frame), five different concentrations were utilised, *i.e.*, 40 wt%, 45 wt%, 50 wt%, 55 wt% and 60 wt% as presented in Table 5.1. The other four parameters for hot-press curing utilised in this first step were kept constant, *i.e.*, compressive pressure,  $p_c$ , was 0.75 MPa [8], vacuum atmosphere pressure inside the chamber,  $p_v$ , was 0.070 MPa, dwelling time,  $t$ , was 30 minutes, and holding temperature,  $T$ , was 120 °C [9]. One composite plate was produced for each  $C_e$  value with these plates being cut into specimens, tested and analysed in order to determine the optimum value of the epoxy concentration.

Once the optimum value of  $C_e$  had been established, this value was then applied in optimising the other four fabrication parameters in the later steps. One parameter was optimised in each of the following four steps in the following order:  $p_c$ ,  $p_v$ ,  $t$  and  $T$ . The same procedure, apart from the parameter under optimisation that was varied, was applied in the next four steps of the optimisation procedure.

### **5.2.3. Testing and Evaluation**

As mentioned, mechanical property characterisation was carried out in accordance with ASTM D790-07 [17] with a span-to-depth ratio,  $S/d$ , of 64 being selected in order to ensure that the specimens failed due to flexure rather than

shear. Specimens were subjected to a three-point bend loading configuration until failure or else reaching 5% strain, whichever occurs first. Specimen dimensions and the preparation procedure, as well as the testing procedure, have been presented in detail in sub-section 4.4.2, whilst microstructural characterisation has been discussed in section 4.5. At least five specimens were prepared from each composite plate and subsequently tested. The data presented here are the average values of these specimens.

### 5.3. RESULT AND DISCUSSION

Figure 5.1 is a photo micrograph of the calibration bar at 5× optical magnification. It shows that a length of 687 pixels was equivalent to 1000 µm – these values being calculated using ImageJ software. Therefore, the scaling factor of the micrographs captured under 5× optical magnification can be calculated.

$$F_{s, 5 \times o.m.} = 0.687 \text{ px}/\mu\text{m}. \quad (5.1)$$

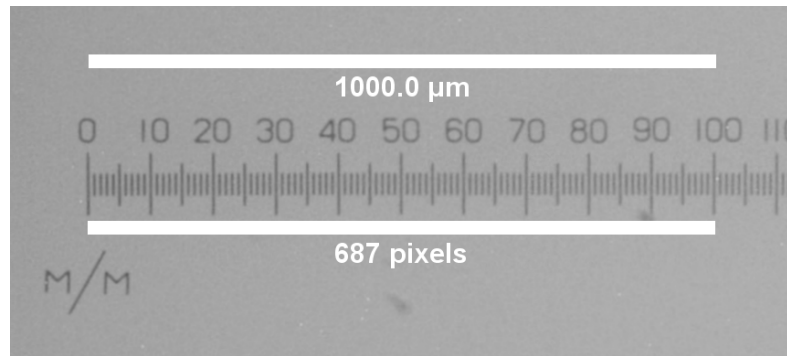


**Figure 5.1.** Photo micrograph of the calibration bar captured under 5× optical magnification showing two scale bars of the same length, one in micron and the other in pixels (px).

Micrograph samples for  $V_f$  and  $V_v$  determination, as well as the flexural property calculation procedures using a spreadsheet, have been presented in Appendix 7 to Appendix 10.

In comparison with those presented in the previously published papers [3, 4], the results currently presented in this report may be slightly different due to the addition of extra sample data being analysed in order to obtain more reliable data.

### ***5.3.1. Epoxy Concentration Determination, $C_e$***

The estimated fibre volume fraction,  $V_f$ , was found to be in the range 51.3%~53.6%, which is relatively constant, for  $C_e$  between 45 wt% and 60 wt%. However, it decreased significantly to ~48.3% when  $C_e$  was increased to 65%. In comparison with Figure 5.2(b), which represents a specimen containing 65 wt% of  $C_e$ , Figure 5.2(a) presents an optical micrograph for a specimen containing 45 wt% of  $C_e$ , showing that the fibre distribution was relatively even within the individual prepreg layers with no obvious matrix-rich areas (dark bands) and suggesting  $V_f$  to be relatively high. Figure 5.2(b) illustrates the presence of matrix-rich regions that were located between adjacent prepreg layers. Such a microstructure indicates that a large proportion of the acetone solution containing 65 wt% of epoxy resin was unable to wet and coat the individual fibres within each layer, instead, the matrix concentrated on the surfaces of the individual prepreps.

The presence of a thick matrix film on the surface of each prepreg layer was believed to have caused significant variations in the thickness of individual prepreg layers, leading to poor flatness of the prepreg surfaces and increasing the possibility of air bubble entrapment between adjacent prepreg layers during the stacking process. Indeed, several large voids, located between adjacent prepreg layers, which appeared dark in colour [18], can be observed in Figure 5.2(b) as noted by the white arrows. In contrast to this, the acetone solutions containing matrix resin contents below 65 wt% were, as expected, found to exhibit lower viscosities which increased their wettability and infiltration into the fibre bundles [8].

Concerning the observation of micrographs during image analysis, the following points were noticed: (i) there was no void development in the through-the-thickness direction of the plates, (ii) most of the larger voids were located between adjacent plies, (iii) voids altered the initial fibre arrangement, and (iv) the majority of the voids were in contact with fibres. Olivier *et al.* reported that, in addition to the volume, void shape and location also need to be considered when predicting the mechanical behaviour of composites containing voids [2].

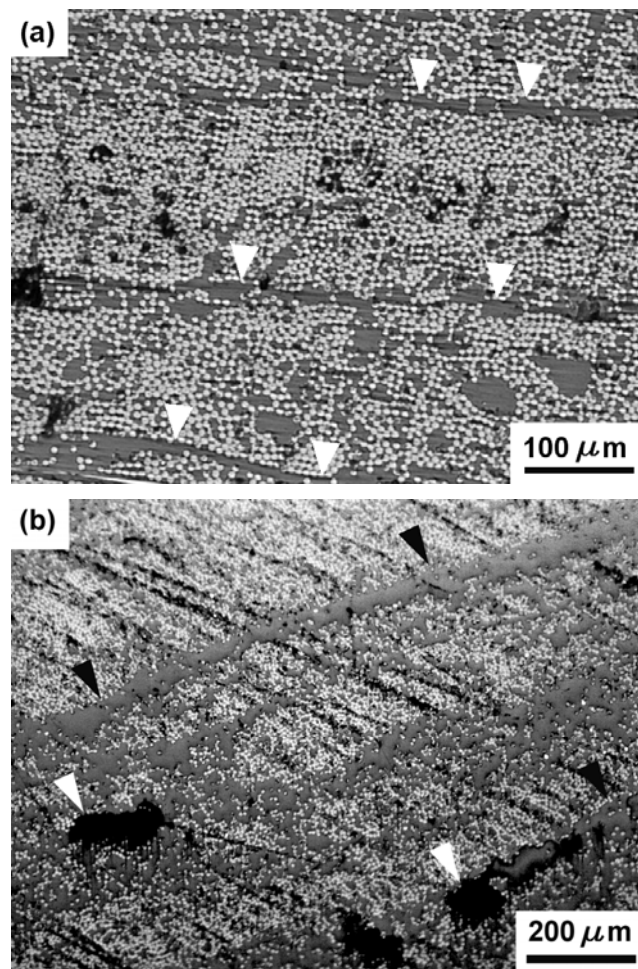


**Figure 5.2.** Optical micrographs of two specimens manufactured from different  $C_e$ -s: (a) 45 wt% of  $C_e$  showing less matrix-rich areas as narrower dark bands (white arrows), and (b) 65 wt% of  $C_e$  showing matrix-rich areas as wider diagonal dark bands (dark arrows) and voids (white arrows) between layers [4].

Figure 5.3 presents the effect of  $C_e$  on the flexural strength, flexural modulus and estimated  $V_f$  and void content,  $V_v$ . The highest values for flexural strength (988 MPa) and flexural modulus (59.3 GPa) were both achieved at a  $C_e$  of 50 wt%. The  $V_f$  for this system was 53.2% which is slightly below the maximum value achieved for the 60 wt% of  $C_e$  (53.6%). Referring to the “rule of mixtures” and considering the fact that  $V_f$  was found to be relatively constant for the range of  $C_e$  from 45% to 60 wt%, the decrease of flexural strength and flexural modulus for  $C_e$  above 50 wt% may be attributed to an increase in  $V_v$  between the individual prepreg layers, similar to the decrease in interlaminar shear strength as reported by Yoshida *et al.* [9]. This also confirmed from the figure that, apart from  $C_e = 60$  wt%, general trend that can be observed is that both flexural strength and flexural modulus increase with the decrease in  $V_v$ , and *vice versa*.

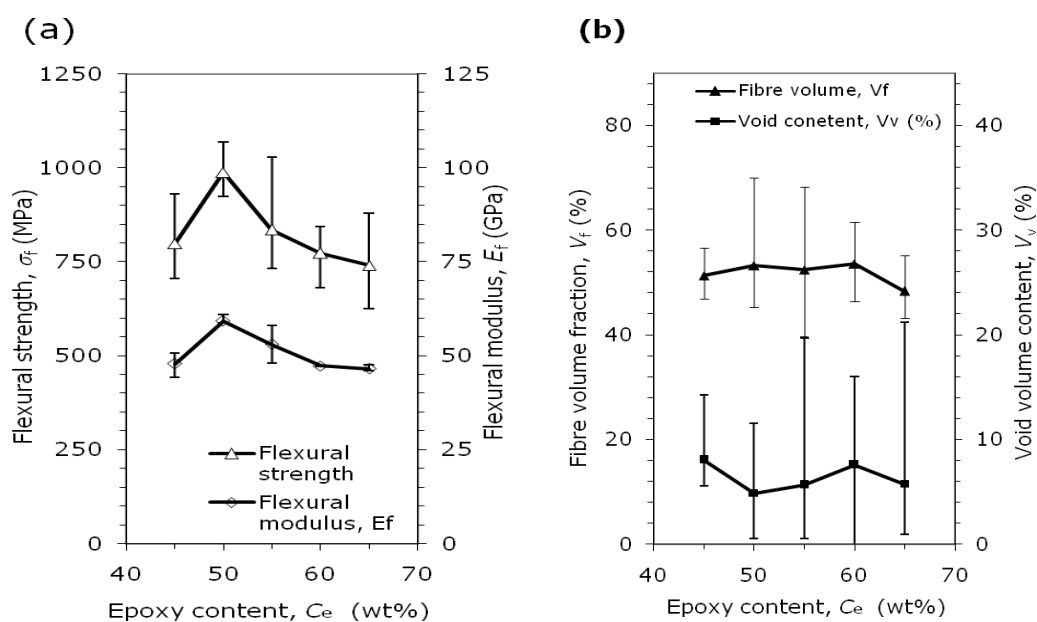


**Figure 5.3.** (a) Influence of  $C_e$  on flexural properties showing narrow of variation, and (b) Estimated fibre volume fraction with relatively narrow range of spread and void volume content with wider range of variation.

It can be concluded from the above discussion that the optimum value of  $C_e$  is 50 wt%, at which point the maximum flexural strength and flexural modulus were achieved together with the minimum  $V_v$ , although its  $V_f$  was slightly lower than that of  $C_e = 60$  wt%.

### 5.3.2. Hot-press Curing Compressive Pressure, $p_c$

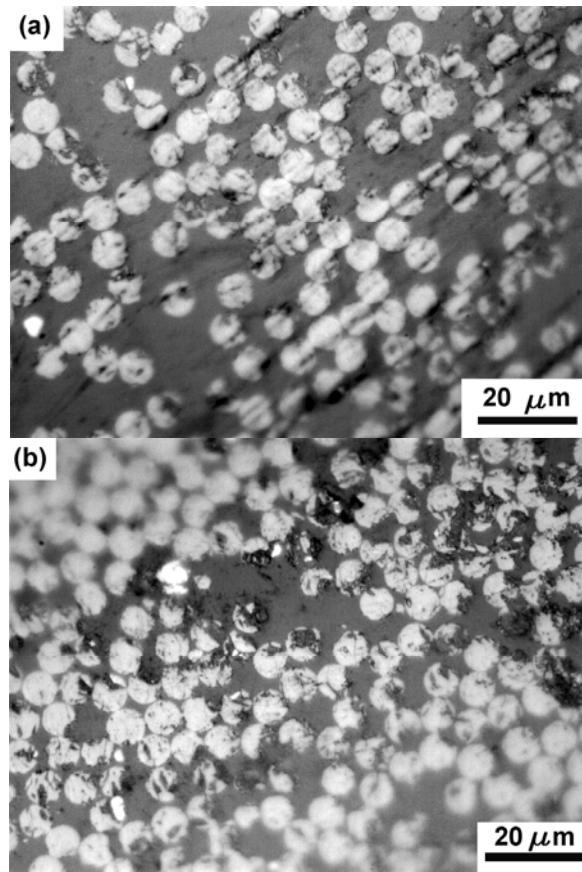


**Figure 5.4.** Optical micrographs of composite specimens: (a) manufactured at 0.25 MPa  $p_c$  illustrating matrix-rich regions and voids (dark spot in matrix area), and (b) manufactured at 1.00 MPa  $p_c$  indicating the presence of denser fibre packing and less voids.

The estimated  $V_f$  was found to vary considerably between a minimum of 50.0% (for a  $p_c$  of 0.50 MPa) and 59.0% (for a  $p_c$  of 1.00 MPa). These results were confirmed by observations during the vacuum hot-press curing procedure where the amount of excess resin squeezed from the prepreg layers was noted to vary for different magnitudes of  $p_c$ . Figure 5.4(a) clearly indicates the presence of a relatively low  $V_f$  (42.3%, the lowest among those of the samples, at 0.25 MPa of  $p_c$ ) when compared to that of Figure 5.4(b) (62.5%, the highest among those of the samples, at 1.0 MPa of  $p_c$ ). Overall, it was noted from optical microscopy that



increasing the  $p_c$  resulted in a lower  $V_v$  within the resultant composite plates. This result was found to agree with that previously reported [1-2].

The degree of fibre misalignment was found to be relatively low as shown in Figure 5.5, as the composite plates were produced using a dry lay-up technique. This result indicates that although a proportion of the fibres were displaced from their initial arrangement, most of these fibres experienced relatively small misalignment angles. In addition to this, unlike what was initially suspected prior to the experiments,  $p_c$  was found not to influence the degree of fibre misalignment.

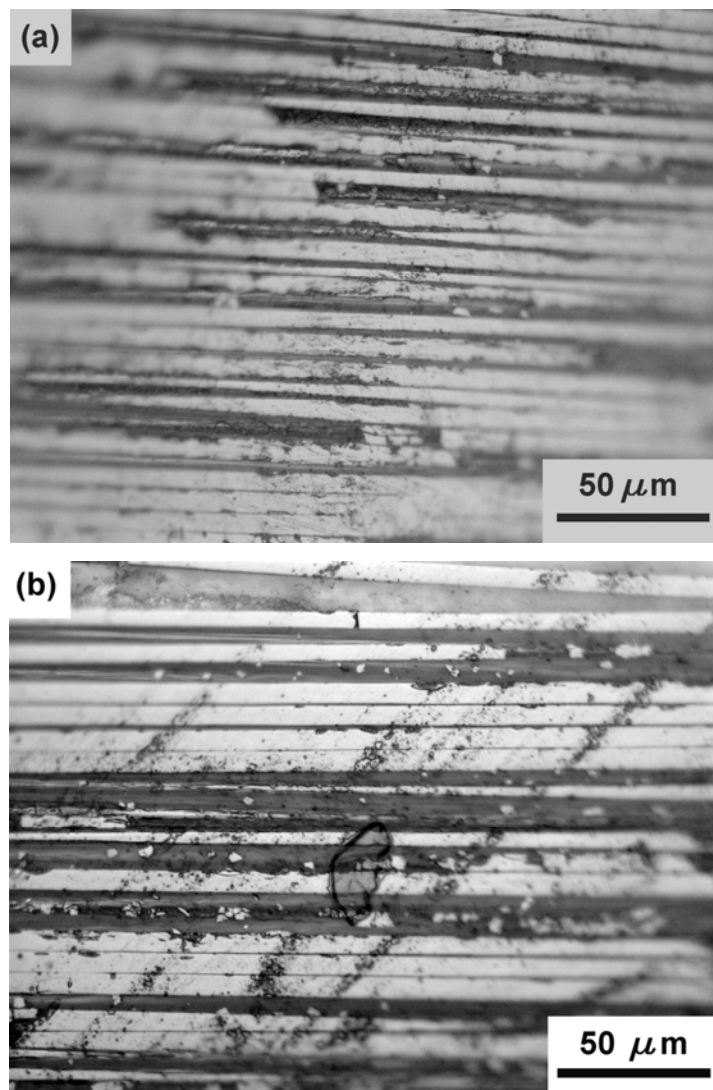


**Figure 5.5.** The effect of  $p_c$  on fibre alignment showing negligible difference in the degree of fibre misalignment: (a)  $p_c = 0.25$  MPa, and (b)  $p_c = 1.25$  MPa.

Figure 5.6 illustrates the relationship between  $p_c$  on one hand, and the flexural properties and estimated  $V_f$  and  $V_v$ , on the other hand. The highest values for flexural strength (1201 MPa) and elastic modulus (59.0 GPa) were found to occur for the specimen manufactured using a  $p_c$  of 1.0 MPa. In particular, the flexural strength was noted to increase significantly (31%) when compared to the maximum value obtained during the first step of optimisation (*i.e.*,  $C_e$ ), corresponding to a  $p_c$  of 0.75 MPa in the present set of specimens. In contrast to this, the flexural modulus was found to be considerably constant. The increase of  $V_v$  with the increase of  $p_c$  from 1 MPa to 1.25 MPa may be attributed to inadequate time of entrapped air for evacuation due to the effect of higher compressive pressure leading to faster matrix consolidation. This was confirmed with the majority of void being observed between two adjacent prepreg layers.

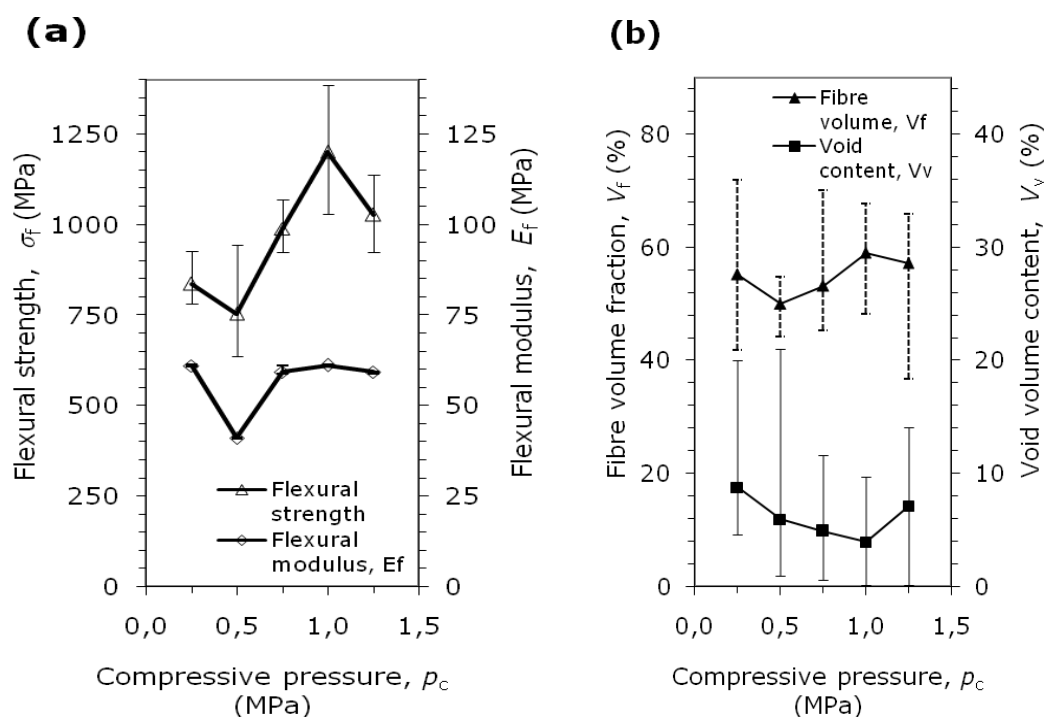
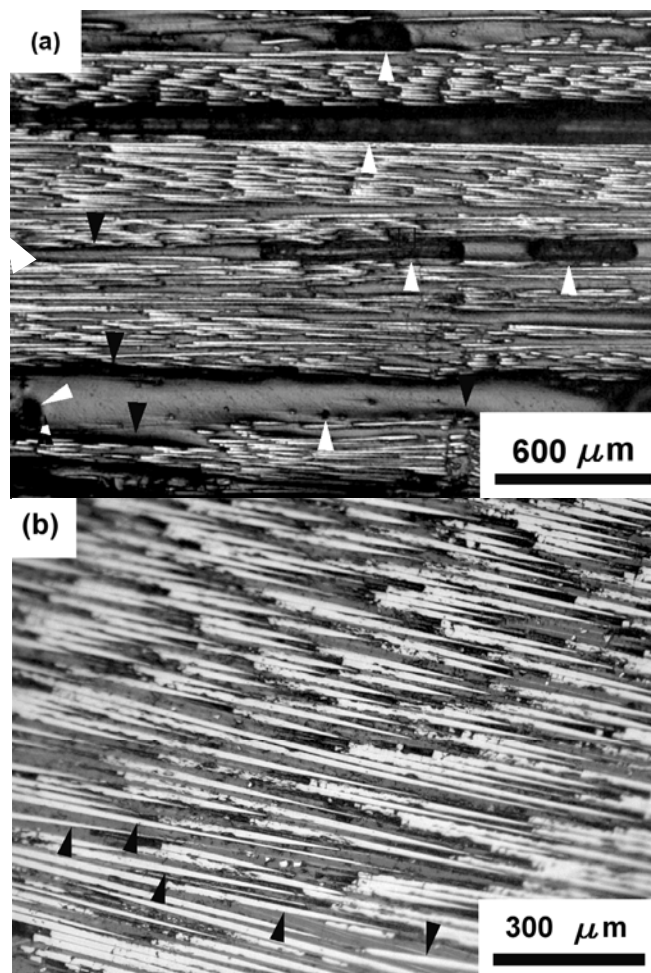


**Figure 5.6.** (a) Influence of  $p_c$  on flexural properties showing narrow range of variation especially for  $E_{ff}$ , and (b) Estimated fibre volume fraction with relatively wide range of variation.

In summary, for  $p_c$  values between 0.25 MPa and 1.25 MPa, the flexural strength and flexural modulus increased due to the decrease in  $V_v$ . Therefore, a  $p_c$  of 1.00 MPa was considered to be the optimum value.

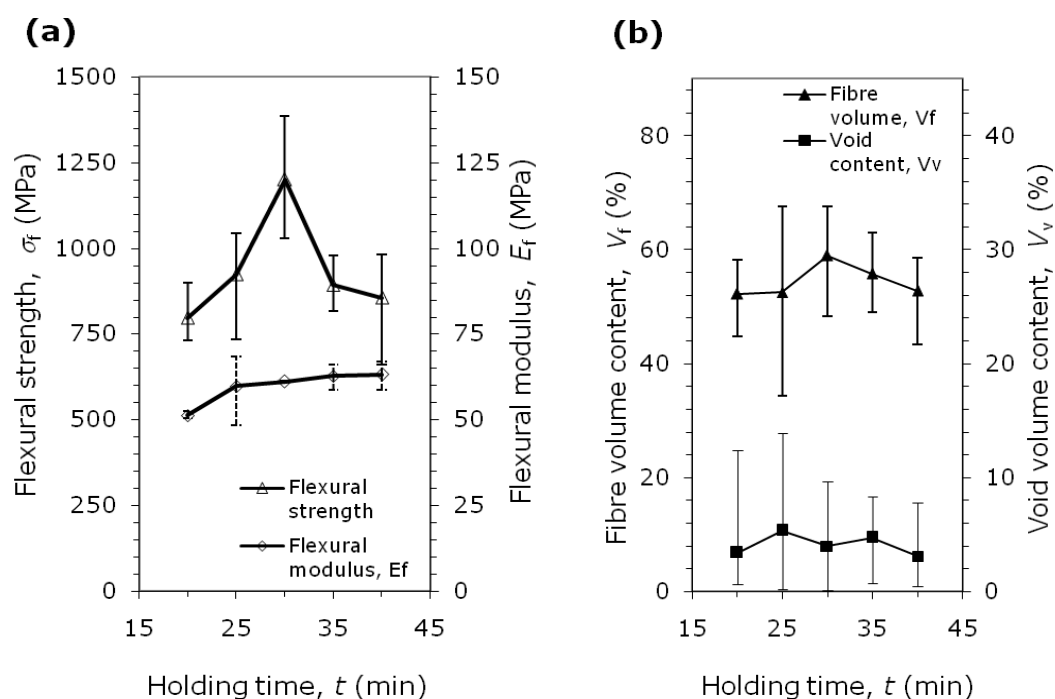
### 5.3.3. Hot-press Curing Holding Time, $t$

Figure 5.7(a) illustrates a longitudinal section of a specimen manufactured using a holding time of 20 minutes. Poor fibre-matrix interface bonding, indicated by the dark colour between fibre bundles, and matrix-rich regions (dark arrows) are obvious. This figure also shows high  $V_v$  (white arrows) that were also mainly located between adjacent prepreg layers as has been observed in the previous rounds of optimisation. These processing deficiencies may be used to explain the relatively low flexural strength (775 MPa) and elastic modulus (49.6 GPa) for this particular specimen.



**Figure 5.7.** Optical micrographs illustrating: (a) imperfect fibre wetting (dark arrows) and the presence of voids (white arrows) between individual prepreg layers in a  $t$  of 20-minute specimen, and (b) fibre misalignment within a  $t$  of 40-minute specimen (dark arrows).

In contrast to this, Figure 5.7(b) illustrates a specimen manufactured using a holding time of 40 minutes, revealing that improvements in inter-layer bonding and decreasing  $V_v$  could be achieved. However, small amounts of fibre misalignment at small off-axis angles, as denoted by the dark arrows, were observed and this would be expected to reduce the mechanical properties of these specimens in comparison with those of plates produced using a 30 minute holding time. Fibre misalignment is known to affect the mechanical properties of the composites [3, 4]. Thus, the flow of matrix and subsequent misalignment of the fibres may be the cause of the decrease flexural strength for specimens produced at  $t$  above 30 minutes.



**Figure 5.8.** (a) Influence of holding time during the vacuum hot-press curing procedure on flexural properties showing narrow range of variation, and (b) Estimated fibre volume fraction with considerably narrow range of spread and void volume content with wider range of variation.

The influence of  $t$  on the flexural properties,  $V_f$  and  $V_v$  has been illustrated in Figure 5.8. The maximum value of flexural strength (1201 MPa) was achieved at a  $t$  of 30 minutes whereas the flexural modulus was approximately 63 GPa for 40 minutes of  $t$ . It can be seen in Figure 5.8 that whilst flexural strength increased

with  $V_f$ , flexural modulus slightly increased with holding time,  $t$ . Therefore, a holding time of 30 minutes was considered to be the optimum value as the optimum flexural strength could be achieved with negligibly lower flexural modulus in comparison to that of the 40 minute holding time specimen.

#### 5.3.4. Hot-press Curing Vacuum Pressure, $p_v$

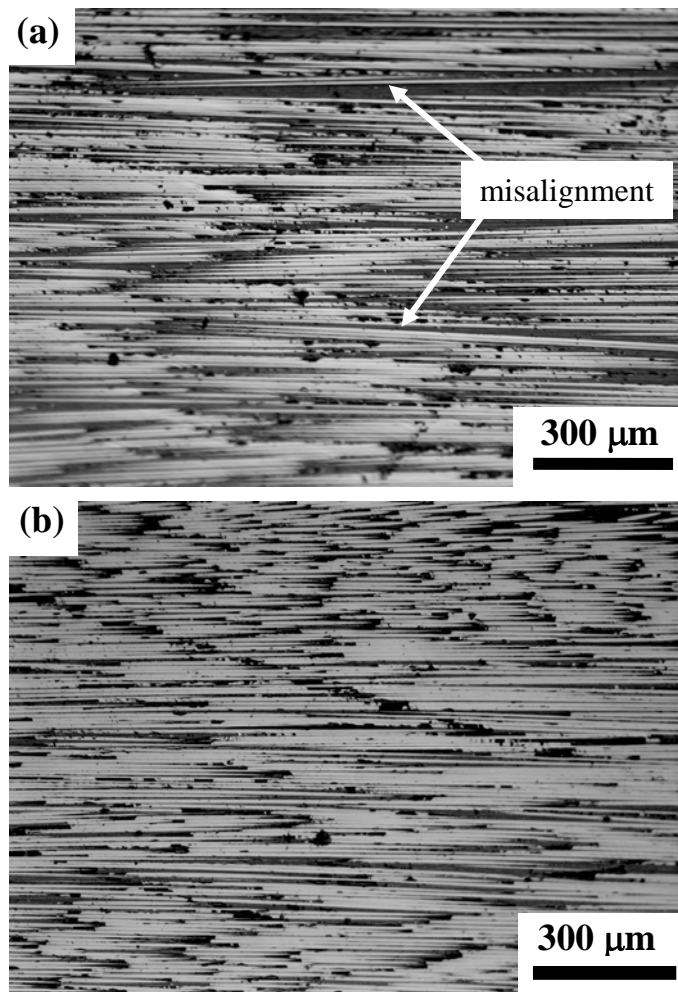


**Figure 5.9.** Samples of in-plane micrographs: (a) at  $p_v = 0.085$  MPa showing ~1.5% up to  $5^\circ$  fibre misalignment, (b) at  $p_v = 0.035$  MPa showing no fibre misalignment can be observed [3].

As the results from the previous stage showed that most fibres underwent misalignment angles between  $0^\circ$  and  $10^\circ$  in both the xy- and xz-planes, increasing the vacuum level did not show a negative effect on the fibre arrangement. When

the vacuum level was further increased from 0.085 MPa up to 0.035 MPa, however, no fibre misalignment could be observed. The small amount of voids removed from the resin system was believed to have caused resin flow to fill in the spaces previously occupied by the voids but was not strong enough to displace fibres from their initial positions. In addition, the presence of voids may lead to fibre misalignment due to local deformation of fibres as has been previously discussed. Figure 5.9(a) shows an in-plane micrograph with approximately ~1.5% of fibres possessing misalignment angles of up to  $5^\circ$ , in contrast to Figure 5.9(b) where no fibre misalignment was noted.

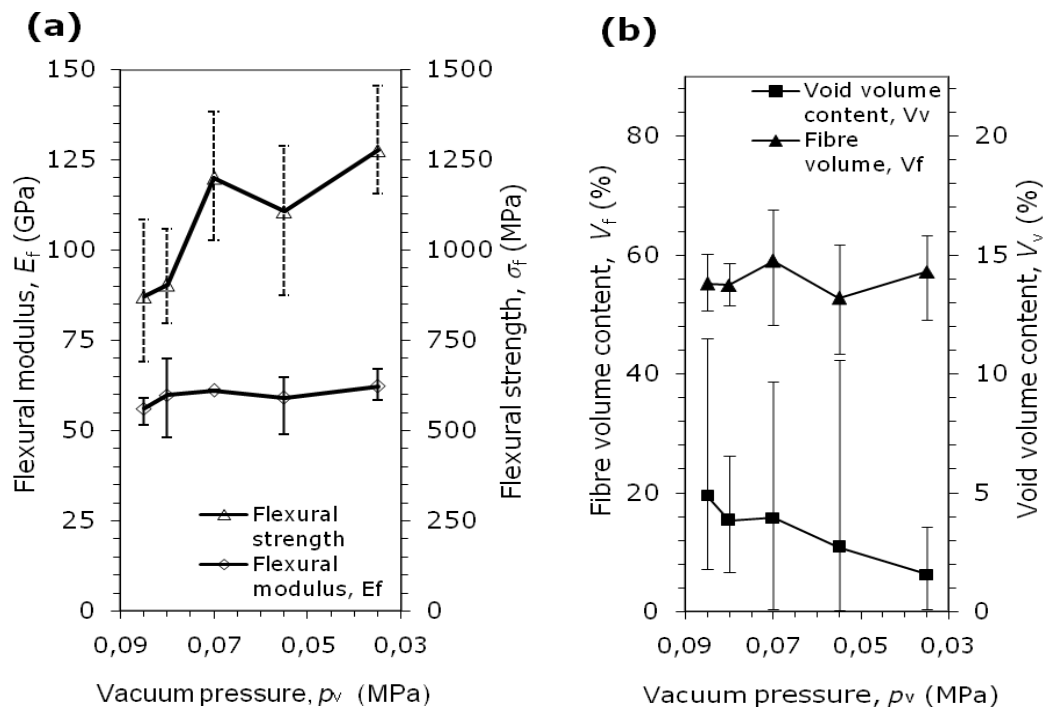


**Figure 5.10.** (a) The influence of vacuum pressure on flexural strength, flexural modulus showing narrow range of variation, and (b) Estimated fibre volume fraction with considerably narrow range of variation and void volume content with wider range of variation, at  $p_c = 1.00$  MPa,  $T = 120^\circ\text{C}$ , and  $t = 30$  minutes.

Figure 5.10 shows a slight decrease in the predicted  $V_f$ , ~0.3%, compared to that of  $p_v = 0.085$  MPa, when the vacuum level increased from 0.085 MPa to 0.080 MPa. Further increasing the vacuum level from 0.080 MPa to 0.070 MPa produced an increase in  $V_f$  back to ~59% and was essentially constant as the vacuum level further increased to 0.035 MPa. Whilst the applied  $p_c$  resulted in

significant variations in the amount of excess resin being squeezed from the prepreg arrangement, at lower vacuum levels, any increase in vacuum evacuated only entrapped voids from the resin system. This result was in contrast to that of Boey and Lye [3] who noted that at higher vacuum levels, some of the resin may be extracted from the prepreg arrangement being pressed, resulting in an increase of fibre content.

Figure 5.10 also shows that, generally speaking,  $V_v$  dropped from ~4.9% to ~1.5%, as the vacuum level increased from 0.085 MPa to 0.035 MPa. At the beginning up to  $p_v = 0.080$  MPa,  $V_v$  dropped quite rapidly with an increase of vacuum level, then it experienced a slower rate of decrease as the vacuum level further increased up to 0.035 MPa – a similar phenomenon has been previously reported [8]. Although the current results may appear to suggest that  $V_v$  may be decreased further with increasing vacuum level, this may not be beneficial from the production processing point of view as the additional effort required to increase the vacuum level further may not be comparable with any extra decrease in  $V_v$ .

The flexural strength and flexural modulus were found to vary from 871 MPa and 56 GPa, respectively (corresponding to 0.085 MPa  $p_v$ ) to 1277 MPa and 62.3 GPa, respectively (corresponding to 0.035 MPa  $p_v$ ). In comparison to the results of the previous step, increases in both flexural strength and flexural modulus were observed, although they were relatively small in nature, *i.e.* 6.35% and 1.96%, respectively. Thus, applying a vacuum pressure inside the curing chamber resulted in a decrease in  $V_v$ . Taking into account the flexural properties,  $V_f$  and  $V_v$ , a vacuum pressure of 0.035 MPa was considered to be optimum.

### 5.3.5. Hot-press Curing Holding Temperature, $T$

The influence of  $T$  on the flexural properties,  $V_f$ , and  $V_v$ , has been presented in Figure 5.11. The values of  $V_f$  were found to vary within a narrow range, from ~54.6% at  $T \sim 140$  °C to ~57.9% at  $T \sim 100$  °C. As the  $T$  increased from 110 °C to 140 °C, the  $V_f$  decreased negligibly. Quicker resin evaporation at higher  $T$  combined with the applied vacuum pressure may be responsible for this slight

decrease of  $V_f$  as the resin vapour would quickly be evacuated from the flowing resin system.

As  $T$  increased from  $\sim 100$  °C up to  $\sim 130$  °C,  $V_v$  decreased from  $\sim 2.46\%$  to  $1.55\%$  and then increased to  $\sim 2.25\%$  at  $T \sim 140$  °C. The decrease of  $V_v$  up to  $T \sim 130$  °C was thought to be caused by the decrease in resin viscosity with larger  $T$  during the initial stages of the heating process prior to the initiation of gelation and cross-linking of the resin molecules – this would aid the removal of voids. In contrast to this, a sharp decrease in resin viscosity due at  $T \sim 140$  °C, leading to insufficient time for the entrapped air to be removed, was suggested as a reason for the increase of  $V_v$  at this temperature. Therefore, a balance needs to be made between the resin solidification rate and vacuum level in order to achieve optimum void evacuation.

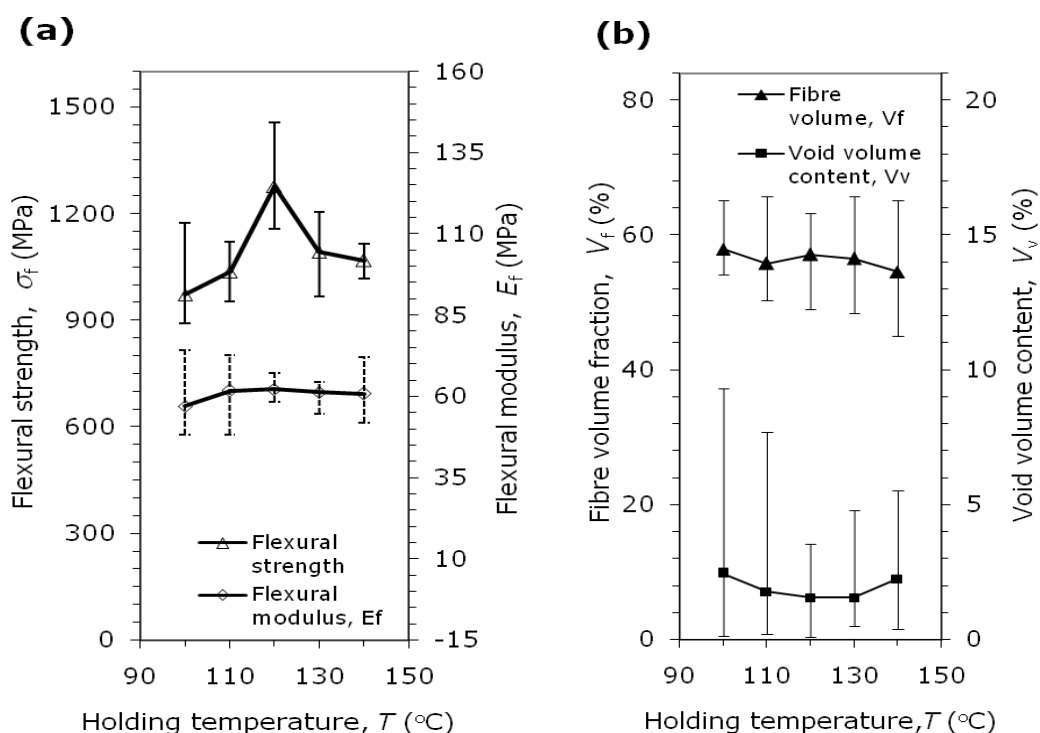


**Figure 5.11.** (a) The influence of  $T$  on flexural strength, flexural modulus considerably showing narrow range of variation, and (b) Estimated  $V_f$  with narrow range of variation and  $V_v$  with relatively wide range of variation, at  $p_c = 1.00$  MPa,  $T = 120$  °C,  $t = 30$  minutes and  $p_v = 0.035$  MPa.

As has been observed in the previous steps, at relatively constant  $V_f$ , the flexural strength showed a negative correlation with their respective  $V_v$ . The



optimum value of  $T$  was found to be the same as that in the previous step, *i.e.*, 120 °C, with the flexural strength and flexural modulus being ~1277 MPa and ~62.3 GPa, respectively.

Although a holding temperature of  $T \sim 120$  °C produced a slightly lower  $V_f$ , its  $V_v$  was the lowest and its flexural properties were the highest, thus a  $T$  of 120 °C was considered to be the optimum value.

## 5.5. CONCLUSIONS

The optimum values of the following processing parameters, *i.e.* (i) epoxy resin content of the acetone solution, (ii) compressive pressure, (iii) holding time, (iv) vacuum pressure inside the curing chamber, and (v) holding temperature during hot-press curing, for the fabrication of a unidirectional CFRP composite have been investigated in five consecutive steps, with the resulting composites having been tested under flexural loading. Whilst  $V_f$  and  $V_v$  were characterised by means of their respective optical micrographs, flexural property characterisation was carried out in the three-point bend loading configuration according to the ASTM D790-03 standard. Taking into account the highest values of mechanical properties and  $V_f$ , as well as the minimum value of  $V_v$ , the optimum values of the processing parameters for this particular epoxy system were determined to be those presented in Table 5.2.

**Table 5.2.** Optimum values of the processing parameters

Processing parameters	Values
Epoxy concentration, $C_e$ (wt%)	50
Compressive pressure, $p_c$ (MPa)	1.00
Dwelling time, $t$ (minutes)	30
Vacuum pressure, $p_v$ (MPa)	0.035
Holding temperature, $T$ (°C)	120

It should be noted that each parameter under investigation resulted a typical effect on CFRP composite properties being produced. It showed that each of these

parameters influences the properties of the resulted composites in different ways. In addition to this, these optimum values of processing parameters have been evaluated individually in each consecutive step. This approach has been selected considering the fabrication facilities available in the university. In order to be capable of obtaining more complex data, such as any possible interactions among the processing parameters being studied, further study involving more complex experimental approach and more sophisticated fabrication facilities may be carried out. Considering that curing is applied to the matrix, it was expected that matrix type may dominantly control curing characteristics rather than fibre type, and further, these optimum values would also be applied to the fabrication of GFRP and hybrid FRP composites.

## REFERENCES

- [1] F. Y. C. Boey and S. W. Lye, "Void reduction in autoclave processing of thermoset composites : Part 1: High pressure effects on void reduction," *Composites*, vol. 23, pp. 261-265, 1992.
- [2] P. Olivier, J. P. Cottu, and B. Ferret, "Effects of cure cycle pressure and voids on some mechanical properties of carbon/epoxy laminates," *Composites*, vol. 26, pp. 509-515, 1995.
- [3] Sudarisman and I. J. Davies, "Influence of compressive pressure, vacuum pressure, and holding temperature applied during autoclave curing on the microstructure of unidirectional CFRP composites," *Advanced Materials Research*, vol. 41-42, pp. 323-328, 2008.
- [4] Sudarisman and I. J. Davies, "The effect of processing parameters on the flexural properties of unidirectional carbon fibre-reinforced polymer (CFRP) composites," *Materials Science and Engineering: A*, vol. 498, pp. 65-68, 2008.
- [5] D. N. Sutherland, "Random packing of circles in a plane," *Journal of Colloid and Interface Science*, vol. 60, pp. 96-102, 1977.
- [6] M. L. Costa, S. F. M. de Almeida, and M. C. Rezende, "The influence of porosity on the interlaminar shear strength of carbon/epoxy and carbon/bismaleimide fabric laminates," *Composites Science and Technology*, vol. 61, pp. 2101-2108, 2001.
- [7] S. F. M. d'Almeida and Z. d. S. N. Neto, "Effect of void content on the strength of composite laminates," *Composite Structures*, vol. 28, pp. 139-148, 1994.

- [8] L. Liu, B.-M. Zhang, D.-F. Wang, and Z.-J. Wu, "Effects of cure cycles on void content and mechanical properties of composite laminates," *Composite Structures*, vol. 73, p. 303, 2006.
- [9] I. J. Davies and H. Hamada, "Flexural properties of a hybrid composite containing carbon and silicon carbide fibres," *Advanced Composite Materials*, vol. 10, pp. 77-96, 2001.
- [10] P.-O. Hagstrand, F. Bonjour, and J.-A. E. Manson, "The influence of void content on the structural flexural performance of unidirectional glass fibre reinforced polypropylene composites," *Composites Part A: Applied Science and Manufacturing*, vol. 36, pp. 705-714, 2005.
- [11] N. Lissart and J. Lamon, "Damage and failure in ceramic matrix minicomposites: Experimental study and model," *Acta Materialia*, vol. 45, pp. 1025-1044, 1997.
- [12] Sudarisman, I. J. Davies, and H. Hamada, "Compressive failure of unidirectional hybrid fibre-reinforced epoxy composites containing carbon and silicon carbide fibres," *Composites Part A: Applied Science and Manufacturing*, vol. 38, pp. 1070-1074, 2007.
- [13] "Composite Reinforcement - Product Range," Huntingwood, NSW, Australia: Colan Australia Pty. Ltd., Accessed date: 20/10/2006.
- [14] S. R. Malkan and F. K. Ko, "Effect of fibre reinforcement geometry on single shear and fracture behavior of three dimensionally braided glass/epoxy composite pins," *Journal of Composite Materials*, vol. 23, pp. 798-818, 1989.
- [15] A. M. A. El-Habak, "Mechanical behaviour of woven glass fibre-reinforced composites under impact compression load," *Composites*, vol. 22, pp. 129-134, 1991.
- [16] "Technirez HP Laminating System / R2519," Southport, QLD, Australia: ATL Composites Pty. Ltd.
- [17] "ASTM D790-07 Standard test method for flexural properties of unreinforced and reinforced plastic and electrical insulating materials by three-point bending," in *Annual Book of ASTM Standard*. vol. Vol. 08.01 West Conshohocken, PA, USA: ASTM Int., 2005.
- [18] B. W. Kim and J. A. Nairn, "Observations of Fiber Fracture and Interfacial Debonding Phenomena Using the Fragmentation Test in Single Fiber Composites," *Journal of Composite Materials*, vol. 36, pp. 1825-1858, 2002.

Every reasonable effort has been made to acknowledge the owners of copyright materials. I would be pleased to hear from any copyright owner who has been omitted or incorrectly acknowledged.

## CHAPTER 6

# RESULT AND DISCUSSION

The results of the preliminary tests, *i.e.*, compressive tests, in addition to those of the three different hybrid combinations will be presented and discussed in this chapter.

### 6.1. PRELIMINARY TEST: COMPRESSIVE TEST

Compressive tests were carried out on the single fibre-type FRP composites, *i.e.* E-glass fibre/epoxy, S2-glass fibre/epoxy, TR50S carbon fibre/epoxy and IM7-12k carbon fibre/epoxy composites, as reference materials for the hybrid FRP composites under investigation. The compressive properties of these reference materials would be expected to strongly influence the flexural behaviour [1] of the resultant hybrid FRP composites – the reason for this being that previous research has indicated that that majority of failures for FRP composites subjected to flexural loading have initiated at the compressive side [2-9]. Compressive tests were carried out in accordance with ASTM D3410-03 [10].

#### 6.1.1. Specimens

The specimen geometry and dimensions utilised in this work have been presented previously in Figure 4.10. Four aluminium end-tabs [11-13] were affixed to each test coupon for the purposes of gripping and the secure transfer of load into the specimen. The adhesive used to glue the tabs onto the specimens was epoxy, *i.e.*, the same as the matrix material. Each specimen was instrumented with two strain gauges, one on each side of the specimen, for the direct measurement of strain. Details of specimen preparation and testing procedure have been presented

in sub-section 4.4.1 of this thesis whilst the tabbing press, alignment jig and test fixture utilised in this experiment have been depicted in Figures 4.4 to 4.6.

The method utilised for predicting fibre and void volume contents has been presented in sub-section 4.4.3. The predicted fibre volume fraction was calculated using equation (4.11) from image analysis results carried out using open source software, ImageJ [14], based on optical micrographs of sample slices perpendicular to the fibre direction. At least ten specimens were removed from different points within each composite plate panel to be analysed, and their average values were presented in Table 6.1, along with their predicted void volume content obtained using the same method. Micrograph samples can be found in Appendix 7. Considering that all fabrication parameters had been controlled for being invariant during the fabrication of all the plates, the higher void volume content of the TR<sub>6</sub> plate may be caused by fabrication procedure for being fully manual.

**Table 6.1.** Mean values and standard deviations of fibre volume content and void volume content of single fibre-type composite plate

<b>Materials</b>	<b>Fibre volume fraction, <math>V_f</math> (%)</b>	<b>Void volume content, <math>V_v</math> (%)</b>
E-glass fibre/epoxy	$53.3 \pm 6.4$	$1.50 \pm 0.83$
S2-glass fibre/epoxy	$54.7 \pm 7.2$	$1.16 \pm 0.43$
TR50S carbon fibre/epoxy	$53.5 \pm 9.1$	$4.25 \pm 0.57$
IM7-12k carbon fibre/epoxy	$52.4 \pm 8.6$	$2.33 \pm 2.04$

### **6.1.2. Stress-Strain Relation**

Representative stress-strain relationships of the single fibre-type FRP composite specimens were noted to be essentially linear to failure as depicted in Figure 6.1 – two sets of stress-strain data (*i.e.*, using both strain gauges) have been presented for each material. It should be noted that the strains given in the horizontal axis are those obtained from direct measurement using strain gauges (Appendix 11), whilst the stress values were calculated using the maximum loads

divided by the respective initial cross-sectional areas of the specimens – mechanical properties of the constituent materials have been presented in Table 5.2. The highest compressive strength (Figure 6.2) was exhibited by the S2-glass fibre/epoxy (S2gF/Ep) specimens, followed by those of E-glass fibre/epoxy (EgF/Ep), IM7 carbon fibre/epoxy (IM7/Ep), and TR50S carbon fibre/epoxy (TR50S/Ep) specimens, respectively. The compressive moduli for each specimen were derived from the initial regions of the stress-strain relationships. Careful examination of Figure 6.1 revealed that the highest compressive modulus was expected from the IM7/Ep specimens, closely followed by TR50S/Ep, with those of S2gF/Ep and EgF/Ep being considerably lower.

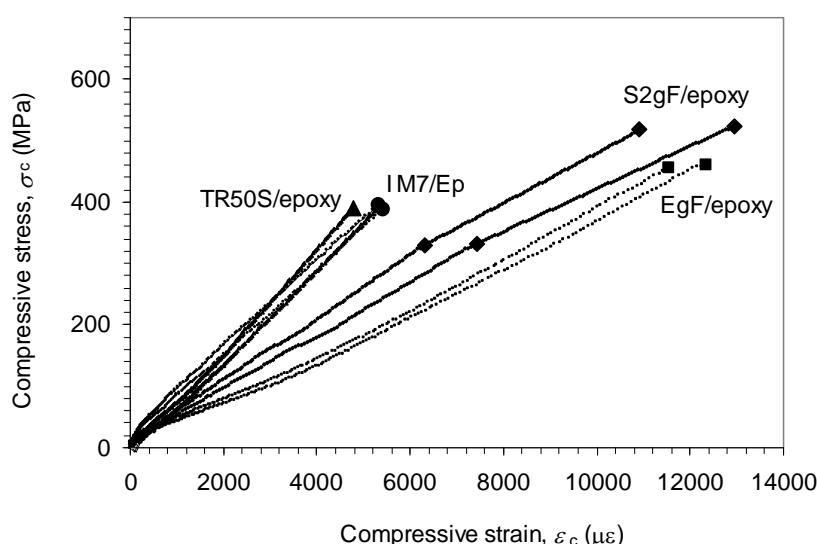


**Figure 6.1.** Representative stress-strain relation curves of compressive FRP composite specimens showing considerably linear stress-strain relation up to close to failure.

Apart from the S2gF/Ep composite specimens, all of the curves were noted to exhibit linear stress-strain relationships to failure. In contrast to this, the stress-strain response of the S2gF/Ep specimens (obtained from strain gauges installed on opposite faces of these specimens) experienced a change in slope at a compressive stress of approximately 330 MPa. This change in slope was attributed to the initiation of global compressive buckling of the specimens as revealed by the gap between the two stress-strain curves, this being a well known phenomenon that frequently occurs during the compressive testing of high

strength composite materials. In the absence of this effect, *i.e.*, if global buckling of this composite could have been prevented, the compressive strength of this specimen would have been expected to be higher.

In addition, all of the composite specimens exhibited catastrophic failure, in contrast to gradual failure that is sometimes noted in CFRP and GFRP composites. Although a gradual drop in load for cylindrical CFRP specimens loaded in compression has been previously reported [15], catastrophic failure for the same specimen geometry albeit with a smaller diameter has also been reported [16]. Davies and colleagues [17] also observed catastrophic failure for their rectangular cross-sectioned CFRP specimens with an aspect ratio of  $\sim 3.5$ . Catastrophic failure, as indicated by a sudden load drop at the point of failure, was also observed in these compressive tests with the cross-sectional geometry of the specimens being rectangular with an aspect ratio of  $\sim 5$ . Considering their respective specimen geometry and dimensions, the slenderness ratio,  $\lambda = \left( \frac{I}{A} \right)^{-1/2} \cdot l_o$ , as a measure of buckling rigidity of the specimens was calculated. The slenderness ratio of the specimens in [15] was found to be  $\sim 8.0$ , those in [16] and [17] were  $\sim 11.8$  and  $\sim 11.0$ , respectively, and in this test the value was  $\sim 11.0$ . The difference in these values was thought to be a significant contributory factor to the diversity in failure modes observed.

### 6.1.3. Compressive Properties

Comparison of the compressive strength and modulus for the FRP specimens tested has been depicted in Figure 6.2. As revealed earlier, the S2-glass fibre/epoxy (S2gF/Ep) specimens exhibited the highest compressive strength (476 MPa) followed in order by the E-glass fibre/epoxy (EgF/Ep) (430 MPa), IM7 carbon fibre/epoxy (IM7/Ep) (426 MPa) and TR50S carbon fibre/epoxy (TR50S/Ep) (384 MPa) specimens. For comparison purposes, from referring to Table 4.1 for the constituent properties and Table 6.1 for fibre volume content, the predicted tensile strengths and moduli, in accordance with the rule of mixtures, have been presented in Table 6.2 for these specimens.

**Table 6.2.** Predicted tensile properties of FRP composites under investigation according to the rule of mixtures

Materials	Strength (MPa)	Modulus (GPa)
E-glass fibre/epoxy	1576	34.5
S2-glass fibre/epoxy	2710	49.2
TR50S carbon fibre/epoxy	2660	130.1
IM7-12k carbon fibre/epoxy	2914	144.2

Comparing the compressive data given in Figure 6.2 to their respective predicted tensile values shown in Table 6.2 suggests a similar order for the compressive moduli in both cases although the compressive and tensile moduli are not linearly proportional. Figure 6.2 also indicates that the compressive moduli of the CFRP specimens are significantly than those of the GFRP specimens (due to the higher elastic modulus of the carbon fibres compared to glass fibres). In comparison to their respective predicted tensile modulus values, the compressive moduli for GFRP, *i.e.*, the EgF/Ep and S2gF/Ep, specimens were 95.2% and

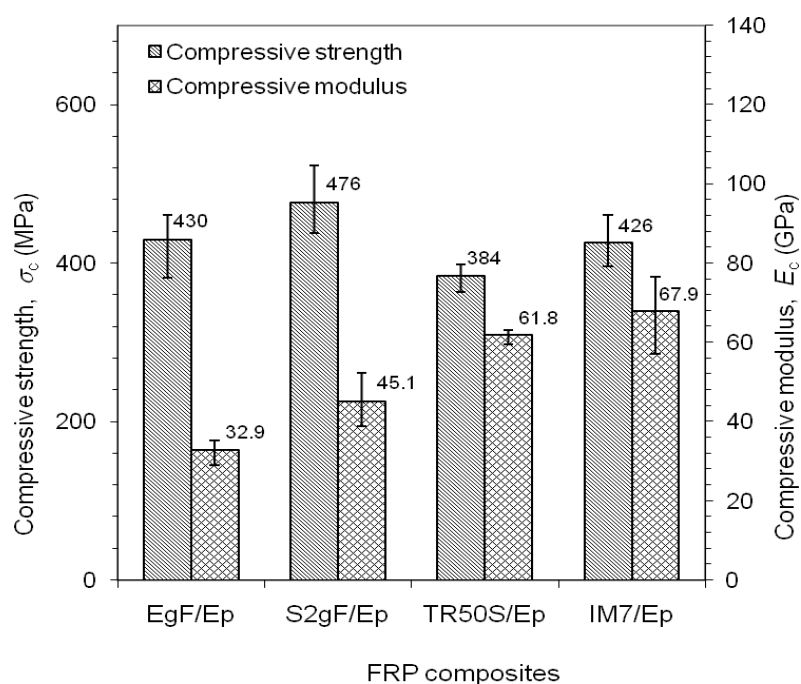


**Figure 6.2.** Compressive properties of single fibre-type composite specimens under investigation showing narrow spread of variation indicating homogeneous properties within each individual composite plate.



91.8%, respectively, while those of CFRP, the TR50S/Ep and IM7/Ep, specimens were only 47.5% and 47.1%, respectively, *i.e.*, the compressive moduli of the CFRP specimens were significantly below those predicted in Table 6.2.

In contrast to this, the compressive strengths of the GFRP specimens were higher than those of the CFRP specimens, in terms of both their nominal values and also their relative values in comparison with their predicted tensile strengths, *i.e.*, 27.3% and 17.6% for the GFRP specimens in comparison with 14.4% and 14.6% for the CFRP specimens. Similar findings have previously been reported by other researchers [15, 18, 19]. For example, Oya and Johnson [20] reported that the compressive strength of various types of carbon fibre ranged from 12.5% to 15.3% of their respective tensile strength, while in [21] they found these values had increased to 29% and 51%, respectively. The higher compressive-to-tensile property ratios for the glass fibres may be attributed to their amorphous crystalline structure [22, p. 25]. The smaller filament diameter of the S2-glass fibre (9  $\mu\text{m}$ , Table 4.1) in comparison to that of the E-glass fibre (17  $\mu\text{m}$ , Table 4.1), leading to a smaller slenderness ratio and thus lower buckling rigidity for individual S2-glass fibres, may be responsible for the significantly lower compressive-to-tensile strength ratio of the S2gF/Ep specimens, 17.6%, compared to that of the EgF/Ep specimens, 27.3%.

In light of the compressive data mentioned above, and considering the stress distribution through the thickness of composite beams subjected to flexural loading, it is clear that the potential exists for the improvement of composite flexural behaviour through the layering of different FRP prepregs in various sequences and proportions.

## **6.2. HYBRID FRP COMPOSITES CONTAINING DIFFERENT TYPES OF GLASS FIBRE**

When compared to high performance carbon and SiC fibres, the cost of common glass fibres such as E-glass is known to be substantially lower and therefore more widely utilised in engineering applications. In recent years, a higher performance and higher cost glass fibre, known as S2-glass, has found

growing use in high value applications such as airplane fuselages. Preliminary work carried out by the authors on E-glass/epoxy and S2-glass/epoxy unidirectional composites (Figure 6.2) indicated the compressive strength of this particular S2-glass/epoxy composite to be considerably higher when compared to that of the E-glass/epoxy composite counterpart.

Potential may thus exist for the improvement of flexural behaviour in E-glass/epoxy composites through the partial substitution of S2-glass fibres at the compressive side of the specimen. Therefore, in the present work the authors have investigated the flexural properties and subsequent failure behaviour of unidirectional hybrid FRP composites containing a mixture of E-glass and S2-glass fibres embedded within an epoxy matrix.

### **6.2.1. Physical properties**

#### **6.2.1.1. Stacking configurations**

Composite plates with six different stacking configurations, including the standard E-glass/epoxy and S2-glass/epoxy composites, were fabricated, subsequently tested and analysed with each plate comprising of five glass fibre/epoxy prepreg layers. Considering the previous findings in that the failure of composite beams under flexural loading was mainly initiated at the compressive face [23-27], in the present work the stronger fibre, *i.e.*, S2-glass fibre, was positioned at the compressive side during flexural testing. The stacking configurations of the hybrid GFRP composites under investigation have been illustrated in Figure 6.3.

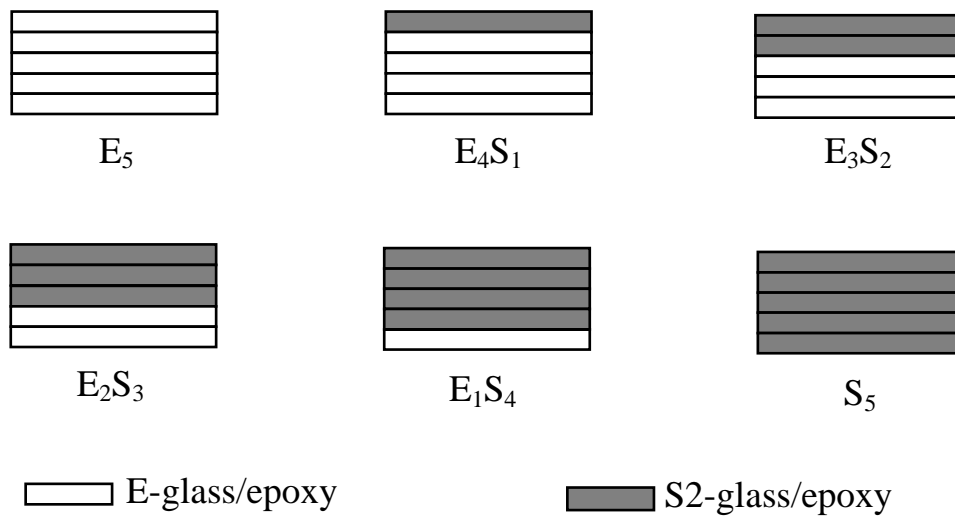


**Figure 6.3.** Visual illustration of the stacking configurations of the hybrid composites under investigation.

#### 6.2.1.2. Density, fibre content and void content

The predicted bulk density and fibre volume calculations, in accordance with the rule of mixtures using equations (3.39) and (3.38), respectively. Considering the fact that the compressive specimens were cut from the same composite plate panels, *i.e.*, the  $S_0E_5$  composite for the EgF/Ep samples and the  $S_5E_0$  composite for the S2gF/Ep samples, and that the fibre volume contents

**Table 6.3.** Mean values and standard deviations of calculated density, fibre volume content and void volume content of the hybrid GFRP composites

Stacking configuration	Bulk density, $\rho$ (g.cm <sup>-3</sup> )	Fibre volume content, $V_f$ (%)		Void volume content, $V_v$ (%)
		Rule of mixtures	Image analysis	
$S_0E_5$	$1.87 \pm 0.086$	$52.1 \pm 5.76$	$53.3 \pm 6.50$	$1.50 \pm 0.84$
$S_1E_4$	$1.88 \pm 0.080$	$52.9 \pm 5.34$	$53.6 \pm 6.66$	$1.43 \pm 0.76$
$S_2E_3$	$1.89 \pm 0.141$	$53.8 \pm 9.47$	$53.9 \pm 6.82$	$1.36 \pm 0.68$
$S_3E_2$	$1.89 \pm 0.087$	$53.9 \pm 5.87$	$54.1 \pm 6.98$	$1.30 \pm 0.60$
$S_4E_1$	$1.90 \pm 0.120$	$54.7 \pm 8.06$	$54.4 \pm 7.14$	$1.23 \pm 0.52$
$S_5E_0$	$1.91 \pm 0.135$	$54.9 \pm 9.06$	$54.7 \pm 7.30$	$1.16 \pm 0.44$

predicted using the rule of mixtures for these hybrid systems were found to be in good agreement with those of these two groups of compressive samples, the void content of the hybrid systems was predicted based on the proportional content of these two types of GFRPs constituting each hybrid system, *i.e.*, the void content of the hybrid composites was calculated based on the known fibre volume fractions of the  $S_0E_5$  and  $S_5E_0$  composites together with the bulk densities of the hybrid composites with the results being presented in Table 6.3.

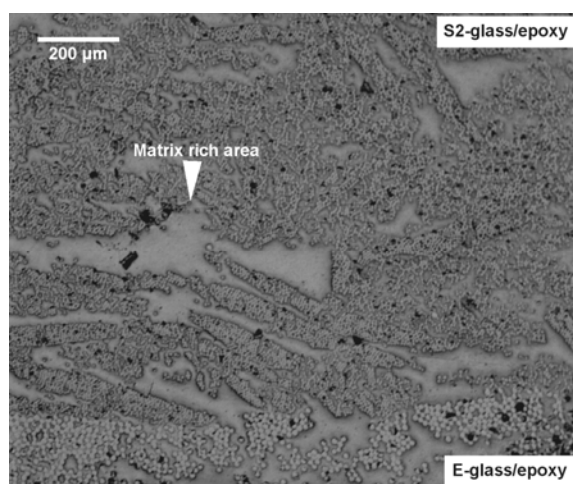


**Figure 6.4.** Optical micrograph of hybrid GFRP composites containing one layer E-glass epoxy prepreg and four layers of S2-glass/epoxy prepreps showing unevenly distributed fibres, matrix rich areas and void (dark spots).

Table 6.3 shows that although the fibre volume content predicted in accordance with the rule of mixtures was found to be in a good agreement with those calculated based on the fibre volume contents of the parent GFRP composites, *i.e.*, E-glass/epoxy and S2-glass/epoxy, the variations in values was reasonably wide, ranging from  $\pm 5.34\%$  for the  $S_1E_4$  hybrid GFRP plate to  $9.47\%$  for the  $S_2E_3$  hybrid GFRP plate. This wide range of values suggested that the fibre was relatively unevenly distributed within the plates with this result being attributed to the difficulty in ensuring consistency of processing parameter for a fully manual hand lay-up fabrication procedure. This conclusion was confirmed from Figure 6.4 which illustrates a relatively uneven distribution of fibres within

the matrix. Further research employing automated processes is recommended for the production of high quality composites and validation of the present results.

### 6.2.2. Mechanical Properties

Sample of load-displacement data obtained from the flexural tests along with an example of the detailed calculations of mechanical properties, *i.e.*, flexural stress, flexural modulus, flexural strain, strain to maximum stress, strain to failure, energy storage capacity to maximum stress and work of fracture have been presented in a spreadsheet in Appendix 10. The magnitude of the stress at each loading point was calculated using equation (3.6a) or (4.8) depending on the  $S/d$  values of the specimens, whilst that of the strain was calculated in accordance with equations (4.7) by substituting the respective value of toe-corrected cross-head displacements for the value of  $D$ . Figure 6.5(c) illustrates stress-strain curves derived from Figure 6.5(b).

#### 6.2.2.1. Stress-strain response

Representative load-displacement and stress-strain curves for a single type of hybrid composite have been presented in Figures 6.5 to 6.7. Figure 6.5(a) shows that the samples demonstrated a reasonably linear stress-strain response up to failure. The sharp drop in load upon reaching the maximum load indicated that the specimens failed catastrophically as had been previously reported [5]. During initial loading of the specimens, the specimen would typically experience settlement onto the test fixture and may exhibit surface indentation effects at the loading points, *i.e.*, the loading nose and two support rolls indented into the surface of the specimen due to the presence of matrix rich regions within the composite [28, 29]. When equilibrium between the load and indentation deformation was reached, the magnitude of the load started to increase with increasing cross-head displacement up to the point of initial failure. Eventually, specimens underwent failure following a sudden drop of load within in a short

period of time. Figure 6.5(b) is the same load-displacement relationship as shown in Figure 6.5(a) following a toe correction procedure as dictated by the employed standard [30]. Flexural properties of the specimens were derived from Figure 6.5(b) and an additional 17 similar plots that represented the other two  $S/d$  values of this configuration together with three  $S/d$  values for each of the other five stacking configurations.

Figure 6.6 shows the effect of the hybrid ratio ( $r_h$ ), *i.e.*, S2-glass fibre-to-total fibre content ratio, on the stress-strain response and maximum stress of representative samples. Those that exhibited approximately average values in their respective groups were selected as representative samples presented in Figure 6.6. The short span samples ( $S/d = 16$ ) depicted in Figure 6.6(a) indicated that samples exhibited an approximately linear stress-strain relationship up to almost the point of failure. Apart from the  $S_1E_4$ -4 sample that underwent excessive elongation, the samples experienced either an abrupt load drop or else a significant load drop within a short period of time. Whilst the  $S_0E_5$ -1 and  $S_5E_0$ -3 samples demonstrate the lowest (585 MPa) and highest (672 MPa) flexural strengths, respectively, the hybrid composite samples exhibited flexural strengths being these two values. This result suggested that a hybrid effect for flexural strength was not observed for the  $S/d = 16$  samples. This result was attributed to the failure mode being shear for these samples, with the shear strength within the plane transverse to the fibre direction being predominantly controlled by the matrix properties. Figure 6.6(a) also illustrates that the initial slopes of the curves, *i.e.*, flexural modulus, for each of the samples appeared to be within a narrow range.

In contrast to this, the  $S/d = 32$  samples presented in Figure 6.6(b) all exhibited a sudden drop in load at the point of failure and associated with catastrophic failure as previously reported [5] – this followed a linear stress-strain relationship to the point of maximum stress. Although the lowest flexural strength in this group of specimens was exhibited by the  $S_0E_5$ -1 composite, representing the pure E-glass/epoxy system, the maximum flexural strength was demonstrated by the  $S_4E_1$ -3 sample which represented a hybrid GFRP composite containing four layers of S2-glass/epoxy prepregs and one layer of E-glass/epoxy prepreg. This suggests that a hybrid effect may exist for flexural strength, depending on further

examination of the values for the specimens in this configuration (as will be discussed later).

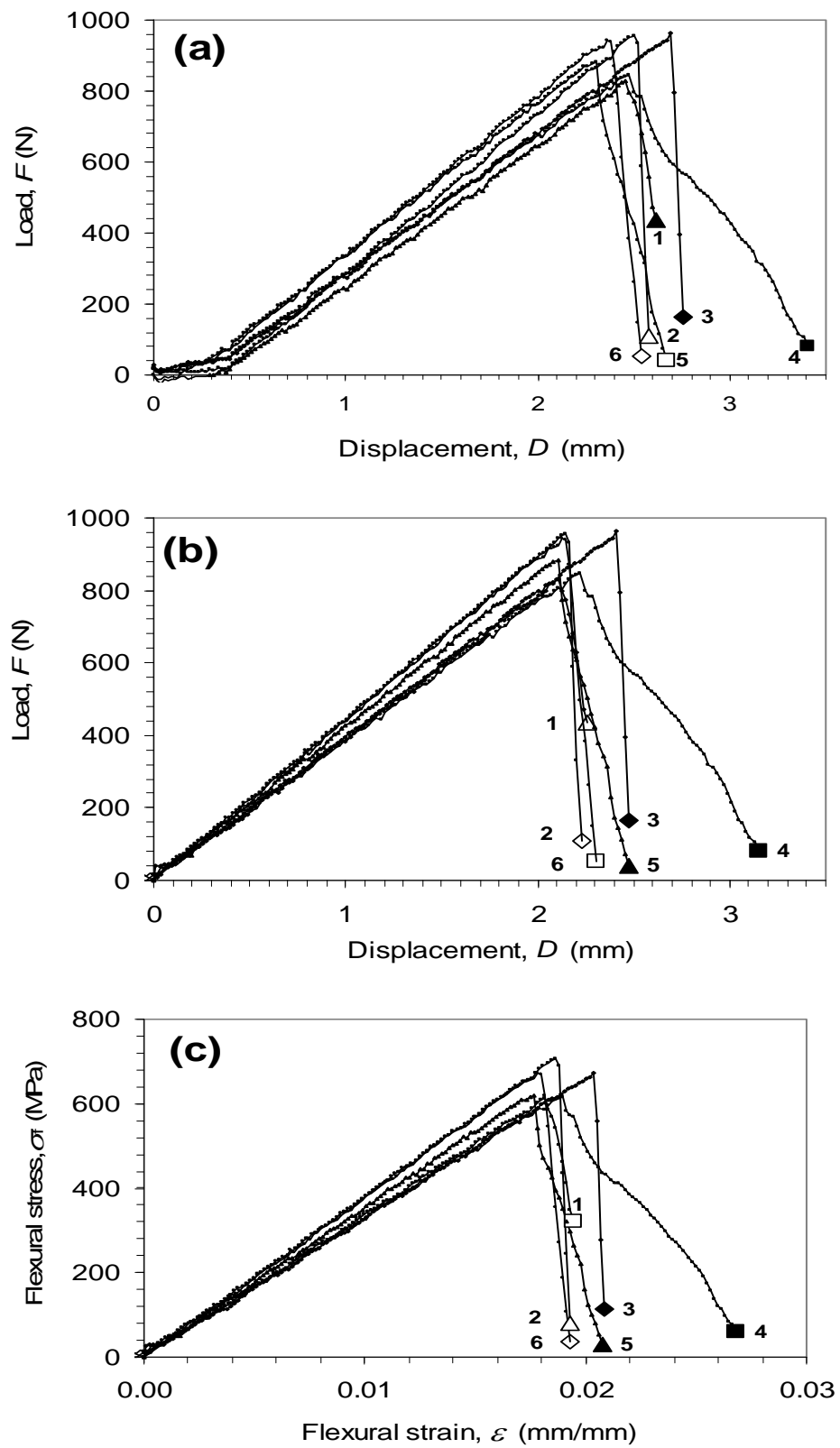


**Figure 6.5.** Representative load-displacement and stress-strain relations of the  $S_3E_2$  samples tested at  $S/d = 16$ . (a) Load-displacement relation before toe correction, (b) After toe correction, (c) Stress-strain relation.



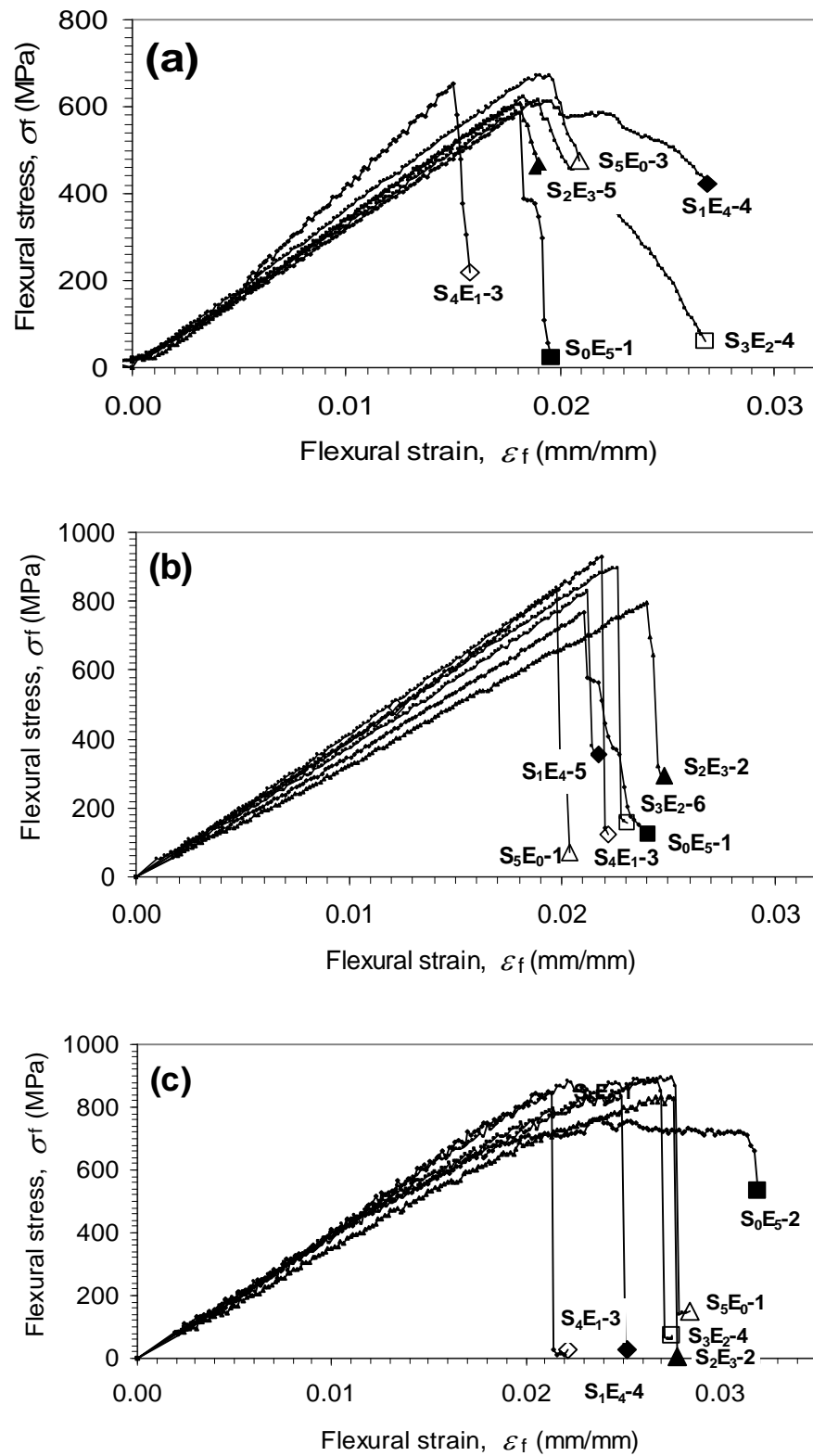


**Figure 6.6.** The effect of hybrid ratio on stress-strain relation of each of the hybrid GFRP composite plate panels: (a)  $S/d = 16$ , (b)  $S/d = 32$ , (c)  $S/d = 64$ .

Close analysis of Figure 6.6(b) lead to the conclusion that the variation in flexural strength appears to be wider for the  $S/d = 32$  samples compared to that of the  $S/d = 16$  samples – this was attributed to the fact that failure in the  $S/d = 16$  specimens was due to a matrix dominated effect (*i.e.*, shear failure) that would presumably be similar for all specimens.

The effect of hybrid ratio on the stress-strain response for samples tested at  $S/d = 64$  has been presented in Figure 6.6(c). Unlike those of the  $S/d = 32$  samples that underwent catastrophic failure immediately after achieving their maximum stress level, the specimens tested at  $S/d = 64$  often experienced a significant decrease in slope close to the point of maximum stress with further increases in strain prior to eventual failure. Comparison between the data for the  $S/d = 32$  specimens (Figure 6.6(b)) and  $S/d = 64$  specimens (Figure 6.6(c)) suggested the flexural strength and variation in flexural modulus values to be essentially similar.

As inferred above, an increase in flexural strength as  $S/d$  changed from 16 to 32 (or 16 to 64) was observed when comparing Figures 6.6(a), 6.6(b) and 6.6(c). In contrast to this, increasing  $S/d$  from 32 to 64 did not appear to result in any significant further increase in flexural strength, neither did the flexural modulus increase significantly as  $S/d$  changed from 16 to 64. Such a phenomenon was confirmed within each individual stacking configuration as illustrated in each of the graphs presented in Figure 6.7. In addition, Figure 6.7 also demonstrates the increase of strain-to-failure with the increase of  $S/d$  – the trends noted above will be further mentioned later.

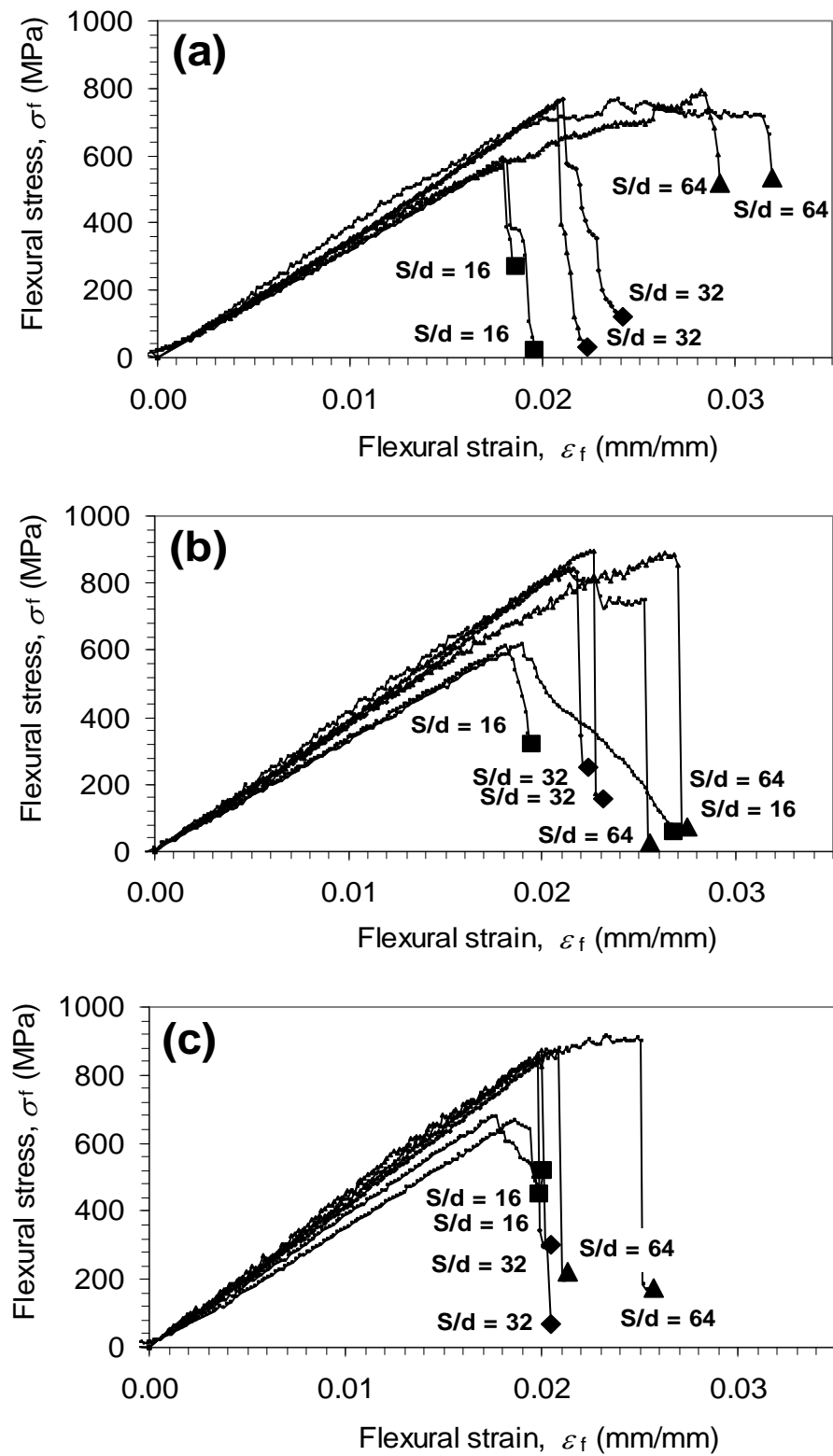


**Figure 6.7.** The effect of span-to-depth ratio on stress-strain relation of representative composite plate panels: (a)  $S_0E_5$  (E-glass/epoxy) composite plate, (b)  $S_3E_2$  (hybrid S2-E-glass/epoxy) composite plate, (c)  $S_5E_0$  (S2-glass/epoxy) composite plate.

#### 6.2.2.2. Failure mechanisms

A representative optical micrograph of a sectioned and polished  $S/d = 16$  specimen following failure has been presented in Figure 6.8. With regards to observation noted during the tests, most specimens tested at  $S/d = 16$  appeared to fail following the initiation of interlaminar shear cracks at the neutral plane, this being followed by crushing and splitting on the compressive side as reported by Lee *et. al.* [31] and fibre breakage at the tensile side. Whilst unidirectional FRP composites are known to be weak transverse to the fibre direction, higher interlaminar shear-to-normal stress ratios at the neutral plane (as has been pointed out by Davies and Hamada [32]), may be responsible for this type of failure, *i.e.*, specimens with weak shear strengths (such as unidirectional FRP composites) will tend to fail due to shear effects provided that the  $S/d$  ratio is sufficiently low. A typical fracture surface for such a specimen depicted in Figure 6.8 reveals the presence of longitudinal cracks at the neutral axis (white arrows) together with splitting and buckled fibres at the compressive surface (top side of the micrograph). The presence of such cracks at the neutral plane would appear to confirm that the specimens tested at  $S/d = 16$  failed in a shear mode.

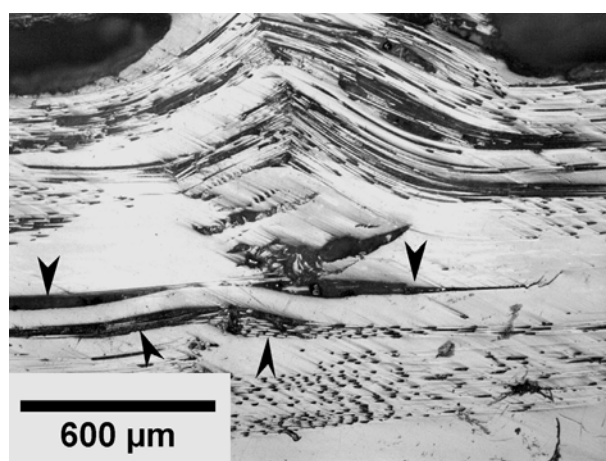


**Figure 6.8.** A typical compressive side of fracture region of specimens tested at  $S/d = 16$  showing splitting (dark arrows) and fibre buckling (top).

An optical micrograph illustrating typical failure of a specimen tested at  $S/d = 32$  has been depicted in Figure 6.9. In comparison with that of  $S/d = 16$ , less

splitting appeared for the  $S/d = 32$  specimens. Fibre buckling and the presence of a kink band at the compressive side, which is known to be a typical failure mode for unidirectional composites at large  $S/d$  ratios, can be clearly seen in this figure. This result would appear to confirm that a ratio of  $S/d = 32$  was sufficiently high so as to suppress shear failure. This type of failure was similar to that previously observed in hybrid composites containing carbon and SiC fibres [32]. In the present case, however, additional splitting and/or local buckling appeared to be present at the compressive side. Buckling, combined with splitting failure, has previously been reported for GFRP composites subjected to compressive loading [15, 33]. In addition to the fibre-matrix interfacial fracture toughness, those authors found that the axial moduli ratio between fibre and matrix, fibre diameter and fibre content were all parameters that influenced the compressive failure mechanism.

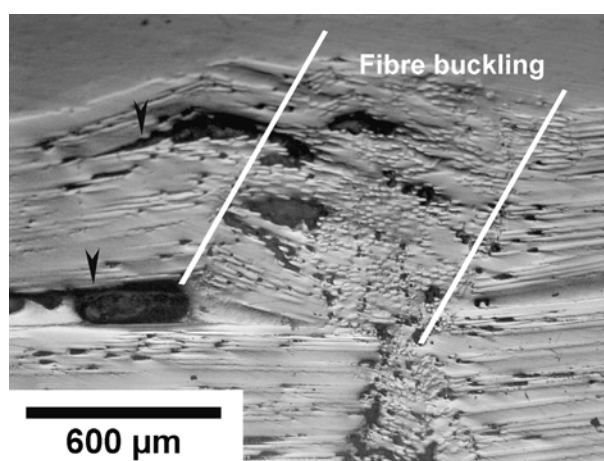


**Figure 6.9.** A typical fracture region of specimens tested at  $S/d = 32$  showing fibre buckling (top) and less splitting (dark arrows).

Specimens tested at  $S/d = 64$ , such as that typically indicated in Figure 6.10, revealed the presence of similar fracture surfaces to those tested at  $S/d = 32$  with kink bands and fibre buckling combined with possible fibre crushing appearing to dominate failure. The splitting length for the  $S/d = 64$  specimens appeared to be shorter than those exhibited for the  $S/d = 16$  specimens (Figure 6.8), confirming that the use of larger  $S/d$  ratios would reduce the interlaminar-to-normal stress

ratio, thereby leading to reducing splitting and the promotion of fibre buckling and kinking. Again, this failure mode was similar to that expected for high strength unidirectional composites subjected to flexural loading.

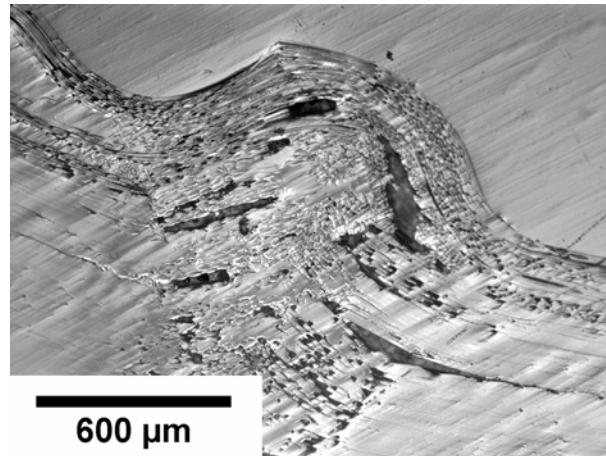


**Figure 6.10.** A typical fracture surface of specimens tested at  $S/d = 64$  showing fibre buckling and kinking domination (top) and less splitting can be observed.

#### 6.2.2.3. Flexural strength

The effect of S2-glass fibre volume, as a fraction of total fibre volume fraction, on flexural strength has been presented in Figure 6.11 as a function of  $S/d$  ratio. As expected, the flexural strength ( $\sigma_f$ ) of the S2-glass fibre/epoxy composite samples (*i.e.*,  $r_h = 1.0$ ) was higher than that of the  $r_h = 0.0$  samples (*i.e.*, E-glass fibre/epoxy composite) for all  $S/d$  ratios. For example, at  $S/d = 16$  the flexural strength was 596 MPa for the E-glass/epoxy specimens and 662 MPa for the S2-glass/epoxy specimens, *i.e.*, an increase of approximately 11.1%. At the largest  $S/d$  ratio the values increased from 716 MPa to 883 MPa, *i.e.* an increase of 23.3%. This trend was attributed to the compressive strength of the S2-glass fibres being higher compared to that of the E-glass fibres.

Figure 6.11 illustrates a general trend that, for each  $S/d$  ratio,  $\sigma_f$  gradually increased as the E-glass fibres were replaced by S2-glass fibres, and whilst the flexural strengths of the samples tested at  $S/d = 32$  appeared to be extremely close

to those of their respective counterparts tested at  $S/d = 64$ , those of the samples tested at  $S/d = 16$  were significantly lower. This trend was similar to that noted previously by Davies and Hamada [32] for the flexural strength of hybrid composites containing carbon and SiC fibres, and also to that previously reported by the author [5] for hybrid E-S2-glass fibre/epoxy composites with different S2-glass fibre-to-total fibre volume content ratios.

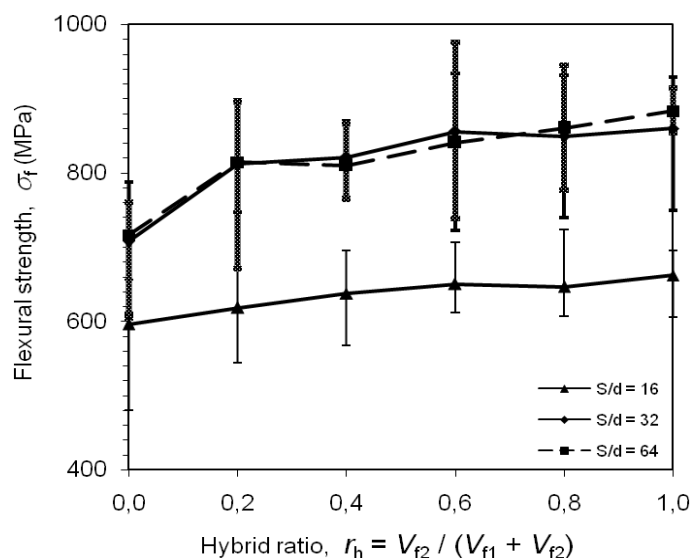


**Figure 6.11.** The influence of hybrid ratio (S2-glass fibre volume/total fibre volume) on flexural strength of hybrid GFRP composites showing increase of flexural strength with the increase in S2-glass fibre volume. Considerably small magnitude of variation can be observed.

Whilst the flexural strength of specimens tested at  $S/d = 16$  exhibited a relatively linear trend up to 100% substitution of S2-glass/epoxy prepreg for E-glass/epoxy prepreg, those of specimens tested at  $S/d = 32$  and  $S/d = 64$  sharply increased (by 14.7% for  $S/d = 32$  and 13.7% for  $S/d = 64$ ) upon the replacement of a single layer, ~20%, of E-glass/epoxy prepreg by S2-glass/epoxy prepreg. A considerably significant increase in flexural strength, up to 20.8% and 17.4% for specimens tested at  $S/d = 32$  and  $S/d = 64$ , respectively, was observed for further substitutions up to ~60% of the total fibre content. Further increases in the substitution level beyond this point did not appear to result in any further significant increases in flexural strength and, indeed, appeared to follow the rule

of mixtures. Such a phenomenon may be attributed to the stress distribution through the thickness of a beam (Figure 3.3) being maximum at the outermost layer, and thus, the first layer of substitution (*i.e.*, introduction of a stronger fibre) at the point of maximum expected stress will result in the optimal harnessing of the strength potential of the substituting fibre leading to a significant increase in flexural stress at the point of failure.

When comparing the trends in flexural strengths as a function of span-to-depth ratio depicted in Figure 6.11, it is clear that flexural strength values for  $S/d$  of 16 were significantly lower to those of either  $S/d = 32$  or  $S/d = 64$ . For example,  $\sigma_f$  for the  $r_h = 0.6$  specimens was 650 MPa for  $S/d = 16$  which increased to 855 MPa and 841 MPa for  $S/d$  ratios of 32 and 64, respectively, *i.e.*, 30% higher. The generally lower  $\sigma_f$  values for  $S/d = 16$  was explained in terms of the competing failure mechanisms being observed in unidirectional composites subjected to 3-point bending as has been previously reported [5, 32]. Whereas the specimen may fail in a flexural mode (with the strength being calculated using equations (3.6a) or (4.8) for  $S/d \leq 16$  or  $S/d > 16$ , respectively), another competing mechanism is that of interlaminar shear failure at the neutral plane (at the mid-depth of a beam for single fibre-type specimens or calculated using equation (3.18) for a hybrid cross-section) where the generated shear stress is the highest. In this case the shear strength,  $\tau_{\max}$ , would be calculated using equation (3.10).

For specimens tested at  $S/d = 16$ , the relationship between  $\sigma_f$  and  $\tau_{\max}$  may be calculated from equations (3.6a) and (3.10) which results in

$$\frac{\sigma_f}{\tau_{\max}} = \frac{S}{d} \quad (6.1)$$

which suggests that specimens tested at  $S/d = 16$  would generate relatively high shear stresses at their neutral planes in comparison with the normal stresses generated at the outermost layer. Recalling that unidirectional composites are known to possess significantly lower interlaminar shear strengths when compared to their longitudinal normal strength [34], such composites would thus be expected to fail due to shear at the neutral axis for smaller  $S/d$  ratios, whereas those tested at higher  $S/d$  will tend to fail due to pure flexure. Therefore, the fact



that  $\sigma_f$  for all of the specimens under investigation tested at  $S/d = 16$  produced significantly lower values (596-662 MPa) in comparison with those of the other two  $S/d$  values (708-883 MPa) can be attributed to the  $\tau_{\max}/\sigma_f$  ratio being higher for  $S/d = 16$  when compared to  $S/d = 32$  or 64.

Strain at maximum stress,  $\epsilon_{\max}$ , for these hybrid configurations has been presented in Table 6.4 with the table showing that strain at maximum stress generally increased as the span-to-depth ratio increased.

**Table 6.4.** Strain at maximum stress of hybrid GFRP specimens

$S/d$	Hybrid ratio, $r_h$					
	0.0	0.2	0.4	0.6	0.8	1.0
<b>16</b>	1.84	1.94	1.88	1.86	1.56	1.78
<b>32</b>	2.01	2.09	2.24	2.22	2.02	2.03
<b>64</b>	2.56	2.42	2.41	2.33	2.14	2.21

These results would thus confirm that partial substitution (even by a relatively small amount, *e.g.*, ~20% in the present case) of higher cost, higher strength S2-glass for low cost E-glass fibres may produce a significant improvement in the flexural strength beyond that expected by the rule of mixtures, *i.e.*, a positive hybrid effect.

#### 6.2.2.4. Flexural modulus

The influence of hybrid ratio and  $S/d$  ratio on the flexural modulus of the hybrid GFRP composites has been presented in Figure 6.12. Apart from those with  $r_h = 0.2$ , a generally similar trend in flexural modulus ( $E_f$ ) was noted to that previously seen for flexural strength (Figure 6.11) with  $E_f$  increasing as the S2-glass fibre content also increased. Similar to that seen for flexural strength, the author concluded that an optimum trade-off of improved performance versus minimum S2-glass usage, was achieved for the specimens containing the single prepreg layer substitution,  $r_h = 0.2$ , with increases of 6.0%, 8.8% and 8.7% for  $S/d$

= 16, 32 and 64, respectively, when compared to the pure E-glass/epoxy composite. However, these values were noticeably similar to those expected from the rule of mixtures prediction when taking into account the difference in elastic modulus of the single fibre-type composites (numerical values given in Figure 6.2 for compressive properties and Table 6.1 for predicted tensile properties) and the changes in total fibre volume fraction. For all of the  $S/d$  ratios tested, the highest  $E_f$  values were recorded for the S2-glass/epoxy specimens that were also found to contain the highest total predicted fibre volume fraction (Table 6.3). Therefore, the increase in  $E_f$  as a function of S2-glass fibre content were attributed mainly to the small increase in total fibre volume fraction for each hybrid configuration as the amount of S2-glass fibre increased and also to the difference in the elastic modulus of the respective fibres.

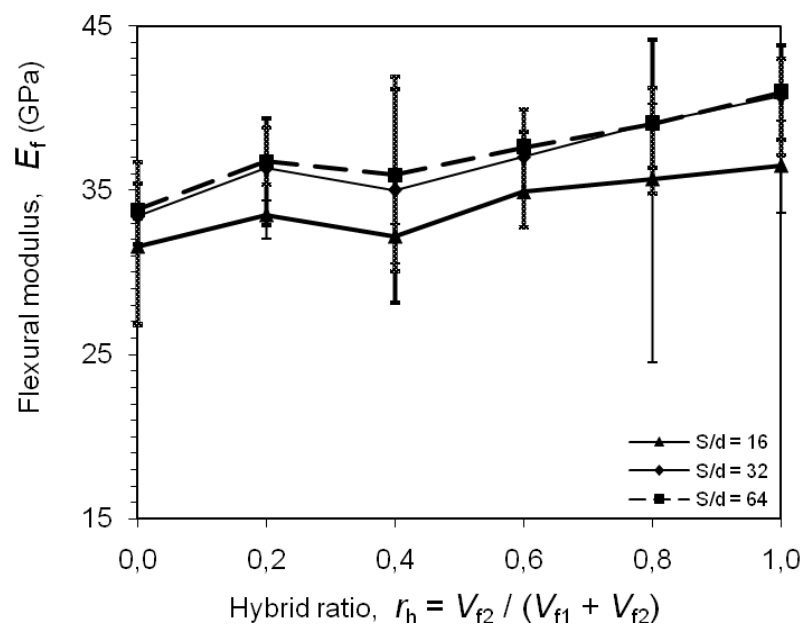


**Figure 6.12.** The influence of hybrid ratio (S2-glass fibre volume/total fibre volume) on flexural modulus of hybrid GFRP composites showing increase of flexural strength with the increase in S2-glass fibre volume.

### 6.2.2.5. Energy absorption capacity to maximum stress

Energy absorption capacity is an important consideration for many structural designs and applications of composite materials. The specific amount of energy absorbed by the samples up to the maximum stress,  $\gamma_{\max}$ , calculated using equation (4.10) has been depicted in Figure 6.13. The figure shows a similar general trend as for flexural strength and flexural modulus with  $\gamma_{\max}$  generally increasing with  $S/d$ . This result can be explained by recalling equation (4.10) where  $\gamma_{\max}$  is linearly proportional to the magnitudes of load and displacement at a given point up to the maximum stress. From equation (4.7) the value of crosshead displacement,  $D$ , in terms of strain is given as

$$D = \frac{1}{6} \cdot d \cdot \left( \frac{S}{d} \right)^2 \cdot \varepsilon \quad (6.2)$$

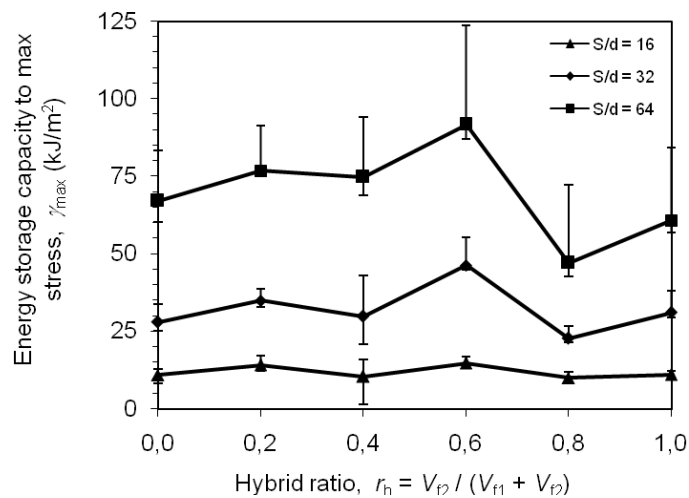


**Figure 6.13.** The influence of hybrid ratio on the energy absorption capacity to maximum stress,  $\gamma_{\max}$ , of hybrid GFRP composites. Small range of variations indicating homogeneous material properties within a plate can be observed.

Therefore, from equations (3.6a) and (4.8) the magnitude of the applied lateral force,  $F$ , in terms of stress for specimens tested at  $S/d \leq 16$  and  $S/d > 16$  [30], respectively, can be obtained as

$$F = \frac{2w}{3 \times \frac{S}{d}} \cdot \sigma \quad \text{for } S/d \leq 16 \quad (6.3a)$$

$$F = \frac{2w}{3 \times \frac{S}{d} \times f_c} \cdot \sigma \quad \text{for } S/d > 16 \quad (6.3b)$$

where  $f_c$  is a correction factor according to the adopted test standard [30] in the stress calculation for long span beams, *i.e.*,  $S/d > 16$ , with

$$f_c = \left[ 1 + 6 \cdot \left( \frac{D}{S} \right)^2 - 4 \cdot \left( \frac{d}{S} \right) \left( \frac{D}{S} \right) \right] \quad (6.4a)$$

Substitution of equation (6.2) into equation (6.4a) results in the value of the correction factor in terms of flexural strain as being

$$f_c = \frac{1}{6} \cdot \varepsilon^2 \cdot \left( \frac{S}{d} \right)^2 - \frac{2}{3} \varepsilon + 1 \quad (6.4b)$$

The values of  $f_c$  at maximum stress can be calculated using equation (6.4b) with the substitution of their respective strain values being presented in Table 6.4. These values were found to vary from  $f_c = 1.056$  for  $r_h \sim 0.0$  to  $f_c = 1.071$  for  $r_h \sim 0.4$ , all for specimens tested at  $S/d = 32$ . In contrast to this, the values for specimens tested at  $S/d = 64$  were found to vary from  $f_c = 1.298$  for  $r_h \sim 0.8$  to  $f_c = 1.431$  for  $r_h \sim 0.0$ .

Substitution of equations (6.2), (6.3a) and (6.3b) into equation (4.10) will result in the formulas for  $\gamma_{\max}$  in terms of stress and strain for short span beams, *i.e.*,  $S/d \leq 16$  [30], and long span beams as follows.

$$\gamma_{\max} = \frac{S/d}{6} \cdot \sum_{i=0}^{i=n-1} \left( \frac{\sigma_i + \sigma_{i+1}}{2} \right) (\varepsilon_{i+1} - \varepsilon_i) \quad \text{for } S/d \leq 16 \quad (6.5a)$$

$$\gamma_{\max} = \frac{S/d}{6 \cdot f_c} \cdot \sum_{i=0}^{i=n-1} \left( \frac{\sigma_i + \sigma_{i+1}}{2} \right) (\varepsilon_{i+1} - \varepsilon_i) \quad \text{for } S/d > 16 \quad (6.5b)$$

If the magnitudes of flexural strength and strain at maximum stress remain unchanged with the increase of  $S/d$ , whereas in fact they increased (Figure 6.11 and Table 6.4), combining equations (6.5a) and (6.5b) and substitution of the values of  $S/d$  of 16, 32 and 64, yield

$$\gamma_{\max-32} \approx \frac{2}{f_c} \cdot \gamma_{\max-16} \quad (6.6a)$$

$$\gamma_{\max-64} \approx \frac{4}{f_c} \cdot \gamma_{\max-16} \quad (6.6b)$$

Equations (6.6a) and (6.6b) thus describe the change in  $\gamma_{\max}$  as a function of  $S/d$ . In addition to this, an increase of  $\gamma_{\max}$  would also be expected from the contributions from the increases in  $\sigma_f$  and  $\varepsilon_{\max}$ , and the effect of the correction factor,  $f_c$ , as given in equations (6.6a) and (6.6b). Recall that in comparison with those tested at  $S/d = 16$ , the flexural strength of specimens tested at  $S/d = 32$  was found to significantly increase, *i.e.*, from 18.8% for the  $r_h \sim 0.0$  samples to 31.4% for the  $r_h \sim 0.2$  samples, as also did  $\varepsilon_{\max}$  (from 7.3% for the  $r_h \sim 0.2$  samples to 29.9% for the  $r_h \sim 0.8$  samples). Thus, for an increase in  $S/d$  from 16 to 32, the values of  $\gamma_{\max}$  would be expected to increase by a minimum of  $\sim 147\%$  to a maximum of  $\sim 223\%$  depending on the hybrid configuration. For similar reasons, specimens tested at  $S/d = 64$  would be expected to demonstrate an increase in  $\gamma_{\max}$  (compared to the  $S/d = 16$  case) of between 368% and 463%.

Figure 6.13 illustrates the comparison of  $\gamma_{\max}$  for the three  $S/d$  values tested as a function of the various stacking configurations under investigation. The increase in  $\gamma_{\max}$  as  $S/d$  increased from 16 to 32 was found to vary from 129.0% to 211.7% (increased from  $10.0 \text{ kJ}\cdot\text{m}^{-2}$  to  $22.8 \text{ kJ}\cdot\text{m}^{-2}$  for  $r_h \sim 0.8$ , and from  $14.8 \text{ kJ}\cdot\text{m}^{-2}$  to  $46.3 \text{ kJ}\cdot\text{m}^{-2}$  for  $r_h = 0.6$ , respectively). These two limits are both slightly lower than, but reasonably comparable with, the predicted values mentioned above, *i.e.*, 146% and 223% for the lower and upper limits, respectively. Further

increasing the value of  $S/d$  to 64 resulted in an even greater increase in  $\gamma_{\max}$ . In comparison to those of  $S/d = 16$ ,  $\gamma_{\max}$  for the specimens tested at  $S/d = 64$  exhibited an increase of between 373.8% and 612.3% (increasing from 10.0  $\text{kJ}\cdot\text{m}^{-2}$  to 47.1  $\text{kJ}\cdot\text{m}^{-2}$  for  $r_h \sim 0.8$ , and from 10.5  $\text{kJ}\cdot\text{m}^{-2}$  to 74.8  $\text{kJ}\cdot\text{m}^{-2}$  for  $r_h \sim 0.4$ , respectively). These experimental values are spread over a slightly wider range in comparison with those of the predicted values (468.4% to 562.8%).

### 6.2.3. Summary

A series of 5-ply unidirectional composites containing E-glass and/or S2-glass fibres within an epoxy matrix have been manufactured and subsequently tested and analysed. The specimens were subjected to a three-point bend (TPB) loading configuration in accordance with Procedure A of the ASTM D790-07 standard [30] in order to evaluate their flexural properties. Following the tests, the fracture surfaces of specimens were sectioned, cast in polyester blocks and polished prior to examination under an optical microscope.

It was determined that a  $S/d$  ratio of at least 32 was required in order to promote flexural failure (as opposed to shear failure). A general trend noted for specimens tested at  $S/d = 32$  and  $S/d = 64$  was that both flexural strength and flexural modulus increased with a replacement of E-glass fibre by S2-glass fibre. In addition to this, both properties also achieved significant increases as the  $S/d$  ratio increased from 16 to 32, but further increasing  $S/d$  from 32 to 64 produced only a slight further improvement in both flexural strength and flexural modulus. A significant increase (up to 20.8%) in flexural strength was observed for a substitution of up to ~60% S2-glass fibre for E-glass fibre, however, the most promising increase (13.7% to 14.7%) was noticed for smaller amounts of (~20%) fibre substitution – this being considered to be the optimum substitution amount from the point of view of performance increase versus minimum S2-glass fibre usage (the S2-glass being considerably more expensive compared to that of the E-glass fibre).

In contrast to this, the flexural modulus was found to generally increase as the proportion of S2-glass fibre was increased to 100% fibre with, again, the

replacement of a single outermost layer demonstrating the most significant increase (8.7% to 8.8%) in flexural modulus. Specimens tested at  $S/d = 16$  did not show any significant increase in flexural properties due to most of the specimens having failed by shear instead of by a flexural mode as had been exhibited by the composites tested at  $S/d = 32$  and  $S/d = 64$ . The energy absorption capacity up to the point of maximum stress appeared not to increase significantly with hybridisation, however, a significant increase for this property was noted when  $S/d$  increased from 16 to 32 and again from 32 to 64 – this trend being attributed to the increase in flexural strength, increase in strain at maximum stress, and most dominantly by the increase in  $S/d$ .

Optical microscopy confirmed that specimens tested at  $S/d = 16$  tended to exhibit significant shear cracking at the neutral plane whereas specimens tested at  $S/d = 32$  and  $S/d = 64$  indicated the presence of kink bands and fibre buckling which is known to be typical for high strength unidirectional composites under flexural loading. Overall, it is concluded that hybrid composites may play a role in increasing the flexural performance of GFRP composites through the incorporation of relatively small amounts of high cost fibres.

### **6.3. HYBRID FRP COMPOSITES CONTAINING DIFFERENT GRADES OF CARBON FIBRE**

Although from the economical point of view, CFRP composites are less advantageous in comparison with GFRP composites, the superiority of their mechanical and thermal properties [35] has lead to a wider variety of applications ranging from sporting goods to aircraft structures [36, 37]. One of the disadvantages of CFRP composites is that, as shown earlier, their compressive strength is generally lower even in comparison with low cost E-glass/epoxy composites [15] – compressive properties of the FRP composites under current investigation have been presented in Figure 6.2.

It has previously been reported that the failure of CFRP beams under flexural loading was almost always initiated at the compressive face [19, 27, 32]. Potential may therefore exist for the improvement of flexural behaviour in CFRP

composites through the partial substitution of higher (compressive) strength carbon fibres at the compressive side of the specimens. Consequently, in the present section the author has investigated the flexural behaviour of unidirectional hybrid FRP composites containing a mixture of lower strength TR50S PAN-based carbon fibre [38] and higher strength IM7-12k PAN-carbon fibre [39] embedded within an epoxy matrix.

### ***6.3.1. Physical properties***

#### **6.3.1.1. Stacking configurations**

Six different stacking configurations, including the pure TR50S carbon fibre/epoxy and IM7-12k carbon fibre/epoxy composites plates, have been fabricated, subsequently tested and analysed. Six layers of carbon fibre/epoxy prepreg, comprising of either entirely TR50S/epoxy, entirely IM7-12k/epoxy, or else a hybrid mix of these, were stuck together in order to produce a preform and subsequently cured under vacuum in a hot press at 120 °C for 30 minutes (using the optimised curing conditions previously determined). The reason for six layers being used for the CFRP composites, as opposed to five layers for the GFRP composites, was the reduced thickness of the individual CFRP prepreg layers – a larger number of layers thus being required in order to obtain nominally similar thickness CFRP and GFRP composites. The stacking configurations for the hybrid GFRP composites under investigation have been presented in Figure 6.14.



## 6.3.1.2. Density, fibre content and void content

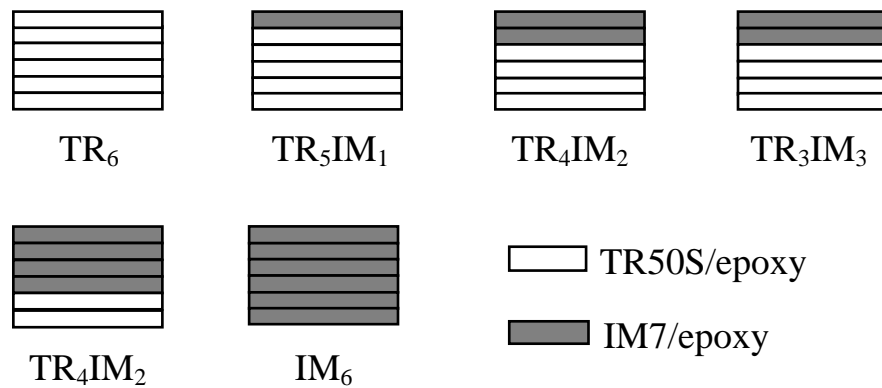


**Figure 6.14.** Visual illustration of the stacking configurations of the hybrid CFRP composites under investigation.

**Table 6.5.** Mean values and standard deviations of the calculated density, fibre volume content and void volume content of the hybrid CFRP composites

Stacking configuration	Bulk density, $\rho$ (g.cm <sup>-3</sup> )	Fibre volume content, $V_f$ (%)		Void volume content, $V_v$ (%)
		Density-based	Image analysis	
$TR_6$	$1.493 \pm 0.045$	$55.2 \pm 6.14$	$53.5 \pm 9.10$	$4.25 \pm 0.57$
$TR_5IM_1$	$1.492 \pm 0.046$	$55.1 \pm 6.29$	$53.3 \pm 9.02$	$3.93 \pm 0.82$
$TR_4IM_2$	$1.490 \pm 0.057$	$54.8 \pm 7.80$	$53.1 \pm 8.93$	$3.61 \pm 1.06$
$TR_3IM_3$	$1.490 \pm 0.046$	$54.8 \pm 6.30$	$53.0 \pm 8.85$	$3.29 \pm 1.31$
$TR_2IM_4$	$1.484 \pm 0.061$	$54.0 \pm 8.41$	$52.8 \pm 8.77$	$2.97 \pm 1.55$
$IM_6$	$1.480 \pm 0.051$	$53.5 \pm 7.00$	$52.4 \pm 8.60$	$2.33 \pm 2.04$

The calculations for predicted bulk density and fibre volume content in accordance with the rule of mixtures using equations (3.39) and (3.38), respectively. Recalling the fact that compressive specimens were previously cut from some of the same composite plates, *i.e.*,  $TR_6$  for the TR50S/Ep samples and  $IM_6$  for the IM7/Ep samples, the fibre volume fractions predicted using the rule of mixtures for these hybrid systems were found to be in good agreement with the experimentally determined values for these two groups of pure CFRP composites (*i.e.*,  $TR_6$  and  $IM_6$ ). Therefore, the void content of these hybrid systems was

predicted based on the proportional content of the two types of CFRP prepregs that constituted each hybrid system with the results being presented in Table 6.5.

The fibre volume fractions for each hybrid composite were predicted in accordance with the rule of mixtures based on their respective bulk densities and proportionally based on their respective constituent properties calculated from image analysis. These two prediction methods demonstrated a very good correlation with those of the bulk density-based predictions being slightly higher (ranging from 1.07% for the IM<sub>6</sub> sample to 1.85% for the TR<sub>3</sub>IM<sub>3</sub> sample) in comparison with the image analysis method. Again, as had been noticed for the hybrid GFRP situation, the variation of fibre content within each plate was relatively high, from 6.14% (TR<sub>6</sub>) to 8.41% (TR<sub>2</sub>IM<sub>4</sub>) for  $V_f$  based on their respective bulk densities and even higher for those based on the proportional contribution of the layer properties, *i.e.*, 5.60% (IM<sub>6</sub>) to 9.10% (TR<sub>6</sub>). The predicted void content in each composite has been presented in the last column of Table 6.5 and was noted to exhibit a similar trend to that of fibre volume content, *i.e.*, narrow range in average values amongst the plates but a wider variation in values within each plate. These values imply that both the fibres and voids were not homogeneously distributed within each plate. Considering that the average values of both the fibre and void volume contents were relatively consistent within each plate, it was concluded that the fully manual hand lay-up fabrication procedure utilised in this work may have been responsible for this uneven distribution of fibre and void within each plate. In addition, the higher void volume content of the TR<sub>6</sub> plate, may also be caused by this fully manual fabrication procedure because all fabrication parameters had been controlled for being invariant during the fabrication of all the plates. Examples of optical micrographs at different magnifications have been depicted in Figure 6.15 and they confirm the presence of uneven fibre distribution.

### 6.3.2. Mechanical Properties

Sample of load-displacement data obtained from the flexural testing of hybrid CFRP samples along with a spreadsheet sample of detailed calculation of mechanical properties, *i.e.*, flexural stress, flexural modulus, flexural strain, strain to maximum stress, strain to failure, energy storage capacity to maximum stress and work of fracture has been presented in Appendix 10. The magnitude of the stress at each loading point was calculated using equation (3.6a) or (4.8) for the  $S/d = 16$  and  $S/d = 32$  and 64 specimens, respectively, whilst the strain was calculated in accordance with equation (4.7) following substitution of the respective values of toe-corrected cross-head displacement for the value of  $D$ .

#### 6.3.2.1. Stress-strain response

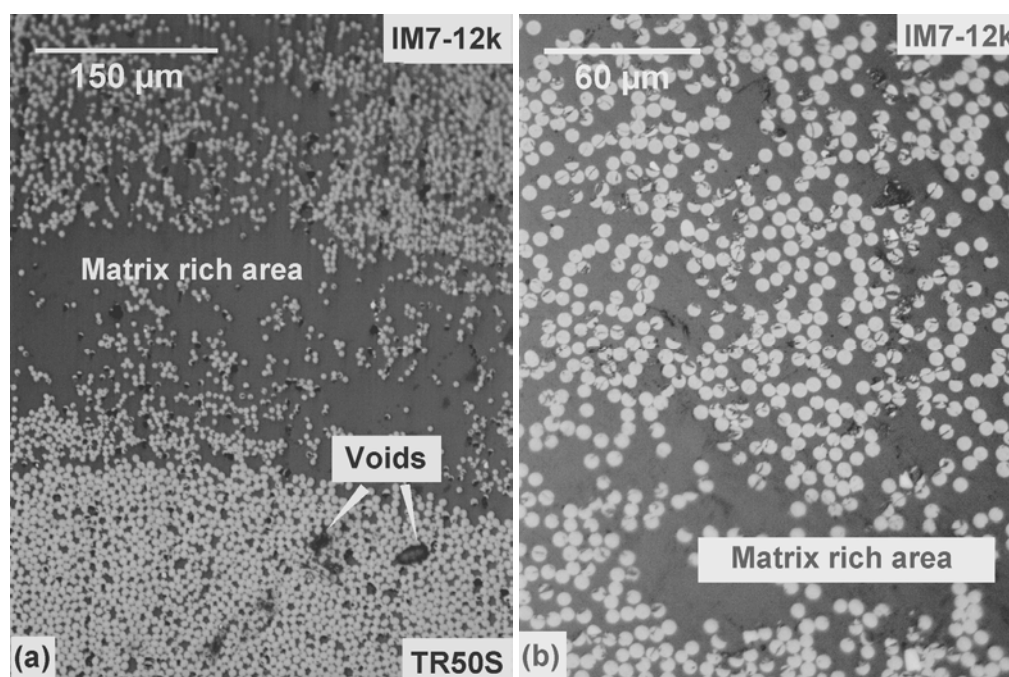


**Figure 6.15.** Optical micrograph of hybrid CFRP composites containing TR50S and IM7 carbon fibres showing unevenly distributed fibres, matrix rich areas and void. (a) Matrix rich area presents in an interface of a TR50S/epoxy-IM7/epoxy prepreg layers, (b) Uneven fibre distribution, with smaller variation was also observed within a IM7/epoxy prepreg layer.

Representative load-displacement and stress-strain curves for the hybrid CFRP composite under investigation have been presented in Figures 6.17 to 6.19. Figure 6.17(a) demonstrates a reasonably linear stress-strain response prior to achieving maximum stress for samples containing one layer of IM7/epoxy and five layers of TR50S/epoxy prepregs tested at  $S/d = 16$ . Unlike that observed for the hybrid GFRP cases, a sudden drop in load after reaching the maximum load was not observed for the CFRP composites, instead, a gradual drop in load was noted. It is suggested that this may, at least partially, be due to the shift of loading point toward the supports (Figure 6.16) leading to the alteration of equation (3.6a) as the actual moment force generated by the applied load (recorded by the load-cell) would actually be lower than the true value due to a reduction in the length of the moment arm.

Similar to the case of the GFRP composites, adjustment of the specimens onto the test fixture during the early stages of loading was also noticed for the CFRP specimens. Surface indentation effects at the loading points, *i.e.*, the loading nose and two support rolls, on the specimens (due to the presence of matrix rich areas) [28, 29] were thought to be responsible for this phenomenon. Figure 6.17(b) are the same load-displacement curves as those in Figure 6.17(a) following the application of a toe correction procedure for the displacement as dictated by the relevant ASTM standard [30]. Flexural properties of the specimens were derived from Figure 6.17(b) in addition to another 17 similar plots representing the other two  $S/d$  values for this configuration together with three  $S/d$  values for each of the remaining five stacking configurations.

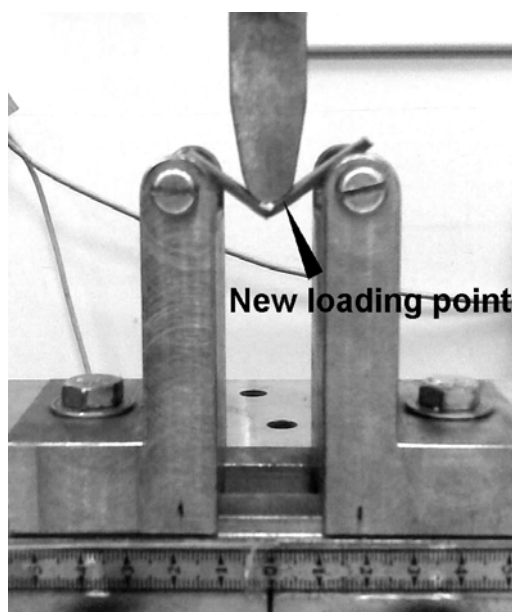


**Figure 6.16.** Shift of loading point after first failure of specimens tested at  $S/d = 16$  resulting in the length of moment arm being reduced or the load recorded by the load cell to produced the same magnitude of moment force being increased.

The effect of hybrid ratio ( $r_h$ ), *i.e.*, IM7 carbon fibre-to-total fibre content ratio, on the stress-strain response and maximum stress of representative samples has been depicted in Figure 6.18 with typical stress-strain relationships for short span ( $S/d = 16$ ) samples being presented in Figure 6.18(a). Apart from that of the IM<sub>2</sub>TR<sub>4</sub> samples, the stress-strain relationships were generally linear up to the point of maximum stress. Most of the samples exhibited a gradual drop in load after achieving the maximum stress, in addition to experiencing further elongation. The highest flexural strength (839 MPa) was achieved by the IM<sub>2</sub>TR<sub>4</sub> specimens which was 8.3% higher than that of the TR<sub>6</sub> specimens and slightly higher (3.4%) than that of the IM<sub>6</sub> specimens. A general trend that can be observed from Figure 6.18(a) is that the initial slopes of the curves (representing the flexural modulus) for each respective specimen appeared to be within a narrow range of values.

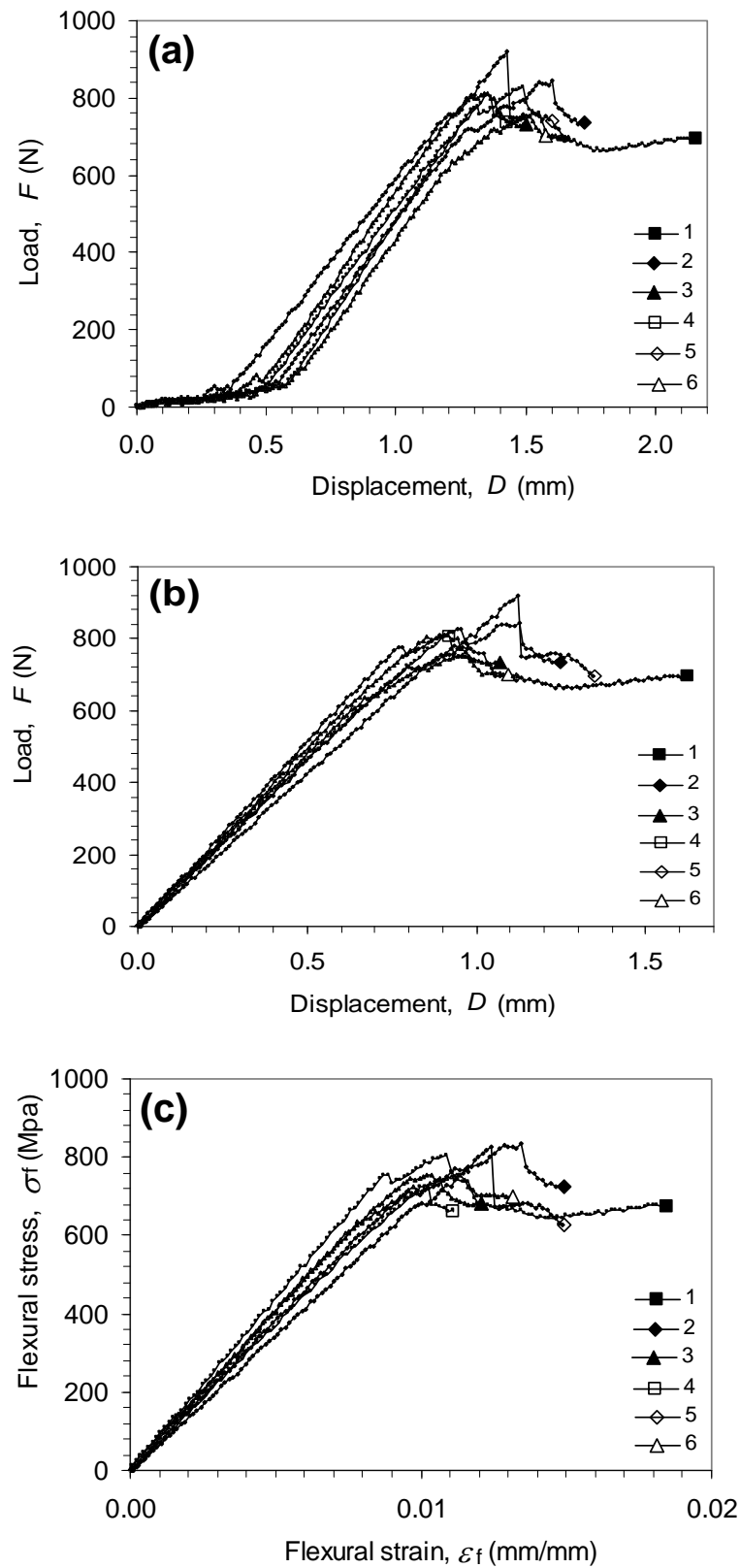
In contrast to this, the  $S/d = 32$  samples presented in Figure 6.18(b) exhibited a sudden drop in load associated with catastrophic failure as previously reported, after following a linear stress-strain relationship to the point of

maximum stress [27]. The lowest flexural strength (832 MPa) was exhibited by the IM<sub>1</sub>TR<sub>5</sub> sample whilst the highest value (869 MPa) was achieved by the IM<sub>6</sub> sample (*i.e.*, the pure IM7 carbon fibre/epoxy composite). Although a slight increase in flexural strength, to a maximum of 2.65% for the IM<sub>4</sub>TR<sub>2</sub> specimens, was noticed, the flexural strength of the IM<sub>6</sub> samples appeared to be higher (3.76%) in comparison with that of the TR<sub>6</sub> specimens. This suggests that, at first sight, a hybrid effect may not exist for the flexural strength although this depends on the values of the other specimens for this configuration and will be discussed again later. Closer observation of Figure 6.18(b) leads to the conclusion that the variation in flexural modulus, as represented by the initial slope of each curve, appeared to be within a narrow range.

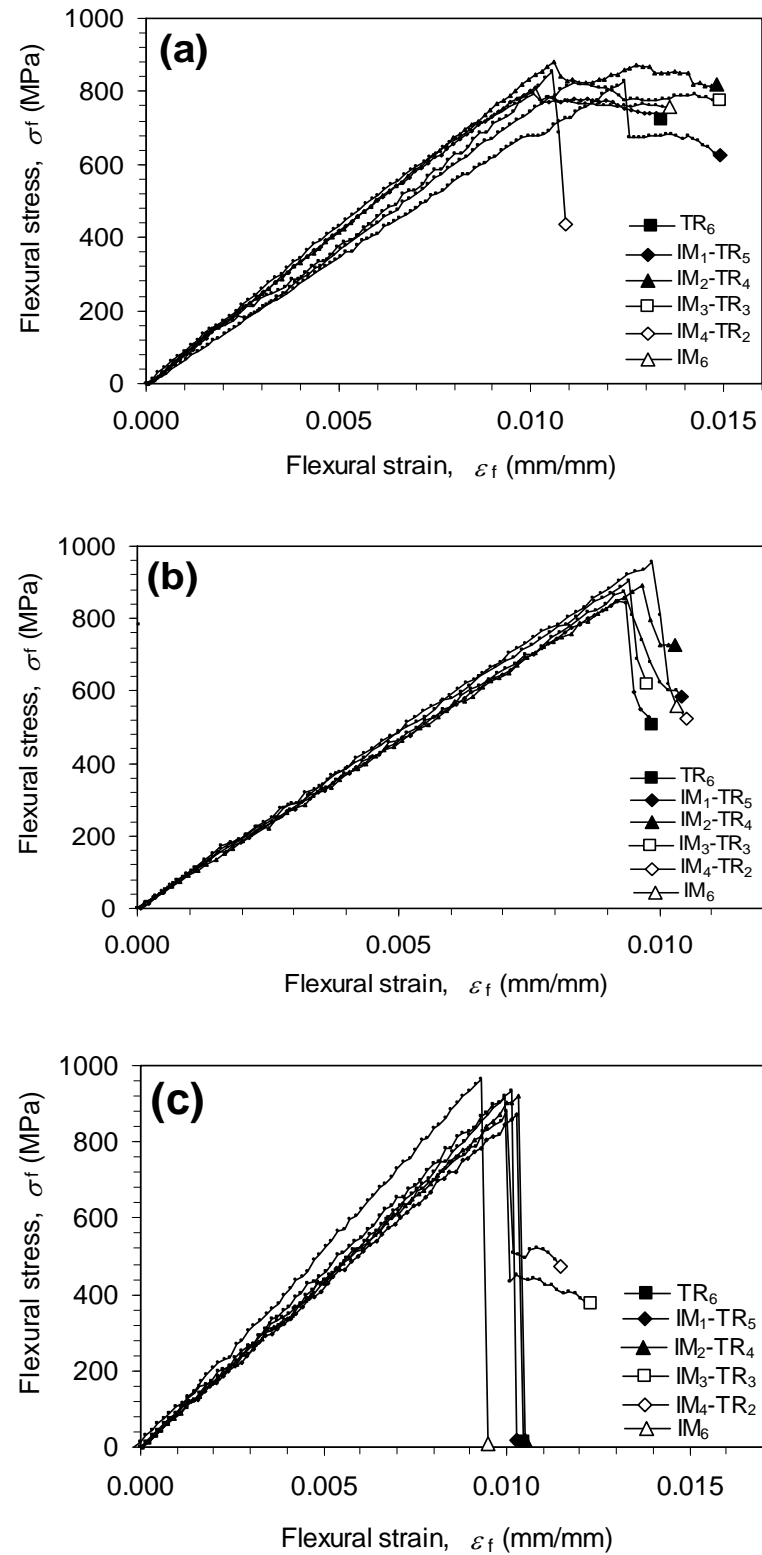
Comparison between Figure 6.18(b) and Figure 6.18(a) indicated that the flexural strength achieved for the  $S/d = 32$  samples were considerably higher for  $S/d = 32$  (from 1.7% for the IM<sub>2</sub>TR<sub>4</sub> specimens to 8.0% for the TR<sub>6</sub> specimens) compared to that of their respective  $S/d = 16$  specimens.

Figure 6.18(c) illustrates the effect of hybrid ratio on stress-strain response for samples tested at  $S/d = 64$ . A similar pattern of stress-strain relationships to that of samples tested at  $S/d = 32$  was noticed. The samples underwent catastrophic failure marked with an abrupt drop of load immediately after achieving their maximum stress level. In comparison with Figure 6.18(b), the maximum flexural stress appears to be similar with a slightly wider variation in flexural modulus.

An increase in flexural strength as  $S/d$  increased from 16 to 32 (or 16 to 64) was apparent from comparing figures 6.18(a), 6.18(b) and 6.18(c). In contrast to this, increasing  $S/d$  from 32 to 64 does not appear to significantly increase flexural strength, neither does the flexural modulus increase with the increase of  $S/d$  from 16 to 64. Such phenomena were confirmed within each individual stacking configuration, *e.g.*, illustrated in each of the graphs presented in Figure 6.19 for the case of hybrid CFRP composites containing three IM7/epoxy and three TR50S/epoxy prepreg layers. In addition, Figure 6.18 also demonstrates that the strain-to-maximum stress was comparable for the three values of  $S/d$ .

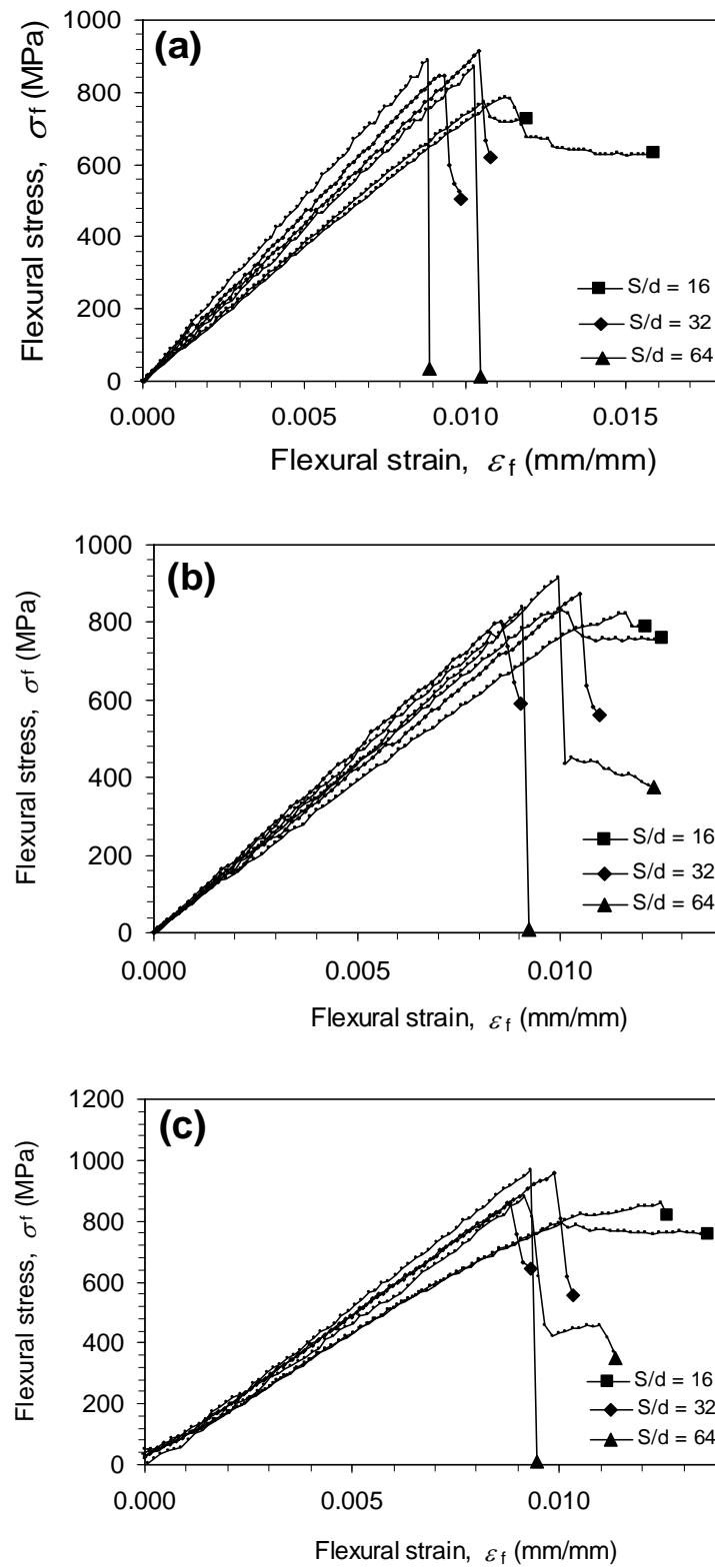


**Figure 6.17.** Representative load-displacement and stress-strain relations of IM<sub>1</sub>TR<sub>5</sub> samples tested at  $S/d = 16$ . (a) Load-displacement relation before toe correction, (b) After toe correction, (c) Stress-strain relation.



**Figure 6.18.** The effect of hybrid ratio on stress-strain relation of each of the hybrid CFRP composite plate panels: (a)  $S/d = 16$ , (b)  $S/d = 32$ , (c)  $S/d = 64$ .

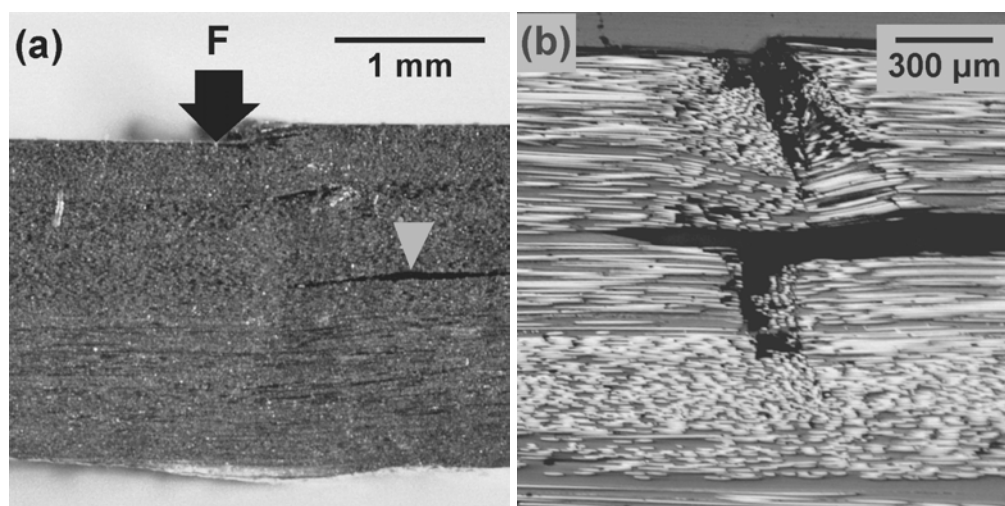




**Figure 6.19.** The effect of hybrid ratio on stress-strain relation of each of the hybrid CFRP composite plate panels: (a) TR<sub>6</sub> samples, (b) IM<sub>1</sub>TR<sub>5</sub> samples, (c) IM<sub>6</sub> samples.

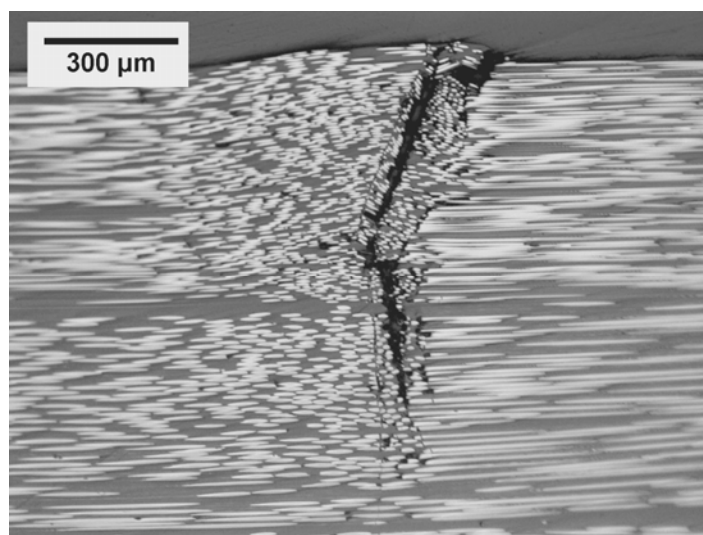
### 6.3.2.2. Failure mechanism

Figure 6.20 illustrates representative optical micrographs taken at two different magnifications of sectioned and polished specimens tested at  $S/d = 16$  following failure. Shear failure at the mid-plane, as reported in [40], was noted for most of the specimens during actual testing at  $S/d = 16$  and this was confirmed in Figure 6.20(a). Taken at a higher magnification, Figure 6.20(b) shows shear cracks present at a deeper layer in addition to out-of-plane buckling and fibre kinking on the compressive side, as has been previously reported [24]. Whilst unidirectional FRP composites are known of be relatively weak transverse to the fibre direction, a higher interlaminar shear-to-normal stress ratio at the neutral plane, as has been pointed out by Davies and Hamada [32], leading to the initiation of shear failure in accordance with the maximum distortion energy theory mathematically presented in equation (3.61), was believed responsible for this type of failure mode. Thus, the presence of longitudinal cracks at the neutral plane would tend to confirm that the specimens tested at  $S/d = 16$  failed in a shear mode.



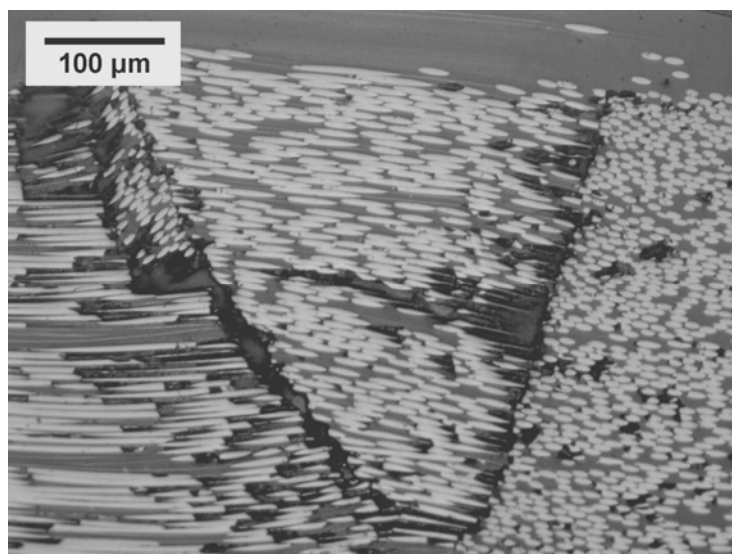
**Figure 6.20.** A typical shear failure region of hybrid CFRP specimens tested at  $S/d = 16$ . (a) Low magnification image showing interlaminar laminar delamination (white arrows), and (b) Larger magnification image showing interlaminar delamination and fibre buckling and kinking in the topside.

An optical micrograph illustrating failure of a representative specimen tested at  $S/d = 32$  has been presented in Figure 6.21. Unlike that previously observed for the hybrid GFRP case, splitting was not apparent in any of the specimens tested at  $S/d = 32$ . Instead, fibre buckling combined with kinking at the compressive side, which is known to be a typical failure mode for unidirectional composites at large  $S/d$  ratios [32], was observed. From this result it was concluded that a  $S/d$  ratio of 32 was sufficiently high to promote flexural failure. The fibre buckling failure mode has been reported for GFRP, CFRP as well as SiC-FRP composites subjected to compressive loading [15, 33, 41]. As mentioned previously, other parameters known to influence the compressive failure mechanism include fibre-matrix interfacial fracture toughness, axial moduli ratio between fibre and matrix, fibre diameter and fibre content.



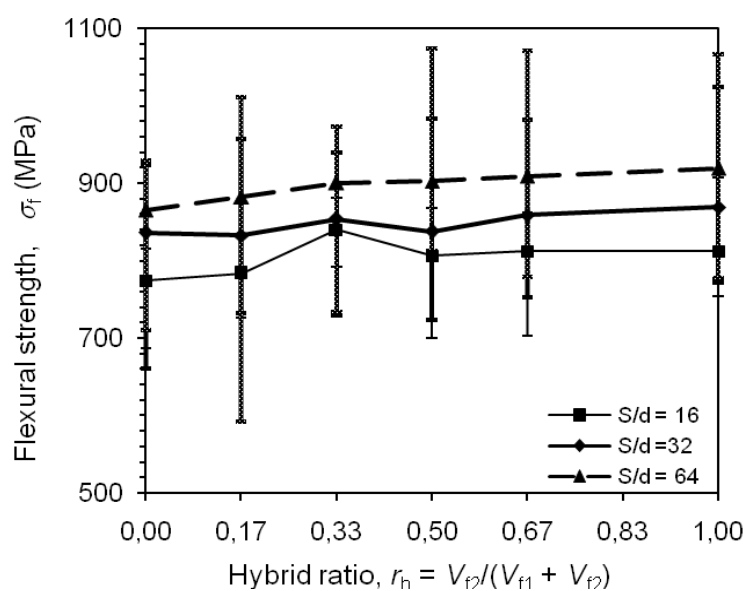
**Figure 6.21.** A typical fracture region of hybrid CFRP specimens tested at  $S/d = 32$  showing fibre buckling and kinking.

Figure 6.22 represents a typical optical micrograph for a specimens tested at  $S/d = 64$  and reveals a similar fracture surface to that tested at  $S/d = 32$  (Figure 6.21) with out-of-plane buckling (right hand side of the micrograph) and kinking of fibres combined with fibre crushing. Once again, splitting was not observed for this hybrid CFRP case. This failure mode was similar to that expected for high strength unidirectional composites subjected to flexural loading.



**Figure 6.22.** A typical fracture region of hybrid CFRP specimens tested at  $S/d = 64$  showing fibre out-of-plane buckling and kinking domination in the compressive side.

#### 6.3.2.3. Flexural strength



**Figure 6.23.** The influence of hybrid ratio (IM7 carbon fibre volume/total fibre volume) on flexural strength of hybrid CFRP composites showing slight increase of flexural strength with the increase in IM7 carbon fibre volume. Considerably wide range of variations indicates inhomogeneity of the composite plates.

The effect of IM7 carbon fibre volume fraction and  $S/d$  ratio on flexural strength has been presented in Figure 6.23. Considering that the compressive strength of the IM7 carbon fibre/epoxy composite samples was higher than that of the TR50S carbon fibre epoxy specimens, the flexural strength ( $\sigma_f$ ) for the IM7 carbon fibre/epoxy composite samples (*i.e.*,  $r_h = 1.0$ ) was also expected to be higher than that of the  $r_h = 0.0$  samples (*i.e.*, TR50S carbon fibre/epoxy composite samples). Figure 6.23 demonstrates that for some points,  $r_h = 0.33$  and  $r_h = 0.67$ , the flexural strength of the specimens tested at  $S/d = 16$  was slightly higher compared to that of the  $r_h = 1.0$  specimens. The difference in failure modes from that of specimens tested at  $S/d = 16$ , which failed due to shear, may be associated with the different trends noticed in the effect of IM7 carbon fibre volume on flexural strength. For example, at  $S/d = 32$  the flexural strength was 836 MPa for the TR50S carbon fibre/epoxy specimens and 869 MPa for the IM7 carbon fibre/epoxy specimens, *i.e.*, a slight increase of approximately 3.8%. At the largest  $S/d$  ratio, the flexural strength increased from 865 MPa to 919 MPa, *i.e.* a slight increase of 5.9%. Considering that failure was always initiated at the compressive face for these specimens and that the compressive strength of the IM7 carbon fibre/epoxy specimens was only approximately 10.9% higher than that of the TR50S carbon fibre/epoxy specimens (Figure 6.2), such a small increase in flexural strength at higher  $S/d$  ratios is reasonably acceptable.

Figure 6.23 also shows that flexural strength increases with an increase in  $S/d$  as has been previously reported [5, 28, 32, 41, 42]. This increase may be associated with the change in failure mode, as has been recommended by the adopted test standard [30], where shorter beams ( $S/d = 16$ ) were found to fail by shear mode and longer beams ( $S/d = 32$  and  $64$ ) failed due to a true flexural mode. Such an increase can be explained further by recalling equations (6.1) and (3.61). Equation (6.1) shows that, for  $S/d = 16$  specimens, a relatively lower longitudinal normal stress is required to generate a relatively high shear stress at the mid-plane. As a consequence of this, the last term in Equation (3.61), which represents the contribution of shear stress into the flexural mode, becomes larger. Thus, the condition defined in Equation (3.61), *i.e.*, initiation of failure, can be achieved at a lower flexural stress in comparison to that of the longer beams. Similar to that

previously noticed for hybrid GFRP composites, a sharper increase up to a maximum of 8.3% (from 774 MPa to 839 MPa for the  $S/d = 16$  specimens) in flexural strength was observed for lower amounts of substitution, up to 33%, of IM7/epoxy prepreg layers for TR50S/epoxy prepreg layers because of the reason previously discussed.

Although a significant increase in flexural strength was observed for lower amounts of substitutions of IM7 carbon fibre/epoxy prepreps for TR50S carbon fibre/epoxy prepreps, a significantly higher compressive modulus combined with only slightly higher compressive strength for IM7/Ep specimens (Figure 6.2) may lead to the compressive strength being slightly higher in order to suppress the increase in internal compressive stresses generated at the compressive face due to the increase in compressive modulus as indicated in equations (3.12a) and (3.12b) for the hybrid configurations. Therefore, the presence of a hybrid effect for flexural strength was not observed for this set of hybrid CFRP composites.

The strain at maximum stress,  $\varepsilon_{\max}$ , for these hybrid CFRP specimens has been presented in Table 6.6. The table shows that that strain at maximum stress appears not to be significantly influenced by the increase in span-to-depth ratio.

**Table 6.6.** Strain at maximum stress of hybrid CFRP specimens (%)

$S/d$	Hybrid ratio, $r_h$					
	0.0	0.17	0.33	0.50	0.67	1.0
16	1.08	1.14	1.10	1.15	1.02	1.17
32	0.96	0.94	0.97	0.95	0.96	0.96
64	1.01	0.98	0.97	0.96	0.95	0.94

It can be summarised that, although the flexural stress increased with the increase in IM7 fibre content, such a small increase could not be safely attributed to a hybrid effect. The most likely reason for this increase may have been an increase in internal load (stress) at the compressive face due to the substitution of carbon fibre possessing significantly higher modulus combined with only slightly higher compressive strength.

## 6.3.2.4. Flexural modulus

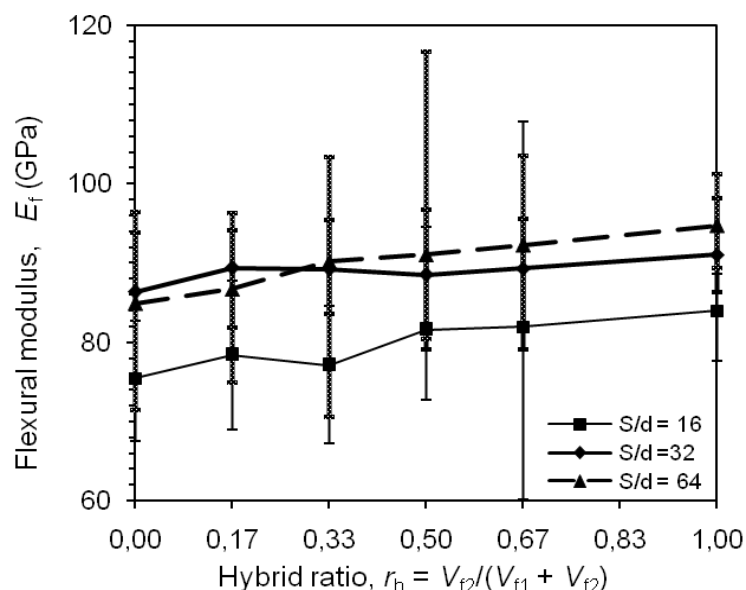


**Figure 6.24.** The influence of hybrid ratio on flexural modulus of hybrid CFRP composites showing an increase in flexural modulus with the increase in IM7 carbon fibre volume content and wide range of variations.

A general trend that can be observed for flexural modulus (shown in Figure 6.24) is that the flexural modulus ( $E_f$ ) increases with an increase of IM7 carbon fibre content represented by the increase of  $r_h$ . Although this increase appeared to obey the rule of mixtures, again, a sharper increase as represented by the slope of left hand side of the segments in Figure 6.24 was demonstrated by the initial layer of prepreg substitution. These values were generally similar to those expected from the rule of mixtures prediction when considering the difference in elastic compressive modulus of the single fibre-type composites (numerical values being given in Figure 6.2 for compressive properties and Table 6.1 for predicted tensile properties) in combination with the changes in total fibre volume fraction. For all  $S/d$  ratios the highest  $E_f$  values were recorded for the IM7 carbon fibre/epoxy specimens which were also found to contain the highest total predicted fibre volume fraction (Table 6.5). Therefore, the small increases in  $E_f$  as a function of IM7 carbon fibre content were attributed mainly to the minor increase in total fibre volume fraction for each hybrid configuration together with the difference in

elastic modulus for the respective fibres. Therefore, a general conclusion that can be drawn for flexural modulus in these CFRP composites is that a hybrid effect was not observed; the increase appeared to obey the rule of mixtures rather than any synergistic effect of hybridisation.

#### 6.3.2.5. Energy absorption capacity to maximum stress

The specific amount of energy absorbed by the samples up to the maximum stress for the hybrid CFRP specimens,  $\gamma_{\max}$ , calculated using equation (4.10), has been presented in Figure 6.25. The figure shows a similar general trend to that of flexural strength and flexural modulus with regards to the effect of  $S/d$  on the energy absorption capacity to maximum stress, *i.e.*, higher  $S/d$  values giving larger  $\gamma_{\max}$ . This can be explained by recalling equation (4.10) where  $\gamma_{\max}$  is linearly proportional to the magnitudes of load and displacement at a given point up to maximum stress. The maximum values of  $\gamma_{\max}$  for the three adopted  $S/d$  values were  $9.88 \text{ kJ}\cdot\text{m}^{-2}$  (IM<sub>3</sub>TR<sub>3</sub> specimens),  $15.43 \text{ kJ}\cdot\text{m}^{-2}$  (IM<sub>3</sub>TR<sub>3</sub> specimens), and  $30.95 \text{ kJ}\cdot\text{m}^{-2}$  (TR<sub>6</sub> specimens), for  $S/d$  values of 16, 32 and 64, respectively.

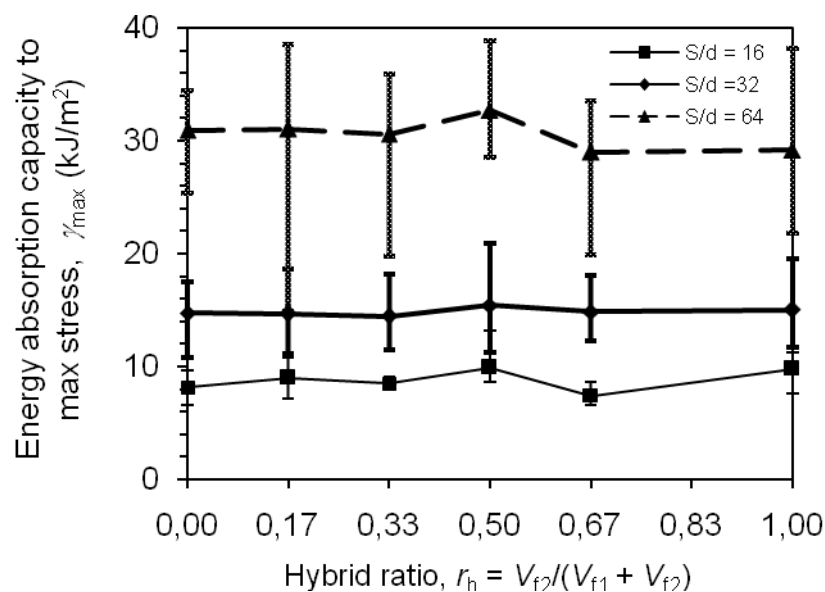


**Figure 6.25.** The influence of hybrid ratio on the energy absorption capacity to maximum stress,  $\gamma_{\max}$ , of hybrid CFRP composites. Considerably wide range of variations indicating inhomogeneous properties of the plates can be observed.



The significant increase in  $\gamma_{\max}$  with increasing  $S/d$  may be contributed to the parameters utilised to calculate  $\gamma_{\max}$  and how these parameters behave in response to the change in  $S/d$  – detailed discussion on this topic was previously addressed in sub-section 6.2.2.5 and has been summarised below. If the magnitudes of flexural strength and strain at maximum stress remain unchanged with increasing  $S/d$  (whereas in fact they increased (Figure 6.23 and Table 6.6)), and if the effect of  $S/d$  on the load-stress relationship is neglected, then equations (6.6a) and (6.6b) suggest that  $\gamma_{\max}$  for the  $S/d = 32$  and 64 specimens would be twice and four times, respectively, that of the  $S/d = 16$  specimens. In addition to this, the increase of  $\gamma_{\max}$  would also be influenced by the increase in  $\sigma_f$  and effect of the correction factor,  $f_c$ , as given in equations (6.6a) and (6.6b). In comparison with those tested at  $S/d = 16$ , whilst the change in strain at maximum stress was relatively small, varying from  $-0.134\%$  (at  $r_h \sim 0.67$ ) to  $-0.557\%$  (at  $r_h \sim 0.50$ ), the flexural strength of the specimens tested at  $S/d = 32$  was found to slightly increase, *i.e.*, varying from  $1.69\%$  for the  $r_h \sim 0.33$  samples to  $8.00\%$  for the  $r_h \sim 0.00$  samples. Therefore,  $\gamma_{\max}$  would be expected to increase by a minimum of  $\sim 71.5\%$  for  $r_h = 0.50$  to a maximum of  $\sim 98.6\%$  for  $r_h = 0.67$ . For similar reasons, specimens tested at  $S/d = 64$  would be expected to demonstrate an increase in  $\gamma_{\max}$  of a minimum of  $261\%$  for  $r_h = 1.00$  to a maximum of  $318\%$  for  $r_h = 0.00$ .

The increase in  $\gamma_{\max}$  when  $S/d$  was increased from 16 to 32 was found to vary from  $53.9\%$  to  $100.4\%$  (increasing from  $9.76 \text{ kJ}\cdot\text{m}^{-2}$  to  $15.01 \text{ kJ}\cdot\text{m}^{-2}$  for  $r_h = 1.00$  and from  $7.41 \text{ kJ}\cdot\text{m}^{-2}$  to  $14.88 \text{ kJ}\cdot\text{m}^{-2}$  for  $r_h \sim 0.67$ , respectively). This range of values was slightly wider than the predicted values, *i.e.*,  $71.5\%$  and  $98.6\%$  for the lower and upper limits, respectively. Further increasing the value of  $S/d$  to 64 resulted in a greater increase in  $\gamma_{\max}$ . In comparison to those of  $S/d = 16$ , the value of  $\gamma_{\max}$  for the specimens tested at  $S/d = 64$  exhibited an increase of  $199\%$  to  $291.3\%$  (increasing from  $9.8 \text{ kJ}\cdot\text{m}^{-2}$  to  $29.2 \text{ kJ}\cdot\text{m}^{-2}$  for  $r_h = 1.00$  and from  $7.1 \text{ kJ}\cdot\text{m}^{-2}$   $S/d = 16$  to  $29.0 \text{ kJ}\cdot\text{m}^{-2}$  for  $r_h \sim 0.67$ , respectively). These experimental values are again spread over a wider range in comparison with those of the predicted values ( $261\%$  to  $316\%$ ). In comparison to that of the hybrid GFRP

composites,  $\gamma_{\max}$  for the hybrid CFRP specimens was found to be significantly lower.

### 6.3.3. Summary

Hybrid CFRP composites containing higher strength and higher modulus IM7 carbon fibre and/or lower strength and lower modulus carbon fibre within an epoxy matrix were manufactured, tested and subsequently analysed. In order to evaluate their flexural properties, the specimens were subjected to a three-point bend (TPB) loading configuration in accordance with Procedure A of the ASTM D790-07 standard [30]. Following the tests, the fracture surfaces of specimens were sectioned, cast in polyester blocks and polished prior to examination under an optical microscope.

It was revealed that specimens tested at a  $S/d$  ratio of at least 32 failed due to fibre buckling and kinking – contrary to those tested at  $S/d = 16$  that failed in a shear mode along their neutral plane. This result suggested that a  $S/d$  ratio of 32 was sufficient in order to promote flexural failure as opposed to the shear failure exhibited by specimens tested at  $S/d = 16$ . A general trend noticed was that flexural strength, flexural modulus and storage energy capacity to maximum stress did not demonstrate any synergistic effect, *i.e.*, hybrid effect, instead, the replacement of stronger and stiffer IM7 carbon fibre for TR50S carbon fibre resulted in a slight increase in flexural properties that appeared to obey the rule of mixtures. The absence of a hybrid effect was thought to have been primarily caused by the internal stresses generated at the compressive face due to the increase in flexural modulus being higher than the respective increase in flexural strength introduced by the stronger fibre. This therefore suggests that a lower modulus fibre, combined with higher compressive strength, may be instead appropriate for the improvement of flexural properties for hybrid composite beams. Unlike the absence of a hybridisation effect for flexural modulus and strength, however, a considerable increase in flexural properties was noted as  $S/d$  was increased from 16 to 32 (or 16 to 64). Energy absorption capacity up to maximum stress appeared not to increase with hybridisation, although a

significant increase in energy absorption capacity up to maximum stress was obvious for the increase of  $S/d$  from 16 to 32 and further from 32 to 64. This increase may be contributed to the increase in flexural strength and most dominantly by the increase in  $S/d$ .

Optical microscopy confirmed that specimens tested at  $S/d = 16$  exhibited significant shear cracking at the neutral plane whereas specimens tested at  $S/d = 32$  and  $S/d = 64$  indicated the presence of fibre buckling and kinking which is typical of that for high strength unidirectional composites under flexural loading.

#### **6.4. HYBRID FRP COMPOSITES CONTAINING MIXED GLASS AND MEDIUM STRENGTH CARBON FIBRES**

The relatively low ratio of compressive-to-tensile strength of carbon fibre [21, 43, 44] may be a drawback for the use of carbon fibre reinforced polymer (CFRP) composites as structural members subjected to compressive and/or flexural loading. Whilst E-glass fibre possesses a lower tensile strength in comparison to even low strength carbon fibre [5, 29], it conversely demonstrates a higher compressive strength in comparison to high strength carbon fibre/vinylester composites at the same fibre volume fraction [15]. Further to this, Wonderly *et al.* pointed out that the compressive-to-tensile strength ratio of glass fibre reinforced polymer (GFRP) composite was relatively high at 0.73 [19] with Mallick crediting this phenomenon to the amorphous structure of the glass fibre [22].

Considering these findings, in this section an attempt was made to improve the flexural properties of CFRP composites through partial substitution of E-glass fibre for carbon fibre on the compressive side of the specimen.

### 6.4.1. Physical properties

#### 6.4.1.1. Stacking configurations

Six different stacking configurations, including the pure E-glass fibre/epoxy composite and pure TR50S carbon fibre/epoxy composite, were investigated. In order to produce composite plates with a thickness of approximately 2 mm, either four, five or six layers, depending on the particular configuration, were utilised – the variation in layer number being due to the E-glass/epoxy prepreg being thicker than that of the TR50S/epoxy case. The average thicknesses of the cured CF/Ep and GF/Ep prepreg layers, calculated from their respective single fibre-type FRP specimen thicknesses, were found being 0.377 mm and 0.614 mm, respectively.

The TR50S carbon fibre/epoxy prepreps, E-glass fibre/epoxy prepreps, or a mixture of both, were stuck together in order to produce a preform and subsequently cured under vacuum in a hot press at 120 °C for 30 minutes according to the optimal curing conditions determined previously. The stacking configurations of the hybrid GFRP composites under investigation have been presented in Figure 6.26.

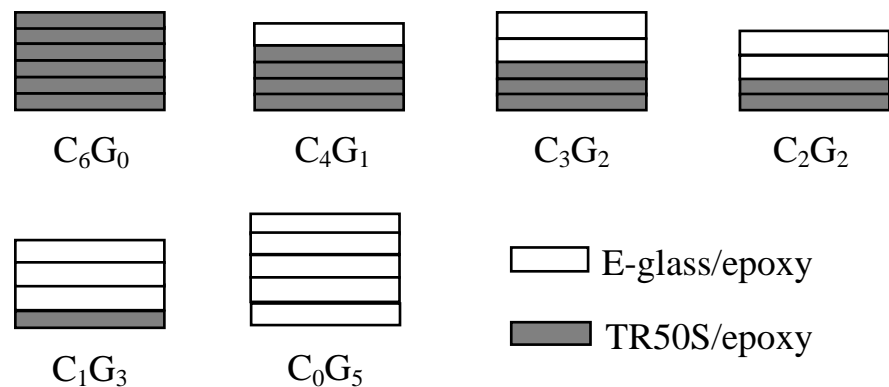


**Figure 6.26.** Schematic illustration of the stacking configurations of the hybrid CFRP composites under investigation.

**Table 6.7.** Physical characteristics of the hybrid composite plates  
(Showing mean values and standard deviations)

Stacking configuration	Bulk density, $\rho$ (g.cm <sup>-3</sup> )	Fibre volume content, $V_f$ (%)		Void volume content, $V_v$ (%)
		Density-based	Image analysis	
C <sub>6</sub> G <sub>0</sub>	1.42 ± 0.006	48 ± 0.9	---	48.0
C <sub>4</sub> G <sub>1</sub>	1.43 ± 0.151	62 ± 8.4	51 ± 9.1	58.6
C <sub>3</sub> G <sub>2</sub>	1.49 ± 0.022	61 ± 6.1	50 ± 3.2	55.0
C <sub>2</sub> G <sub>2</sub>	1.44 ± 0.030	47 ± 2.0	49 ± 7.5	48.3
C <sub>1</sub> G <sub>3</sub>	1.58 ± 0.026	63 ± 1.6	51 ± 9.1	52.9
C <sub>0</sub> G <sub>5</sub>	1.87 ± 0.024	---	52 ± 1.6	52.0

#### 6.3.1.2. Density and fibre content

Physical characteristics of the composite plates have been presented in Table 6.7 with the fibre volume fractions being determined from optical micrographs of slices cut perpendicular to the fibre direction – the calculation can be found in Appendix 9. The hybrid ratio,  $r_h$ , defined as the volume ratio of glass fibre with respect to the total fibre content,  $V_{fG}/V_f$ , was calculated using equation (6.7) that was equivalent to volume fraction given in reference [45].

$$r_h = \frac{1}{1 + \left( \frac{t_{CF/Ep}}{t_{GF/Ep}} \right) \left( \frac{V_{f-CF/Ep}}{V_{f-GF/Ep}} \right)} \quad (6.7)$$

where  $t$  and  $V_f$  are the layer thickness and fibre volume fraction within the respective layer, respectively.

Total fibre content,  $V_{f-total}$ , in Table 6.7 was calculated using the following formula.

$$V_{f-\text{total}} = \frac{n_C \cdot t_C}{n_C \cdot t_C + n_G \cdot t_G} \cdot V_{f-C} + \frac{n_G \cdot t_G}{n_G \cdot t_G + n_G \cdot t_G} \cdot V_{f-G} \quad (6.8)$$

where the subscripts  $C$  and  $G$  refer to carbon/epoxy and glass/epoxy preregs, respectively, and  $n$  and  $t$  are the number of prepreg layers and the average thickness of individual prepreg layers, respectively. Table 6.7 shows that for the hybrid configurations, apart from the  $C_2G_2$  case, the carbon/epoxy prepreg layers (third column in Table 6.7) exhibited a higher fibre content compared to the glass/epoxy prepreg layers (fourth column), and thus produced a total fibre content higher for the configurations containing thicker carbon/epoxy prepreg layers. The variation in total fibre content for the hybrid composites was significant, ranging from 46.0% for the pure CFRP composite plate to 58.6% for the  $C_4G_1$  hybrid configuration plate. Such a major variation in fibre volume fraction was also expected to have a significant influence on the resulting flexural properties.

#### **6.4.2. Mechanical Properties**

##### **6.4.2.1. Stress-strain response**

The mechanical property data presented in this section was extracted from the output of flexural testing with the raw data and spreadsheet calculation example similar to that being presented in Appendix 10. Figures in this sub-section, and the following sub-sections present the pure CFRP and GFRP composites as possessing a hybrid ration,  $r_h$  of zero and unity, respectively, with values between these endpoints representing hybrid composites. Load-deflection and stress-strain curves for a single type of hybrid composite have been presented in Figure 6.27. A reasonably linear stress-strain response prior to the point of maximum stress (Figure 6.27(a)) was noted for this hybrid composite containing one layer of carbon fibre/epoxy and three layers of E-glass fibre/epoxy preregs tested at  $S/d = 16$ . Apart from specimen number 5, a gradual decrease in load was noted past the point of maximum load. This may partially be credited to the stacking configuration of this hybrid composite being dominated by glass

fibre/epoxy layers possessing a higher failure strain (2.36% [46]) in comparison with the pure CFRP composite (0.75% [47]). Specimen adjustment onto the test fixture in the early stages of loading was again noted for these composites and thus Figure 6.27(b) illustrates the same data as shown in Figure 6.27(a) following a toe correction procedure carried out in accordance with the respective ASTM standard [30]. Stiffer prepreg layers, *i.e.* glass/epoxy prepregs, being displaced from their initial placement in different magnitudes and patterns, as can be observed in Figure 6.30 and 6.31, may be responsible for the variation in bending stiffness of the samples being observed in Figure 6.27. Flexural properties of the specimens were derived from Figure 6.27(b) in addition to another 17 similar plots representing the other two  $S/d$  values for this configuration in addition to three  $S/d$  values for each of the other five stacking configurations.

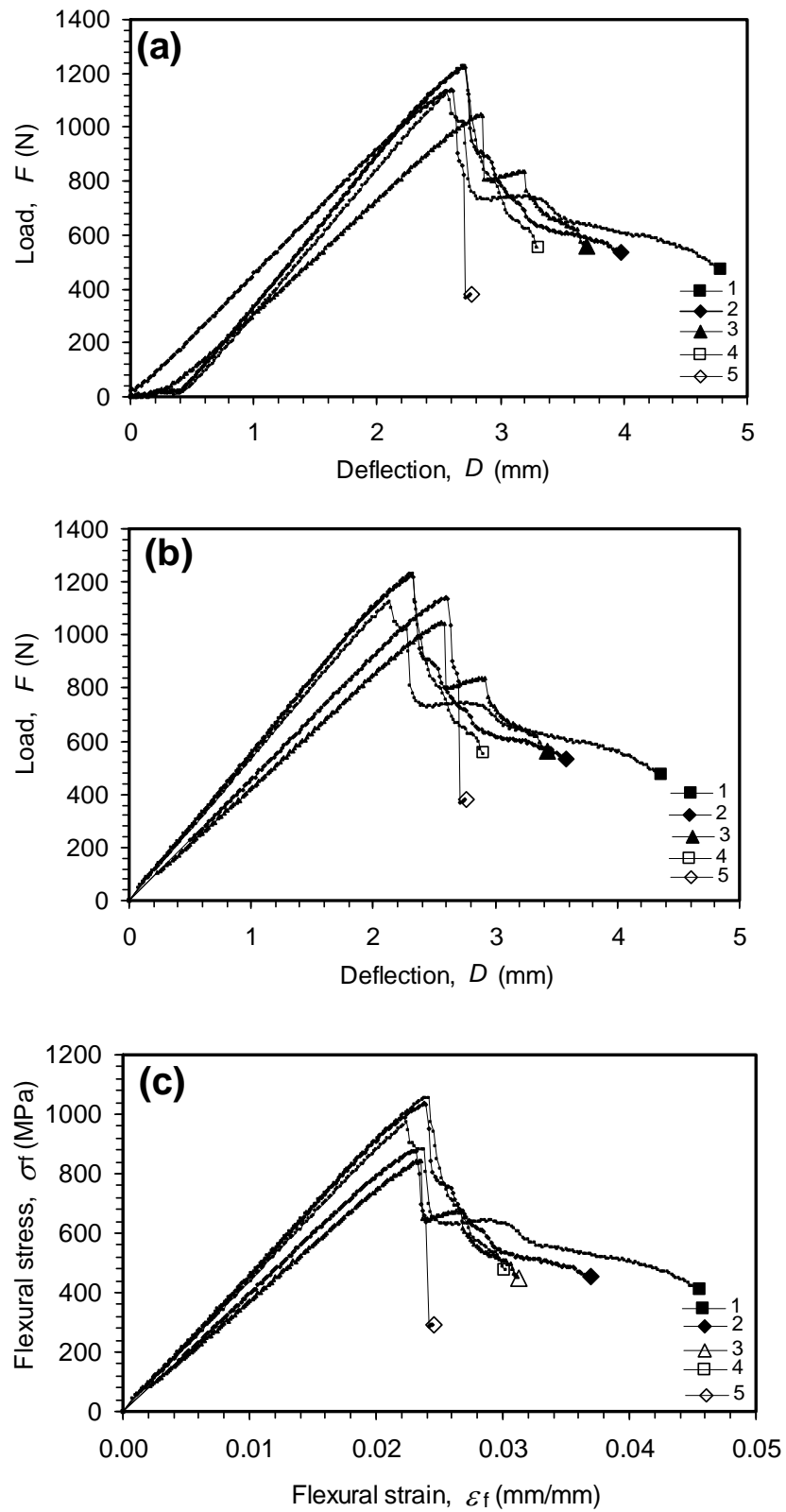


**Figure 6.27.** Representative load-displacement and stress-strain relations of hybrid composite samples ( $C_1G_3$ ). (a) Before to correction, (b) After toe correction, and (c) Stress-strain relation.



The effect of hybrid ratio ( $r_h$ ), *i.e.* E-glass fibre-to-total fibre content ratio, on the stress-strain response of representative samples has been presented in Figure 6.28. These representative samples are those that exhibited approximately average values in their respective groups. Typical stress-strain relationships of  $S/d = 16$  samples presented in Figure 6.28(a) show approximate linear stress-strain curves from the initial loading to a certain level of stress. Whilst the pure CFRP ( $C_6G_0$ ) and GFRP ( $C_0G_5$ ) samples exhibit catastrophic failure, all of the representative hybrid samples demonstrated a gradual drop in load and/or excessive elongation prior to failure. The highest flexural strength (1065 MPa) was achieved by the  $C_2G_2$  specimens which is 76.8% and 28.3% higher than that of the  $C_6G_0$  (602 MPa) and  $C_0G_5$  (830 MPa) specimens, respectively.

A general trend that can be observed in Figure 6.28(a) is that, apart from that of the  $C_0G_5$  specimens, the initial slopes of the curves (representing the flexural modulus) for each respective sample appears within a narrow range and closer to that of the pure CFRP ( $C_6G_0$ ) specimens. The reason for this was that the elastic modulus of the TR50S carbon fibre (240 GPa [48]) is known to be significantly higher than that of the E-glass fibre (72.3 GPa [49]).

In contrast to this, apart from the  $C_4G_1$  specimens, the  $S/d = 32$  samples presented in Figure 6.28(b) exhibited an abrupt drop in load associated with catastrophic failure following a linear stress-strain relationship to the point of maximum stress as previously reported [27]. Whilst the highest flexural strength (1230 MPa) was demonstrated by the  $C_1G_3$  sample representing the hybrid configuration containing one layer of carbon fibre/epoxy prepreg and three layers of E-glass fibre/epoxy prepreg, the lowest flexural strength (691 MPa) was exhibited by the  $C_6G_0$  sample. This significant increase (77.9%) in flexural strength suggests that a hybrid effect would most probably be observed and will be later discussed further. A similar trend to that previously observed for  $S/d = 16$  was observed in Figure 6.28(b) whereupon the variation in flexural modulus represented by the slope of each individual curve appeared within a narrow range. On comparison between Figure 6.28(b) and Figure 6.28(a) it was concluded that the flexural stress achieved for the  $S/d = 32$  samples was considerably higher

(from 8.94% for the C<sub>2</sub>G<sub>2</sub> specimens to 32.8% for the C<sub>4</sub>E<sub>1</sub> specimens) than that of their respective  $S/d = 16$  samples.

Figure 6.28(c) illustrates the effect of hybrid ratio on stress-strain response for the samples tested at  $S/d = 64$  with the pattern of stress-strain relationships being similar to those of the samples tested at  $S/d = 32$ . The GFRP composite behaviour appeared to dominate the stress-strain relationships, apart from that of the C<sub>6</sub>G<sub>0</sub> composite, in that the specimens demonstrated a significant non-linearity after reaching a certain level of stress up to failure. This nonlinearity may be related to matrix shear yielding and band broadening at the compressive side just prior to initiation of local fibre buckling, as has been noted by Daniel *et al.* [50]. In comparison with Figure 6.28(b), the maximum flexural stress appears to be similar but with a significantly wider variation in flexural modulus.

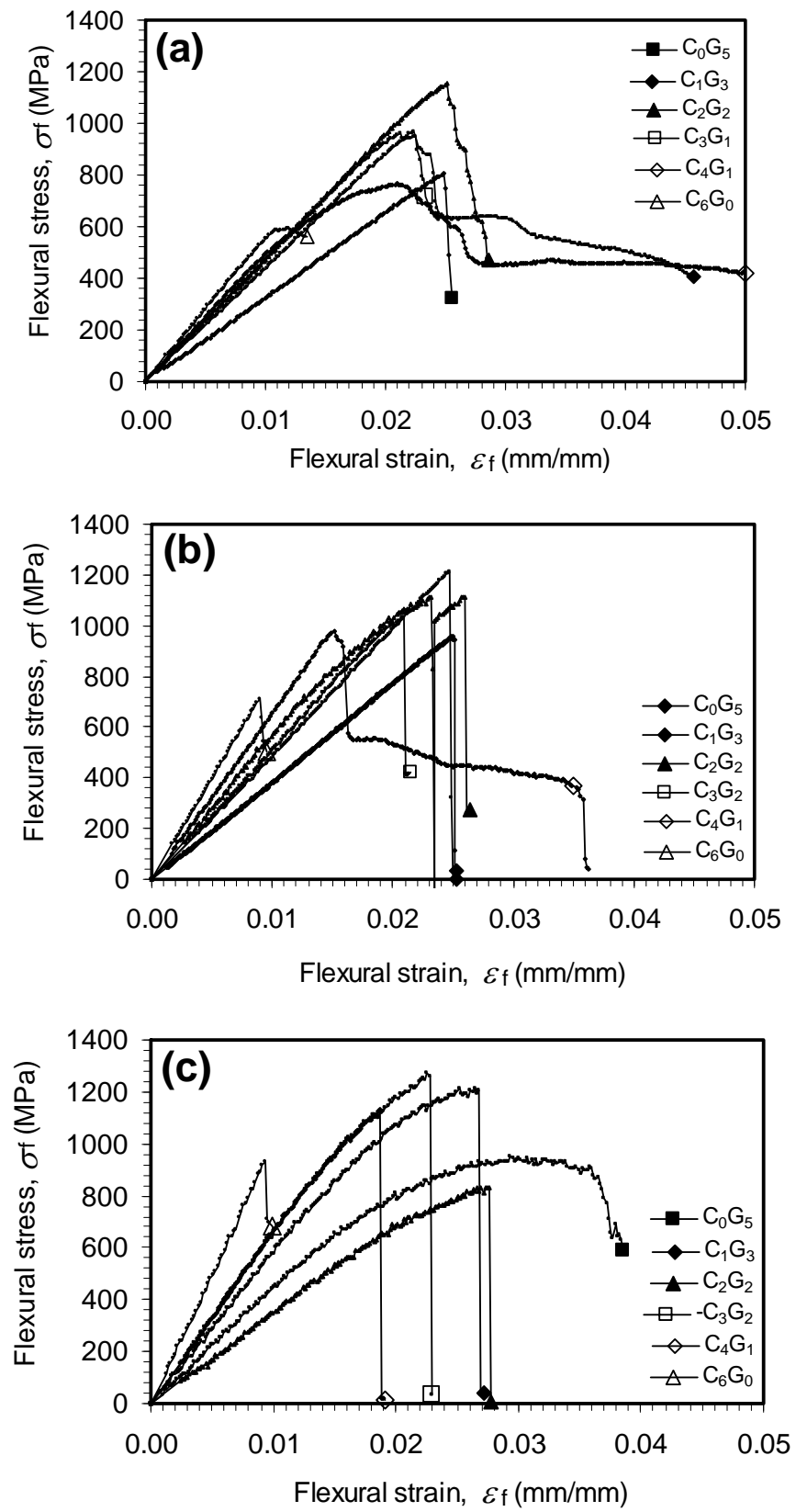


**Figure 6.28.** Representative illustration of the effect of hybrid ratio on stress-strain relation. (a)  $S/d = 16$ , (b)  $S/d = 32$ , (c)  $S/d = 64$ .

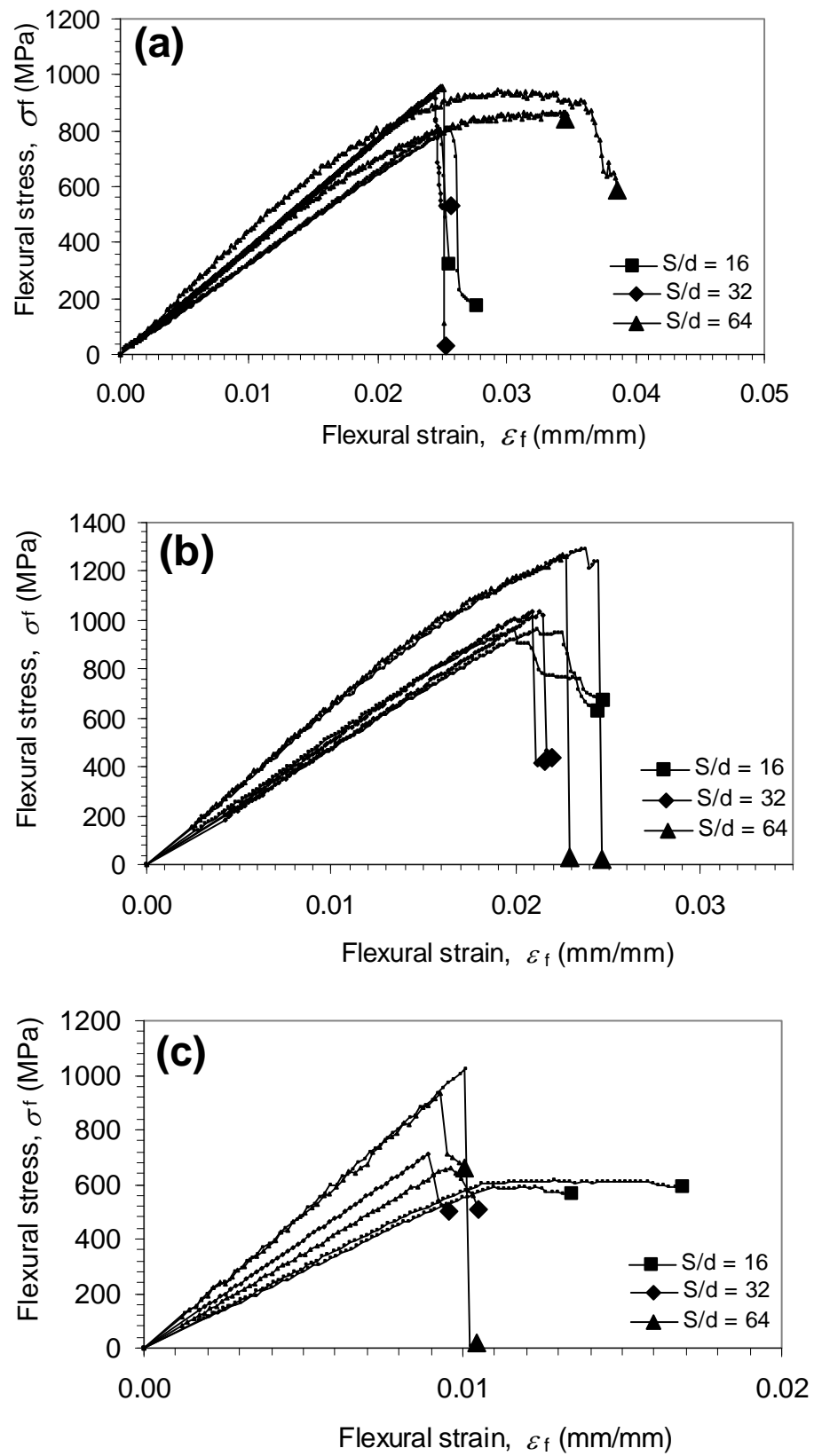


**Figure 6.29.** Representative illustration of the effect of S/d on stress-strain relation. (a)  $C_0G_5$  samples, (b)  $C_3G_2$  samples, (c)  $C_6G_0$  samples.

A general trend that can be drawn by comparing figures 6.27(a), 6.27(b) or 6.27(c) is a noticeable increase in flexural strength with increasing  $S/d$  from 16 to 32 (or 16 to 64). In contrast to this, the increase of  $S/d$  from 32 to 64 appears not to significantly increase flexural strength; neither does the flexural modulus increase significantly with the increase of  $S/d$  from 16 to 64. Such phenomena were confirmed, for example, within each individual stacking configuration, *e.g.*, illustrated in each of the graphs presented in Figure 6.29 for the case of hybrid FRP composites containing three IM7/epoxy and three TR50S/epoxy prepreg layers. In addition, Figure 6.28 and Figure 6.29 also demonstrate that significant increases in strain to maximum stress was noticed upon hybridisation, but no significant difference in strain-to-maximum stress was noticed amongst the three values of  $S/d$ .

#### 6.4.2.2. Failure mechanism

Bader and colleagues [8] reported that fibre surface treatment had the potential to change the mode of failure to be more brittle and also reduce the strength of their CF/epoxy tensile specimens whereas Daniel *et al.* [7] noted that failure in CF/epoxy composites subjected to compressive loading initiated with matrix shear or shear yielding followed by fibre buckling and fracture. Furthermore, band broadening took place at increasing compressive stress with thicker specimens producing more complex kink band geometries.

Failure mechanisms in aluminium-carbon short fibre hybrid-reinforced thermoplastic composites have previously been reported by Schmidt-Thomas *et al.* [9]. They noted that changes in temperature significantly affected the failure mode and morphology as well as mechanical properties with increases in temperature drastically degrading mechanical properties. Alternatively, Hwang and Mao [10] reported their work on compressive failure mechanisms in carbon-glass hybrid FRP composites and noted that increases in length and decreases in depth of a delamination caused decreased buckling loads. In addition, an increase in the number of glass/epoxy prepreg layers in interply hybrid composites resulted in decreased failure loads.

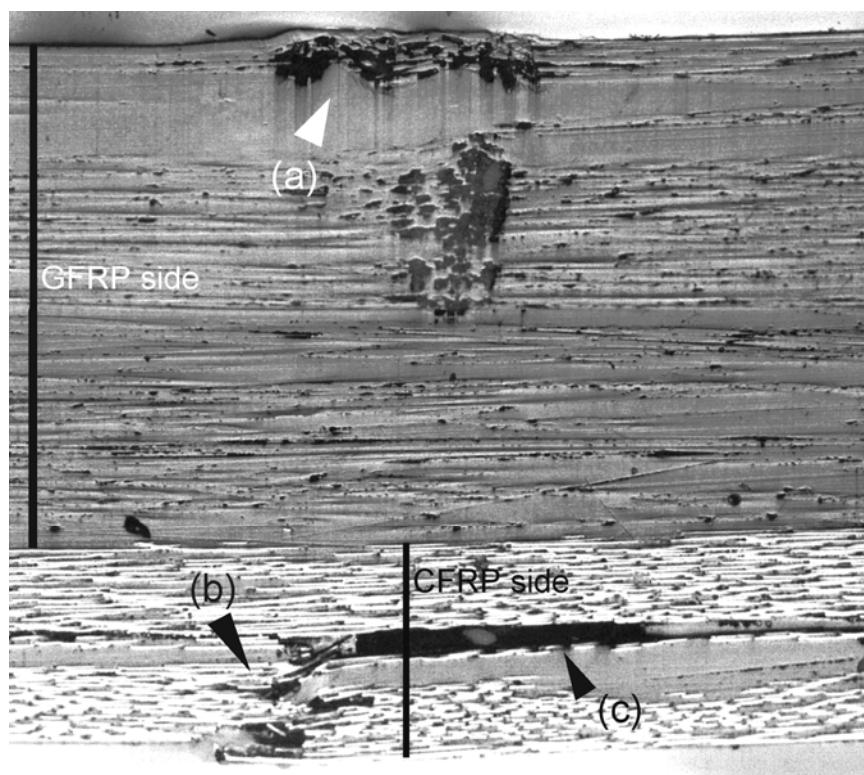


**Figure 6.30.** Fracture region of a  $C_2G_2$  specimen tested at  $S/d = 16$  showing: (a) fibre kinking, (b) fibre breakage, (c) delamination in a matrix rich region.

A representative optical micrograph for a fracture region in a specimen tested at  $S/d = 16$  has been presented in Figure 6.30. As has been previously discussed, the specimens tested at  $S/d = 16$  exhibited different patterns of stress-strain behaviour to failure as depicted in Figure 6.28(a). The first group experienced catastrophic failure ( $C_6G_0$  and  $C_0G_5$  specimens representing the CFRP and GFRP composites, respectively) characterised by a sudden load drop. The second group ( $C_2G_2$  and  $C_3G_1$  specimens representing hybrid configurations with the CF/epoxy-GF/epoxy layer interface closest to the mid-depth of the beam) failed after undergoing a gradual decrease in load within a relatively short period of time that was thought to be associated with band broadening at the compressive side [15, 24] followed by longitudinal crack formation at relatively low strains [51] and eventually fibre breakage in the tensile side as presented in Figure 6.30.

Figure 6.31 illustrates a typical failure region for specimens tested at  $S/d = 32$ . As presented in Figure 6.28(b), specimens tested at  $S/d = 32$ , apart from the C<sub>4</sub>G<sub>1</sub> specimens that did not fail even at 5% strain, experienced catastrophic failure as indicated by the sudden drop in load. The strain at maximum stress,  $\epsilon_{\max}$ , for the hybrid specimens was found to be between that of the CFRP and GFRP composites. It was noted that  $\epsilon_{\max}$  increased with the proportion of GF/epoxy prepreg layers, although not linearly proportional. A reduced effect of shear stress at higher  $S/d$ , as previously suggested by Davies and Hamada [13], may have been caused by the reduction in the period of time available for matrix shear yielding processes.

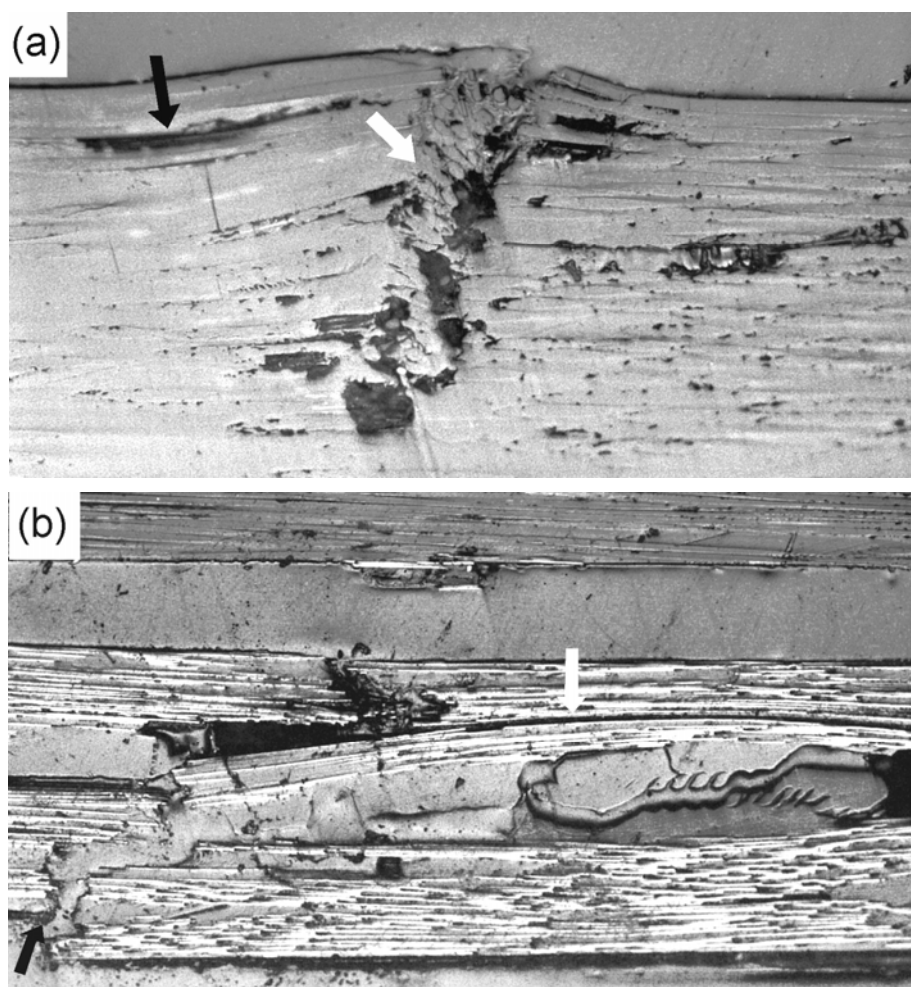


**Figure 6.31.** Fracture region of a C<sub>2</sub>G<sub>2</sub> specimen with  $S/d = 32$ . (a) Compressive face showing out-of-plane buckling and kinking (white arrow) and splitting (dark arrow), and (b) tensile surface showing fibre breakage (dark arrow) and delamination (white arrow).

It can be noticed from Figure 6.31(a) that the compressive surface failed through a combination of out-of-plane fibre buckling (white arrow) and splitting (black arrow). Such a compressive failure mode in GFRP composites has been reported by Lee and Waas [14]. At the tensile side shown in Figure 6.31(b), fibre breakage due to local tensile stresses combined with delamination near a resin rich region was clearly observable.

Referring to Figure 6.28(c) illustrating specimens tested at  $S/d = 64$ , apart from that of the CFRP composite that failed at strain less than 1%, a linear stress-strain relationship up to  $\sim 1\%$  strain can be noticed. Increases in strain resulted in a decrease in slope for the  $\sigma_f - \varepsilon$  plots. Another characteristic noted in Figure 6.28 was the fact that  $\varepsilon_{\max}$  for the hybrid specimens was found to be between those of the pure CFRP and GFRP composites, with an obvious trend that  $\varepsilon_{\max}$  increased with an increase in GF content.

Figure 6.32 illustrates a portion of a fractured specimen tested at  $S/d = 64$ . The GFRP portion at the compressive side exhibited out-of-plane buckling

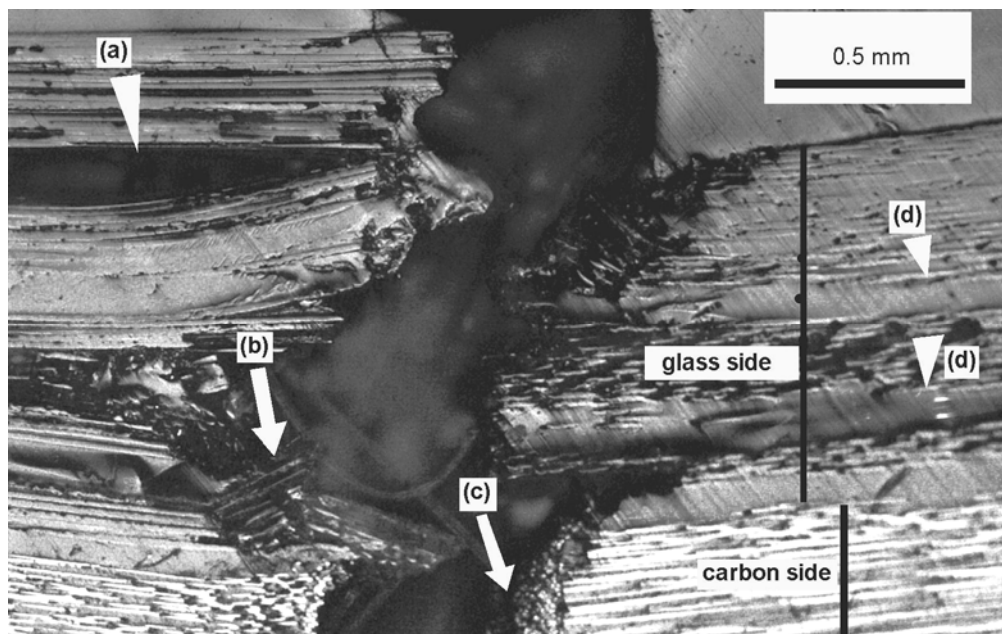


**Figure 6.32.** Compressive side of fracture region of a  $C_2G_2$  specimen with  $S/d = 64$ : (a) splitting, (b) in-plane buckling producing kink band, (c) out-of-plane buckling in carbon side, (d) matrix-rich areas between two prepreg layers [4].



combined with splitting. A kink band was observed to cross the interface of the CF/epoxy-GF/epoxy layers indicating that the upper part of the CF/epoxy layer was bearing a local compressive load. Recall that the average thickness of the CF/epoxy prepreg was 0.377 mm while that of the GF/epoxy prepreg was 0.614 mm, thus indicating that the CF/epoxy-GF/epoxy interface lay below the mid-plane of the beam, thus the neutral axis had been shifted towards the tensile face. This result further implied that the compressive modulus of the GFRP layer was lower than the tensile modulus of the CFRP layer, because, in a ‘composite cross section’ the neutral axis will be shifted toward the stiffer material [52, pp. 393-403].

#### 6.4.2.2. Flexural strength

Figure 6.33 exhibited a general trend whereby  $\sigma_f$  increased with increasing  $r_h$  as previously reported in Kang *et al.* [53] and increasing  $S/d$ . The reduced influence of shear as  $S/d$  increased was thought to be responsible for the general increase in  $\sigma_f$  as  $S/d$  increased [32]. These results can be applied to the maximum distortion energy failure criterion presented mathematically in equation (3.61) that

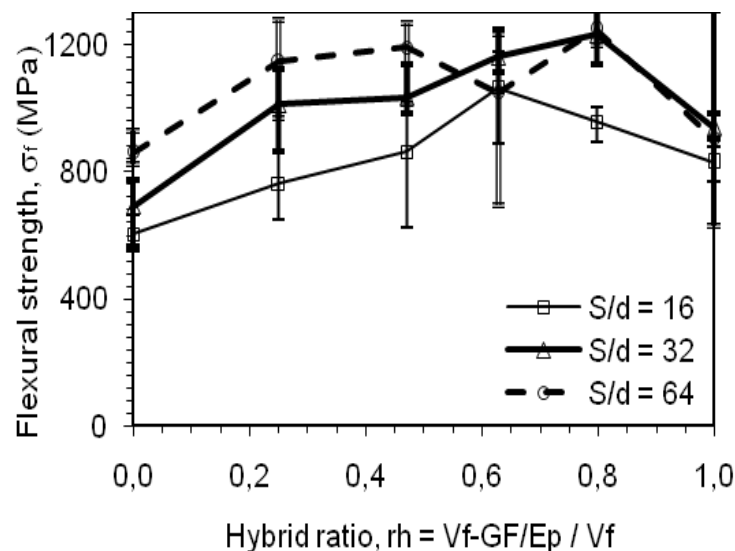


**Figure 6.33.** The effect of hybrid ratio on flexural strength showing the increase of flexural strength with the increase of hybrid ratio. Comparatively narrow range of variations indicating homogenous properties within a plate can be observed.

results in an increased value of the last term leading to satisfying the inequality for initial failure. Apart from the specimens tested at  $S/d = 16$ ,  $\sigma_f$  increased with partial substitution, up to  $\sim 80\%$ , of glass fibre for carbon fibre. The maximum  $\sigma_f$  (1065 MPa) at  $S/d = 16$  was achieved at  $r_h \sim 63\%$  and then decreased to that of the GFRP specimen in an approximately linear pattern. In contrast to all other specimens tested at  $S/d = 64$  that failed by flexure, those of C<sub>2</sub>G<sub>2</sub> failed by interlaminar shear this was thought to explain the lower than expected  $\sigma_f$  for this specimen. Considering that some of the hybrid composites exhibited higher flexural strength compared to either of the pure GFRP or CFRP specimens, a positive hybrid effect in flexural strength was obviously noticeable. The flexural strength of the parent composite materials observed here were noticeably higher than those reported in [1], *i.e.* 568 MPa and 798 MPa for the case of AS4 graphite fibre/epoxy and E-glass fibre/epoxy composite, respectively, tested at  $S/d = 40$ . For specimens tested at  $S/d = 32$ , the highest flexural strength (1230 MPa) was achieved at  $r_h \sim 0.80$ . This value was approximately 77.9% and 30.9% higher than that of the pure CFRP (691 MPa) and GFRP (940 MPa) specimens, respectively. Specimens tested at  $S/d = 64$  exhibited their maximum flexural strength (1248 MPa) at  $r_h \sim 0.80$  which was comparable with that of the same hybrid configuration tested at  $S/d = 32$ . This implies that further improvement in flexural strength may not be obtained for  $S/d$  values higher than 32. Although these maximum values were significantly lower than that previously reported (1855 MPa) for unidirectional hybrid carbon-boron FRP composites [54], the total fibre volume content obtained here (52.9%) was significantly lower than that reported in [54], *i.e.* 75%. The author in [54] also reported the flexural strength for pure CFRP and pure BFRP composites to be 1174 MPa (at  $V_f = 53.1\%$ ) and 1788 MPa (at  $V_f = 50.0\%$ ), respectively. That the flexural strength of the parent materials were lower than those of [54] may be responsible for the lower overall flexural strength of the resulting hybrid FRP composites in the present work, which may be closely associated with their respective overall fibre volume fractions.

Another feature of the  $\sigma_f - r_h$  correlation shown in Figure 6.33 was that a smaller amount of GF substitution, up to  $\sim 25\%$ , resulted in a relatively greater

increase in  $\sigma_f$ , represented by a steeper slope of the initial left hand side of the curve. Such a result has previously been reported [5, 32, 42] for different hybrid combination and may be explained as follows. At small amounts of substitution, the GF/Ep layers were placed at the outer layer of the compressive side where the maximum compressive stress occurs. For additional GF/Ep layers, the substitution would be located closer to the neutral plane where the compressive stress is significantly reduced, such that the compressive strength of this GF/Ep layer would not be optimally harnessed until initial buckling occurs at the outermost layer and propagates toward this layer.

**Table 6.8.** Strain at maximum stress of the hybrid carbon-glass FRP composites under investigation (%)

$S/d$	Hybrid ratio, $r_h$					
	0.00	0.25	0.47	0.63	0.80	1.00
16	1.19	2.11	2.14	2.52	2.33	2.52
32	0.94	1.53	2.05	2.62	2.46	2.43
64	0.92	1.90	2.10	2.29	2.45	3.24

The strain at maximum stress,  $\varepsilon_{\max}$ , for these unidirectional hybrid carbon-glass FRP composites has been presented in Table 6.8. Noting that the strain at maximum stress for the unidirectional GFRP composite (1.84%) was significantly higher than that of the CFRP composites (0.48%) [1], it was expected that  $\varepsilon_{\max}$  should increase with increasing  $r_h$  – this trend was indeed observed in Table 6.8. Li *et al.* [55] noted the same result from the incorporation of ultrahigh modulus polyethylene fibre into their CFRP samples.

It was also observed that the relative increase in  $\varepsilon_{\max}$  was greater when the amount of glass fibre substitution was smaller. The table shows that, for  $S/d = 16$  and  $S/d = 32$ ,  $\gamma_{\max}$  increases with an increase of  $r_h$  up to  $r_h \sim 0.63$ . Generally speaking, at low glass fibre content, *i.e.*, smaller values of  $r_h$ , the strain at maximum stress was predominantly controlled by the carbon fibre behaviour, and *vice versa*.

It can be stated that a hybrid effect for flexural strength was clearly observed up to a maximum of ~80% and ~63% substitution of glass fibre for carbon fibre, respectively, for longer span beams ( $S/d = 32$  and  $S/d = 64$ ) and shorter span beams ( $S/d = 16$ ). The significant increase in flexural strength demonstrated by the first layer substitution was attributed to the optimum harnessing of the compressive potential of the glass fibre when placed at the location of maximum compressive stress. In addition, the strain at maximum stress also exhibited an improvement with increasing glass fibre content.

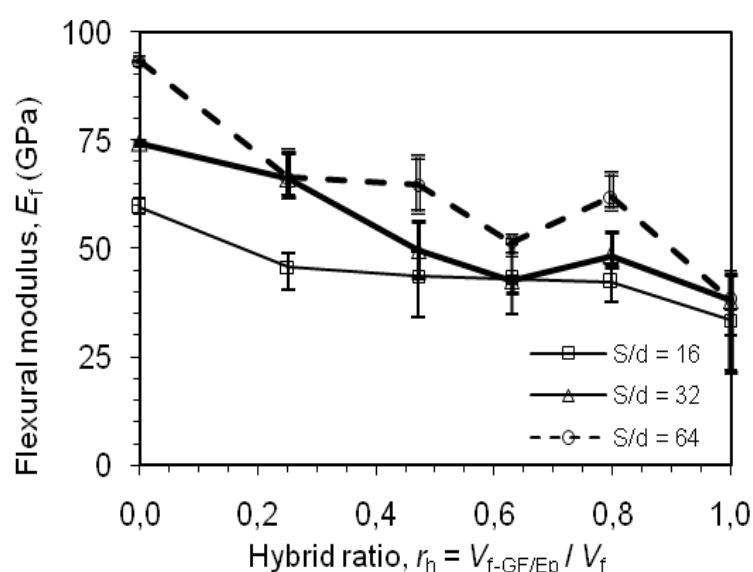


**Figure 6.34.** The effect of hybrid ratio on flexural modulus showing a decrease in flexural strength with the increase of hybrid ratio. Homogeneous property distribution represented by narrow range of variations can be observed.

#### 6.4.2.3. Flexural modulus

Considering the fact that the compressive modulus of glass fibre (72.3 GPa [49]) was significantly lower than that of carbon fibre (240 GPa [48]), it was expected that the flexural modulus,  $E_f$ , would decrease with increasing  $r_h$  and this was indeed the case as noted in Figure 6.34. The general trend was that  $E_f$  increased with increasing  $S/d$  but decreased with increasing  $r_h$ . The general increase in  $E_f$  with  $S/d$  was consistent with the reduced contribution of shear

deformation with increasing  $S/d$  as the equations for  $E_f$  do not take into account the proportion of the specimen deflection due to shear. In addition to this, the general increase in  $E_f$  with  $S/d$  was noted to be larger for CFRP specimens than for GFRP specimens. Whilst some flexural modulus values, *e.g.*,  $r_h \sim 0.80$  for  $S/d = 64$ , showed a slight positive hybrid effect, overall, the flexural modulus appeared to obey the rule of mixtures relationship.

Similar to that observed for the influence of hybrid ratio on flexural strength, a more significant decrease in  $E_f$ , as represented by the initial slope of the left hand side of the segment in Figure 6.34, was observed for relatively small amounts of glass fibre substitution was the reason being the same as that noted for the flexural strength case. The decrease in  $E_f$  for the  $C_2G_2$  specimens in comparison to that of the  $C_3G_2$  specimens was attributed to the lower  $V_f$  of these specimens, as previously shown in Table 6.7.

#### 6.4.2.4. Energy storage capacity to maximum stress, $\gamma_{\max}$

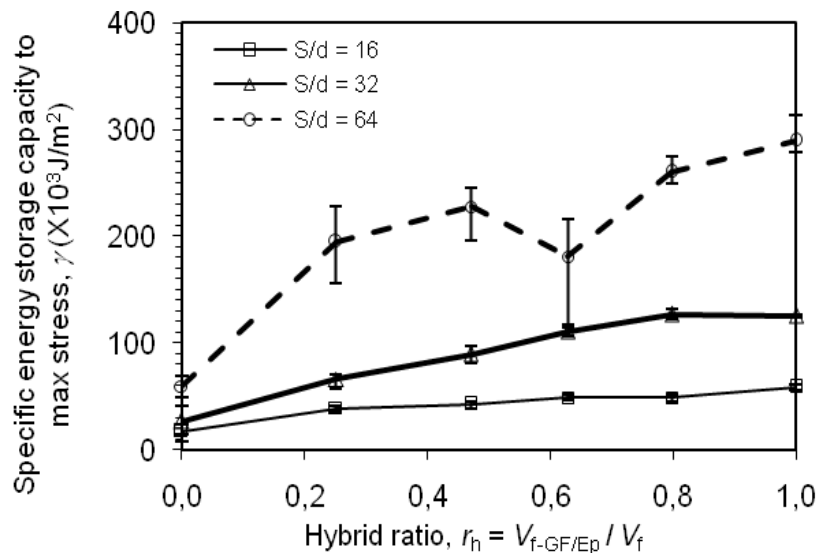


**Figure 6.35.** The effect of hybrid ratio on specific energy storage capacity-to-maximum stress showing an increase of  $\gamma$  as the hybrid ratio increases. Whilst homogeneous material properties indicated by narrow range of variations can be observed for  $S/d = 16$ , and  $S/d = 32$ , wider range of variations was noticed for  $S/d = 64$ .

Figure 6.35 illustrates that  $\gamma_{\max}$  generally increased with both increasing  $r_h$  and  $S/d$ . Apart from the  $S/d = 16$  specimens that tended to obey the rules of mixtures and the  $C_2G_2$  specimens at  $S/d = 64$ , the other hybrid specimens exhibited a positive hybrid effect. For each individual curve of the three  $S/d$  values investigated, the lowest and highest  $\gamma_{\max}$  values were consistently exhibited by the CFRP ( $r_h \sim 0.00$ ) and GFRP ( $r_h \sim 1.00$ ) composite specimens, respectively. These lowest and highest values were  $8.6 \text{ kJ}\cdot\text{m}^{-2}$  and  $29.4 \text{ kJ}\cdot\text{m}^{-2}$  for  $S/d = 16$ ,  $13.2 \text{ kJ}\cdot\text{m}^{-2}$  and  $62.8 \text{ kJ}\cdot\text{m}^{-2}$  for  $S/d = 32$ , and  $29.7 \text{ kJ}\cdot\text{m}^{-2}$  and  $144.7 \text{ kJ}\cdot\text{m}^{-2}$  for  $S/d = 64$ . The low  $\gamma_{\max}$  value for  $C_2G_2$  specimens at  $S/d = 64$  was thought due to the low total  $V_f$  for that particular composite as shown in Table 6.7.

The energy storage capacity-to-maximum stress,  $\gamma_{\max}$ , was predicted from the respective flexural stress and flexural strain behaviour as given in equation (4.10) with the hybrid effect appearing to be influenced by  $r_h$ ; the higher the  $r_h$ , the less the hybrid effect. The increase in energy storage  $\gamma_{\max}$  with increasing  $S/d$  ratio was attributed to the increase in flexural strength, strain at maximum stress together with the direct effect of the increase in  $S/d$  as has been discussed in detail previously in sub-section 6.2.2.4. A maximum hybrid effect for  $\gamma_{\max}$  was achieved at  $S/d = 64$  and  $r_h \sim 0.25$ .

#### 6.4.3. Summary

Six different stacking configurations, including those of the parent composite materials, of FRP composites containing either all carbon fibre/epoxy, all E-glass fibre/epoxy or a mixture of them have been fabricated, tested in accordance with Procedure A of the ASTM D790-07 [30] standard, and evaluated. A general trend noted is that flexural strength, strain to maximum stress, and energy storage capacity to maximum stress were found to increase with the replacement of E-glass fibre/epoxy prepreg layers for TR50S carbon fibre/epoxy prepreg layers. A maximum increase in these properties was consistently demonstrated by replacement of the first layer at the compressive face of the specimen. In contrast to this, the flexural modulus exhibited a trend of obeying the

rule of mixtures, *i.e.*, flexural modulus decreases with an increase of E-glass fibre content due to the elastic modulus of E-glass fibre being significantly lower than that of the TR50S carbon fibre. In addition to this, the span-to-depth ratio was found to influence the flexural properties of the hybrid composites with the flexural strength increasing with span-to-depth ratio due to the reduced effect of shear stresses (when compared to axial stresses) under these situations. A positive hybrid effect was noted for flexural strength, strain at maximum stress for most hybrid configurations, and specific energy storage capacity at maximum stress apart from the  $S/d = 16$  specimens.

Optical micrographs revealed that failure was initiated at the compressive face in the form of fibre buckling followed by kink band formation, shear cracking in weaker regions (either neutral plane or matrix rich area), and eventually fibre breakage at the tensile face. Whilst failure at the compressive side was observed to be dominated by fibre buckling, kinking and splitting, that at the tensile side exhibited shear delamination and fibre breakage.

The hybrid effect was clearly noted to have a larger effect when the hybrid ratio was small and this was attributed to the relative position of the GF/Ep layer(s) with respect to the neutral plane. In contrast to this, the elastic modulus appeared to obey the rule of mixtures equation with a decreasing trend following substitution of the lower modulus glass fibres.

## REFERENCES

- [1] S. C. Khatri and M. J. Koczak, "Thick-section AS4-graphite/E-glass/PPS hybrid composites: Part II. Flexural response," *Composites Science and Technology*, vol. 56, pp. 473-482, 1996.
- [2] I. J. Davies, H. Hamada, and M. Shibuya, "Compressive and flexural strength of polymer composites containing a mixture of carbon and silicon carbide fibres: Part 1 - Flexural properties," in *T. Tanimoto and T. Morii (editors): Proceedings of the 6th Japan International SAMPE Symposium*, Tokyo, Japan, October 26-29, 1999, pp. 571-574, Japan Chapter of SAMPE, Tokyo, Japan.
- [3] D. Liu and Sudarisman, "Photoelastic study of fully-stressed composite beams," in *Proceedings of the 1995 Spring Conference, Society for*

- Experimental Mechanics*, Grand Rapids, MI, U.S.A., June 12-14, 1995, pp. 861-866.
- [4] Sudarisman, B. de San Miguel, and I. J. Davies, "Failure mechanism of unidirectional hybrid FRP composites containing carbon and E-glass fibres subjected to three-point bend loading," in *Proceedings of the International Conference on Materials and Metallurgical Engineering 2009*, 24-25 June, Surabaya, Indonesia, 2009, pp. FA 5-8.
  - [5] Sudarisman and I. J. Davies, "Flexural failure of unidirectional hybrid fibre-reinforced polymer FRP) composites containing different grades of glass fibre," *Advanced Materials Research*, vol. 41-42, pp. 357-362, 2008.
  - [6] P.-O. Hagstrand, F. Bonjour, and J.-A. E. Manson, "The influence of void content on the structural flexural performance of unidirectional glass fibre reinforced polypropylene composites," *Composites Part A: Applied Science and Manufacturing*, vol. 36, pp. 705-714, 2005.
  - [7] Z. Zheng and J. J. Engblom, "Computational and experimental characterization of continuously fiber reinforced plastic extrusions: Part II - Long-term flexural loading," *Journal of Reinforced Plastics and Composites*, vol. 23, pp. 799-810, 2004.
  - [8] Z. Zheng and J. J. Engblom, "Computational and experimental characterization of continuously fiber reinforced plastic extrusions: Part I - Short-term flexural loading," *Journal of Reinforced Plastics and Composites*, vol. 23, pp. 777-793, 2004.
  - [9] M. Ramulu, P. B. Stickler, N. S. McDevitt, I. P. Datar, D. Kim, and M. G. Jenkins, "Influence of processing methods on the tensile and flexure properties of high temperature composites," *Composites Science and Technology*, vol. 64, pp. 1763-1772, 2004.
  - [10] "ASTM D3410 Standard test method for compressive properties of polymer matrix composite materials with unsupported gage section by shear loading," in *Annual Book of ASTM Standard*. vol. Vol. 03.01? West Conshohocken, PA, USA: ASTM Int., 2005, pp. 128-144.
  - [11] A. R. Bunsell and B. Harris, "Hybrid carbon and glass fibre composites," *Composites*, vol. 5, pp. 157-164, 1974.
  - [12] R. F. Dickson, G. Fernando, T. Adam, H. Reiter, and B. Harris, "Fatigue behaviour of hybrid composites," *Journal of Materials Science (Historical Archive)*, vol. 24, pp. 227-233, 1989.
  - [13] S. Sivashanker, N. A. Fleck, and M. P. F. Sutcliffe, "Microbuckle propagation in a unidirectional carbon fibre-epoxy matrix composites," *Acta Materials*, vol. 44, pp. 2581-2590, 1996.
  - [14] "ImageJ, Image Processing and Analysis in Java," Bethesda, MD, U.S.A., National Institute of Health: <http://rsb.info.nih.gov/ij/>, Accessed date: November 12<sup>th</sup>, 2005.



- [15] S. H. Lee, and A. M. Waas, "Compressive response and failure of fiber reinforced unidirectional composites," *International Journal of Fracture*, vol. 100(3), pp. 275-306, 1999.
- [16] C. J. Creighton and T. W. Clyne, "The compressive strength of highly-aligned carbon-fibre/epoxy composites produced by pultrusion," *Composites Science and Technology*, vol. 60(4), pp. 525-533, 2000.
- [17] I. J. Davies, H. Hamada, and M. Shibuya, "Flexural and compressive properties of polymer matrix composites containing a mixture of carbon and silicon carbide fibres: Part 2 - Compression," in *H. Fukuda, T. Ishikawa, Y. Kogo (editors): Proceedings of the 9th US-Japan conference on composite materials*, Mishima, Shizuoka, Japan, July 3-4, 2000, pp. 373-374, Japan Society for Composite Materials, Tokyo, Japan.
- [18] C. S. Yerramalli and A. M. Waas, "A nondimensional number to classify composite compressive failure," *Journal of Applied Mechanics*, vol. 71, pp. 402-408, 2004.
- [19] C. Wonderly, J. Grenestedt, G. Fernlund, and E. Cepus, "Comparison of mechanical properties of glass fiber/vinyl ester and carbon fiber/vinyl ester composites," *Composites Part B: Engineering*, vol. 36, pp. 417-426, 2005.
- [20] N. Oya and D. J. Johnson, "Direct measurement of longitudinal compressive strength in carbon fibres," *Carbon*, vol. 37, pp. 1539-1544, 1999.
- [21] N. Oya and D. J. Johnson, "Longitudinal compressive behaviour and microstructure of PAN-based carbon fibres," *Carbon*, vol. 39, pp. 635-645, 2001.
- [22] P. K. Mallick, *Fibre-reinforced composites: materials, manufacturing and design*. New York: Marcel Dekker, p. 25, 1988.
- [23] G. Belingardi, M. P. Cavatorta, and C. Frasca, "Bending fatigue behavior of glass-carbon/epoxy hybrid composites," *Composites Science and Technology, Experimental Techniques and Design in Composite Materials*, vol. 66, pp. 222-232, 2006.
- [24] T. Keller and M. Schollmayer, "Plate bending behavior of a pultruded GFRP bridge deck system," *Composite Structures*, vol. 64, pp. 285-295, 2004.
- [25] Y. A. Khalid, F. A. Ali, B. B. Sahari, and E. M. A. Saad, "Performance of composite I-beams under axial compression and bending load modes," *Materials & Design*, vol. 26(2), pp. 127-135, 2005.
- [26] O. Sayman, M. Uyaner, and N. Tarakcioglu, "Elastic-plastic stress analysis in a thermoplastic composite cantilever beam loaded by bending moment," *Journal of Reinforced Plastics and Composites*, vol. 21, pp. 175-192, 2002.
- [27] G. Zhou and J. Hood, "Design, manufacture and evaluation of laminated carbon/epoxy I-beams in bending," *Composites Part A: Applied Science and Manufacturing*, vol. 37, pp. 506-517, 2006.

- [28] Sudarisman and I. J. Davies, "The effect of processing parameters on the flexural properties of unidirectional carbon fibre-reinforced polymer (CFRP) composites," *Materials Science and Engineering: A*, vol. 498, pp. 65-68, 2008.
- [29] Sudarisman and I. J. Davies, "Influence of compressive pressure, vacuum pressure, and holding temperature applied during autoclave curing on the microstructure of unidirectional CFRP composites," *Advanced Materials Research*, vol. 41-42, pp. 323-328, 2008.
- [30] "ASTM D790-07 Standard test method for flexural properties of unreinforced and reinforced plastic and electrical insulating materials by three-point bending," in *Annual Book of ASTM Standard*. vol. Vol. 08.01 West Conshohocken, PA, USA: ASTM Int., 2005.
- [31] S. H. Lee, C. S. Yerramalli, and A. M. Waas, "Compressive splitting response of glass-fiber reinforced unidirectional composites," *Composites Science and Technology*, vol. 60, pp. 2957-2966, 2000.
- [32] I. J. Davies and H. Hamada, "Flexural properties of a hybrid composite containing carbon and silicon carbide fibres," *Advanced Composite Materials*, vol. 10, pp. 77-96, 2001.
- [33] C. S. Yerramalli and A. M. Waas, "Compressive splitting failure of composites using modified shear lag theory," *Int J. Fracture*, vol. 115, pp. 27-40, 2002.
- [34] C. Nightingale and R. J. Day, "Flexural and interlaminar shear strength properties of carbon fibre/epoxy composites cured thermally and with microwave radiation," *Composites Part A: Applied Science and Manufacturing*, vol. 33, pp. 1021-1030, 2002.
- [35] C. Reder, D. Loidl, S. Puchegger, D. Gitchthaler, H. Paterlik, K. Kromp, G. Khatibi, A. Betzwar, P. Zimprich, and B. Weiss, "Non-contacting strain measurement of ceramic and carbon single fibres by using the laser speckle method," *Composites Part A: Applied Science and Manufacturing*, vol. 34, pp. 1029-1033, 2003.
- [36] "Program Fact Sheet BOEING 787 Dreamliner," Seattle: The Boeing Company, <http://www.boeing.com/commercial/787family/programfacts.html>, Accessed date: 14<sup>th</sup> September 2008.
- [37] A. Jacob, "The popularity of carbon fibre," *Reinforced Plastics*, vol. 50, pp. 22-24, 2006.
- [38] "GRAFIL: Worldwide leader in carbon fiber manufacturing," Sacramento, CA, USA: Gafil, Inc.
- [39] *Hexcel Tow<sup>TM</sup> IM7 (5000) Carbon Fiber Product Data*. Stamford, CT, U.S.A.: Hexcel Corporation, [http://www.hexcel.com/NR/rdonlyres/BD219725-D46D-4884-A3B3-AFC86020EFDA/0/HexTow\\_IM7\\_5000.pdf](http://www.hexcel.com/NR/rdonlyres/BD219725-D46D-4884-A3B3-AFC86020EFDA/0/HexTow_IM7_5000.pdf), Accessed date: November 10<sup>th</sup>, 2008.
- [40] J. Z. Zhao, S. V. Hoa, X. R. Xiao, and I. Hanna, "Global-Local approaches using partial hybrid finite element analysis of stress field in

- laminated composites with mid-plane delamination under bending," *Journal of Reinforced Plastics and Composites*, vol. 18, pp. 827-843, 1999.
- [41] Sudarisman, I. J. Davies, and H. Hamada, "Compressive failure of unidirectional hybrid fibre-reinforced epoxy composites containing carbon and silicon carbide fibres," *Composites Part A: Applied Science and Manufacturing*, vol. 38, pp. 1070-1074, 2007.
  - [42] Sudarisman, B. de San Miguel, and I. J. Davies, "The Effect of Partial Substitution of E-glass Fibre for Carbon Fibre on the Mechanical Properties of CFRP Composites," in *Proceedings of the International Conference on Materials and Metallurgical Engineering 2009*, 24-25 June, Surabaya, Indonesia, 2009, pp. MI 116-119.
  - [43] N. Oya and H. Hamada, "Effect of reinforcing fibre properties on various mechanical behavior of unidirectional carbon/epoxy laminates," *Sci. Eng. Compos. Mater.*, vol. 5, pp. 105-129, 1996.
  - [44] M. Shioya and M. Nakatani, "Compressive strengths of single carbon fibres and composite strands," *Composites Science and Technology*, vol. 60, pp. 219-229, 2000.
  - [45] M. G. Phillips, "Composition parameters for hybrid composite materials," *Composites*, vol. 12, pp. 113-116, 1981.
  - [46] S. Deng, L. Ye, and Y.-W. Mai, "Influence of fibre cross-sectional aspect ratio on mechanical properties of glass fibre/epoxy composites I. Tensile and flexure behaviour," *Composites Science and Technology*, vol. 59, pp. 1331-1339, 1999.
  - [47] M. D. Gilchrist, A. J. Kinloch, F. L. Matthews, and S. O. Osiyemi, "Mechanical performance of carbon-fibre- and glass-fibre-reinforced epoxy I-beams: I. Mechanical behaviour," *Composites Science and Technology*, vol. 56(1), pp. 37-53, 1996.
  - [48] "PYROFIL<sup>TM</sup> - TR50S-12K," Sacramento, CA, USA: Grafil, Inc., 2008.
  - [49] "System Information: OC<sup>TM</sup> Advantex<sup>®</sup> 162A," Toledo, OH, U.S.A.: OWENS CORNING: <http://www.owenscorningchina.com/upload/File/591228664.pdf> Accessed date: November 22<sup>th</sup>, 2008.
  - [50] I. M. Daniel, H.-M. Hsiao, and S.-C. Wooh, "Failure mechanisms in thick composites under compressive loading," *Composites Part B: Engineering*, vol. 27, pp. 543-552, 1996.
  - [51] P. J. Callus, A. P. Mouritz, M. K. Bannister, and K. H. Leong, "Tensile properties and failure mechanisms of 3D woven GRP composites," *Composites Part A: Applied Science and Manufacturing*, vol. 30, pp. 1277-1287, 1999.
  - [52] J. M. Gere, *Mechanics of Materials*, 2nd ed. Southbank, VIC, Australia: Thomson, 2004.

- [53] T. J. Kang, S. J. Shin, K. Jung, and J. K. Park, "Mechanical, thermal and ablative properties of interply continuous/spun hybrid carbon composites," *Carbon*, vol. 44, pp. 833-839, 2006.
- [54] M. Wang, Z. Zhang, and Z. Sun, "The Hybrid Model and Mechanical Properties of Hybrid Composites Reinforced with Different Diameter Fibers," *Journal of Reinforced Plastics and Composites*, vol. 28, pp. 257-264, 2009.
- [55] Y. Li, X. J. Xian, C. L. Choy, M. Guo, and Z. Zhang, "Compressive and flexural behavior of ultra-high-modulus polyethylene fiber and carbon fiber hybrid composites," *Composites Science and Technology*, vol. 59, pp. 13-18, 1999.

Every reasonable effort has been made to acknowledge the owners of copyright materials. I would be pleased to hear from any copyright owner who has been omitted or incorrectly acknowledged.

## **CHAPTER 7**

# **CONCLUSION AND RECOMMENDATION**

### **7.1. CONCLUSIONS**

Three different fibre combinations, *i.e.*, different types of glass fibre (E-glass and S2-glass), different grades of carbon fibre (IM7 and TR50S), and combination of carbon fibre and glass fibre, were utilised in order to manufacture unidirectional hybrid fibre-reinforced polymer matrix composites that were then tested under three-point bend loading in accordance with Procedure A of the ASTM D790-07 standard. Prior to producing hybrid fibre composite plate panels, the equipment required to manufacture and test the composites (*e.g.*, autoclave, oven, prepreg frame, test jig, *etc.*) was first designed and developed by the author. The next step of the research was to investigate the influence of processing parameters on the mechanical properties and void content of the composites and determine an optimum processing route. Once this had been achieved, the compressive mechanical properties of the parent composite materials (that would be later used to produce hybrid composite materials) were evaluated. Only after this had been achieved were the flexural properties investigated for three groups of hybrid composite. The following main conclusions were reached from this work.

#### ***7.1.1. Fabrication Parameters Optimisation***

Five processing parameters in the fabrication procedure for the epoxy matrix composites were optimised as follows: (i) epoxy concentration within the epoxy/acetone solution used for fibre embedment, (ii) mechanical compressive pressure applied onto the preform under curing, (iii) vacuum pressure inside the

curing chamber, (iv) dwell time during curing, and (v) holding temperature for curing. The criteria utilised to determine the optimum conditions were the maximum fibre content, minimum void content, maximum flexural strength, and highest flexural modulus. The following values were found to be the optimum conditions.

1. Epoxy concentration,  $C_e \sim 50$  wt%
2. Compressive pressure,  $p_c \sim 1.00$  MPa
3. Vacuum pressure,  $p_v \sim 0.035$  MPa
4. Dwelling time,  $t \sim 30$  minutes
5. Holding temperature,  $T \sim 120$  °C.

### ***7.1.2. Compressive Mechanical Properties of Parent Composite Materials***

Compressive test results demonstrated an approximately linear stress-strain relationship to the point of failure. The highest *compressive strength* was achieved by the S2-glass/epoxy specimens and then followed by E-glass/epoxy, IM7/epoxy, and TR50S/epoxy. This result was found to be in good agreement with previously reported data [1-3]. The higher compressive-to-tensile strength ratio for the glass fibres was attributed to their amorphous crystalline structure [4, p. 25]. Contrary to this, the CFRP composite samples demonstrated higher *compressive moduli* in comparison with those of the GFRP composite samples. The differences in compressive strength and compressive modulus amongst these parent composite materials led to the conclusion that potential existed to improve the flexural properties of a lower compressive strength FRP composite through incorporation of higher compressive strength fibre in order to produce a hybrid FRP system.

### ***7.1.3. Hybrid FRP Composites Containing Different Types of Glass Fibres***

A considerable positive hybrid effect was noticed for flexural strength and flexural modulus, particularly for longer span samples. Specimens tested at  $S/d = 32$  and  $S/d = 64$  demonstrated a significant increase in flexural properties from the addition of a relatively small amount of S2-glass fibre to the E-glass composite.

The most remarkable increase in flexural strength and flexural modulus (13.7% to 14.7% and 8.7% to 8.8%, respectively) was noted when the hybrid ratio was small ( $r_h \sim 0.2$ ) and this was attributed to the relative position of the stronger S2-glass/epoxy prepreg layer with respect to the neutral axis, *i.e.*, the S2-glass was placed at the compressive face of the specimen. Shear failure exhibited by specimens tested at  $S/d = 16$  was thought responsible for the absence of a hybrid effect as the shear strength (in unidirectional composites) within the plane of failure is matrix dominated and relatively insensitive to fibre properties. It was thus determined that a  $S/d$  ratio of at least 32 was required in order to promote flexural failure (as opposed to shear failure). In addition, it was also noticed that flexural properties increased with the increase of  $S/d$  ratio and this was credited to the change in failure mode from shear failure to flexural failure.

Significant increases (up to 20.8%) in flexural strength were observed for a substitution of up to ~60% of S2-glass fibre for E-glass fibre. Unlike that observed in flexural strength, the flexural modulus was found to increase for up to 100% of fibre replacement. In contrast to this, the energy absorption capacity up to the point of maximum stress,  $\gamma_{\max}$ , appeared not to increase with hybridisation, although a significant increase in  $\gamma_{\max}$  was noted as  $S/d$  increased from 16 to 32 and then to 64. This increase in  $\gamma_{\max}$  was explained in terms of the increase in flexural strength, increase in strain at maximum stress and, more importantly, by the increase in  $S/d$ . Therefore, hybrid composites may play a role in increasing flexural performance through the incorporation of relatively small amounts of high strength fibres.

#### ***7.1.4. Hybrid FRP Composites Containing Different Grades of Carbon Fibres***

A general trend noted for this group of hybrid composites was that the flexural strength, flexural modulus and storage energy capacity to maximum stress did not demonstrate any synergistic effect, *i.e.*, hybrid effect. Although a replacement of stronger and stiffer IM7 carbon fibre for TR50S carbon fibre resulted in a slight increase in the flexural properties, it appeared to only obey the rule of mixtures. The absence of a hybrid effect for this case may be mainly

caused by the internal stresses generated at the compressive face due to the increase in flexural modulus being higher than the respective increase in flexural strength introduced by the stronger fibre. Therefore, this suggests that a fibre combining a lower modulus and higher compressive strength is needed in order to optimise the improvement of composite beam flexural properties through the production of hybrid composite beams.

Although no hybrid effect was noted, the flexural properties did increase as the span-to-depth ( $S/d$ ) ratio during testing was increased. This increase was attributed to the increase in flexural strength and, more importantly, the decrease in the ratio of shear stress to normal stress as  $S/d$  increased. Specimens tested at  $S/d$  ratios of at least 32 failed due to fibre buckling and kinking whereas those tested at  $S/d = 16$  failed in a shear mode along their neutral plane. From this it was suggested that a minimum value of  $S/d = 32$  is sufficient in order to promote flexural failure.

#### ***7.1.5. Hybrid FRP Composites Containing Glass and Carbon Fibres***

A positive hybrid effect for this group of hybrid composites (TR50S carbon and E-glass) was noted for the cases of flexural strength, strain at maximum stress (for most of the hybrid configurations), and specific energy storage capacity at maximum stress (apart from the  $S/d = 16$  specimens). The most significant increase in flexural strength due to hybridisation (26.6%, 46.5% and 33.8% for  $S/d = 16, 32$  and  $64$ , respectively) was demonstrated by replacement of a single layer of fibre (~25 vol.%) at the compressive face of the specimen. In contrast to this, flexural modulus was seen to obey the rule of mixtures, *i.e.*, flexural modulus decreased with increasing E-glass fibre content due to the elastic modulus of the E-glass fibre being significantly lower than that of the TR50S carbon fibre. In addition to this, the flexural strength was found to increase with increasing span-to-depth ratio due to the reduced influence of shear stresses.

Optical micrographs revealed that failure was initiated at the compressive face in the form of fibre buckling followed by kink band formation, shear cracking in weaker regions (either the neutral plane or matrix rich areas), and



eventually fibre breakage at the tensile face. Whilst failure at the compressive side was observed to be dominated by fibre buckling, kinking and splitting, that at the tensile side exhibited shear delamination and fibre breakage.

Considering the result of the three different hybrid combinations under investigation, a hybrid effect would be most likely to be obviously observed when the fibre introduced at the compressive side possessed a significantly lower modulus combined with significantly higher compressive strength, as demonstrated by the hybrid TR50S carbon - E-glass FRP composites. Such a result may be attributed to the decrease of internal stresses generated at the compressive side due to the decrease in compressive modulus being relatively small in comparison with the increase of compressive strength of the fibre introduced at this side. Slightly stronger fibres combined with a higher compressive modulus, when introduced at the compressive face, results in the absence of a hybrid effect as was noted for the case of hybrid CFRP composites containing different grades of carbon fibre. In this case, the increase in compressive strength of the fibre introduced at the compressive side was not sufficient to suppress the increase of internal stresses generated at this side due to the increase in compressive modulus of the introduced fibre. In between these two cases was the situation of the hybrid GFRP composites that contained different types of glass fibre where a hybrid effect was observed but was not as obvious as the case for the hybrid carbon-glass FRP composites.

The span-to-depth ratio,  $S/d$ , was noted to influence flexural properties with the flexural properties increasing as the  $S/d$  ratio increased. In addition,  $S/d = 32$  was determined to be sufficient in order to produce flexural failure as opposed to shear failure that had been noted for shorter span beams, *i.e.*, smaller  $S/d$  values.

## **7.2. RECOMMENDATION FOR FUTURE WORK**

Based on the outcomes of the work contained within this thesis a number of possibilities for further studies concerning the improvement of performance for composite structural members subjected to flexural loading through the

production of hybrid composites using a fully manual hand lay-up procedure were identified.

1. Improvements in quality of the existing manufacturing facilities in the Department of Mechanical Engineering, Curtin University of Technology by employing a more sophisticated control system. For example, fibre orientation and tension control during fibre wrapping in order to produce more accurate fibre orientation and homogeneous fibre tension, in addition to more accurate temperature control in the partial curing stage inside the oven so as to ensure a consistent curing temperature.
2. A study to determine the compressive-to-tensile modulus ratio and compressive-to-tensile strength ratio in order to produce a more significant hybrid effect in a more effective and efficient manner for the production of hybrid FRP composites.
3. Within the elastic limit, the neutral plane of composite beams under progressive loading may be shifted toward the tensile face as the load, *i.e.*, the magnitude of the bending moment, increases. A study to determine the relationship between neutral plane position and bending moment may be useful in helping to solve the problem introduced in point 2 above.
4. The number of fibre types being combined to produce hybrid fibre composites could be extended to more than two in order to optimally harness the property potential of the constituent materials. However, this will undoubtedly be more complex compared to the studies that have thus far been carried out utilising only two different types or grades of fibres.

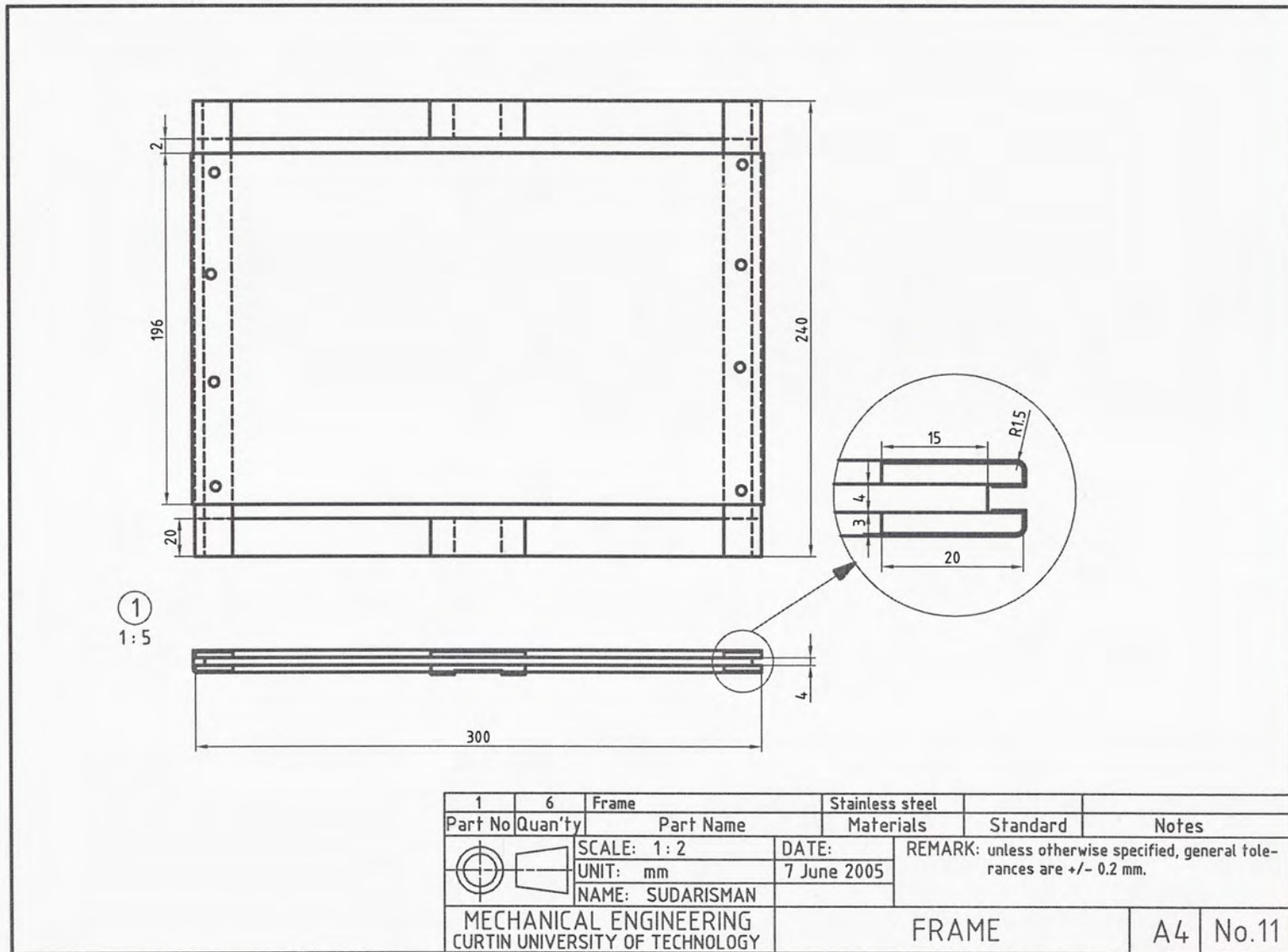
## REFERENCES

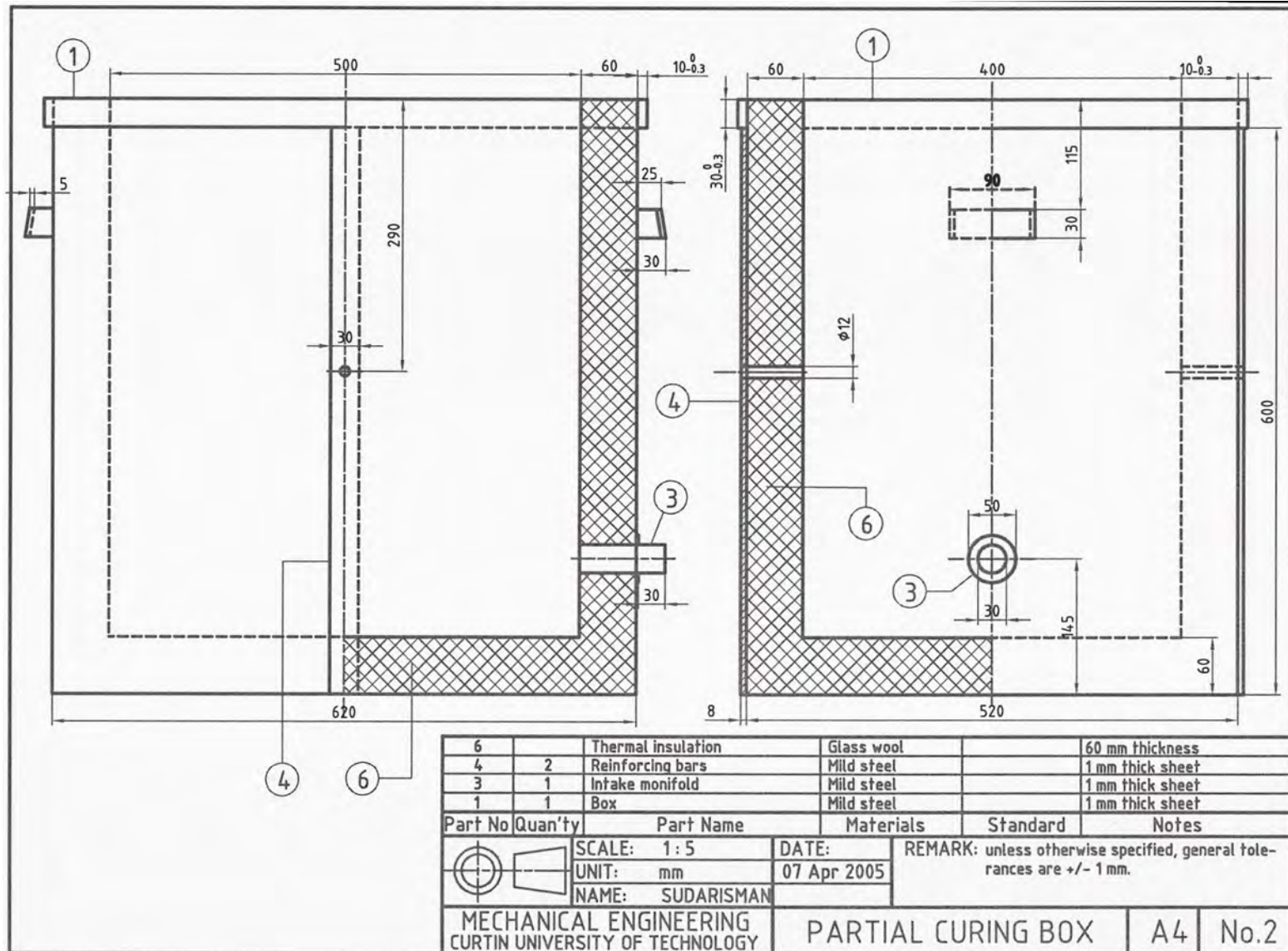
- [1] S. H. Lee, and A. M. Waas, "Compressive response and failure of fiber reinforced unidirectional composites," *International Journal of Fracture*, vol. 100(3), pp. 275-306, 1999.
- [2] C. Wonderly, J. Grenestedt, G. Fernlund, and E. Cepus, "Comparison of mechanical properties of glass fiber/vinyl ester and carbon fiber/vinyl ester composites," *Composites Part B: Engineering*, vol. 36, pp. 417-426, 2005.

- [3] C. S. Yerramalli and A. M. Waas, "A nondimensional number to classify composite compressive failure," *Journal of Applied Mechanics*, vol. 71, pp. 402-408, 2004.
- [4] P. K. Mallick, *Fibre-reinforced composites: materials, manufacturing and design*. New York: Marcel Dekker, p. 25, 1988.
- [5] "ASTM D790-07 Standard test method for flexural properties of unreinforced and reinforced plastic and electrical insulating materials by three-point bending," in *Annual Book of ASTM Standard*. vol. Vol. 08.01 West Conshohocken, PA, USA: ASTM Int., 2005.

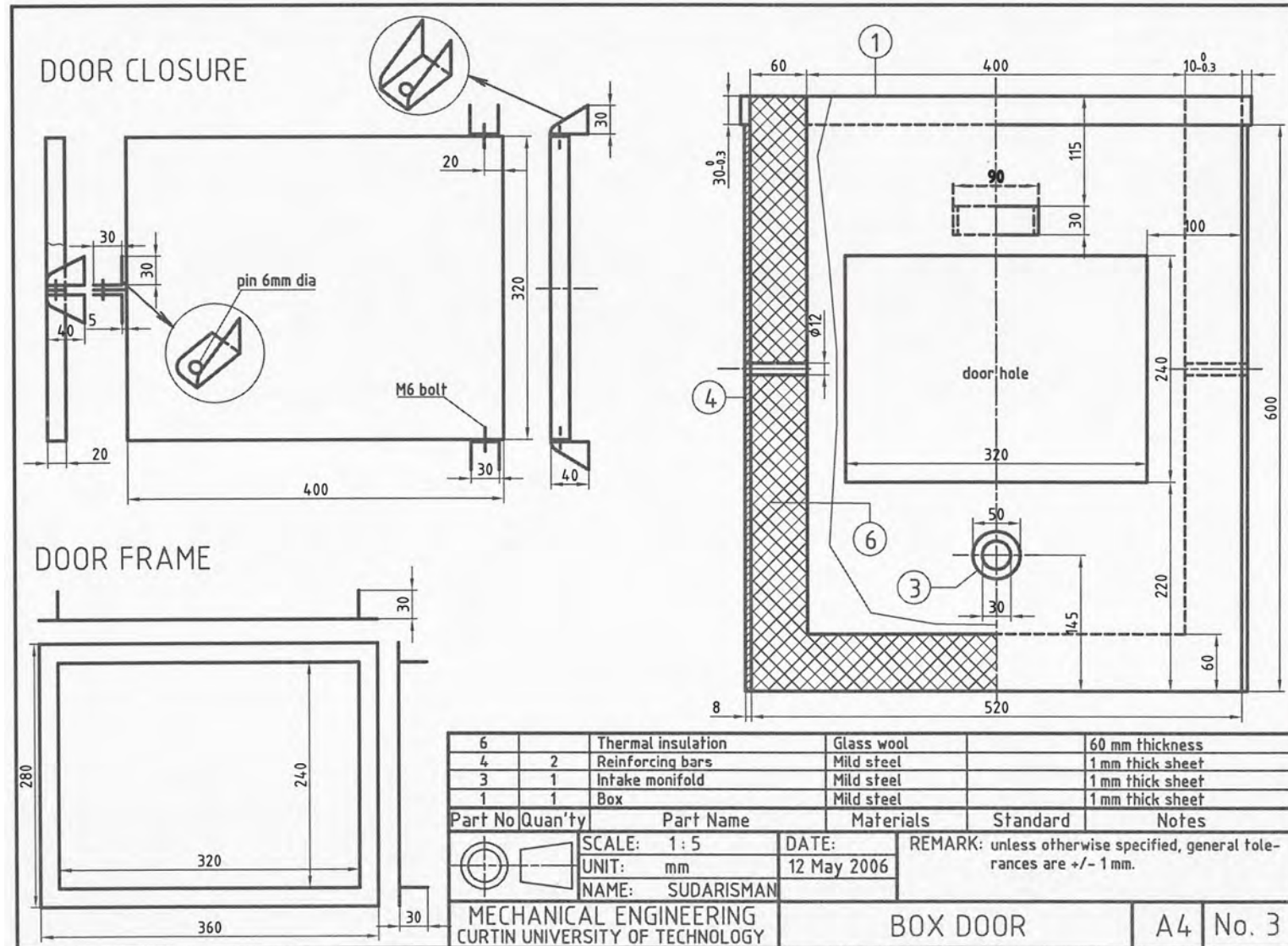
Every reasonable effort has been made to acknowledge the owners of copyright materials. I would be pleased to hear from any copyright owner who has been omitted or incorrectly acknowledged.

**Appendix 1.** Stainless steel frame.

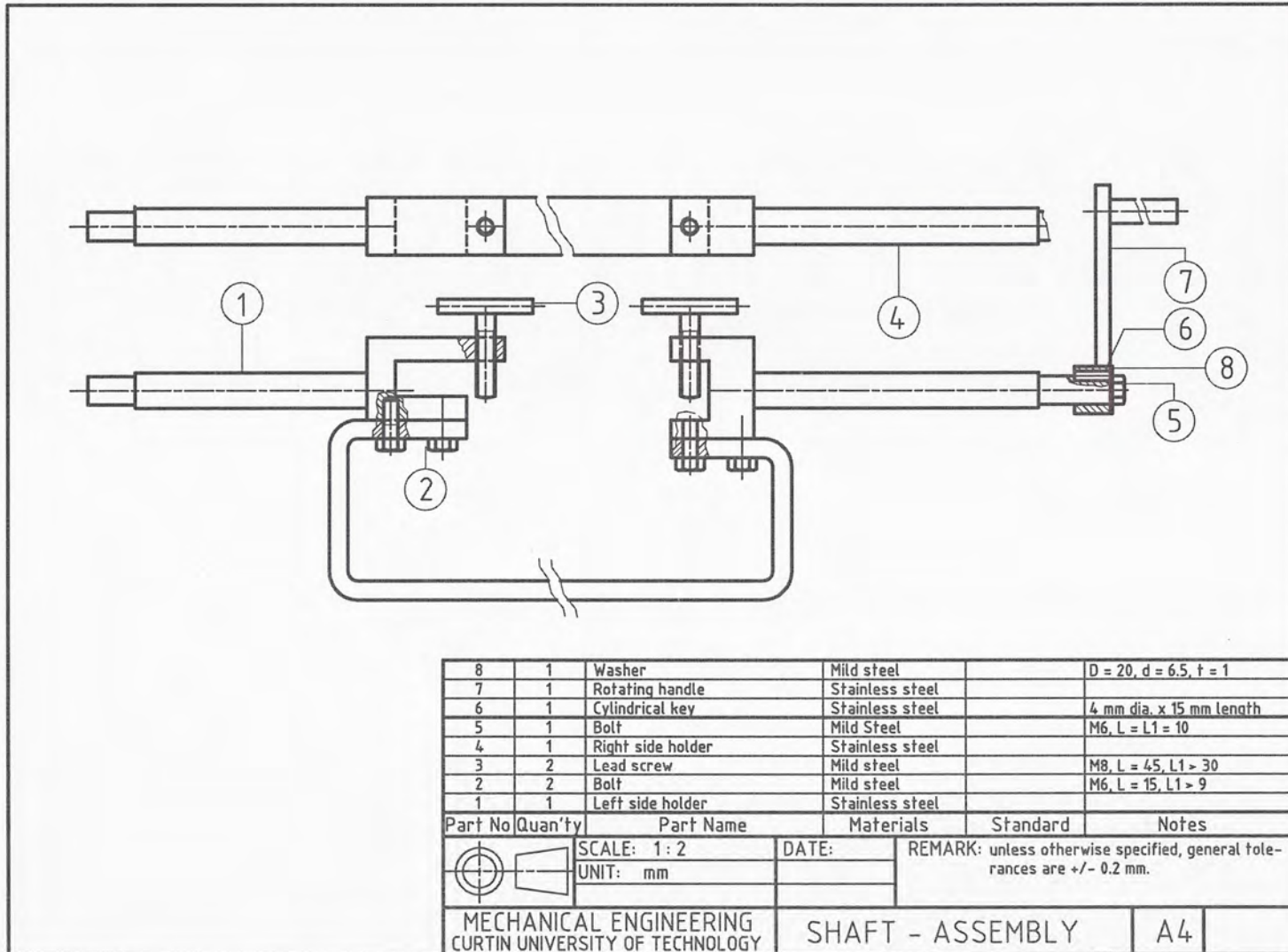


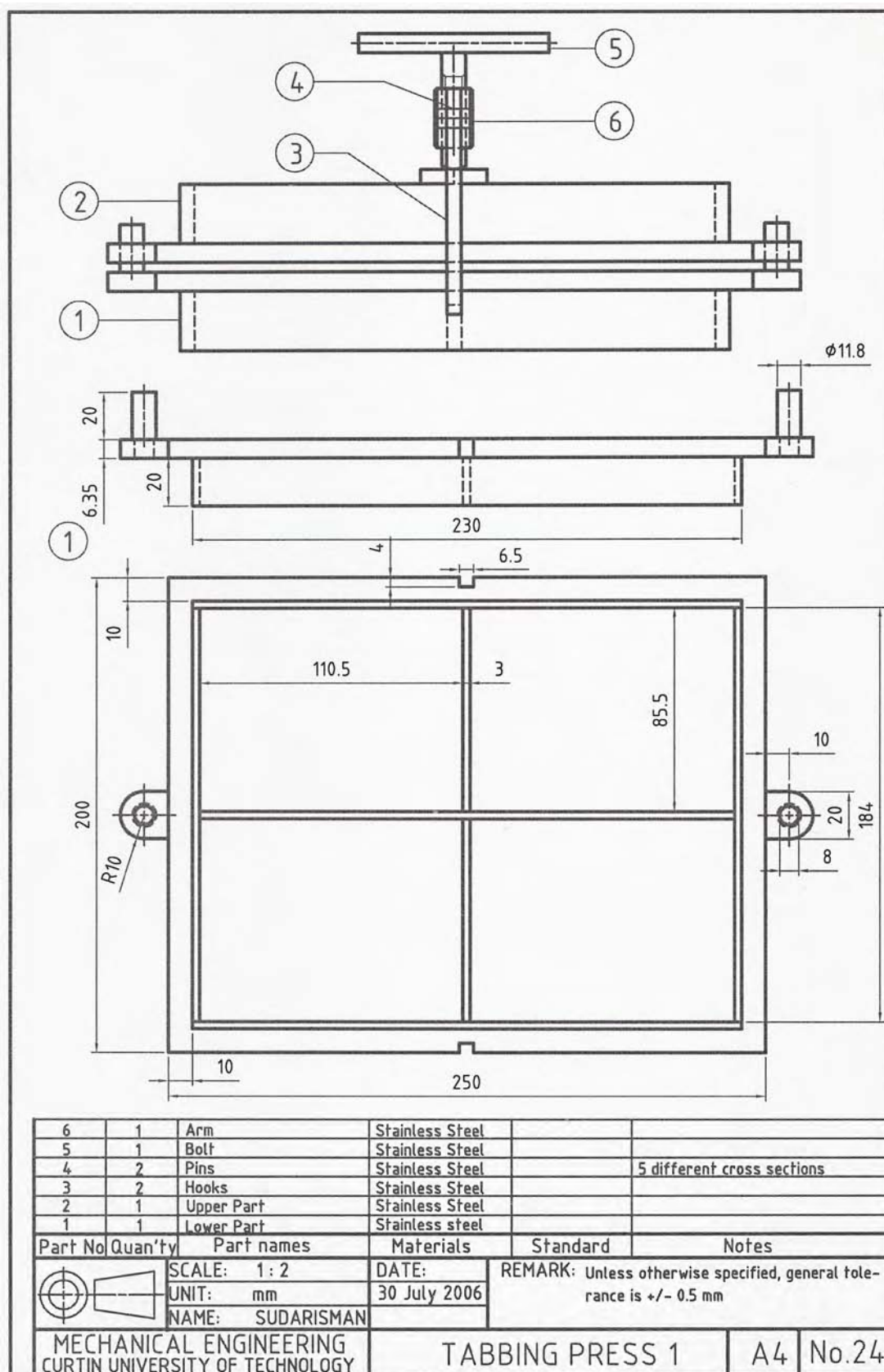
**Appendix 2.** Oven.

**Appendix 2.** Oven (Continuation)

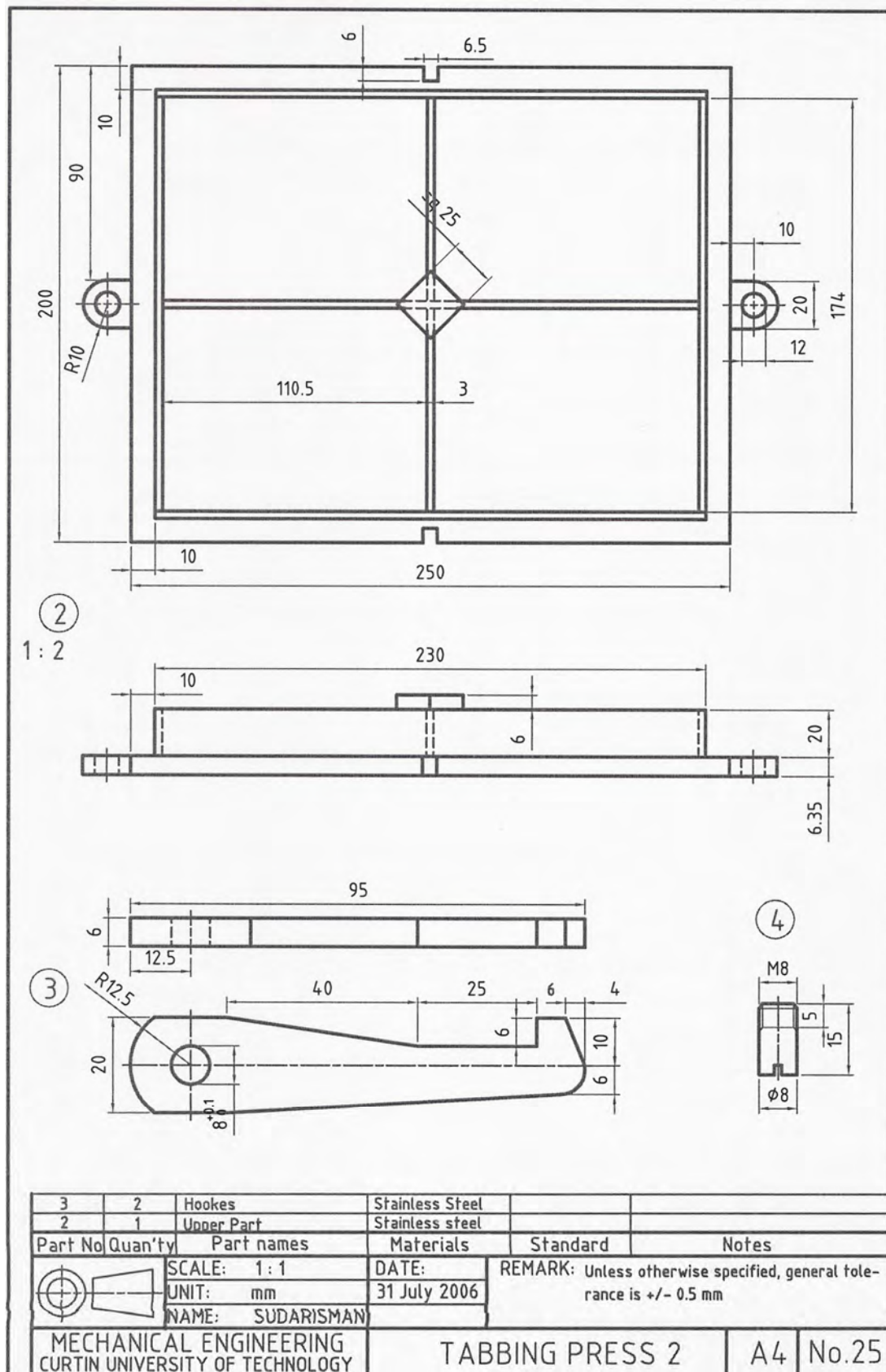




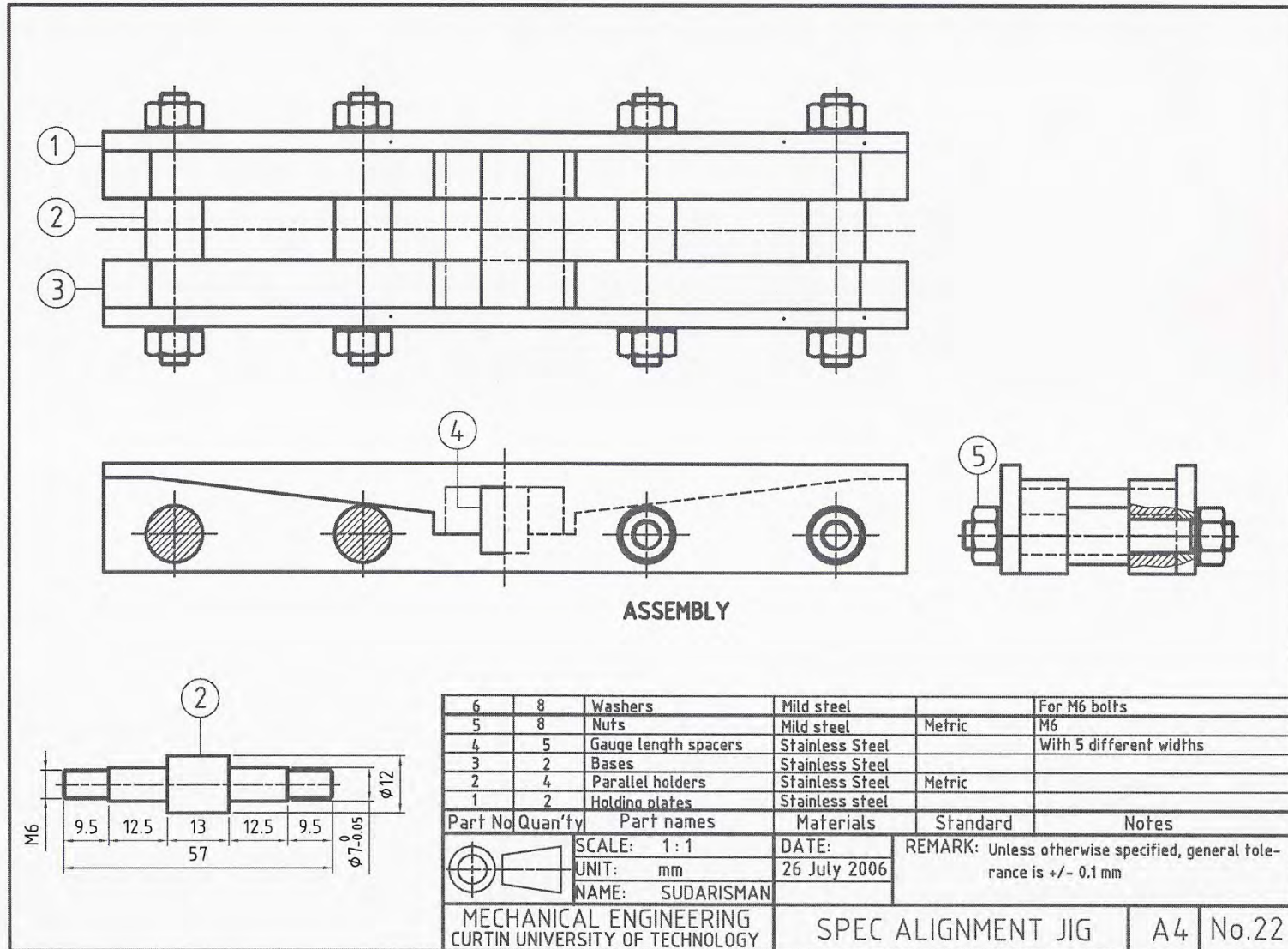
**Appendix 2.** Oven (Continuation)

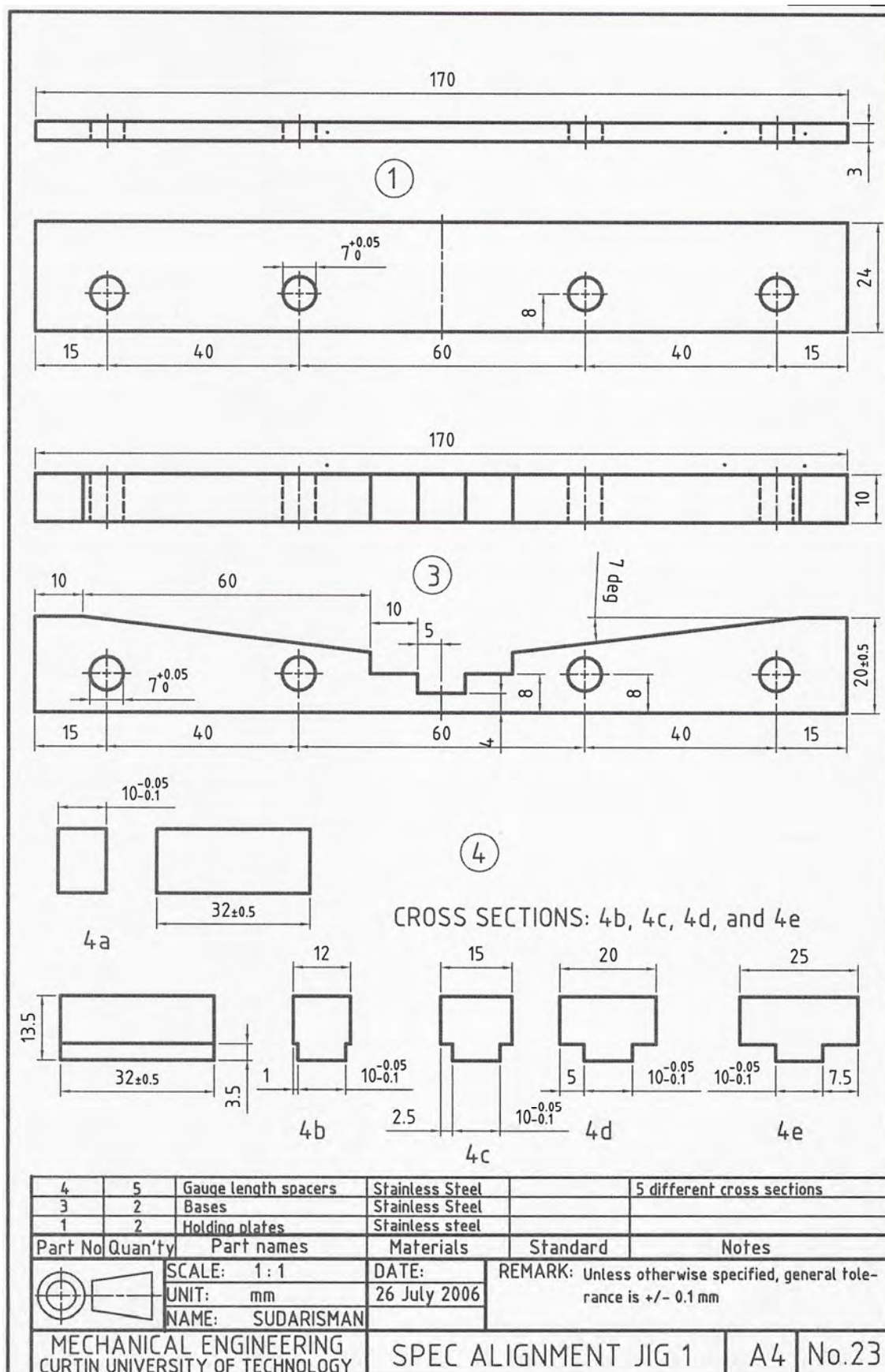
**Appendix 3.** Tabbng Press



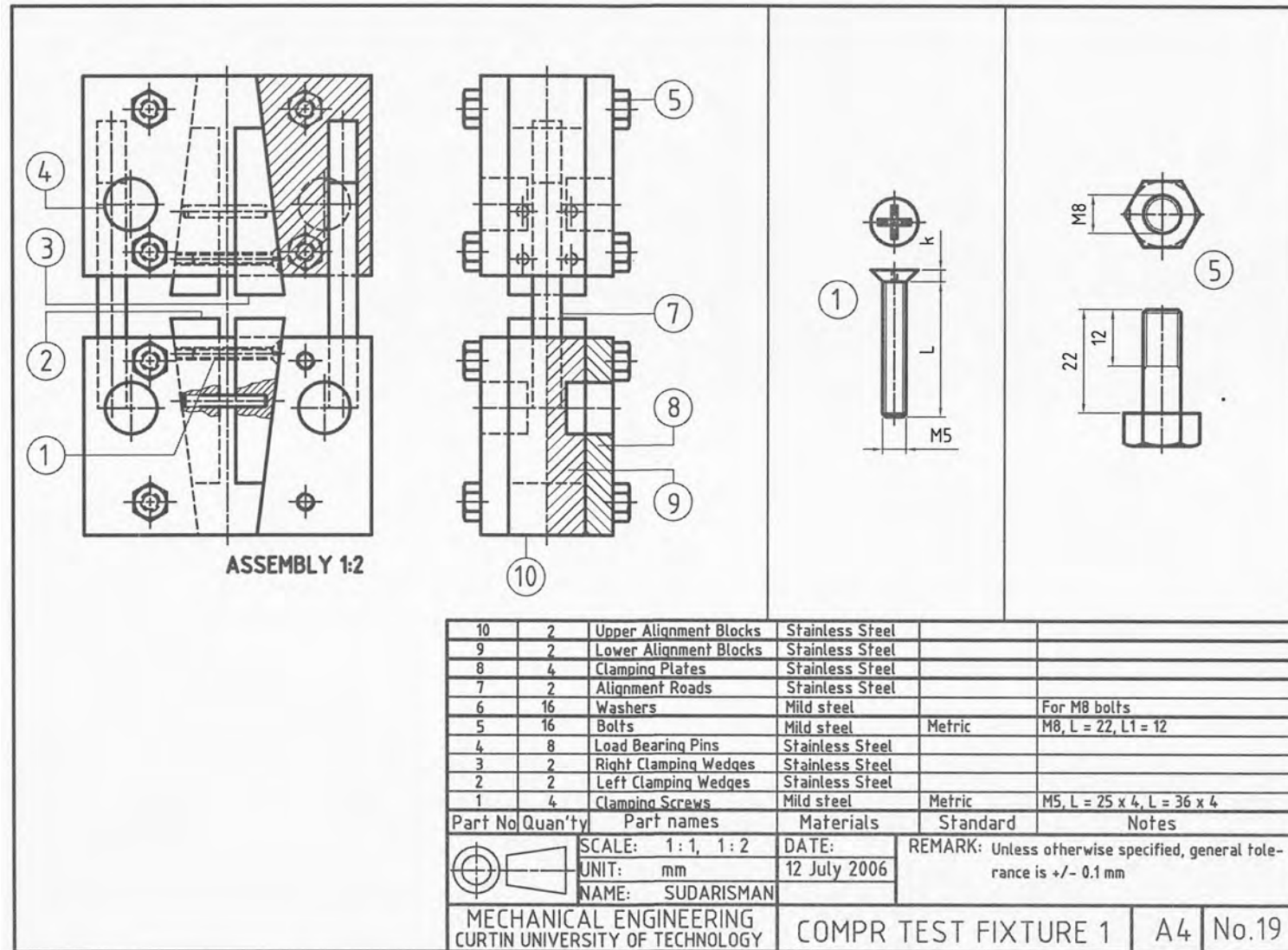
**Appendix 3.** Tabbing Press (*Continuation*)

**Appendix 4.** Alignment Jig

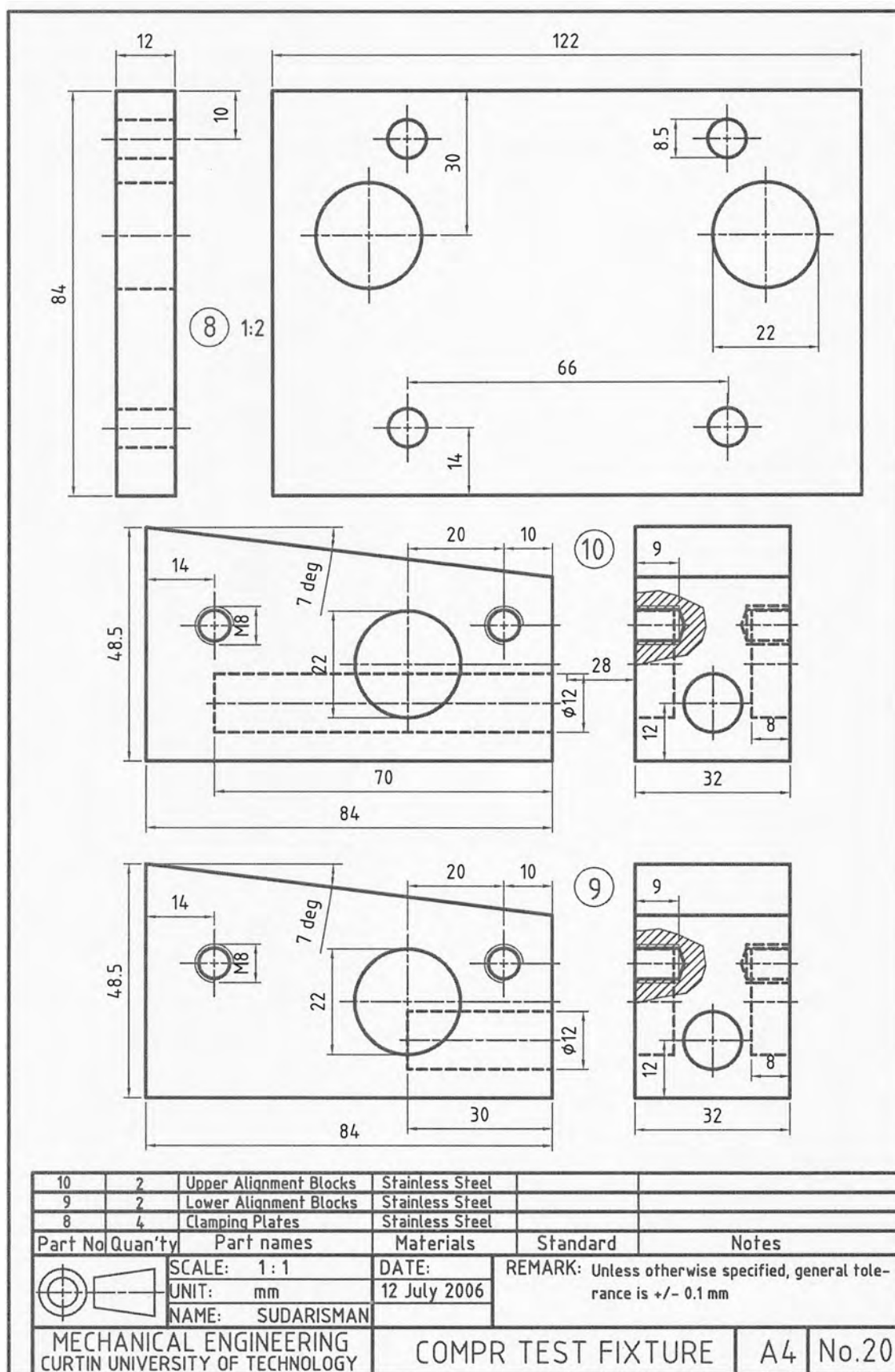


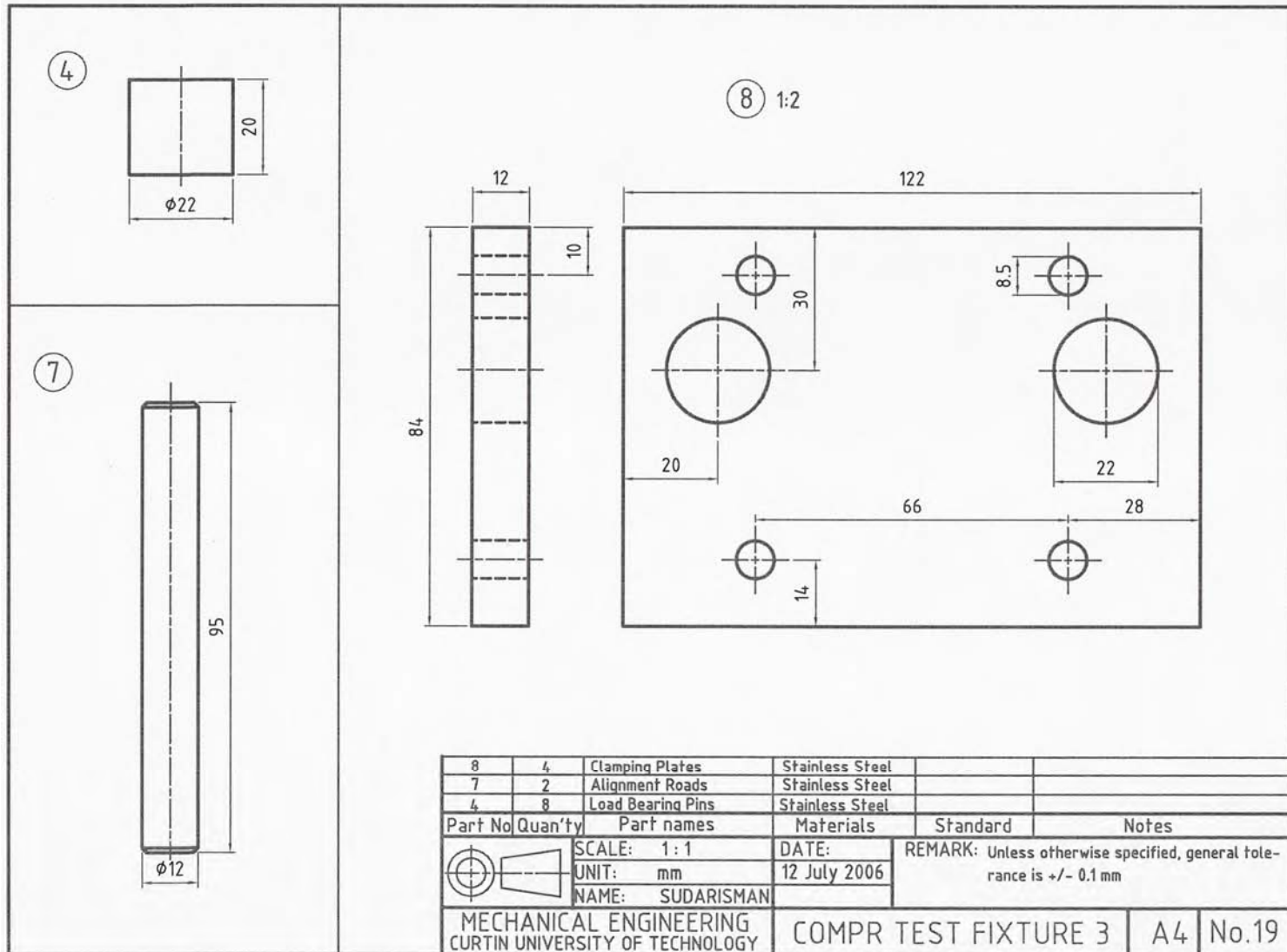
**Appendix 4.** Alignment Jig (*Continuation*)

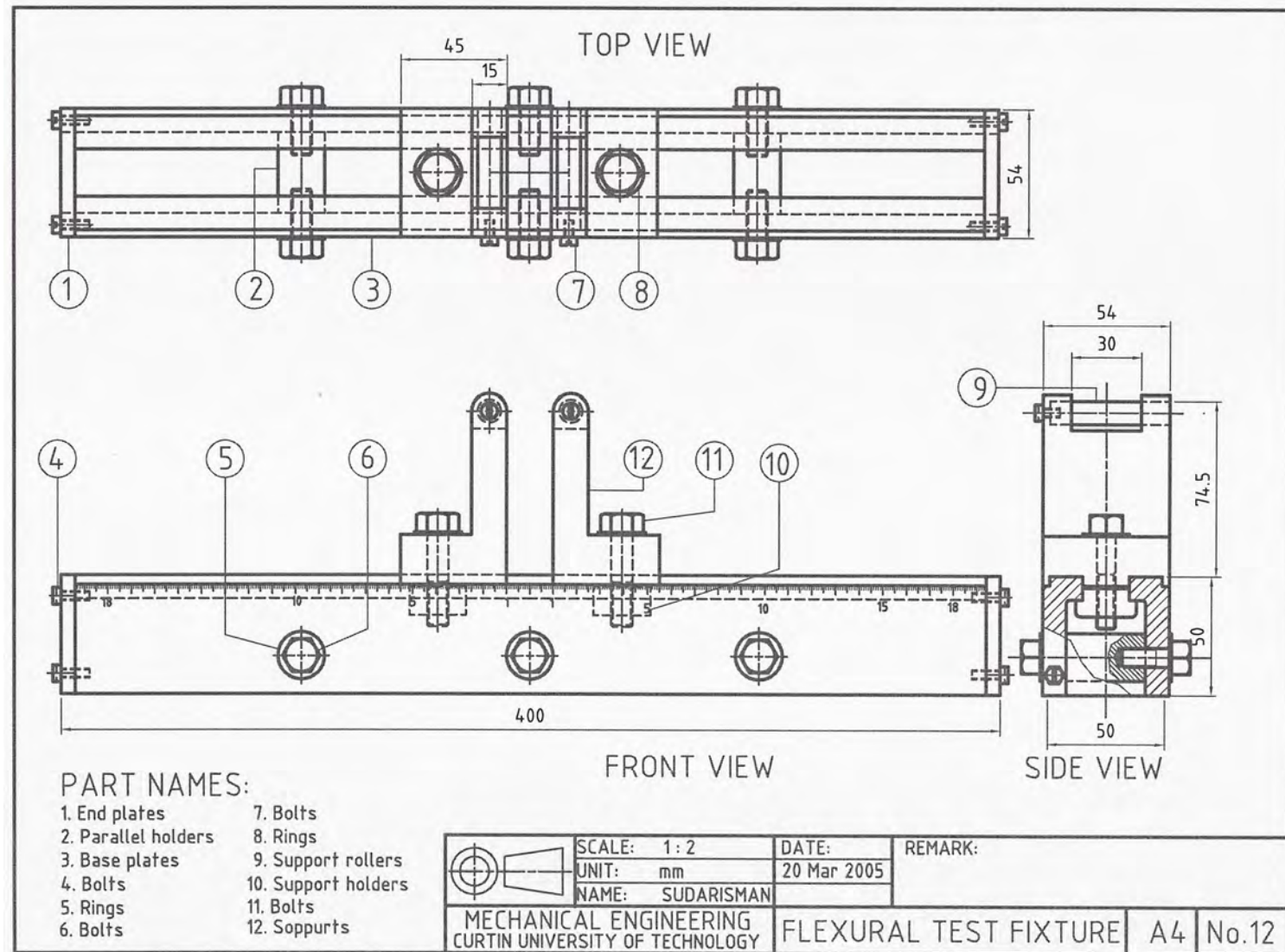
### Appendix 5. Compressive Test Fixtures

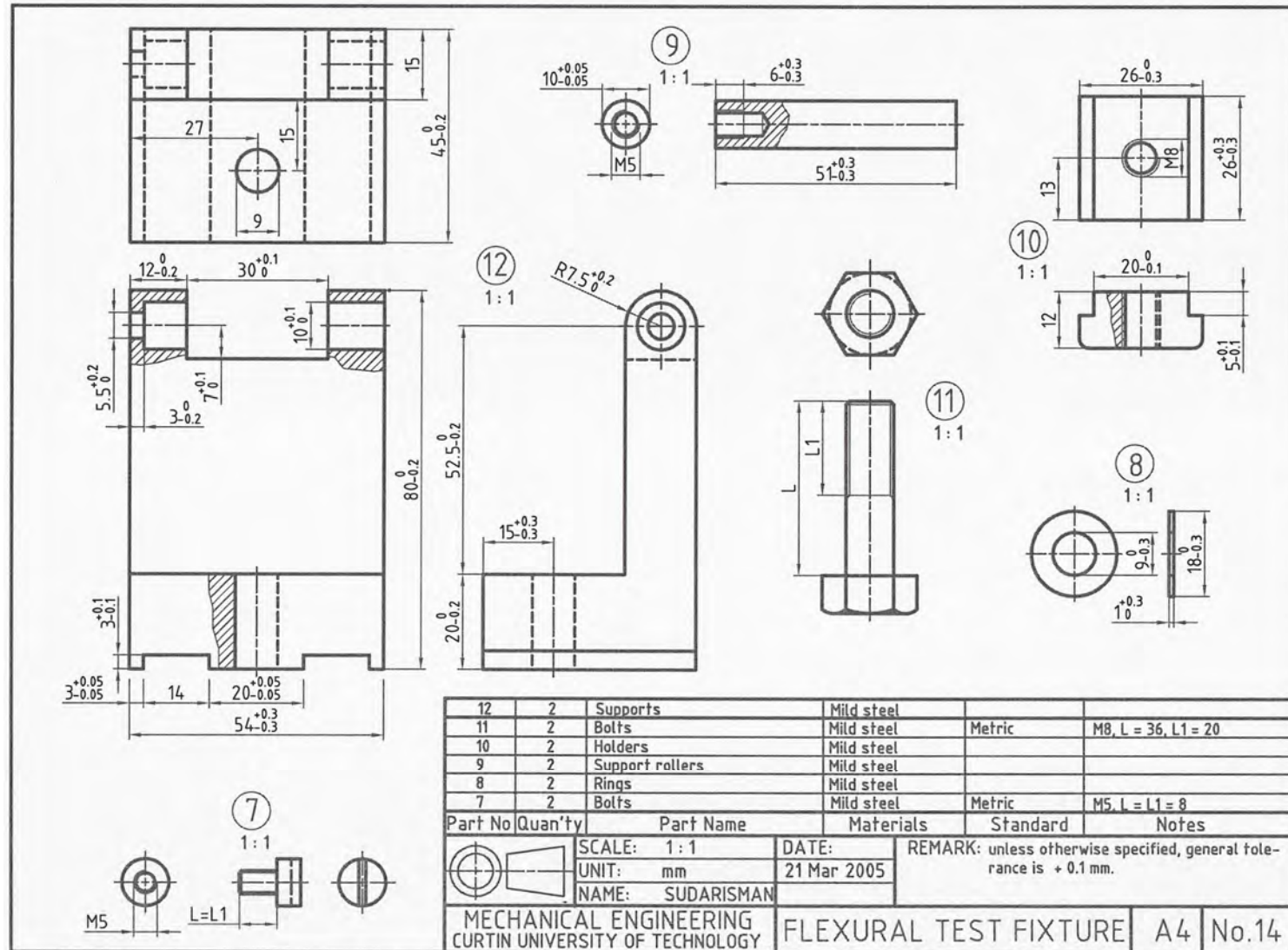




**Appendix 5.** Compressive Test Fixtures (*Continuation*)

**Appendix 5.** Compressive Test Fixtures (*Continuation*)

**Appendix 6.** Flexural Test Fixtures

**Appendix 6.** Flexural Test Fixtures (*Continuation*)



**Appendix 7.** Micrograph samples for image analysis

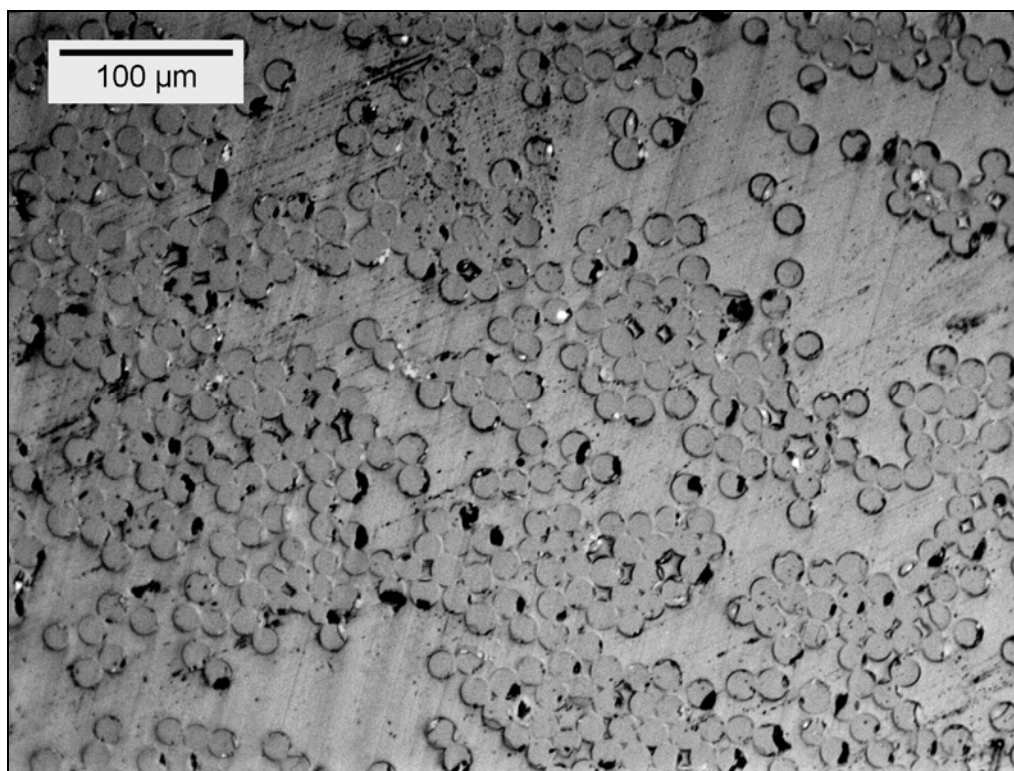


**Figure A7.1.** A micrograph sample of glass fibre/epoxy prepreg layer prepared for fibre and void content determination by means of micrograph analysis.

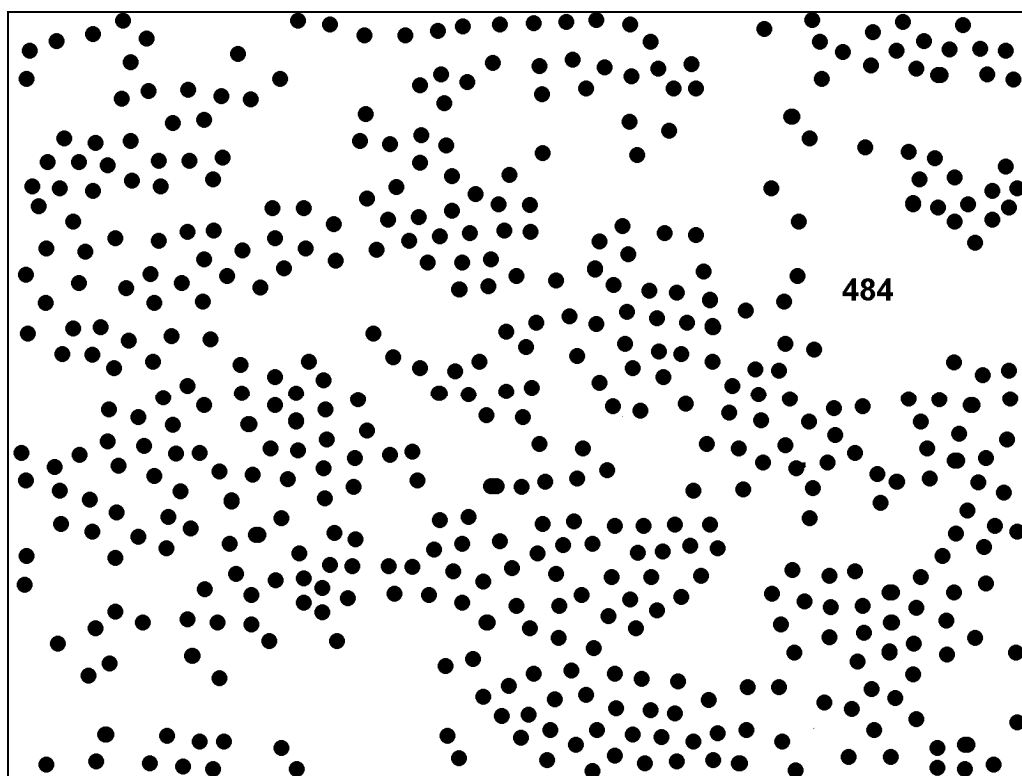


**Figure A7.2.** Dark-coloured dots representing fibres of Figure A5.2(a) after being marked and filtered showing the number of fibres (484) counted by the ImageJ open source software.

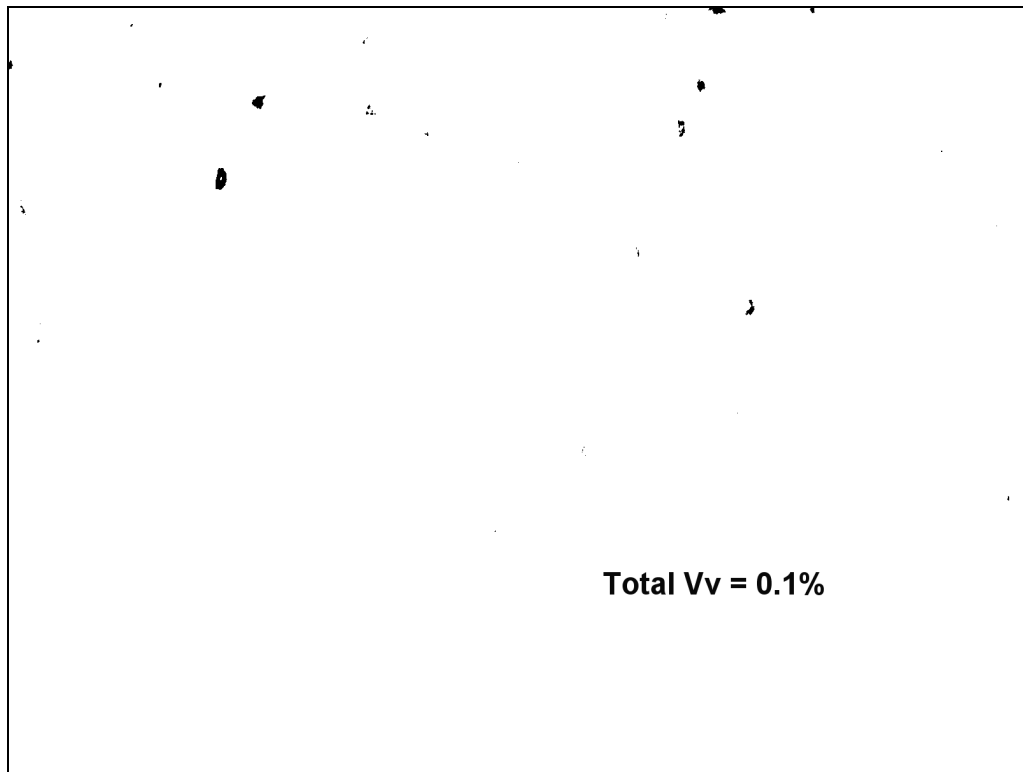


**Figure A7.3.** Dark spots representing voids of Figure A5.2(a) after being traced and filtered showing void content,  $V_v$ , of 0.1% counted by the ImageJ open source software.

**Appendix 8.** Spreadsheet sample: fibre diameter measurement and calculation.

**Table A8.** Sample: COLAN Fibre diameter measurement  
Optical magnification: 50X Scaling factor is: 13.74 px/ $\mu$ m

Sam- ple #	Diameter		Sam- ple #	Diameter		Sam-pl #	Diameter		Sam- ple #	Diameter	
	px	Mic- ron		px	Mic- ron		px	Mic- ron		px	Mic- ron
1	98	7.13	31	108	7.86	61	108	7.86	91	98	7.13
2	112	8.15	32	110	8.01	62	94	6.84	92	103	7.50
3	108	7.86	33	101	7.35	63	109	7.93	93	100	7.28
4	103	7.50	34	105	7.64	64	95	6.91	94	110	8.01
5	101	7.35	35	109	7.93	65	102	7.42	95	103	7.50
6	110	8.01	36	94	6.84	66	103	7.50	96	101	7.35
7	100	7.28	37	104	7.57	67	108	7.86	97	96	6.99
8	99	7.21	38	102	7.42	68	104	7.57	98	112	8.15
9	102	7.42	39	101	7.35	69	115	8.37	99	105	7.64
10	101	7.35	40	103	7.50	70	106	7.71	100	95	6.91
11	90	6.55	41	105	7.64	71	105	7.64	101	97	7.06
12	99	7.21	42	109	7.93	72	103	7.50	102	109	7.93
13	101	7.35	43	123	8.95	73	92	6.70	103	92	6.70
14	95	6.91	44	93	6.77	74	108	7.86	104	97	7.06
15	100	7.28	45	114	8.30	75	103	7.50	105	111	8.08
16	95	6.91	46	112	8.15	76	111	8.08	106	107	7.79
17	111	8.08	47	107	7.79	77	113	8.22	107	102	7.42
18	103	7.50	48	106	7.71	78	100	7.28	108	105	7.64
19	104	7.57	49	100	7.28	79	109	7.93	109	99	7.21
20	109	7.93	50	98	7.13	80	97	7.06	110	103	7.50
21	111	8.08	51	99	7.21	81	110	8.01	111	106	7.71
22	108	7.86	52	114	8.30	82	99	7.21	112	96	6.99
23	101	7.35	53	110	8.01	83	107	7.79	113	102	7.42
24	106	7.71	54	109	7.93	84	104	7.57	114	104	7.57
25	109	7.93	55	107	7.79	85	95	6.91	115	98	7.13
26	103	7.50	56	112	8.15	86	106	7.71	116	108	7.86
27	111	8.08	57	106	7.71	87	95	6.91	117	105	7.64
28	116	8.44	58	101	7.35	88	99	7.21	118	99	7.21
29	96	6.99	59	103	7.50	89	110	8.01	119		
30	105	7.64	60	103	7.50	90	108	7.86	120		

	px	$\mu$ m	(%)			
<b>Mean =</b>	103.86	7.56		<b>Min =</b>	6.55	<b>n = 118</b>
<b>StDev =</b>	5.956	0.43	5.734	<b>Max =</b>	8.95	

Magnification: 5X = 1.374 px/ $\mu$ m  
 10X = 2.748 px/ $\mu$ m  
 20X = 5.496 px/ $\mu$ m  
 50X = 13.74 px/ $\mu$ m  
 100X = 27.48 px/ $\mu$ m

**Appendix 9.** Spreadsheet sample:  $V_f$  and  $V_v$  calculation procedure**Table A9.** Spreadsheet sample for fibre and void content (%)  
(Optimisation Procedure, Stage 1 -  $C_e$ )

Optical Magnification ==>		<b>5X</b>	<b>10X</b>
Linear scale factor		1.374	2.748
Average fibre dia = 7.559272691	$\mu\text{m} =$	10.386441	20.772881
Average single fibre area =		84.7273	338.9092
Image size = 800*600 px^2 =		480000	480000

	Spec #	Number of fibres	Void area (px^2)	Volume content		Optical Magnif ↓
				Fibre	Void	
<b>1</b>	11	782	4567	55.21	1.0	10
	12					10
	13	635	7971	44.83	1.7	10
	14	726	14687	51.26	3.1	10
	15	612	9565	43.21	2.0	
	16	667	101633	47.09	21.2	10
	Aver			48.32	5.77	
<b>1</b>	21	658	0	46.46	0.0	10
	22	773	68483	54.58	14.3	10
	23	732	4616	51.68	1.0	10
	24					
	25	872	76988	61.57	16.0	10
	26	759	31739	53.59	6.6	10
	Aver			53.58	7.58	
<b>1</b>	31	609	7330	43.00	1.5	10
	32	924	21008	65.24	4.4	10
	33	658	95075	46.46	19.8	10
	34					
	35	966	10330	68.21	2.2	10
	36	557	2693	39.33	0.6	10
	Aver			52.45	5.68	
<b>1</b>	41	642	55543	45.33	11.6	10
	42	689	18238	48.65	3.8	10
	43	992	2613	70.04	0.5	10
	44	716	31496	50.55	6.6	10
	45	728	9486	51.40	2.0	10
	46					
	Aver			53.19	4.89	
<b>1</b>	51	664	68645	46.88	14.3	10
	52	689	34023	48.65	7.1	10
	53	704	36388	49.71	7.6	10
	54	776	27799	54.79	5.8	10
	55					
	56	802	26802	56.63	5.6	10
Aver				51.33	8.07	

## **Appendix 10.** Spreadsheet sample for flexural property calculation.

### NOTES:

A particular cell,  $C$ , in the following spreadsheet is identified with its column,  $i$ , and its row,  $j$ . Whilst capital letter(s) is (are) assigned to identify a column, a number is used to identify a row, *e.g.*  $C_{ij}$  = cell AD187 is a cell located in column AD at row 187.

### Cell formulas:

G22 to L22, $m$ :	=SLOPE( $i_14:i_1200, i_24:i_2200$ ), $i_1$ = AU, AV, AW, ... AZ, $i_2$ = AO, AP, AQ ... AT.
G23 to L23, $c$ :	=INTERCEPT( $i_14: i_1200, i_24: i_2200$ ), $i_1$ = AU, AV, AW, ... AZ, $i_2$ = AO, AP, AQ ... AT.
G24 to L24, $r$ :	=CORREL( $i_14:i_1200, i_24:i_2200$ ), $i_1$ = AO, AP, AQ ... AT, $i_2$ = AU, AV, AW, ... AZ.
G25 to L25, $\Delta D$ :	= $-i_{23}/i_{22}$ , $i$ = G, H, I, ... L.
G26 to L26, $F_{\max}$ :	=MAX( $i:i$ ), $i$ = BA, BC, BE, BG, BI, BK.
G27 to L27, $D$ :	=VLOOKUP( $i_126, i_2: i_3, 2, \text{FALSE}$ ), $i_1$ = G, H, I, ... L, $i_2$ = BA, BC, BE, BG, BI, BK, $i_3$ = BB, BD, BF, BH, BJ, BL.
G31 to L31, $\sigma_f$ :	=MAX( $i:i$ ), $i$ = BM, BO, BQ, BS, BU, BW.
G32 to L32, $E$ :	= $i_{22} * \$D\$8^3 / (4 * i_{28}) / 1000$ , $i$ = G, H, I, ... L.
G33 to L33, $\varepsilon_{\max}$ :	=VLOOKUP( $i_133, i_2: i_3, 2, \text{FALSE}$ ), $i_1$ = G, H, I, ... L, $i_2$ = BM, BO, BQ, BS, BU, BW, $i_3$ = BN, BP, BR, BT, BV, BX.
G34 to L34, $\varepsilon_{\text{fail}}$ :	=MAX( $i:i$ ), $i$ = BN, BP, BR, BT, BV, BX.
G35 to L35, $\gamma_{\max}$ :	= $i_1202 / (2 * i_228 * i_229)$ , $i_1$ = BY, BZ, CA, ... CD, $i_2$ = G, H, I, ... L.
G37 to L37, $\gamma_{\text{fail}}$ :	= $i_1203 / (2 * i_228 * i_229)$ , $i_1$ = BY, BZ, CA, ... CD, $i_2$ = G, H, I, ... L.

Where  $c$  (N) is the constant of the equation of initial linear part of an  $F$ – $D$  curve,  $r$  is the coefficient of the  $F$ – $D$  correlation,  $\Delta D$  (mm) is the displacement correction,  $\sigma_f$  (MPa) is the flexural strength,  $\varepsilon_{\max}$  (mm/mm) is the strain at maximum stress,  $\varepsilon_{\text{fail}}$  (mm/mm) is the strain to failure,  $\gamma_{\max}$  (kJ/mm<sup>2</sup>) is the specific energy storage capacity to maximum stress, and  $\gamma_{\text{fail}}$  (kJ/mm<sup>2</sup>) is the specific work of fracture.

Corrected or true crosshead displacement was calculated as follows:

$$D = D_o - \Delta D$$

Where  $D_o$  is the recorded crosshead displacement (mm).

Elastic modulus, stress and strain were calculated using equations given in following page.

**Appendix 10. Continuation.**

	A	B	C	D	E	F	G	H	I	J	K	L	M	N	O
1	<b>(IM7<sub>4</sub> + TR50S<sub>2</sub>) hybrid/epoxy, S/d = 64</b>														
2	Name:	Risman	Process	1. Copy Disp(mm) and Load (kN) data from Raw Data Sheet											
3	Operator ID:	Derek Oxley		2. Enter linear cut-offs by observing Original Data Plot											
4	Test date:	22/10/2008		3. Under 'Data from Testing Sheet' Alter name of reference file as appropriate											
5	Specimen name:	Composite Material		4. Delete Data As Appropriate-blank & non linear											
6	Fixture type:	3-point													
7	Crosshead speed:	13.37 mm/min													
8	Span-to-Depth Ratio:	64													
9															
10	<b>Data From Testing Sheet</b>														
11	Sample	width	depth	span											
12	1	12.52	2.00	128.00											
13	2	11.98	1.85	118.19											
14	3	12.51	2.07	132.48											
15	4	12.57	1.93	123.31											
16	5	12.69	1.99	127.15											
17	6	12.48	1.92	123.09											
18															
19															
20	<b>Linear Cut-Offs</b>			Min											
21	<b>(Read From Plot)</b>			Max											
22	<b>Toe Correction Analysis</b>			m	15.6	18.9	17.8	17.9	16.5	18.4					
23				c	-15.7	-9.3	-19.4	-18.2	-4.2	-7.2					
24				r	0.999	0.999	0.998	0.999	0.999	0.999					
25				toe correction (x-intercept)	1.00	0.49	1.09	1.02	0.25	0.39					
26	<b>Maximum Point</b>			Max Load (N)	221.3	232.8	208.2	240.0	217.5	187.8					
27				True Displacement at Max Load (mm)	14.38	12.44	12.06	13.47	13.57	10.18					
28	<b>Sample Dimensions</b>			width (mm)	12.52	11.98	12.51	12.57	12.69	12.48					
29				depth (mm)	2.00	1.85	2.07	1.93	1.99	1.92					
30				span (mm)	128.00	118.19	132.48	123.31	127.15	123.09	<b>Aver</b>	<b>StDev</b>			
31	<b>Results</b>			Flexural Strength (Mpa)	906.33	1071.09	806.07	1012.64	879.18	778.18	908.9	114.56			
32				Flexural Modulus (GPa)	81.87	103.58	93.14	93.36	85.00	96.71	92.28	7.884			
33				Strain to Max Stress	1.05%	0.99%	0.85%	1.02%	1.00%	0.78%	0.95%	0.109%			
34				Strain to Failure or test being stopped	1.09%	1.04%	0.90%	1.06%	1.17%	1.22%	1.08%	0.112%			
35				Specific Work to Max Stress (kJ/m <sup>2</sup> )	32.4	33.2	24.9	33.5	29.9	19.9	29.0	5.47			
36				Work of Fracture (kJ)	1647.2	1492.0	1306.5	1647.3	1778.9	1729.6	1600	173.8			
37				Specific Work of fracture (kJ/m <sup>2</sup> )	65.8	67.5	50.5	68.0	70.5	72.1	65.7	7.81			
38															

Continue to the next column

**Appendix 10. Continuation.**

	P	Q	R	S	T	U	V	W	X	Y	Z	AA	AB
1	Original data												
2	t (sec)	Specimen 1		Specimen 2		Specimen 3		Specimen 4		Specimen 5		Specimen 6	
3		D (mm)	F (kN)	D (mm)	F (kN)	D (mm)	F (kN)	D (mm)	F (kN)	D (mm)	F (kN)	D (mm)	F (kN)
4	0	0.000	0.0002	0.000	0.000	0.00	0.0004	0.000	-0.0030	0.000	-0.0051	0.000	-0.0015
5	1	-0.223	0.0048	-0.224	-0.003	-0.22	0.0015	-0.223	0.0040	-0.222	-0.0092	-0.236	-0.0011
6	2	-0.445	-0.0030	-0.445	-0.005	-0.45	-0.0017	-0.446	-0.0034	-0.446	-0.0066	-0.470	-0.0074
7	3	-0.670	-0.0026	-0.668	-0.015	-0.67	-0.0048	-0.669	-0.0037	-0.669	-0.0126	-0.705	-0.0107
8	4	-0.891	-0.0071	-0.892	-0.016	-0.89	-0.0067	-0.892	-0.0088	-0.892	-0.0148	-0.940	-0.0137
9	5	-1.114	-0.0082	-1.115	-0.013	-1.11	-0.0110	-1.115	-0.0113	-1.114	-0.0158	-1.175	-0.0168
10	6	-1.338	-0.0115	-1.337	-0.018	-1.34	-0.0086	-1.338	-0.0135	-1.338	-0.0196	-1.410	-0.0180
11	7	-1.560	-0.0141	-1.561	-0.023	-1.56	-0.0150	-1.560	-0.0161	-1.560	-0.0236	-1.644	-0.0206
12	8	-1.783	-0.0153	-1.783	-0.026	-1.78	-0.0150	-1.783	-0.0175	-1.783	-0.0266	-1.879	-0.0262
13	9	-2.006	-0.0172	-2.006	-0.028	-2.01	-0.0186	-2.005	-0.0225	-2.006	-0.0302	-2.114	-0.0301
14	10	-2.229	-0.0232	-2.229	-0.034	-2.23	-0.0219	-2.229	-0.0244	-2.229	-0.0320	-2.349	-0.0369
15	11	-2.452	-0.0273	-2.452	-0.037	-2.45	-0.0275	-2.452	-0.0277	-2.451	-0.0367	-2.584	-0.0380
16	12	-2.674	-0.0271	-2.675	-0.043	-2.68	-0.0288	-2.674	-0.0325	-2.674	-0.0424	-2.819	-0.0441
17	13	-2.897	-0.0304	-2.898	-0.047	-2.90	-0.0368	-2.897	-0.0341	-2.897	-0.0436	-3.054	-0.0491
18	14	-3.120	-0.0350	-3.121	-0.051	-3.12	-0.0371	-3.120	-0.0378	-3.121	-0.0465	-3.290	-0.0505
19	15	-3.343	-0.0380	-3.344	-0.055	-3.34	-0.0414	-3.343	-0.0426	-3.344	-0.0537	-3.525	-0.0578
20	16	-3.566	-0.0395	-3.566	-0.057	-3.57	-0.0470	-3.566	-0.0467	-3.566	-0.0545	-3.759	-0.0613
21	17	-3.789	-0.0398	-3.789	-0.063	-3.79	-0.0474	-3.789	-0.0500	-3.789	-0.0591	-3.994	-0.0669
22	18	-4.012	-0.0472	-4.012	-0.067	-4.01	-0.0534	-4.012	-0.0555	-4.011	-0.0634	-4.230	-0.0698
23	19	-4.235	-0.0514	-4.235	-0.073	-4.23	-0.0578	-4.235	-0.0559	-4.235	-0.0641	-4.464	-0.0750
24	20	-4.457	-0.0529	-4.458	-0.074	-4.46	-0.0593	-4.457	-0.0631	-4.458	-0.0682	-4.699	-0.0796
↓													
37	33	-7.356	-0.0994	-7.355	-0.130	-7.35	-0.1105	-7.355	-0.1135	-7.356	-0.1179	-7.755	-0.1355
38	34	-7.579	-0.1013	-7.579	-0.133	-7.58	-0.1148	-7.578	-0.1146	-7.578	-0.1200	-7.990	-0.1390
39	35	-7.801	-0.1065	-7.801	-0.137	-7.80	-0.1193	-7.801	-0.1203	-7.800	-0.1257	-8.225	-0.1432
40	36	-8.024	-0.1094	-8.024	-0.141	-8.02	-0.1210	-8.024	-0.1251	-8.023	-0.1283	-8.460	-0.1470
41	37	-8.246	-0.1129	-8.247	-0.149	-8.25	-0.1262	-8.246	-0.1308	-8.247	-0.1323	-8.695	-0.1518
42	38	-8.470	-0.1173	-8.470	-0.151	-8.47	-0.1324	-8.469	-0.1353	-8.470	-0.1334	-8.930	-0.1593
43	39	-8.692	-0.1199	-8.692	-0.157	-8.69	-0.1369	-8.692	-0.1359	-8.692	-0.1388	-9.165	-0.1591
44	40	-8.915	-0.1215	-8.915	-0.159	-8.92	-0.1395	-8.916	-0.1407	-8.915	-0.1425	-9.399	-0.1658
45	41	-9.138	-0.1303	-9.138	-0.165	-9.14	-0.1454	-9.139	-0.1470	-9.138	-0.1456	-9.635	-0.1705
46	42	-9.361	-0.1331	-9.362	-0.170	-9.36	-0.1505	-9.361	-0.1494	-9.361	-0.1525	-9.869	-0.1736
47	43	-9.583	-0.1378	-9.585	-0.175	-9.58	-0.1506	-9.583	-0.1529	-9.584	-0.1531	-10.105	-0.1783
48	44	-9.806	-0.1395	-9.807	-0.180	-9.81	-0.1568	-9.806	-0.1599	-9.807	-0.1580	-10.339	-0.1824
49	45	-10.030	-0.1415	-10.030	-0.182	-10.03	-0.1600	-10.030	-0.1592	-10.030	-0.1619	-10.574	-0.1878
50	46	-10.253	-0.1492	-10.253	-0.185	-10.25	-0.1635	-10.253	-0.1641	-10.252	-0.1618	-10.809	-0.1429
51	47	-10.476	-0.1489	-10.476	-0.189	-10.48	-0.1630	-10.476	-0.1665	-10.475	-0.1708	-11.044	-0.1330
52	48	-10.698	-0.1536	-10.699	-0.192	-10.70	-0.1678	-10.698	-0.1730	-10.698	-0.1715	-11.279	-0.1307
53	49	-10.921	-0.1561	-10.922	-0.199	-10.92	-0.1739	-10.921	-0.1768	-10.921	-0.1754	-11.514	-0.1322
54	50	-11.144	-0.1601	-11.144	-0.201	-11.14	-0.1754	-11.144	-0.1819	-11.144	-0.1764	-11.750	-0.1283
55	51	-11.367	-0.1618	-11.367	-0.206	-11.37	-0.1835	-11.367	-0.1823	-11.368	-0.1825	-11.985	-0.1274
56	52	-11.591	-0.1670	-11.591	-0.210	-11.59	-0.1844	-11.590	-0.1872	-11.590	-0.1842	-12.220	-0.1278
57	53	-11.813	-0.1685	-11.813	-0.212	-11.81	-0.1874	-11.813	-0.1938	-11.812	-0.1880	-12.454	-0.1288
58	54	-12.035	-0.1727	-12.036	-0.215	-12.04	-0.1897	-12.035	-0.1941	-12.035	-0.1917	-12.689	-0.1280
59	55	-12.258	-0.1770	-12.259	-0.222	-12.26	-0.1933	-12.258	-0.1970	-12.259	-0.1920	-12.925	-0.1291
60	56	-12.481	-0.1768	-12.481	-0.228	-12.48	-0.1985	-12.481	-0.2065	-12.482	-0.1969	-13.160	-0.1282
61	57	-12.705	-0.1826	-12.704	-0.228	-12.70	-0.2053	-12.704	-0.2070	-12.705	-0.1968	-13.395	-0.1305
62	58	-12.927	-0.1855	-12.928	-0.233	-12.93	-0.2079	-12.928	-0.2083	-12.927	-0.2058	-13.629	-0.1325
63	59	-13.151	-0.1925	-13.150	0.008	-13.15	-0.2082	-13.151	-0.2138	-13.149	-0.2066	-13.864	-0.1320
64	60	-13.374	-0.1945	-13.374	0.008	-13.37	0.0141	-13.373	-0.2176	-13.374	-0.2105	-14.099	-0.1306
65	61	-13.597	-0.1968	-13.598	0.009	-13.60	0.0006	-13.594	-0.2230	-13.595	-0.2114	-14.334	-0.1306
66	62	-13.820	-0.1991			-13.82	-0.0008	-13.818	-0.2230	-13.818	-0.2175	-14.570	-0.1334
67	63	-14.040	-0.2027					-14.041	-0.2266	-14.042	-0.1260	-14.806	-0.1321
68	64	-14.265	-0.2041					-14.265	-0.2327	-14.264	-0.1240	-15.040	-0.1316
69	65	-14.487	-0.2070					-14.489	-0.2400	-14.487	-0.1224	-15.275	-0.1280
70	66	-14.710	-0.2127					-14.711	0.0050	-14.709	-0.1266	-15.510	-0.1325
71	67	-14.933	-0.2149					-14.934	0.0057	-14.933	-0.1274	-15.745	-0.1300
72	68	-15.156	-0.2173							-15.157	-0.1262	-15.980	-0.1282
73	69	-15.379	-0.2213							-15.379	-0.1238	-16.215	-0.1298
74	70	-15.602	0.0020							-15.601	-0.1191	-16.450	-0.1277
75	71	-15.825	0.0037							-15.825	-0.1148		
76	72									-16.048	0.0117		
77	73									-16.134	0.0069		
↓													
202													
203													

Continue to the next column



**Appendix 10. Continuation.**

	AC	AD	AE	AF	AG	AH	AI	AJ	AK	AL	AM	AN
1	<b>First Plot: All Data (original plot)</b>											
2	<b>Displacement, D (mm)</b>						<b>Load, F (N)</b>					
3	1	2	3	4	5	6	1	2	3	4	5	6
4	0.00	0.00	0.00	0.00	0.00	0.00	-0.2	0.1	-0.4	3.0	5.1	1.5
5	0.22	0.22	0.22	0.22	0.22	0.24	-4.8	3.0	-1.5	-4.0	9.2	1.1
6	0.45	0.45	0.45	0.45	0.45	0.47	3.0	4.9	1.7	3.4	6.6	7.4
7	0.67	0.67	0.67	0.67	0.67	0.71	2.6	14.7	4.8	3.7	12.6	10.7
8	0.89	0.89	0.89	0.89	0.89	0.94	7.1	16.1	6.7	8.8	14.8	13.7
9	1.11	1.11	1.11	1.11	1.11	1.18	8.2	13.4	11.0	11.3	15.8	16.8
10	1.34	1.34	1.34	1.34	1.34	1.41	11.5	17.9	8.6	13.5	19.6	18.0
11	1.56	1.56	1.56	1.56	1.56	1.64	14.1	22.7	15.0	16.1	23.6	20.6
12	1.78	1.78	1.78	1.78	1.78	1.88	15.3	26.0	15.0	17.5	26.6	26.2
13	2.01	2.01	2.01	2.01	2.01	2.11	17.2	28.1	18.6	22.5	30.2	30.1
14	2.23	2.23	2.23	2.23	2.23	2.35	23.2	33.6	21.9	24.4	32.0	36.9
15	2.45	2.45	2.45	2.45	2.45	2.58	27.3	36.8	27.5	27.7	36.7	38.0
16	2.67	2.68	2.68	2.67	2.67	2.82	27.1	42.7	28.8	32.5	42.4	44.1
17	2.90	2.90	2.90	2.90	2.90	3.05	30.4	47.4	36.8	34.1	43.6	49.1
18	3.12	3.12	3.12	3.12	3.12	3.29	35.0	50.7	37.1	37.8	46.5	50.5
19	3.34	3.34	3.34	3.34	3.34	3.52	38.0	54.8	41.4	42.6	53.7	57.8
20	3.57	3.57	3.57	3.57	3.57	3.76	39.5	56.6	47.0	46.7	54.5	61.3
21	3.79	3.79	3.79	3.79	3.79	3.99	39.8	62.8	47.4	50.0	59.1	66.9
22	4.01	4.01	4.01	4.01	4.01	4.23	47.2	67.0	53.4	55.5	63.4	69.8
23	4.23	4.24	4.23	4.23	4.23	4.46	51.4	72.9	57.8	55.9	64.1	75.0
24	4.46	4.46	4.46	4.46	4.46	4.70	52.9	74.2	59.3	63.1	68.2	79.6
↓												
37	7.36	7.36	7.35	7.35	7.36	7.76	99.4	129.5	110.5	113.5	117.9	135.5
38	7.58	7.58	7.58	7.58	7.58	7.99	101.3	133.2	114.8	114.6	120.0	139.0
39	7.80	7.80	7.80	7.80	7.80	8.22	106.5	137.5	119.3	120.3	125.7	143.2
40	8.02	8.02	8.02	8.02	8.02	8.46	109.4	140.9	121.0	125.1	128.3	147.0
41	8.25	8.25	8.25	8.25	8.25	8.69	112.9	149.1	126.2	130.8	132.3	151.8
42	8.47	8.47	8.47	8.47	8.47	8.93	117.3	150.9	132.4	135.3	133.4	159.3
43	8.69	8.69	8.69	8.69	8.69	9.16	119.9	157.4	136.9	135.9	138.8	159.1
44	8.92	8.92	8.92	8.92	8.92	9.40	121.5	158.9	139.5	140.7	142.5	165.8
45	9.14	9.14	9.14	9.14	9.14	9.63	130.3	164.8	145.4	147.0	145.6	170.5
46	9.36	9.36	9.36	9.36	9.36	9.87	133.1	170.0	150.5	149.4	152.5	173.6
47	9.58	9.58	9.58	9.58	9.58	10.10	137.8	174.6	150.6	152.9	153.1	178.3
48	9.81	9.81	9.81	9.81	9.81	10.34	139.5	179.5	156.8	159.9	158.0	182.4
49	10.03	10.03	10.03	10.03	10.03	10.57	141.5	181.7	160.0	159.2	161.9	187.8
50	10.25	10.25	10.25	10.25	10.25	10.81	149.2	185.3	163.5	164.1	161.8	142.9
51	10.48	10.48	10.48	10.48	10.47	11.04	148.9	188.7	163.0	166.5	170.8	133.0
52	10.70	10.70	10.70	10.70	10.70	11.28	153.6	192.4	167.8	173.0	171.5	130.7
53	10.92	10.92	10.92	10.92	10.92	11.51	156.1	198.7	173.9	176.8	175.4	132.2
54	11.14	11.14	11.14	11.14	11.14	11.75	160.1	200.8	175.4	181.9	176.4	128.3
55	11.37	11.37	11.37	11.37	11.37	11.98	161.8	206.2	183.5	182.3	182.5	127.4
56	11.59	11.59	11.59	11.59	11.59	12.22	167.0	209.7	184.4	187.2	184.2	127.8
57	11.81	11.81	11.81	11.81	11.81	12.45	168.5	212.5	187.4	193.8	188.0	128.8
58	12.04	12.04	12.04	12.04	12.03	12.69	172.7	215.3	189.7	194.1	191.7	128.0
59	12.26	12.26	12.26	12.26	12.26	12.92	177.0	221.5	193.3	197.0	192.0	129.1
60	12.48	12.48	12.48	12.48	12.48	13.16	176.8	227.8	198.5	206.5	196.9	128.2
61	12.71	12.70	12.70	12.70	12.70	13.39	182.6	228.5	205.3	207.0	196.8	130.5
62	12.93	12.93	12.93	12.93	12.93	13.63	185.5	232.8	207.9	208.3	205.8	132.5
63	13.15	13.15	13.15	13.15	13.15	13.86	192.5	-7.7	208.2	213.8	206.6	132.0
64	13.37	13.37	13.37	13.37	13.37	14.10	194.5	-7.8	-14.1	217.6	210.5	130.6
65	13.60	13.60	13.60	13.59	13.60	14.33	196.8	-9.0	-0.6	223.0	211.4	130.6
66	13.82		13.82	13.82	13.82	14.57	199.1		0.8	223.0	217.5	133.4
67	14.04			14.04	14.04	14.81	202.7			226.6	126.0	132.1
68	14.26			14.26	14.26	15.04	204.1			232.7	124.0	131.6
69	14.49			14.49	14.49	15.27	207.0			240.0	122.4	128.0
70	14.71			14.71	14.71	15.51	212.7			-5.0	126.6	132.5
71	14.93			14.93	14.93	15.75	214.9			-5.7	127.4	130.0
72	15.16				15.16	15.98	217.3				126.2	128.2
73	15.38				15.38	16.21	221.3				123.8	129.8
74	15.60				15.60	16.45	-2.0				119.1	127.7
75	15.83				15.82		-3.7				114.8	
76					16.05						-11.7	
77					16.13						-6.9	
↓												
202												
203												

Continue to the next column.



**Appendix 10. Continuation.**

	AO	AP	AQ	AR	AS	AT	AU	AV	AW	AX	AY	AZ
1	<b>Second Plot: Linear Data</b>											
2	<b>Displacement (mm), linear part</b>						<b>Load N, linear part</b>					
3	1	2	3	4	5	6	1	2	3	4	5	6
4												
5												
6												
7												
8												
9												
10												
11												
12												
13												
14												
15												
16												
17						3.054						49.1
18	3.120	3.121	3.120	3.120	3.121	3.290	35.0	50.7	37.1	37.8	46.5	50.5
19	3.343	3.344	3.343	3.343	3.344	3.525	38.0	54.8	41.4	42.6	53.7	57.8
20	3.566	3.566	3.566	3.566	3.566	3.759	39.5	56.6	47.0	46.7	54.5	61.3
21	3.789	3.789	3.789	3.789	3.789	3.994	39.8	62.8	47.4	50.0	59.1	66.9
22	4.012	4.012	4.012	4.012	4.011	4.230	47.2	67.0	53.4	55.5	63.4	69.8
23	4.235	4.235	4.235	4.235	4.235	4.464	51.4	72.9	57.8	55.9	64.1	75.0
24	4.457	4.458	4.458	4.457	4.458	4.699	52.9	74.2	59.3	63.1	68.2	79.6
↓												
37	7.356	7.355	7.355	7.355	7.356	7.755	99.4	129.5	110.5	113.5	117.9	135.5
38	7.579	7.579	7.578	7.578	7.578	7.990	101.3	133.2	114.8	114.6	120.0	139.0
39	7.801	7.801	7.801	7.801	7.800	8.225	106.5	137.5	119.3	120.3	125.7	143.2
40	8.024	8.024	8.024	8.024	8.023	8.460	109.4	140.9	121.0	125.1	128.3	
41	8.246	8.247	8.247	8.246	8.247	8.695	112.9	149.1	126.2	130.8	132.3	
42	8.470	8.470	8.470	8.469	8.470	8.930	117.3	150.9	132.4	135.3	133.4	
43	8.692	8.692	8.692	8.692	8.692	9.165	119.9	157.4	136.9	135.9	138.8	
44	8.915	8.915	8.915	8.916	8.915	9.399	121.5	158.9	139.5	140.7	142.5	
45	9.138	9.138	9.138	9.139	9.138	9.635	130.3	164.8	145.4	147.0	145.6	
46	9.361	9.362	9.362	9.361	9.361	9.869	133.1	170.0	150.5	149.4	152.5	
47	9.583	9.585	9.584	9.583	9.584							
48	9.806	9.807	9.806	9.806	9.807							
49												
50												
51												
52												
53												
54												
55												
56												
57												
58												
59												
60												
61												
62												
63												
64												
65												
66												
67												
68												
69												
70												
71												
72												
73												
74												
75												
76												
77												
↓												
202												
203												

*Continue to the next column.*

**Appendix 10. Continuation.**

	BA	BB	BC	BD	BE	BF	BG	BH	BUI	BJ	BK	BL
1	<b>Third Plot: =Toe Corrected Displacements</b>											
2	1		2		3		4		5		6	
3	F (N)	D (mm)	F (N)	D (mm)	F (N)	D (mm)	F (N)	D (mm)	F (N)	D (mm)	F (N)	D (mm)
4	7.1	-0.111	4.9	-0.046	11.0	0.021	11.3	0.098	9.2	-0.030	7.4	0.079
5	8.2	0.112	14.7	0.177	8.6	0.244	13.5	0.321	6.6	0.194	10.7	0.314
6	11.5	0.336	16.1	0.401	15.0	0.468	16.1	0.543	12.6	0.417	13.7	0.549
7	14.1	0.558	13.4	0.624	15.0	0.690	17.5	0.766	14.8	0.640	16.8	0.784
8	15.3	0.781	17.9	0.846	18.6	0.912	22.5	0.989	15.8	0.862	18.0	1.019
9	17.2	1.004	22.7	1.070	21.9	1.135	24.4	1.213	19.6	1.085	20.6	1.254
10	23.2	1.227	26.0	1.292	27.5	1.358	27.7	1.435	23.6	1.307	26.2	1.488
11	27.3	1.450	28.1	1.515	28.8	1.582	32.5	1.658	26.6	1.531	30.1	1.723
12	27.1	1.672	33.6	1.738	36.8	1.804	34.1	1.881	30.2	1.754	36.9	1.958
13	30.4	1.895	36.8	1.961	37.1	2.027	37.8	2.104	32.0	1.977	38.0	2.194
14	35.0	2.118	42.7	2.184	41.4	2.250	42.6	2.327	36.7	2.199	44.1	2.429
15	38.0	2.341	47.4	2.407	47.0	2.473	46.7	2.550	42.4	2.422	49.1	2.663
16	39.5	2.564	50.7	2.630	47.4	2.696	50.0	2.773	43.6	2.645	50.5	2.899
17	39.8	2.787	54.8	2.853	53.4	2.919	55.5	2.995	46.5	2.868	57.8	3.134
18	47.2	3.010	56.6	3.075	57.8	3.141	55.9	3.218	53.7	3.092	61.3	3.369
19	51.4	3.233	62.8	3.298	59.3	3.364	63.1	3.441	54.5	3.314	66.9	3.603
20	52.9	3.455	67.0	3.521	64.5	3.587	64.0	3.664	59.1	3.537	69.8	3.839
21	59.0	3.678	72.9	3.744	69.2	3.809	68.2	3.887	63.4	3.759	75.0	4.074
22	62.8	3.902	74.2	3.967	67.9	4.033	71.8	4.110	64.1	3.982	79.6	4.308
23	66.2	4.125	79.5	4.189	75.1	4.256	76.1	4.333	68.2	4.206	84.0	4.544
24	67.8	4.347	84.9	4.412	78.8	4.479	81.9	4.555	71.4	4.428	90.6	4.778
↓												
37	112.9	7.244	137.5	7.310	132.4	7.376	135.3	7.453	120.0	7.326	143.2	7.834
38	117.3	7.468	140.9	7.533	136.9	7.599	135.9	7.676	125.7	7.548	147.0	8.069
39	119.9	7.690	149.1	7.756	139.5	7.821	140.7	7.899	128.3	7.771	151.8	8.304
40	121.5	7.913	150.9	7.979	145.4	8.044	147.0	8.122	132.3	7.994	159.3	8.539
41	130.3	8.136	157.4	8.201	150.5	8.268	149.4	8.345	133.4	8.217	159.1	8.774
42	133.1	8.359	158.9	8.424	150.6	8.491	152.9	8.567	138.8	8.440	165.8	9.009
43	137.8	8.581	164.8	8.647	156.8	8.713	159.9	8.790	142.5	8.663	170.5	9.244
44	139.5	8.804	170.0	8.871	160.0	8.936	159.2	9.014	145.6	8.886	173.6	9.478
45	141.5	9.028	174.6	9.094	163.5	9.159	164.1	9.237	152.5	9.108	178.3	9.714
46	149.2	9.251	179.5	9.316	163.0	9.382	166.5	9.459	153.1	9.331	182.4	9.949
47	148.9	9.474	181.7	9.539	167.8	9.605	173.0	9.682	158.0	9.555	187.8	10.184
48	153.6	9.696	185.3	9.762	173.9	9.828	176.8	9.904	161.9	9.778	192.9	10.418
49	156.1	9.919	188.7	9.985	175.4	10.050	181.9	10.128	161.8	10.000	193.0	10.654
50	160.1	10.142	192.4	10.208	183.5	10.273	182.3	10.351	170.8	10.222	193.7	10.888
51	161.8	10.365	198.7	10.431	184.4	10.496	187.2	10.574	171.5	10.446	193.2	11.123
52	167.0	10.589	200.8	10.653	187.4	10.720	193.8	10.797	175.4	10.669	198.3	11.359
53	168.5	10.811	206.2	10.876	189.7	10.943	194.1	11.019	176.4	10.892	197.4	11.594
54	172.7	11.033	209.7	11.100	193.3	11.165	197.0	11.242	182.5	11.115	197.8	11.829
55	177.0	11.256	212.5	11.322	198.5	11.387	206.5	11.465	184.2	11.337	198.8	12.063
56	176.8	11.479	215.3	11.545	205.3	11.610	207.0	11.688	188.0	11.560	198.0	12.299
57	182.6	11.703	221.5	11.768	207.9	11.835	208.3	11.911	191.7	11.783	199.1	12.534
58	185.5	11.925	227.8	11.990	208.2	12.056	213.8	12.134	192.0	12.006	198.2	12.769
59	192.5	12.149	228.5	12.213	-14.1	12.280	217.6	12.357	196.9	12.230	193.5	13.004
60	194.5	12.372	232.8	12.437	-0.6	12.504	223.0	12.578	196.8	12.452	192.5	13.239
61	196.8	12.595	-7.7	12.659	0.8	12.726	223.0	12.802	205.8	12.675	192.0	13.473
62	199.1	12.818	-7.8	12.883			226.6	13.025	206.6	12.897	193.6	13.708
63	202.7	13.038	-9.0	13.107			232.7	13.249	210.5	13.122	193.6	13.944
64	204.1	13.263					240.0	13.473	211.4	13.343	193.4	14.180
65	207.0	13.485					-5.0	13.694	217.5	13.566	192.1	14.415
66	212.7	13.708					-5.7	13.918	126.0	13.789	191.6	14.649
67	214.9	13.931							124.0	14.012	198.0	14.884
68	217.3	14.154							122.4	14.235	192.5	15.119
69	221.3	14.377							126.6	14.457	193.0	15.354
70	-2.0	14.600							127.4	14.680	192.2	15.589
71	-3.7	14.824							126.2	14.905	192.8	15.824
72									123.8	15.127	192.7	16.059
73									119.1	15.349		
74									114.8	15.572		
75									-11.7	15.795		
76									-6.9	15.882		
77												
↓												
202												
203												

Continue to the next column.



**Appendix 10. Continuation.**

	BM	BN	BO	BP	BQ	BR	BS	BT	BU	BV	BW	BX
1	<b>Fourth Plot: Stress (MPa) - Strain (mm/mm) Data</b>											
2	1		2		3		4		5		6	
3	Stress	Strain	Stress	Strain	Stress	Strain	Stress	Strain	Stress	Strain	Stress	Strain
4	27.1	0.000	21.5	0.000	40.9	0.000	44.7	0.000	35.0	0.000	29.7	0.000
5	31.5	0.000	63.9	0.000	32.0	0.000	53.4	0.000	25.0	0.000	42.9	0.000
6	44.3	0.000	69.7	0.000	55.6	0.000	63.7	0.000	47.9	0.000	54.8	0.000
7	54.0	0.000	58.4	0.000	55.6	0.000	69.3	0.001	56.3	0.000	67.2	0.001
8	58.8	0.001	77.6	0.001	68.9	0.001	89.1	0.001	60.1	0.001	72.1	0.001
9	65.8	0.001	98.6	0.001	81.1	0.001	96.7	0.001	74.4	0.001	82.3	0.001
10	88.7	0.001	112.7	0.001	101.9	0.001	109.8	0.001	89.8	0.001	104.7	0.001
11	104.6	0.001	122.0	0.001	106.9	0.001	128.7	0.001	101.3	0.001	120.4	0.001
12	104.0	0.001	145.9	0.001	136.4	0.001	135.2	0.001	114.9	0.001	147.5	0.001
13	116.7	0.001	159.8	0.002	137.8	0.001	150.0	0.002	122.0	0.001	152.3	0.002
14	134.2	0.002	185.4	0.002	153.6	0.002	168.8	0.002	139.9	0.002	176.6	0.002
15	145.9	0.002	206.2	0.002	174.3	0.002	185.5	0.002	161.7	0.002	196.7	0.002
16	151.6	0.002	220.3	0.002	176.0	0.002	198.5	0.002	166.3	0.002	202.4	0.002
17	152.9	0.002	238.3	0.002	198.2	0.002	220.5	0.002	177.2	0.002	231.7	0.002
18	181.1	0.002	246.4	0.002	214.6	0.002	222.1	0.002	204.8	0.002	245.8	0.003
19	197.4	0.002	273.2	0.003	220.5	0.002	250.7	0.003	207.9	0.002	268.5	0.003
20	203.1	0.003	291.9	0.003	239.8	0.003	254.5	0.003	225.8	0.003	280.1	0.003
21	226.9	0.003	317.8	0.003	257.2	0.003	271.4	0.003	242.1	0.003	301.4	0.003
22	241.7	0.003	323.6	0.003	252.8	0.003	286.0	0.003	244.8	0.003	320.1	0.003
23	254.9	0.003	346.7	0.003	279.8	0.003	303.3	0.003	260.7	0.003	338.1	0.003
24	261.0	0.003	370.6	0.003	293.7	0.003	326.5	0.003	273.4	0.003	364.6	0.004
↓												
37	439.6	0.005	608.2	0.006	498.4	0.005	545.9	0.006	464.1	0.005	584.3	0.006
38	457.2	0.005	624.1	0.006	515.7	0.005	548.8	0.006	486.7	0.006	600.7	0.006
39	467.7	0.006	661.2	0.006	526.2	0.006	569.0	0.006	497.7	0.006	621.3	0.006
40	474.4	0.006	670.2	0.006	548.9	0.006	595.5	0.006	513.8	0.006	653.1	0.007
41	509.7	0.006	699.8	0.007	568.8	0.006	605.8	0.006	518.6	0.006	653.0	0.007
42	521.2	0.006	707.5	0.007	569.8	0.006	621.0	0.007	540.2	0.006	681.7	0.007
43	540.1	0.006	735.0	0.007	594.1	0.006	650.1	0.007	555.1	0.006	701.9	0.007
44	547.7	0.006	759.2	0.007	607.0	0.006	648.1	0.007	568.3	0.007	715.8	0.007
45	556.2	0.007	781.3	0.007	621.2	0.006	669.0	0.007	596.0	0.007	736.5	0.007
46	587.1	0.007	804.5	0.007	619.8	0.007	679.9	0.007	599.1	0.007	754.6	0.008
47	586.7	0.007	815.6	0.008	638.9	0.007	707.7	0.007	619.2	0.007	778.2	0.008
48	606.0	0.007	833.2	0.008	663.0	0.007	724.4	0.008	635.4	0.007	593.0	0.008
49	616.8	0.007	849.9	0.008	669.9	0.007	746.5	0.008	635.7	0.007	553.1	0.008
50	633.5	0.007	868.0	0.008	701.8	0.007	749.3	0.008	672.1	0.008	544.5	0.008
51	641.5	0.008	898.0	0.008	706.2	0.007	770.4	0.008	676.2	0.008	551.8	0.008
52	662.9	0.008	909.2	0.008	718.6	0.008	799.1	0.008	692.6	0.008	536.7	0.009
53	670.1	0.008	935.3	0.009	728.7	0.008	801.9	0.008	697.6	0.008	533.6	0.009
54	687.8	0.008	952.9	0.009	743.4	0.008	815.2	0.009	723.0	0.008	536.4	0.009
55	706.2	0.008	967.6	0.009	764.7	0.008	856.1	0.009	730.6	0.008	541.7	0.009
56	706.5	0.008	982.3	0.009	792.1	0.008	859.8	0.009	747.2	0.009	539.5	0.009
57	731.1	0.009	1012.8	0.009	803.4	0.008	866.7	0.009	763.0	0.009	545.5	0.010
58	743.9	0.009	1043.5	0.010	806.1	0.009	891.4	0.009	765.6	0.009	542.7	0.010
59	773.5	0.009	1048.8	0.010	-54.8	0.009	908.9	0.009	786.5	0.009	553.4	0.010
60	782.6	0.009	1071.1	0.010	-2.4	0.009	933.3	0.010	787.7	0.009	563.1	0.010
61	793.3	0.009	-35.6	0.010	3.3	0.009	935.0	0.010	825.2	0.009	562.4	0.010
62	804.2	0.009	-36.2	0.010			952.1	0.010	829.9	0.010	557.5	0.010
63	820.5	0.010	-41.9	0.010			979.8	0.010	847.2	0.010	559.0	0.011
64	827.7	0.010					1012.6	0.010	852.7	0.010	572.4	0.011
65	841.1	0.010					-21.2	0.010	879.2	0.010	568.2	0.011
66	866.0	0.010					-24.1	0.011	510.1	0.010	567.2	0.011
67	876.7	0.010							503.2	0.010	553.2	0.011
68	888.0	0.010							497.6	0.010	574.0	0.012
69	906.3	0.011							515.9	0.011	564.7	0.012
70	-8.4	0.011							520.1	0.011	558.1	0.012
71	-15.1	0.011							516.4	0.011	566.4	0.012
72									507.8	0.011	558.9	0.012
73									489.8	0.011		
74									473.1	0.011		
75									-48.4	0.012		
76									-28.3	0.012		
77												
↓												
202												
203												

Continue to the next column.



**Appendix 10. Continuation.**

	BV	BW	BX	BY	BZ	CA	CB	CC	CD
1	<b>Work (Area under Load-Disp Curve, kJ)</b>								
2				1	2	3	4	5	6
3									
4				-0.39088	-0.11254	0.11662	0.55399	-0.13836	0.29269
5				1.705	2.184	2.190	2.760	1.766	2.137
6				2.211	3.458	2.646	3.285	2.135	2.868
7				2.845	3.279	3.325	3.742	3.052	3.586
8				3.286	3.487	3.737	4.448	3.399	4.091
9				3.627	4.547	4.518	5.243	3.947	4.526
10				4.493	5.408	5.493	5.799	4.794	5.488
11				5.614	6.015	6.297	6.706	5.603	6.606
12				6.047	6.888	7.298	7.406	6.328	7.870
13				6.417	7.847	8.224	8.015	6.946	8.805
14				7.305	8.858	8.755	8.958	7.628	9.655
15				8.125	10.045	9.849	9.969	8.825	10.939
16				8.657	10.919	10.518	10.784	9.610	11.722
17				8.845	11.754	11.251	11.746	10.060	12.715
18				9.683	12.397	12.368	12.421	11.182	13.980
19				10.987	13.328	13.031	13.241	12.016	15.050
20				11.602	14.465	13.782	14.210	12.663	16.086
21				12.489	15.598	14.874	14.737	13.612	16.996
22				13.624	16.373	15.378	15.587	14.228	18.154
23				14.360	17.100	15.946	16.468	14.763	19.238
24				14.886	18.287	17.106	17.587	15.563	20.498
↓									
37				24.744	30.172	28.775	29.660	26.474	33.124
38				25.704	31.033	29.967	30.273	27.290	34.064
39				26.437	32.324	30.807	30.874	28.313	35.080
40				26.900	33.385	31.753	32.071	29.104	36.579
41				28.065	34.305	33.081	32.936	29.625	37.387
42				29.317	35.246	33.499	33.646	30.296	38.149
43				30.097	36.074	34.146	34.870	31.351	39.540
44				30.960	37.432	35.311	35.678	32.114	40.348
45				31.378	38.348	36.121	36.028	33.185	41.423
46				32.508	39.350	36.452	36.785	34.128	42.355
47				33.114	40.265	36.866	37.781	34.741	43.521
48				33.600	40.911	38.017	38.934	35.723	38.821
49				34.511	41.827	38.870	40.057	35.908	32.430
50				35.292	42.480	40.011	40.670	37.009	30.963
51				35.935	43.522	41.012	41.185	38.219	30.868
52				36.705	44.456	41.508	42.462	38.741	30.708
53				37.271	45.291	42.033	43.101	39.220	30.060
54				37.969	46.502	42.619	43.600	40.075	29.953
55				38.854	47.055	43.458	44.976	40.741	30.082
56				39.564	47.683	45.078	46.170	41.418	30.185
57				40.256	48.611	46.349	46.371	42.252	30.267
58				40.832	49.841	46.002	47.054	42.897	30.217
59				42.273	51.021	21.808	47.932	43.412	30.408
60				43.205	51.585	-1.652	48.795	43.878	30.831
61				43.536	24.969	0.024	49.951	44.726	31.048
62				44.266	-1.741	-5.404	50.107	45.811	30.866
63				44.136	-1.889		51.359	46.858	30.703
64				45.717			53.027	46.720	31.158
65				45.678			26.021	47.813	31.216
66				46.864			-1.192	38.349	30.923
67				47.593				27.817	30.480
68				48.171				27.461	30.628
69				49.038				27.617	30.864
70				24.436				28.399	30.318
71				-0.638				28.443	30.287
72								27.728	30.229
73								26.991	
74								26.163	
75								11.494	
76								-0.804	
77									
↓									
202	<b>Work to max Stress</b>			1623.4	1470.6	1291.7	1622.5	1509.2	955.1
203	<b>Work of fracture</b>			1647.2	1492.0	1306.5	1647.3	1778.9	1729.6

**Appendix 11.** Spread sheet sample for compressive property calculation.**E-glass/Epoxy FRP Composites**

**Name:** Risman  
**Operator ID:** D Oxley  
**Test date:** 11/06/2008  
**Specimen name:** Composite Material  
**Fixture type:** Compression  
**Crosshead speed:** 1.5 mm/min

**Cross-sectional areas (mm<sup>2</sup>):**  
**w** **d** **A**  
**Eg-1** 10.02 3.02 30.26  
**Eg-2** 10.05 2.953 29.69  
**Eg03** 10.06 3.153 31.71

Time sec	Eg-1	Eg-2	Eg-3	Stress (MPa)			Strain gauge reading (µε)					
	Load kN	Load kN	Load kN	Eg-1	Eg-2	Eg-3	Eg-1		Eg-2		Eg-3	
0	0.0340	0.0134	0.0141	-1.13	-0.46	-0.45	2	-2	-1	0	2	0
1	-0.1128	-0.0909	-0.0412	3.76	3.09	1.31	-15	-37	-12	-4	2	-1
2	-0.1474	-0.1094	-0.0538	4.92	3.72	1.71	-60	-57	-33	-68	2	0
3	-0.1821	-0.1244	-0.0659	6.08	4.23	2.09	-75	-68	-113	-97	2	-1
4	-0.2095	-0.1376	-0.0719	6.99	4.68	2.28	-83	-73	-128	-103	-13	-33
5	-0.2293	-0.1542	-0.0810	7.65	5.25	2.57	-94	-84	-145	-122	-54	-51
6	-0.2527	-0.1716	-0.0874	8.43	5.84	2.77	-102	-90	-158	-133	-67	-61
7	-0.2690	-0.1858	-0.0934	8.98	6.32	2.96	-110	-99	-175	-151	-75	-66
8	-0.2905	-0.2038	-0.1046	9.70	6.94	3.32	-120	-102	-193	-165	-84	-76
9	-0.3084	-0.2195	-0.1094	10.29	7.47	3.47	-126	-114	-205	-183	-92	-81
↓												
217	-5.1489	-10.6855	-11.9768	171.87	363.63	380.19	-5517	-302	-1069	-11113	-11182	-10759
218	-4.0335	-10.7685	-12.0643	134.64	366.45	382.97	-5414	-264	-938	-11259	-11282	-10852
219	-4.0576	-10.8185	-12.1567	135.44	368.15	385.90	1014	-226	-830	-11396	-11336	-10929
220	-4.6572	-10.9042	-12.2631	155.46	371.07	389.28	1018	-188	-707	-11537	-11430	-11025
221		-10.9489	-12.3556		372.59	392.22	O/S+	O/S+	-588	-11667	-11507	-11114
222		-11.0481	-12.4494		375.97	395.20	O/S+	O/S+	-598	-11935	-11600	-11213
223		-11.0978	-12.5435		377.66	398.18	O/S+	O/S+	-676	-12169	-11673	-11288
224		-11.1614	-12.6319		379.82	400.99	O/S+	O/S+	-708	-12418	-11769	-11391
225		-11.2155	-12.7055		381.67	403.33	O/S+	O/S+	-682	-12626	-11841	-11469
226		-10.4084	-12.8104		354.20	406.66	O/S+	O/S+	-691	-2846	-11945	-11595
227		-9.6202	-12.9006		327.38	409.52	O/S+	O/S+	-700	-2630	-12011	-11656
228		-8.7150	-12.9995		296.57	412.66			-709	-2383	-12109	-11777
229		-7.7815	-13.0821		264.81	415.28			-718	-2127	-12177	-11855
230		-6.0285	-13.1859		205.15	418.58			O/S+	O/S+	-12240	-11961
231		-4.6344	-13.2675		157.71	421.17			O/S+	O/S+	-12334	-12043
232		-2.0907	-13.3905		71.15	425.07			O/S+	O/S+	-12418	-12166
233		-0.3625	-13.4573		12.34	427.19			O/S+	O/S+	-12501	-12245
234		-0.0768	-13.5689		2.61	430.74					-12573	-12342
235			-13.6477		0.00	433.23					-12664	-12436
236			-13.7650		0.00	436.96					-12744	-12542
237			-13.8446		0.00	439.48					-12837	-12643
238			-13.9521		0.00	442.90					-12914	-12744
239			-14.0246		0.00	445.20					-13008	-12844
240			-14.1242			448.36					-13076	-12944
241			-7.4755			237.30					-4667	-309
242			-4.4948			142.68					-4809	-274
243			-4.6000			146.02					-5003	-239
244			-4.8240			153.14					-4910	-204
245											O/S+	O/S+
246											O/S+	O/S+
247											O/S+	O/S+
248											O/S+	O/S+
249											O/S+	O/S+
250											O/S+	O/S+
251											O/S+	O/S+
252											O/S+	O/S+
253											O/S+	O/S+
254											O/S+	O/S+
255											O/S+	O/S+

Compressive stress (MPa) = Load (kN) / Area (mm<sup>2</sup>) \* 1000